1-1-2012

The proton-coupled folate transporter: biology and therapeutic applications to cancer

Sita Desmoulin
Wayne State University,

THE PROTON-COUPLED FOLATE TRANSPORTER: BIOLOGY AND THERAPEUTIC APPLICATIONS TO CANCER

by

SITA KUGEL DESMOULIN

DISSERTATION

Submitted to the Graduate School

of Wayne State University,

Detroit, Michigan

in partial fulfillment of the requirements

for the degree of

DOCTOR OF PHILOSOPHY

2012

MAJOR: CANCER BIOLOGY (Pharmacology)

Approved by:

_____

Advisor Date

_____

_____

_____

_____

_____

DEDICATION

This dissertation is lovingly dedicated to my family.

To my mother, Monica Kugel, whom I love and admire more than anyone else in the world. Your strength, integrity and enormous capacity to love are my permanent support and my life's inspiration.

To my wonderful bothers Kunal, Nitya and Harish, who bring a continuous source of pride and happiness to my life.

And lastly, to the memory of my father, Helmut Kugel (1938 -1992) who instilled in me a strong work ethic and the feeling of satisfaction that comes from doing your job well, no matter what that job is. His memory motivates me and reminds me daily of the importance of cancer research.

ACKNOWLEDGEMENTS

I would like to thank my advisor, Larry H. Matherly. To whom I owe so much. You've been my friend, my mentor, my teacher and a never-ending fountain of moral support. Thank-you for challenging me to critically think both conceptually and analytically and for cultivating my enthusiasm for science. You have helped to build my self confidence both scientifically and personally and I am grateful for all the time you have given me. In the future, I can only hope that I can be half the advisor that you have been. As I progress towards independence, I am better prepared because of you.

A special thanks to all the members of the Matherly lab, both past and present and to the students and faculty in the Cancer Biology Graduate Program who created a wonderful, supportive and productive environment in which to grow as a scientist. I would also like to thank my committee members, Dr. George Brush, Dr. Bharati Mitra, Dr. Yubin Ge and Dr. Jeffery Taub, for all their time and guidance in helping me complete my dissertation research.

I am thankful to Dr. Aleem Gangjee for providing the novel folate analogs used in my research, to Dr. Lisa Polin for performing the *in vivo* efficacy trials of the novel antifolates, to Dr. Mark Stout for his help with the high performance liquid chromatography analysis of nucleoside triphosphate pools and polyglutamates, to Dr. Eric Hales for his help with the flow cytometry analysis of cell cycle and levels of apoptosis after drug treatment, to Dr. Zhanjun Hou for the many hours of training and guidance and finally, to Christina Cherian for all the help she provided throughout my dissertation research.

Lastly, I would like to acknowledge the funding support I received throughout my graduate studies from the Canadian Institutes of Health (CIHR).

TABLE OF CONTENTS

LIST OF TABLES

LIST OF FIGURES

LIST OF ABBREVIATIONS

Ade	Adenosine
AICAR	5-amino-4-imidazolecarboxamide ribonucleotide
AICARFTase	5-amino-4-imidazolecarboxamide ribonucleotide formyltransferase
AIRS	Aminoimidazole ribonucleotide synthase
AMPK	AMP-activated protein kinase
ALL	Acute lymphoblastic leukemia
AML	Acute myelogenous leukemia
AMT	Aminopterin
AFB	Anion-free buffer
APRT	Adenine phosphoribosyl transferase
CAIRS	Carboxyaminoimidazole ribonucleotide synthase
CBE	$Cl^-/HCO3^-$ exchanger
CHO	Chinese hamster ovary cells
CML	Chronic myelogenous
Cmpd	Compound
CK2	Casein kinase 2
DDATHF	6R diastereomer of 5,10-dideazatetrahydrofolate
dFBS	Dialyzed fetal bovine serum
DHF	Dihydrofolate
DHFR	Dihydrofolate reductase
DPBS	Dulbecco's phosphate-buffered saline
dTMP	Thymidylate

dUMP	Deoxyuridine monophosphate
EL	Extracellular loop
FCCP	Carbonylcyanide p-trifluoromethoxyphenylhydrazone
FITC	Fluorescein isothiocyanate
5-CHO-THF	5-formyl-tetrahydrofolate
FPGS	Folylpoly-γ-glutamate synthase
FR	Folate receptor
GAPDH	Glyceraldehyde-3-phosphate dehydrogenase
GAR	Glycinamide ribonucleotide
GARFTase	Glycinamide ribonucleotide formyltransferase
GARS	Glycinamide ribonucleotide synthase
GlpT	Glycerol-3-phosphate transporter
GPAT	Glutamine phosphoribosylpyrophosphate amidotransferase
HA	Hemagglutinin
HEPES	4-(2-hydroxyethyl)-1-piperazineethanesulfonic acid
HFM	Hereditary folate malabsorption
HPLC	High performance liquid chromatography
HPRT	Hypoxanthine phosphoribosyl transferase
IC_{50}	Fifty percent inhibitory concentration
IL	Intracellular loop
IMP	Inosine monophosphate
IMPCH	Inosine monophosphate cyclohydrolase
LacY	Lactose permease

LMX	Lometrexol
MCT	Monocarboxylate-H^+ efflux symporter
MEM	Minimal essential media
MES	4-morphilinopropane sulfonic acid
MeOH	Methanol
MRS	Magnetic resonance spectroscopy
MRI	Magnetic resonance imaging
mSHMT	Mitochondrial serine hydroxymethyltransferase
MTAP	Methylthioadenosine phosphorylase
MTHFD	5,10-methylene tetrahydrofolate dehydrogenase
MTHFR	5,10-methylene tetrahydrofolate reductase
MTHFS	Methenyl tetrahydrofolate synthase
MTX	Methotrexate
NCI	National Cancer Institute
ND	Not determined
NHE1	Na^+/H^+ exchanger
NRF-1	Nuclear respiratory factor 1
NS	Non-specific
NSCLC	Non-small cell lung cancer
OATP	Organic anion transporting polypeptides
PABA	p-aminobenzoic acid
PAICS	Phosphoribosyl aminoimidazole carboxylase and phosphoribosyl aminoimidazole succinocarboxamide synthetase

PCFT	Proton-coupled folate transporter
PDX	Pralatrexate
PET	Positron emission tomography
PG	Polyglutamate
pHLIP	pH (low) insertion peptide
PI	Propidium iodide
PIPES	Piperazine-N,N′-bis(2-ethanesulfonic acid)
PMX	Pemetrexed
PNGase	Peptide: N-Glycosidase
PRPP	Phosphoribosyl pyrophosphate
PVDF	Polyvinylidene difluoride
RFC	Reduced folate carrier
RTX	Raltitrexed
RT-PCR	Reverse transcription-PCR
RXRα	Retinoid X receptor-α
SAICARS	Succinylaminoimidazolcarboxamide ribonucleotide synthase
SAM	S-adenosylmethionine
SAR	Structure activity relationship
SCID	Severe combined immunodeficient
SEM	Standard error of the mean
TCA	Trichloroacetic acid
Thd	Thymidine
THF	Tetrahydrofolate

TMD	Transmembrane domain
TS	Thymidylate synthase
TSC2	Tuberous sclerosis complex 2
VDR	Vitamin D receptor
Vitamin D3	1,25-dihydroxyvitamin D3
WT	Wild-type
YFP	Yellow fluorescent protein
ZMP	5-amino-4-imidazolecarboxamide ribotide

CHAPTER 1

INTRODUCTION

1.1 General Introduction.

Proliferating tumor cells have unique metabolic requirements characterized by enhanced cell-autonomous nutrient uptake and reorganization of metabolic pathways to support the biosynthesis of macromolecules needed for cell growth and division. This includes the folate-dependent *de novo* synthesis of purines and thymidylate for the synthesis of DNA and RNA.

Early observations made by Farber and colleagues established the importance of folate metabolism in cancer progression. Specifically, folic acid supplementation was found to stimulate leukemic cell growth and enhance disease progression among children with acute lymphoblastic leukemia (ALL) (Farber et al., 1947). Therefore, it was hypothesized that folic acid antagonists may inhibit or arrest the proliferation of cancer cells (Farber and Diamond, 1948). In collaboration with SubbaRow and colleagues of Lederle Laboratories, a series of folic acid analogs including aminopterin (AMT) and methotrexate (MTX) were synthesized. This collaboration signified one of the first examples of rational drug design in cancer drug discovery. When administered to children with ALL in 1948, these antifolates became the first drugs to induce remission in this malignancy (Farber, 1949; Farber and Diamond, 1948). Remarkably, MTX continues to achieve widespread clinical use as an essential component of multidrug regimens for treating ALL (Pui and Evans, 2006), lymphomas, and solid tumors worldwide (Jolivet et al., 1983; Monahan, 2001). Thus, targeting folate metabolism and nucleic acid synthesis has the potential to affect cancers arising from many different tissues. Unfortunately, the efficacy of MTX clinically is limited by a lack of tumor selectivity and the presence of *de*

novo and acquired resistance (Matherly et al., 2007). These limitations have led to decades of drug discovery efforts aimed at characterizing more effective antifolates.

The novel antifolate, pemetrexed (PMX) is one of the antimetabolites that were identified through these drug discovery efforts (Taylor et al., 1992). The FDA approval of PMX for the treatment of malignant pleural mesothelioma in 2004 (Hazarika et al., 2004) and non-small cell lung cancer (NSCLC) in 2008 (Cohen et al., 2009) and the concomitant discovery of the proton-coupled folate transporter (PCFT), the preferred cellular uptake route of PMX, by Goldman and colleagues in 2006 (Qiu et al., 2006) has caused a revival of interest in antifolates for cancer therapy (Goldman et al., 2010). This success has shaped a new therapeutic approach to rational folate analog design based on targeting delivery into the cancer cell by exploiting the tumor-specific expression and/or function of folate transporters. This strategy is expected to increase the tumor selectivity of these antimetabolites and enhance their therapeutic window.

This chapter will review the basic biology of PCFT as it relates to the therapeutic application of PCFT in tumor targeting. It will provide an overview of PCFT function, expression, and transcriptional regulation, as well as discuss structurally and functionally important amino acids and domains. The relationship of PCFT to other folate transporters and the consequences of PCFT mutations in human disease will be described. Finally, this chapter will begin to establish the feasibility of a treatment strategy that targets solid tumors based on PCFT-specific uptake of novel folate based analogs.

1.2 Folate Metabolism.

Folates designate the family of B9 vitamins that are essential cofactors necessary for various one-carbon transfer reactions in intermediary metabolism. Important among these reactions are critical steps in the *de novo* synthesis of thymidylate and purine nucleotide

biosynthesis, the regeneration of methionine from homocysteine, the interconversion of serine and glycine, and the catabolism of histidine and formic acid (Matherly and Goldman, 2003; Sirotnak and Tolner, 1999; Stokstad, 1990). The folate molecule consists of three structural components: a pteridine ring system, a p-aminobenzoic acid (PABA) and an L-glutamate moiety (Figure 1.1) (Assaraf, 2007; Zhao et al., 2009a). Mammalian cells are devoid of the metabolic enzymes necessary for folate biosynthesis. Thus, all folate requirements must be acquired through the diet (Matherly and Goldman, 2003; Sirotnak and Tolner, 1999). Within the mammalian cell, folates are converted to various one-carbon-substituted tetrahydrofolate (THF) cofactors with a one-carbon moiety at the N5 and/or N10 position at the oxidation level of methanol (5-methylTHF), formaldehyde (5,10-methyleneTHF) or formate (10-formylTHF or 5,10-methenylTHF). Additionally, folates undergo polyglutamylation by folylpoly-γ-glutamate synthase (FPGS) in which 2 to 8 linked glutamyl residues are added to the γ-carboxyl on PABA of the THF cofactor. Polyglutamates of THF cofactors are polyanions which are impermeable to the plasma membrane and hence are retained in cells, thus ensuring high levels of intracellular reduced folates (Figure 1.1) (Stokstad, 1990).

Carbon 3 of serine (derived from glycolytic intermediates) is the primary source of one-carbon units for cytoplasmic one-carbon metabolism (Davis et al., 2004), mainly through its conversion to formate in the mitochondria (Anguera et al., 2006; Barlowe and Appling, 1988; Barlowe and Appling, 1990; Garcia-Martinez and Appling, 1993; Gregory et al., 2000; Herbig et al., 2002; Kastanos et al., 1997; MacFarlane et al., 2008; Pasternack et al., 1994; Pasternack et al., 1996; Patel et al., 2003; Quinlivan et al., 2005; Tibbetts and Appling, 2010). The cytoplasmic and mitochondrial compartments are metabolically connected by transport of serine, glycine and formate across mitochondrial membranes. Once transported into the mitochondria, the one-

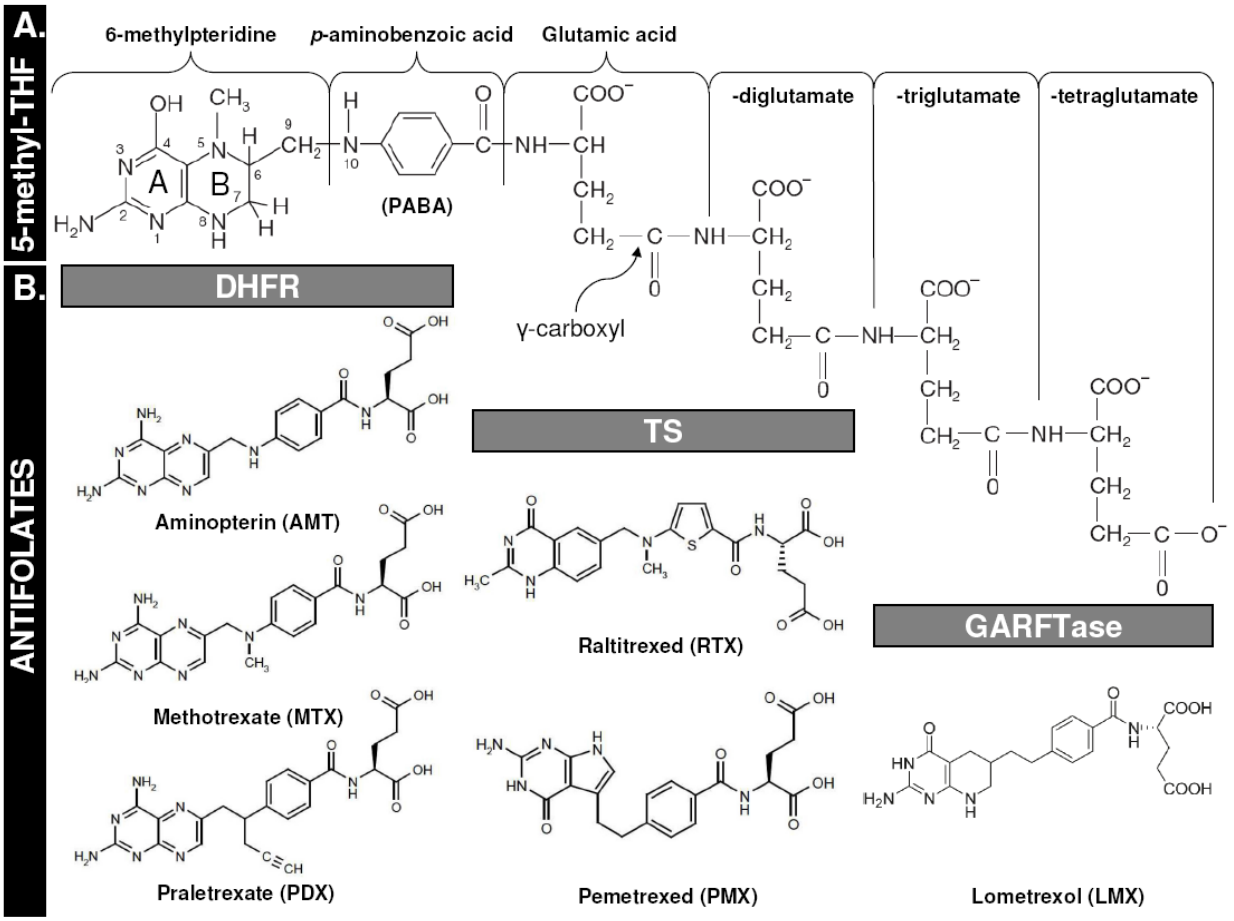

Figure 1.1 Structure of 5-methyl tetrahydrofolate and classical antifolates. 5-methyl-tetrahydrofolate (THF) is the major dietary form and the dominant folate found in blood. The folate molecule consists of a 6-methylpteridine moiety with A and B rings linked at carbon 6 by a methylene bridge to p-aminobenzoylglutamic acid. The N5 and/or N10 position can associate with a methyl (*Panel A*), formyl, methylene or methenyl one carbon moiety, which serve as one-carbon donors in biosynthetic reactions. THF undergoes polyglutamylation by folylpoly-γ-glutamate synthase (FPGS) in which 2 to 8 linked glutamyl residues are added to the γ-carboxyl on PABA of the THF cofactor. *Panel B*, Antifolates are structural analogs of natural folates that inhibit folate-dependent enzymes. Antifolates inhibiting: dihydrofolate reductase (DHFR) are aminopterin (AMT), methotrexate (MTX), and praletrexate (PDX); thymidylate synthase (TS) are raltitrexed (RTX) and pemetrexed (PMX); β-glycinamide ribonucleotide formyltransferase (GARFTase) is lometrexol (LMX). PMX inhibition of 5-amino-4-imidazolecarboxamide ribonucleotide formyltransferase (AICARFTase) and MTX polyglutamate inhibition of TS and AICARFTase is not illustrated.

carbon unit from serine is transferred to THF in a reaction catalyzed by mitochondrial serine hydroxymethyltransferase (mSHMT), which generates 5, 10-methyleneTHF and glycine (reaction **1m**) in Figure 1.2 (Tibbetts and Appling, 2010). In the mitochondria, 5,10-methyleneTHF is converted into 10-formylTHF by the bifunctional MTHFD2 in embryonic tissue (Mejia and MacKenzie, 1985) or MTHFD2L in adult tissues (Bolusani et al., 2011). Bifunctional MTHFD2 has both 5,10-methyleneTHF dehydrogenase (reaction **2m**) and 5,10-methenylTHF cyclohydrolase (reaction **3m**) activities. 10-formylTHF can then be converted by the monofunctional MTHFD1L 10-formylTHF synthetase into formate and reduced THF (reaction **4m**) (Prasannan et al., 2003). Once exported into the cytoplasm, formate reacts with unsubstituted THF, facilitated by the 10-formylTHF synthetase activity of the cytoplasmic trifunctional enzyme C_1-tetrahydrofolate synthase (referred to as MTHFD1) to produce 10-formylTHF (reaction **4**) (Hum et al., 1988; Paukert et al., 1977; Schirch, 1978; Smith et al., 1980; Thigpen et al., 1990). The formyl group of 10-formylTHF can be used in *de novo* purine nucleotide synthesis where it is donated to β-glycinamide ribonucleotide (GAR) and then 5-amino-4-imidazolecarboxamide ribonucleotide (AICAR), which is catalyzed by GAR formyltransferase (GARFTase; reaction **5**) and AICAR formyltransferase (AICARFTase; reaction **6**), respectively. This leads to a net two carbon transfer from 10-formylTHF to C-2 and C-8 of the purine ring, regenerating unsubstituted THF (Hartman and Buchanan, 1959b; Smith et al., 1981; Smith et al., 1980). The 5,10-methenylTHF cyclohydrolase (reaction **3**) and 5,10-methyleneTHF dehydrogenase (reaction **2**) activities of the cytosolic trifunctional MTHFD1 can also convert 10-formylTHF to 5,10-methenylTHF and subsequently 5,10-methyleneTHF (Hum et al., 1988; Paukert et al., 1977; Schirch, 1978; Smith et al., 1980; Thigpen et al., 1990), which can donate the one-carbon unit in the irreversible conversion of deoxyuridine monophosphate

(dUMP) to thymidylate (dTMP, a precursor to DNA), catalysed by thymidylate synthase (TS) (reaction **7** in the cytoplasm and **7n** in the nucleus) (Friedkin and Roberts, 1956; Phear and Greenberg, 1957). The resulting dihydrofolate (DHF) (Humphreys and Greenberg, 1958; McDougall and Blakley, 1960) is reduced by cytoplasmic DHFR to unsubstituted THF (reaction **8**). Alternatively, 5,10-methyleneTHF can be reduced in an irreversible reaction by 5,10-methyleneTHF reductase (MTHFR) to generate 5-methylTHF for entry into the methyl cycle (reaction **9**). 5-methylTHF can donate a one carbon unit in the B12-dependent regeneration of methionine from homocysteine, regenerating the THF, catalyzed by methionine synthase (reaction **10**) (Hatch et al., 1961). Methionine is a precursor for the synthesis of S-adenosylmethionine (AdoMet or SAM), a cofactor and methyl group donor for numerous methylation reactions, including the methylation of cytosine bases in DNA, histones, RNA, neurotransmitters, and other small molecules, phospholipids, and other proteins (Figure 1.2) (Lu, 2000).

1.3 Membrane Transport of Folates.

Due to the highly hydrophilic nature of folates and antifolates, three genetically distinct and functionally diverse transport systems are in place to facilitate their uptake into the cells of peripheral tissues.

1.3.1 Reduced Folate Carrier.

The reduced folate carrier (RFC; SLC19A1), a member of the Major Facilitator Superfamily of solute carriers, is a secondary active anionic exchanger and the major transport system for reduced folates (K_t ~ 2-4 μM) in mammalian cells and tissues at physiologic pH (Figure 1.2) (Goldman et al., 1968; Sirotnak et al., 1968). RFC has a very low affinity for folic acid and as the pH is decreased, the activity for reduced folates is diminished so that there is little

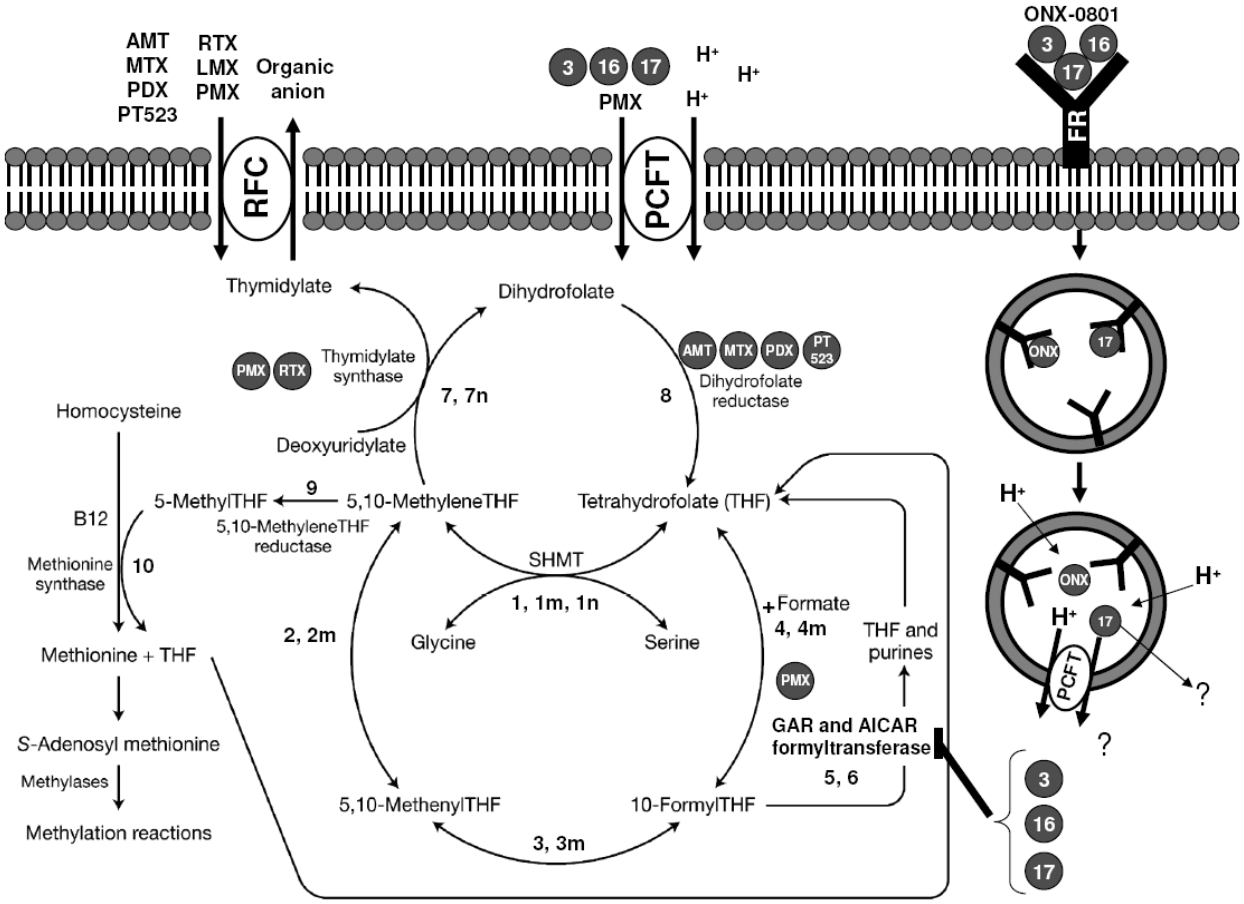

Figure 1.2 Folate transporters, folate metabolic pathways and intracellular enzyme targets of antifolates. Folate and antifolate transport across biological membranes is mediated by the reduced folate carrier (RFC), the proton-coupled folate transporter (PCFT) and the folate receptor (FR). Reactions 1-4 are in both the cytoplasmic and mitochondrial (m) compartments. Reactions 1 and 9 are also present in the nucleus (n). The numbered reactions are catalyzed by the following enzymes: **1**, **1n** and **1m**, serine hydroxymethyltransferase (SHMT). In the mitochondria, reactions **2m** and **3m** are catalyzed by bifunctional MTHFD2 or MTHFD2L and **4m** is catalyzed by monofunctional MTHFD1L. In the cytoplasm, reactions **4**, **3** and **2**: 10-formylTHF synthetase, 5,10-methenylTHF cyclohydrolase and 5,10-methyleneTHF dehydrogenase, respectively, are catalyzed by trifunctional C1-THF synthase in the cytoplasm (MTHFD1); **5**, β-glycinamide ribonucleotide formyltransferase (GARFTase); **6**, 5-amino-4-imidazolecarboxamide ribonucleotide formyltransferase (AICARFTase); **7** and **7n**, thymidylate synthase (TS); **8**, dihydrofolate reductase (DHFR); **9**, 5,10-methyleneTHF reductase (MTHFR); **10**, methionine synthase. Aminopterin (AMT), methotrexate (MTX), praletrexate (PDX), raltitrexed (RTX), lometrexol (LMX), pemetrexed (PMX) (Figure 1.1), ONX-0801 (ONX), compound 3, compound 16 and compound 17 (Figure 3.1).

activity below pH 6.5. The human RFC gene is located on chromosome 21q22.3, and the gene structure appears to be conserved across species, with as many as six non-coding regions and alternative promoters (A1, A2, A, B, C, D and E) spanning 35 kb upstream from the major AUG translational start in coding exon 1, and five major coding exons with conserved intron-exon boundaries. This gives 15 distinct 5'untranslated regions fused to a common splice acceptor at position -49 and the same 1,776 bp coding sequence, which encodes a protein consisting of 591 amino acids (Flatley et al., 2004; Matherly et al., 2007; Payton et al., 2007; Whetstine et al., 2002a). Promoter activity has been confirmed for the 5' regions proximal to the A1/A2, A, B, C and D non-coding regions. Regulation of RFC gene expression is by both ubiquitous (e.g. Sp, USF) and tissue-specific (e.g., Ap2, C/EBp, Ikaros, GATA) transcription factors that, when combined, transactivate or repress transcription in response to tissue-specific stimuli. Additionally, promoter methylation, general architecture and chromatin structure have all been implicated in transcriptional regulation of RFC (Liu et al., 2004; Payton et al., 2005a; Payton et al., 2005b; Whetstine et al., 2002b).

Hydropathy plot analysis of the RFC amino acid sequence predicted a topological model of 12 transmembrane domains (TMDs) and both amino- and carboxyl termini oriented to the cytosol. This was confirmed by hemagglutin epitope insertion, scanning N-glycosylation mutagenesis, and scanning cysteine accessibility methods (Cao and Matherly, 2004; Ferguson and Flintoff, 1999; Liu and Matherly, 2002). RFC is N-glycosylated at an N-glycosylation consensus site in the first intracellular loop (IL1) between TMD1 and TMD2. A large loop domain connecting TMD6 and TMD7 is needed to provide appropriate spacing between TMD1-TMD6 and TMD7-TMD12 segments for optimal transport. Amino acids localized in TMD4, TMD5, TMD7, TMD8, TMD10 and TMD11 were implicated in forming the putative substrate-

binding pocket (Hou et al., 2005; Hou et al., 2006). This structure is consistent with crystal structures for the bacterial Major Facilitator Superfamily proteins, lactose permease (LacY) and glycerol-3-phosphate transporter (GlpT) (Abramson et al., 2003; Huang et al., 2003b). Like other Major Facilitator Superfamily transporters, RFC exists as a homo-oligomer; however, each monomer functions as an independent transport unit and is fully active (Hou and Matherly, 2009; Hou et al., 2010).

Various studies on transcriptional and protein expression levels showed that RFC is ubiquitously expressed in tissues where it participates in transporting folate cofactors into cells, thus suggesting its integral role in specialized tissues that are important for *in vivo* folate homeostasis. Immunohistochemical analysis demonstrated mouse RFC protein expression on the apical brush-border membrane of small intestine and colon, liver hepatocyte membranes, the apical surface of the choroid plexus, the basolateral membrane of renal tubular epithelium, and the apical membrane of cells lining the spinal canal (Wang et al., 2001b). Measuring transcriptional expression of RFC in 76 human tissues and tumor cell lines showed the highest levels in placenta and liver, with considerably higher levels in leukocytes, kidney, lung, bone marrow and small intestine, and low but detectable levels in heart and skeletal muscle (Whetstine et al., 2002a). In at least some tissues (e.g., small intestine), the rodent RFC is responsive to dietary folate availability such that under conditions of folate deficiency, increased levels of RFC transcripts and proteins are observed (Liu et al., 2005). However, as acidic pH in the gut decreases the transport activity of RFC, the significance of this increased expression in the gut is unclear.

1.3.2 Folate Receptor.

Folate receptors (FRs), often referred to as high affinity folate binding proteins, bind and transport folic acid, reduced folate, many antifolates and folate conjugates with a high affinity (Kd~0.1–1 nM). There are three isoforms of human FR, α, β, and γ, encoded by distinct genes (Elwood, 1989; Lacey et al., 1989; Ratnam et al., 1989; Sadasivan and Rothenberg, 1989; Shen et al., 1994; Shen et al., 1995), localized on chromosome 11q13.3-q13.5 (Ragoussis et al., 1992). The human FR isoforms are homologous, with 68~79% identical amino acid sequences and two (β and γ) or three (α) N-glycosylation sites (Roberts et al., 1998; Shen et al., 1997). FRα and β are cell surface glycosyl phosphatidylinositol (GPI)-anchored glycopolypeptides, while FRγ lacks the signal for GPI-anchor attachment and is therefore a secretory protein with unknown function (Shen et al., 1995). Upon binding (anti)folates or folate-conjugates, FR internalizes them by a non-classical endocytic mechanism (Figure 1.2) (Rijnboutt et al., 1996; Sabharanjak and Mayor, 2004). In this process, folates bind to FRs at the cell membrane, invaginate and bud off to form vesicles that are internalized into the intracellular endosomal compartment. Release of the ligand from the receptor occurs with a decrease of pH in the endosome and exit from the intact vesicle occurs presumably by diffusion or a process that operates optimally at low pH (Kamen et al., 1988).

FR is predominantly expressed on the apical (luminal) surface of polarized epithelial cells where it is not in contact with circulating folate (Chancy et al., 2000). In normal tissues, FRα is expressed in the brush-border membrane of the choroid plexus, retinal pigment epithelium, proximal tubules in kidney, fallopian tubes, uterus and placenta (Elnakat and Ratnam, 2004). FRβ expression in normal tissues is only found in placenta and hematopoietic cells (Ratnam et al., 1989). In normal bone marrow and peripheral blood cells, expression of FRβ is restricted to myelomonocytic lineage such as mature neutrophils, and was reported to have little binding

function with folic acid (Pan et al., 2002; Reddy et al., 1999). The polarized expression of FRα and β serves to protect normal tissues from FR-targeted cytotoxic agents in the circulation given intravenously (Weitman et al., 1992). Overexpression of FRα was reported in several malignant tissues including non-mucinous adenocarcinomas of ovary, uterus and cervix and ependymal brain tumors (Elnakat and Ratnam, 2004), and was found to positively correlate with tumor grade and stage in ovarian tumors (Buist et al., 1995; Garin-Chesa et al., 1993; Veggian et al., 1989; Wu et al., 1999). The FRα overexpressed in malignant tissues was shown to retain the high affinity binding of folate (Ross et al., 1994; Weitman et al., 1992). Malignant expression of FRβ is found in all chronic myelogenous leukemia (CML) cells and 70% of acute myelogenous leukemia (AML) cells, but not in ALL (Pan et al., 2002; Ross et al., 1999).

1.3.3 Proton-coupled Folate Transporter.

In addition to RFC and the FRs, a low-pH folate transport mechanism was observed in mammalian cells, but the carrier responsible for this transport activity remained elusive for more than three decades. The transporter that is the basis for this activity and the subject of this dissertation has been recently identified and characterized as a proton-coupled folate transporter (PCFT; SLC46A1) (Nakai et al., 2007; Qiu et al., 2006; Umapathy et al., 2007; Zhao and Goldman, 2007) (Figure 1.2. PCFT is a proton-folate symporter that functions optimally at acidic pH by coupling the uptake of folates with the flow of protons down their electrochemical concentration gradient. Although human PCFT shares only ~14% amino acid identity with human RFC, like RFC, it belongs to the Major Facilitator Superfamily (Zhao and Goldman, 2007; Zhao et al., 2009a). Strategies used to clone PCFT included database mining, using the conserved amino acid sequence of SLC19 family members, and screening of candidate mRNAs in cell lines where the RFC gene was deleted and low pH transport was either retained or

markedly decreased (Qiu et al., 2006). PCFT was initially reported to be a low-affinity heme transporter that is pH-independent (Shayeghi et al., 2005). Although PCFT may be capable of heme transport, its primary function appears to be absorption of folates at low pH. The ability of PCFT to transport folate under acidic conditions is important for folate homeostasis, as dietary folate absorption in the duodenum and upper jejunum occurs via PCFT (Inoue et al., 2008; Qiu et al., 2007).

1.4 Biology of the Proton-Coupled Folate Transporter.

1.4.1 PCFT Tissue Expression.

PCFT is localized to chromosome 17q11.2 in humans and the gene consists of five exons, and codes for a 459 amino acid protein with a predicted molecular mass of ~50 kDa. As mentioned above, the highest expression levels of PCFT in normal tissues were reported in the apical brush-border membrane along the proximal jejunum and duodenum, kidney, liver, placenta, spleen, and choroid plexus (Inoue et al., 2008; Qiu et al., 2006; Qiu et al., 2007; Urquhart et al., 2010). It has been hypothesized that PCFT may still play a role in folate uptake into tissues that do not experience low pH, though whether this is due to localized acidification or solely due to the high level of expression, combined with residual transport of 5-methylTHF at neutral pH, remains to be determined (Qiu et al., 2006). Delivery of folates to the central nervous system has been proposed to involve PCFT and FRα coupling in the choroid plexus, whereby PCFT exports folates from the acidic endocytic compartment created by FRα-mediated endocytosis (Zhao et al., 2009b) (Figure 1.2). For the maintenance of cerebrospinal fluid folate, the presence of one transporter is inadequate in the absence of the other; therefore, when either FR or PCFT is mutated in humans, the syndrome of folate deficiency manifests (Cario et al., 2009; Steinfeld et al., 2009).

A comprehensive examination of PCFT and RFC expression in malignant cell lines and tissues has not previously been performed, however, low pH transport of [^{3}H]MTX was detected in human solid tumor cell lines from the National Cancer Institute (NCI) 60 tumor panel and other sources. In this study MTX influx at pH 5.5 was equal to, or greater than, MTX influx at pH 7.4 in 29 of 32 cell lines (Zhao et al., 2004b). These findings suggest that if the low pH transport can be attributed to PCFT-mediated uptake of MTX, designing therapeutics selective for PCFT uptake over RFC has the potential of increasing solid tumor selectivity of antifolates.

1.4.2 Regulation of PCFT Gene Expression.

Understanding the regulation and silencing of PCFT gene expression is important due to the physiologic and pharmacologic importance of PCFT. The PCFT minimal transcriptional regulatory region is localized between positions -42 and +96 (the transcriptional start site is +1) (Diop-Bove et al., 2009; Stark et al., 2009).

The promoter of the PCFT gene harbors a 1085-bp CpG island (nucleotides −600 through +485) and hence the extent of methylation is a possible mechanism of PCFT transcriptional control. Hypermethylation of the PCFT promoter was shown to be associated with low PCFT gene and protein expression in CCRF-CEM and Jurkat T-cell leukemia cell lines (Gonen et al., 2008) and a MTX-resistant HeLa cell line (R1) (Diop-Bove et al., 2009). In both cases, treatment with the DNA methyltransferase inhibitor, 5-aza-2'-deoxycytidine, resulted in substantial restoration of pH 5.5 transport and PCFT mRNA expression. Folate status can affect methylation of CpG islands of DNA and of histones through their requirement in vitamin-B12-dependent synthesis of methionine, a precursor of SAM (Stokstad, 1990). To this end, hypomethylation can accompany folate deficiency under some conditions (Wasson et al., 2006). Hence, control of PCFT expression through methylation provides an elegant method of altering

uptake in the face of folate excess or deficiency (Zhao et al., 2011a). Additionally, low dose 5-aza-2'deoxycytidine treatment may restore PCFT-mediated transport of antifolates in patients with acquired resistance due to methylation of the PCFT promoter.

PCFT mRNA levels are also controlled by 1,25-dihydroxyvitamin D3 (vitamin D3), and expression of PCFT is increased in a dose-dependent fashion in Caco-2 cells *in vitro* and in duodenal rat biopsies *ex vivo* when treated with vitamin D3. Vitamin D receptor (VDR) heterodimerizes with retinoid X receptor-α (RXRα) in response to vitamin D3 and binds a VDR response element in the PCFT promoter region (-1694/-1680), increasing expression and therefore function of PCFT (Eloranta et al., 2009). This finding suggests that vitamin D3 supplementation could affect the bioavailability or toxicity of PCFT-targeted therapeutics in the clinic and may be an important consideration in the design of clinical trials.

Three adjacent putative binding sites for the nuclear respiratory factor 1 (NRF-1) transcription factor were identified in the PCFT minimal promoter. NRF-1 was found to bind and transactivate the human PCFT promoter leading to an increase in PCFT mRNA levels (Gonen and Assaraf, 2010). NRF-1 is a major regulator of mitochondrial biogenesis (Scarpulla, 2002; Scarpulla, 2006; Scarpulla, 2008; Scarpulla, 2011). Folates play an important role in mitochondrial integrity, and folate deficiency has been found to cause large mitochondrial deletions, cytochrome c dysfunction, membrane depolarization and superoxide overproduction (Chang et al., 2007). Interestingly, NRF-1 has been found to up-regulate the bi-directional transcription of glutamine phosphoribosylpyrophosphate amidotransferase (GPAT) (reaction **1**) and phosphoribosylaminoimidazole carboxylase/phosphoribosylaminoimidazole succinocarboxamide synthetase (PAICS) (reaction **6** and **7**) which are both enzymes needed for *de novo* purine biosynthesis (Figure 1.5) (Brayton et al., 1994; Chen et al., 1997). Thus, NRF-1

may function to coordinate mitochondrial respiration-biogenesis with folate uptake, folate metabolism and *de novo* purine biosynthesis (Gonen and Assaraf, 2010).

1.4.3 Hereditary Folate Malabsorption.

Direct evidence that PCFT is responsible for low-pH transport and intestinal folate absorption came from the discovery that homozygous mutations in the coding region of the PCFT gene leads to the rare autosomal recessive disorder, hereditary folate malabsorption (HFM) (Atabay et al., 2010; Borzutzky et al., 2009; Geller et al., 2002; Lasry et al., 2008; Mahadeo et al., 2010; Mahadeo et al., 2011; Meyer et al., 2010; Min et al., 2008; Qiu et al., 2006; Shin et al., 2011; Shin et al., 2010; Zhao et al., 2007). HFM is characterized by the onset of macrocytic folate-deficiency, anemia, and failure to thrive within the first few months of life. This may be accompanied by hypoimmunoglobulinemia associated with infectious complications, most frequently *Pneumocyctis jiroveci* pneumonia. The syndrome is characterized by developmental delays, gait disorders, peripheral neuropathies, and, in the absence of adequate and timely treatment, seizures (Geller et al., 2002; Mahadeo et al., 2010). Loss of PCFT function leads to impaired intestinal folate absorption, resulting in severe folate deficiency and impaired transport of folates across the choroid plexus into the central nervous system, reflecting the important physiological functions of PCFT folate transport (Zhao et al., 2009a). The fact that subjects who are PCFT null develop severe folate deficiency indicates that RFC does not contribute significantly to folate absorption under these conditions (pH 5.8-6.0) despite its presence in the intestinal epithelium. Many insights into the structure and function of PCFT have been gained by mechanistically evaluating the HFM loss-of-function mutations (Figure 1.3; Figure 1.4; Table 1.1).

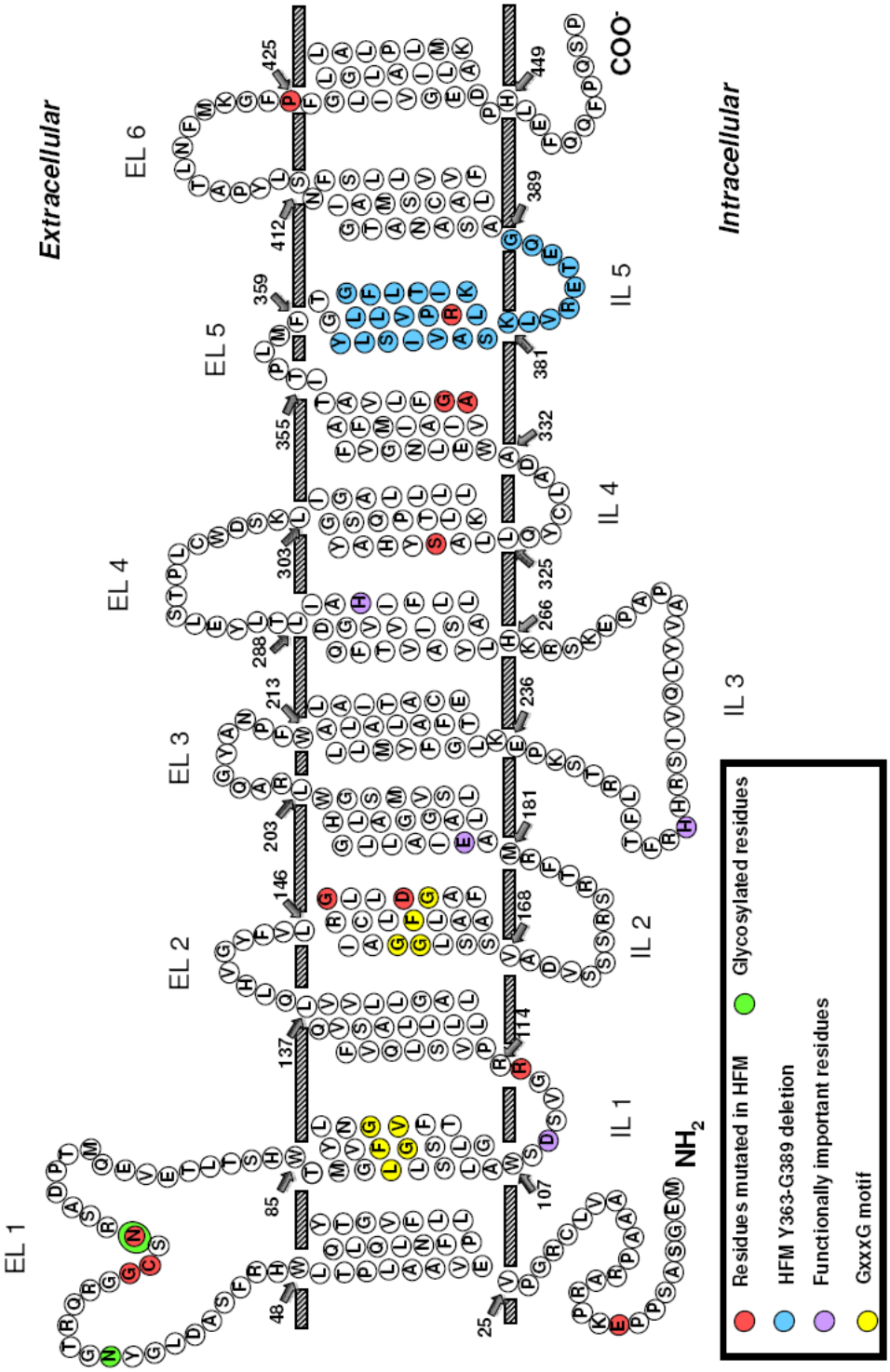

Figure 1.3 Schematic structure of PCFT topology. Structurally or functionally important amino acids, as determined from published mutagenesis studies, are shown as *purple circles*. Amino acids mutated in patients with hereditary folate malabsorption (HFM) are shown as *red* and *blue circles*. GxxxG putative dimerization motifs are shown as *yellow circles* and glycosylated residues N58 and N68 are shown as *green circles*.

Figure 1.4 Amino acid sequence alignment of PCFT homologs from different species.

Table 1.1 Summary of published PCFT mutations in subjects with the clinical diagnosis of hereditary folate malabsorption.

Nucleotide change	Amino acid change	Location of mutation	Cells used for transfection	Crude membrane expression	Cell surface expression	Transport	Transport substrate	Reference
17-18insC	E9Gfs	N-term	ND	ND	ND	ND	ND	Shin et al., 2011
194delG	G65Afs X25	EL1	WT HeLa	no	no	no transport	5-methylTHF	Zhao et al., 2007
194dupG	C66Lfs X99	EL1	ND	ND	ND	ND	ND	Meyer et al., 2010
GC197-198AA	C66X	EL1	R1-11 HeLa	no	no	no transport	5-methylTHF	Min et al., 2008
204-205delCC^	N68Kfs^	EL1	ND	ND	ND	ND	ND	Shin et al., 2011; Atabay et al., 2010
C337A	R113S	IL1	WT HeLa	no	no	no transport	5-methylTHF	Zhao et al., 2007
C337T	R113C	IL1	C5 MTX$^{R0.15}$	ND	yes	no transport	folic acid	Larsy et al., 2008
						no transport	MTX	
G439C	G147R	TMD4	WT HeLa	no	no	13% of WT	5-methylTHF	Zhao et al., 2007
G466T	D156Y	TMD4	R1-11 HeLa	low MW PCFT	no	no transport	MTX	Shin et al., 2010
C954G*	S318R*	TMD8	WT HeLa	low	no	no transport	5-methylTHF	Zhao et al., 2007
C1004A^	A335D^	TMD9	R1-11 HeLa	ND	ND	no transport	MTX	Shin et al., 2011
G1012C	G338R	TMD9	R1-11 HeLa	ND	ND	no transport	MTX	Shin et al., 2011
G1082-1A splice acceptor site	Y362_G389del	TMD10 + IL5	HeLa	low MW PCFT	no intracellular	no transport	5-methylTHF	Qiu et al., 2006; Borzutzky et al., 2009; Mahadeo et al., 2011
C1126T*	R376W*	TMD10	WT HeLa	low	no	no transport	5-methylTHF	Zhao et al., 2007
			R1-11 HeLa	same as WT	same as WT	no transport	5-methylTHF	Mahadeo et al., 2010
						no transport	Folic acid	
						no transport	5-formylTHF	
						no transport	MTX	
						no transport	PMX	
G1127A	R376Q	TMD10	R1-11 HeLa	~50% of WT	~50% of WT	no transport	5-methylTHF	Mahadeo et al., 2010
						no transport	Folic acid	
						no transport	5-formylTHF	
						no transport	MTX	
						~50% of WT ↑ influx Km = Vmax	PMX	
C1274G	P425R	EL6	WT HeLa	no	yes	3.5% of WT	5-methylTHF	Zhao et al., 2007
			R1-11 HeLa	yes	yes	~5% of WT	MTX	Hou et al., 2011

The first exon, particularly nucleotides encoding extracellular loop 1 (EL1) between the first and second transmembrane domains, has a high GC content, 65.8% (75% between residues 63 and 70), and is the most frequent site of PCFT mutations in subjects with HFM (Shin et al., 2011). There are five reported mutations. These include four frame-shifts: c.17-18insC, p.E9Gfs (Shin et al., 2011); c.194delG, p.G65Afs (Zhao et al., 2007); c.194dupG, p.C66Lfs (Meyer et al., 2010); and c.204-205delCC, p.N68Kfs (Atabay et al., 2010; Shin et al., 2011) and a stop codon (c.GC197AA; p.C66X (Min et al., 2008)) (See Table 1.1 for references describing various HFM mutations). These genetic alterations led to truncation of PCFT and loss of PCFT expression and function. Additionally, a number of residues identified in patients with HFM, (c.G439C, p.G147R in TMD4 (Zhao et al., 2007); c.G466T, p.D156Y in TMD4 (Shin et al., 2010); c.C954G, p.S318R in TMD8 (Zhao 2007); c.C1004A, p.A335D in TMD9 (Shin 2011) and c.G1012C, p.G338R in TMD9 (Shin 2011)) (Figure 1.3 and Table 1.1) when mutated lead to no or very low (13% of wild-type (WT) for G147R) levels of transport of either 5-methylTHF or MTX. Point mutations involving either Arg113 to serine (c.C337A, p.R113S (Zhao et al., 2007)) or cysteine (c.C337T, p.R113C (Lasry et al., 2008)) and either Arg376 to tryptophan (c.C1126T, p.R376W (Mahadeo et al., 2010)) or glutamine (c.G1127A, p.R376Q (Mahadeo et al., 2010)) have been found in two unrelated families with HFM. Characterization of these mutations suggested that mutation of Arg113 may affect binding and/or translocation of negatively charged folate substrates and mutation of Arg376 may affect proton binding and therefore modulates the folate-binding pocket in a substrate-dependent manner. Please see section 1.4.4.3 for a more in depth discussion of the importance of these residues for PCFT function. Interestingly, most point mutations associated with HFM occur in TMDs or at TMD junctions. TMD4 and 9 contain the most mutations (Figure 1.3) (Zhao et al., 2011b). The mutation c.G1082-1A is located in the

splice acceptor of intron 2 (intron 2/exon 3 boundary), causing skipping of exon 3 which creates a splice variant that results in deletion of 28 amino acids in TMD10 and IL5 (p.Y362_G389del). This mutation results in a protein with decreased stability and impaired trafficking to the cell membrane and was identified in eight unrelated families of Puerto Rican heritage (Borzutzky et al., 2009; Mahadeo et al., 2011; Qiu et al.). Finally, the residue Pro425 in the EL6 was found to be mutated (c.C1274G, p.P425R) in a family of Arab descent. This mutation only slightly impacted cell surface expression of PCFT, but function was 3.5-5% of WT (Shin et al., 2012; Zhao et al., 2007). Interestingly, combined WT and inactive mutant P425R PCFTs were targeted to the cell surface by surface biotinylation/Western blotting and confocal microscopy, and functionally exhibited a "dominant-positive" phenotype, implying positive cooperativity between monomers comprising oligomeric PCFT and functional rescue of mutant by WT PCFT (Hou et al., 2011) (see section 1.4.4.4).

A possible mechanism of resistance to antifolates selective for PCFT-mediated uptake may be loss of PCFT function; therefore a better understanding of the impact of mutations on PCFT structure and function could provide insight into possibly reversing future cases of resistance.

1.4.4 Structure and Function of PCFT.

1.4.4.1 Topology.

Based on hydropathy plot analysis, the membrane topology of PCFT is predicted to include twelve TMDs with the N- and C- termini directed into the cytoplasm (Figure 1.3) (Zhao and Goldman, 2007; Zhao et al., 2009a). Orientation of the N- and C- termini was validated by immunofluorescence analysis of HA-tagged PCFT. The loop domain between TMD1 and TMD2 was found to be extracellular since the two predicted N-glycosylation sites (Asn58,

Asn68) in this region are glycosylated (Figure 1.3). N-linked glycosylation at the above mentioned sites was validated by Peptide: N-Glycosidase (PNGase) F cleavage of the oligosaccharide, tunicamycin inhibition of N-linked glycosylation and site-directed mutagenesis of Asn58 and Asn68. Trafficking and function of PCFT was not affected by N-glycosylation status (Unal et al., 2008). In MDCK and Caco-2 cells, C-terminal-tagged yellow fluorescent protein (YFP) PCFT was functionally expressed at the apical membrane, which is different from the basolateral localization for RFC (Subramanian et al., 2008). Complete truncation of the PCFT C-terminal region had no significant effect on either apical cell surface targeting or transport function (Subramanian et al., 2008). A disulfide bond exists that is not important to function that links Cys66 in the first extracellular loop to Cys298 in the fourth extracellular loop (Zhao et al., 2010).

1.4.4.2 Transport Characteristics.

PCFT has similar affinities (K_t ~ 0.5-1.0 µM) for reduced (5-methylTHF, 5-formylTHF) and oxidized (folic acid) folates at pH 5.5 and is stereospecific for 5-formylTHF (Zhao and Goldman, 2007). Folic acid and MTX uptake in *Xenopus laevis* oocytes was increased > 200 fold at pH 5.5 when injected with PCFT cRNA (Qiu et al., 2006; Qiu et al., 2007). Increased low-pH (pH 5.5) transport was also observed when PCFT cDNA was transiently transfected into HeLa cells or stably transfected into HepG2 cells (Zhao et al., 2008). When PCFT was silenced with interfering RNAs, the low-pH transport of Caco-2 was reduced by 80% (Qiu et al., 2006). PCFT transport activity was highest at the lowest pH (pH 5.5) and declined as the pH increased (pH 7.4). Uptake by PCFT conformed to Michaelis-Menten kinetics. The K_t increased and V_{max} decreased as the pH increased from pH 5.5 to pH 7.4 (Qiu et al., 2006; Zhao and Goldman, 2007). The activity of PCFT is not affected by removal of extracellular Na^+, K^+, Ca^{+2}, Mg^{+2} or

Cl^- (Qiu et al., 2006). Dissipation of the transmembrane proton-gradient by carbonylcyanide p-trifluoromethoxyphenylhydrazone (FCCP) (a proton ionophore) (Qiu et al., 2006) and nigericin (a K^+/H^+-exchanging ionophore) (Inoue et al., 2008) in *Xenopus* oocytes and HEK293 cells, respectively, reduced transport by PCFT. Studies in *Xenopus* oocytes have demonstrated that folate transport by PCFT is electrogenic, where there is a net translocation of positive charge as each negatively charged folate molecule is transported. Assuming that folates are bivalent anions, more than two protons must be co-transported with each folate molecule to account for the net transport of positive charge (Qiu et al., 2006; Qiu et al., 2007). Cellular acidification that accompanies folate transport into oocytes was measured, confirming proton coupling (Unal et al., 2009a). Conversely, in HEK293 cells, transport by PCFT was insensitive to membrane potential, suggesting potential-independent, non-electrogenic transport, although in either case there was still a requirement for an inwardly directed proton gradient (Inoue et al., 2008). PCFT functions even when there is no transmembrane pH gradient, based partly on the membrane potential. At pH 7.4, when the membrane potential is increased, folate-induced currents are increased (Qiu et al., 2006; Umapathy et al., 2007). At low pH, PCFT has also been found to have channel-like activities, where protons can flow uncoupled from the flow of folates (Mahadeo et al., 2010; Unal et al., 2009a). Anionic compounds, sulasalazine and pyrimethamine were found to be weak inhibitors of PCFT-mediated uptake with K_i values of 42.3 and 161.1 μM, respectively. One could envision that the efficiency of intestinal folate absorption or the efficacy of orally administered PCFT-selective antifolates for cancer therapy would be affected in subjects administered these compounds (Inoue et al., 2008; Nakai et al., 2007; Urquhart et al., 2010). Hence, it is important to gain a better understanding of PCFT substrate affinity and

transport characteristics to create better PCFT substrates and avoid drug interactions during clinical administration.

1.4.4.3 Functionally Important Residues.

Functional analysis of HFM mutations and mutations generated by site-directed mutagenesis have identified residues that are important in PCFT structure and function.

Arg113 was found to be mutated in two unrelated families of Turkish (c.C337A, p.R113S) and Arab (c.C337T, p.R113C) descent by two independent investigators (Lasry et al., 2008; Zhao et al., 2007). The residue Arg113 is found in the highly conserved (Figure 1.4) IL1 motif $D_{109}XXGRR_{114}$ connecting TMD2 and TMD3 in PCFT (Table 1.1; Figure 1.3). When expressed in C5 $MTXR^{0.15}$ CHO cells, R113C PCFT was expressed at the cell surface, but did not transport folic acid or MTX (Lasry et al., 2008). Similarly, when R113S PCFT was expressed in WT HeLa cells, no protein was found at the cell surface and no transport of 5-methylTHF was detected (Zhao et al., 2007). Since the recently crystallized *E coli* GlpT shares several structural and functional characteristics with PCFT and is the closest structural homolog with 13.8% sequence similarity over 424 aligned amino acid residues (from a total of 459), GlpT was used as a template in a homology-based structural model to analyze the structure of the IL1. Homology modeling analysis predicted that the DXXGRR motif forms a β-turn whereas the cationic R113 residue of PCFT is completely buried in a putative hydrophobic cavity, the walls of which are made up of TMD1, TMD3, TMD4, and TMD6. It was suggested that R113 might possibly participate in the binding and/or translocation of negatively charged folate substrates (Lasry et al., 2008). Alanine mutagenesis across this stretch disrupted the β turn and resulted in endoplasmic reticulum retention with loss of transport (Subramanian et al., 2008).

Arg376 is a highly conserved residue (Figure 1.4) that has been found to be mutated in two unrelated families with HFM of Mexican (c.C1126T, p.R376W) (Mahadeo et al., 2010; Zhao et al., 2007) and Chinese (c.G1127A, p.R376Q) descent (Table 1.1; Figure 1.3). When expressed in R1-11 HeLa cells, R376W was expressed in crude membranes and localized to the membrane similar to WT; however, no transport of 5-methylTHF, 5-formylTHF, folic acid, MTX and PMX could be detected (Zhao et al., 2007). When explored more rigorously, it was found that a positive charge is favored at this residue. Interestingly, when this residue was mutated to a polar amino acid, as found in the HFM R376Q mutant, PMX transport activity was preserved at saturating concentrations (influx K_t increased and V_{max} decreased); however, no or very low transport of 5-methylTHF, 5-formylTHF, folic acid and MTX was detected. This mutant was expressed in crude membranes and localized to the membrane at levels 50% of WT. The data suggest that mutation of the R376 residue to glutamine impairs proton binding which, in turn, modulates the folate-binding pocket and depresses the rate of conformational alteration of the carrier, a change that appears to be, in part, substrate dependent (Mahadeo et al., 2010; Mahadeo et al., 2011).

Histidine has been shown to be critical for the function of some of the proton-coupled solute carriers (Fei et al., 1997; Lam-Yuk-Tseung et al., 2003; Metzner et al., 2008). There are ten His residues in PCFT; of these, His84, 247 and 281 are fully conserved across all species (Figure 1.4) and mutation of His281 and His247 to alanines caused loss of MTX transport function at pH 5.5 and pH 7.0. H247A (located in IL3) and H281A (located in TMD7) (Figure 1.3) were expressed to the same extent as WT, except the H247A mutant protein migrated faster by SDS PAGE than WT or H281A. This was not due to protein instability. Independent of changes in V_{max}, H247A had increased affinity for folic acid, 5-formylTHF and 5-methylTHF

compared to WT. The affinities for all the different substrates were very similar, which is in contrast to results for WT PCFT (Unal et al., 2009a). GlpT was used as a template in a homology-based structural model to analyze the role of His247 in PCFT function. The model predicted His247 to be localized in a highly electropositive region at the cytoplasmic opening to the water-filled translocation pathway. Additionally, the model predicted that His247 interacts with Ser172 and limits access of extracellular folate substrates, thus determining the selectivity of PCFT for folate. Ser172 mutated to alanine caused a similar change in influx K_t, as caused by the His247 mutation. Additionally, the mutant exhibited folate-independent proton transport or "slippage". Mutation of His281 to alanine produced a substantially different phenotype, characterized by increased influx K_t and maintenance of a selectivity profile similar to WT PCFT. The magnitude of the increase in folic acid transport as a function of pH was far less; however there was still folate-induced cellular acidification. Therefore, His281 is not needed in proton –coupling but protonation of this residue may result in increased binding of folate substrates (Unal et al., 2009a).

More rigorous evaluation of the HFM mutant, D156Y, revealed that Asp 156 is important for protein stability (Table 1.1; Figure 1.3) (Shin et al., 2010). Loss of stability was observed with a variety of polar, neutral, or positively charged mutants. However, stability and trafficking were preserved with a Gly (relatively polar) or, to a lesser extent, with Ser (polar) substitutions. All the residues that are point mutated in HFM are completely conserved across all the species analyzed, demonstrating their importance for expression and function of PCFT (Figure 1.4). Discovery and characterization of the D156Y mutation in HFM led to rigorous analysis of the other 6 conserved Asp residues in PCFT. Only one, Asp109, is shown to be required for function. No substitution, irrespective of charge or polarity preserved function, even conservative

substitutions. All of the Asp109 mutants were expressed and were detectable at the cell membrane at levels similar to WT, but no MTX transport was detected at high MTX concentrations and when the extracellular proton concentration was increased. This suggested that the loss of activity was not due to an increase in influx K_t, like the R376Q mutation, or that there was a decrease in affinity of a proton-binding site that allosterically alters the conformation of the folate-binding pocket, like the H281A mutation. Additionally, lack of activity at pH 7.4 excludes a role of this residue for proton-coupling. The Asp109 is found in IL1 like the R113S and R113C HFM mutations. When Asp109 was replaced with other amino acids (even glutamate), substrate either does not bind and/or the alternative-access mechanism of transport is impaired (Figure 1.3) (Shin et al., 2010).

Conserved, charged residues located in TMDs are preserved through evolution because they usually contribute by intramolecular interactions to the stabilization of transporter tertiary structure and are therefore important for function of the carrier (Zvelebil et al., 1987). The residue Glu185 when mutated to leucine or alanine resulted in loss of MTX transport at pH 5.5 due to a decrease in the influx V_{max} with no change in influx K_t. The preservation of a negative charge at position 185 is essential, since low pH transport was lost for all E185 substitutions regardless of charge and polarity except for the similarly charged E185D, which maintained a third of WT function. Unexpectedly, transport at pH 7.4 for the E185A mutant was comparable to that of WT. This suggests that Glu185 plays an important role in proton-coupling (Figure 1.3) (Unal et al., 2009b).

1.4.4.4 Oligomerization.

As mentioned previously, PCFT belongs to the Major Facilitator Superfamily of transporters. Since numerous Major Facilitator Superfamily proteins including LacS (Veenhoff

et al., 2001), AE1 (Dahl et al., 2003; Taylor et al., 2001), GLUT1 (Zottola et al., 1995), TetA (Hickman and Levy, 1988; Yin et al., 2000), and RFC (Hou and Matherly, 2009) have been reported to exist as oligomers (e.g., dimers, tetramers, etc.), and given the potential mechanistic and regulatory ramifications of such structures for PCFT, the oligomerization status was evaluated (Hou et al., 2011). The HFM mutation P425R (described in section 1.4.3 and Zhao et al. (2007)) was used in conjunction with an assortment of biochemical and molecular techniques to validate the existence of PCFT homo-oligomers. By protein cross-linking, oligomeric PCFT appeared to predominate over monomeric PCFT. On a non-denaturing blue-native-PAGE, dimeric PCFT was the most predominant species. HA and FLAG/His 10 epitope-tagged PCFT protein monomers co-localized to the plasma membrane. PCFT monomers associate when analyzed using Ni affinity chromatography. FRET was detected between two YPet and ECFP-tagged PCFT monomers. Finally, co-expression of WT PCFT with P425R PCFT monomers led to a dominant-positive transport phenotype. This appeared to involve co-folding and increased surface trafficking of P425R PCFT to the cell surface, as reflected in increased surface levels of mutant PCFT protein by surface biotinylation and Western blotting, and by indirect immunofluorescence and confocal microscopy. Thus, not only does PCFT exist as a homo-oligomer but there is functional cooperation between PCFT monomers in facilitating transport of folate substrates (Hou et al., 2011). Interestingly, the PCFT primary structure includes GXXXG motifs in TMD2 (amino acids 93-97) and TMD4 (amino acids 155-159) (Figure 1.3), analogous to “dimerization motifs” implicated in the oligomerization of other amphipathic proteins, including, ABCG2 and OAT1 (Duan et al., 2011; Polgar et al., 2010). Additionally, a cluster of PCFT nonfunctional mutations have been found in TMD4 (G147R, D156Y and L161R), suggesting that this region may be important in oligomerization (Figure 1.3 and Figure 1.4). A

better understanding of the structural and regulatory determinants of PCFT oligomerization may lead to novel approaches for therapeutically rescuing functionally impaired PCFT mutants in HFM or that may arise as a form of resistance to PCFT-selective novel folate analogs, perhaps with PCFT peptidomimetics or small molecules.

1.5 The Role of Antifolates in Cancer Therapy.

1.5.1 Inhibition of *De Novo* Thymidylate Biosynthesis Pathway.

Antifolates that inhibit DHFR, such as the classic antifolates, AMT and MTX, and the newer generation antifolates, pralatrexate (PDX) and the non-polyglutamable PT523 (Figure 1.1 and 1.2), block the regeneration of unsubstituted THF from DHF. This causes a depletion of THF cofactors and the accumulation of DHF, resulting in cessation of one-carbon-dependent processes (Matherly et al., 1987a; Seither et al., 1989). AMT has a much higher binding affinity for RFC and FPGS than MTX and is therefore transported into the cell and metabolized to polyglutamates much more rapidly (Smith et al., 1996). This increases the activity of AMT clinically, but also increases the toxicity of the compound compared to MTX (Goldin et al., 1955). PDX was discovered through drug development efforts of F.M. Sirotnak and colleagues at Memorial Sloan Kettering Cancer Center and J. DeGraw and coworkers at the Southern Research Institute. They found that 10-deaza-AMT was more potent than MTX (Sirotnak et al., 1984) and that the 10-ethyl derivative of 10-deaza-AMT (edatrexate) had even better efficacy both preclinically and clinically (Beinart et al., 2007; Gralla, 1995; Schmid et al., 1985; Shum et al., 1988; Sirotnak et al., 1993; Vandenberg et al., 1993). Based on the finding of Jones et al. (1981) that the N-10-propargyl analog of 5,8-dideazafolic acid (CB 3717) possessed potent inhibitory activity against TS (discussed in more detail below), 10-propargyl-10-deaza-AMT (PDX) was synthesized and tested to evaluate the effect of the propargyl group on growth

inhibition. It was found that PDX had a 3-fold decreased affinity for DHFR and a 10-fold RFC transport advantage compared to MTX, resulting in 5-fold enhanced anti-proliferative activity (DeGraw et al., 1993; Sirotnak et al., 1998). In September 2009, the FDA approved the use of PDX for the treatment of relapsed, refractory peripheral T-cell lymphoma (Thompson, 2009). Since then, PDX has been evaluated clinically either alone or in combination with other agents in a wide range of malignancies with promising results (Azzoli et al., 2007; Marchi et al., 2010; Toner et al., 2006; Zain and O'Connor, 2010a; Zain and O'Connor, 2010b).

Raltitrexed (RTX; Tomudex) is a potent TS inhibitor and arose from rational drug design efforts of researchers from the Institute for Cancer Research and Astra Zeneca (Figure 1.1 and 1.2) (Calvert et al., 1980). Previous work demonstrated that 5,8-dideazafolic acid was a weak inhibitor of TS; sequential modification of this compound produced N10-propargyl-5,8-dideazafolic acid or CB3717 (Calvert et al., 1986; Jones et al., 1981). In the initial phase I/II clinical trials, this drug had activity against ovarian, liver, and breast cancer but also resulted in troublesome hepatic toxicity and dose-limiting nephrotoxicity, which occurred in 70% of patients at doses greater than 450 mg/m^2)(Jackman and Calvert, 1995). To try and reduce toxicity, efforts were made to make the compound more water soluble at physiological pH; this was achieved by removing the 2-amino group and synthesizing a 2-desamino-2-methyl compound (ICI 198583) (Jackman et al., 1991b). Finally, replacement of the para-aminobenzoate with a thiophene and introduction of a N10-methyl substituent produced ZD1694 or RTX (Jackman et al., 1996; Jackman et al., 1991a; Jackman et al., 1991c). RTX had reduced TS inhibition compared to CB3717 but showed enhanced cellular uptake by RFC and polyglutamylation, leading to more potent tumor growth inhibition both *in vitro* and *in vivo* (Gibson et al., 1993; Jackman et al., 1993; Jackman et al., 1991c). This drug discovery effort exemplifies the power of establishing

structure activity relationships (SAR) through careful cellular, biochemical and pharmacological evaluation to test each chemical modification. RTX was approved for clinical use outside the US for advanced colorectal cancer (Chu et al., 2003).

Antifolates that target TS (Matsui et al., 1996; Yin et al., 1997), and DHFR (Benigni et al., 1983; Lorico et al., 1988) decrease levels of deoxythymidine triphosphate (dTTP), which results in a "thymineless" death. The decreased dTTP levels cause misincorporation of deoxyuridine triphosphate (dUTP) in place of dTTP into newly synthesized DNA. The dUTP is recognized as incorrect and cycles of futile excision-repair ensue, ultimately leading to DNA strand breaks and cell death (Bronder and Moran, 2003).

1.5.2 Inhibition of *De Novo* Purine Biosynthesis Pathway.

Purines serve as building blocks of RNA and DNA; they regulate enzymatic activity as components of vitamins and cofactors, and mediate energy transfer in the cell (King et al., 1983). Most differentiated adult cells can satisfy their purine requirements through purine salvage mechanisms (Howell et al., 1981; Jackson and Harkrader, 1981; King et al., 1983; LeLeiko et al., 1983; Mackinnon and Deller, 1973). Conversely, proliferating cells, such as activated T-cells and tumor cells, require activation of *de novo* purine synthesis in order to meet the greater nucleotide demands for DNA and RNA synthesis (Denkert et al., 2008; Fairbanks et al., 1995; Howell et al., 1981; Jackson and Harkrader, 1981; Kondo et al., 2000). Inhibitors of *de novo* purine biosynthesis inhibit lymphocyte and tumor cell growth, which suggests that purine salvage pathways are insufficient to support nucleotide synthesis (Christopherson et al., 2002; Hovi et al., 1976). Interestingly, even though bone marrow progenitor cells and intestinal crypt cells are highly proliferative they rely principally on purine salvage for their purine demands. This is reflected in the high levels of purine precursors such as hypoxanthine (~7-11 μM, three to four

times higher than plasma levels) in these tissues, which can not only be salvaged but can also directly inhibit *de novo* purine biosynthesis (Howell et al., 1981; King et al., 1983; LeLeiko et al., 1983; Mackinnon and Deller, 1973).

Biosynthetically, adenosine and guanosine nucleotides are derived from inosine monophosphate (IMP), which is synthesized from phosphoribosyl pyrophosphate (PRPP) in both salvage and *de novo* synthesis of purines. PRPP is formed by PRPP synthetase which uses ATP to activate ribose-5-phosphate (made through the pentose phosphate shunt from glucose). In the salvage pathway, PRPP is used by either hypoxanthine phosphoribosyl transferase (HPRT) to convert guanine and hypoxanthine back into GMP and IMP, respectively, or by adenine phosphoribosyl transferase (APRT) to convert adenine back into AMP (Murray, 1971). While the salvage of purines is a one-step conversion, the *de novo* purine synthesis pathway consists of ten reactions catalyzed by 6 enzymes that convert PRPP into IMP, which is subsequently used to synthesize AMP and GMP (Figure 1.5). Synthesis of IMP occurs in the cytosol and requires five moles of ATP, two moles of glutamine, one mole of glycine, one mole of CO_2, one mole of aspartate and two moles of formate per mole of IMP. The enzymatic reaction and intermediates of the *de* novo purine biosynthesis pathway were largely characterized in seminal experiments by Buchanan and colleagues in avian models in the 1950s and 1960s (Hartman and Buchanan, 1959a). They have since been found to be conserved in species ranging from bacteria to humans.

The first reaction is the rate-limiting step and involves the conversion of PRPP into 5-phosphoribosylamine by glutamine phosphoribosylpyrophosphate amidotransferase (GPAT), which entails replacement of the pyrophosphate of PRPP by the amide group of glutamine

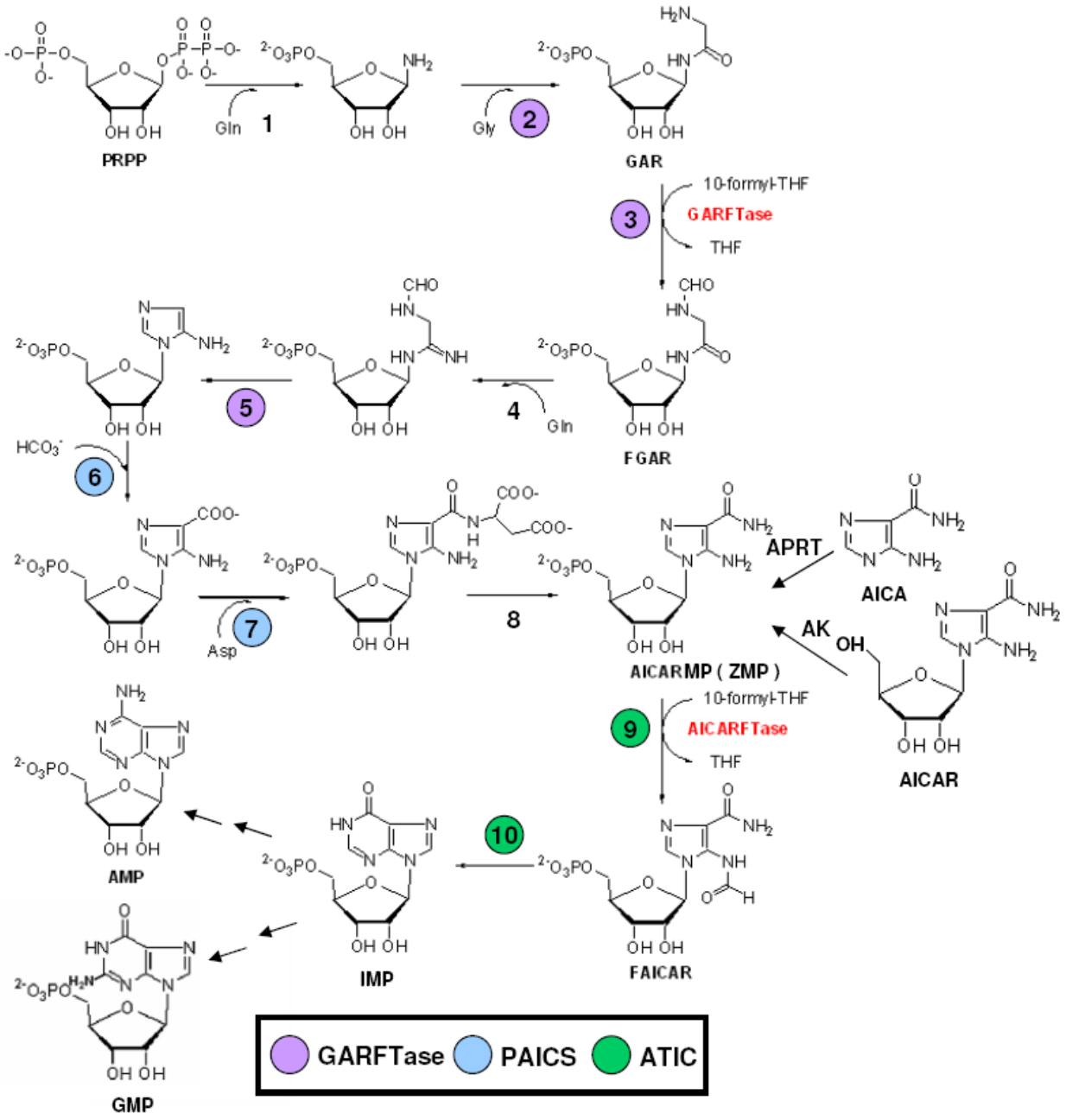

Figure 1.5 ***De novo*** **purine nucleotide biosynthesis pathway.** The *de novo* purine nucleotide biosynthetic pathway from phosphoribosyl pyrophosphate (PRPP) to IMP is shown. The numbered reactions are catalyzed by the following monofunctional enzymes: **1**, glutamine phosphoribosylpyrophosphate amidotransferase (GPAT); **4**, formylglycinamide ribonucleotide synthase (FGAM synthetase); **8**, adenylosuccinate lyase (ASL). Reactions **2**, **3** and **5** are catalyzed by the trifunctional glycinamide ribonucleotide (GAR) formyltransferase (GARFTase) which contains GAR synthase (GARS; reaction **2**), GAR formyltransferase (GARFTase; reaction **3**) and 5-aminoimidazole ribonucleotide synthase (AIRS; reaction **5**) activities. Reactions **6** and **7** are catalyzed by the bifunctional phosphoribosylaminoimidazole carboxylase/ phosphoribosylaminoimidazole succinocarboxamide synthetase (PAICS) enzyme, which

contains carboxyaminoimidazole ribonucleotide synthase (CAIRS; reaction **6**) and 5-aminoimidazole-4-(*N* succinylocarboxamide ribonucleotide synthase (SAICARS; reaction **7**) activities. Reactions **9** and **10** are catalyzed by a bifunctional enzyme, 5-Amino-4-imidazolecarboxamide ribonucleotide formyltransferase/ IMP cyclohydrolase (ATIC) that sequentially catalyzes the last two steps in the pathway for *de novo* synthesis of IMP. ATIC has 5-aminoimidazole-4-carboxamide ribonucleotide (AICAR) formyltransferase (AICARFTase; reaction **9**) and inosine monophosphate cyclohydrolase (IMPCH; reaction **10**) activities. There are two folate-dependent reactions (reaction **3** and **9**) in which 10-formyl tetrahydrofolate serves as the one-carbon donor catalyzed by GARFTase and AICARFTase. 5-aminoimidazole-4-carboxamide (AICA) and AICAR can be metabolized to AICAR monophosphate (ZMP) by either adenine phosphoribosyl transferase (APRT) or adenosine kinase (AK), thus circumventing the reaction catalyzed by GARFTase. For the *in situ* GARFTase assay, incorporation of [^{14}C]glycine into [^{14}C]F-GAR in the presence of azaserine is used as a direct measure of GARFTase activity.

(reaction **1**). Subsequent steps involve three multifunctional enzymes: a trifunctional protein GARFTase, that has GAR synthase (GARS; reaction **2**), GAR formyltransferase (GARFTase; reaction **3**), and 5-aminoimidazole ribonucleotide synthase (AIRS; reaction **5**) activities; a bifunctional enzyme, phosphoribosylaminoimidazole carboxylase/ phosphoribosylaminoimidazole succinocarboxamide synthetase (PAICS), that has carboxyaminoimidazole ribonucleotide synthase (CAIRS; reaction **6**) and 5-aminoimidazole-4-(*N* succinylocarboxamide ribonucleotide synthase (SAICARS; reaction **7**) activities; and a bifunctional enzyme, 5-Amino-4-imidazolecarboxamide ribonucleotide formyltransferase/ IMP cyclohydrolase (ATIC), that has 5-aminoimidazole-4-carboxamide ribonucleotide formyltransferase (AICARFTase; reaction **9**) and IMP cyclohydrolase (IMPCH; reaction **10**) activities. The remaining steps are catalyzed by monofunctional enzymes, formylglycinamide ribonucleotide synthase (FGAM synthetase; reaction **4**) and adenylosuccinate lyase (ASL; reaction **8**). The formate that is used by GARFTase and AICARFTase to supply the number 2 and number 8 carbons of the purine ring is carried by THF in the form of 10-formylTHF (Hartman and Buchanan, 1959a; Hartman and Buchanan, 1959b).

In a continued effort to find other inhibitors of folate metabolism at sites other than DHFR, a “critical bond blocking” strategy was employed by a joint collaboration between E.C. Taylor at Princeton and a team of chemists at Eli Lilly led by Chuan (Joe) Shih. This effort resulted in the synthesis of the 6R diastereomer of 5,10-dideazatetrahydrofolate (DDATHF) or LMX (Figure 1.1), which is structurally identical to natural THF except the nitrogen atoms at positions 5 and 10 that participate in all of the one-carbon transfers are replaced by carbons (Moran et al., 1989; Taylor et al., 1985). LMX is transported into the cell by RFC (Westerhof et al., 1995), polyglutamylated by FPGS (Baldwin et al., 1991) and inhibits GARFTase leading to

ATP and GTP depletion (Figure 1.2) (Beardsley et al., 1989). Phase I clinical investigation of LMX found that without folic acid co-administration, LMX caused severe cumulative toxicity, with myelosuppression (anemia, thrombocytopenia and neutropenia) and mucositis being dose limiting (Ray et al., 1993). With folic acid co-administration, there was a reduction in the clinical toxicity, permitting a dose of greater than 10 times that in the absence of supplementation (Roberts et al., 2000a). It was thought that the delayed and cumulative toxicity may result from gradual release of LMX metabolites from the liver resulting in an extended γ-phase plasma half life (Taber et al., 1991). One hypothesis was that folate depletion increased the expression of FR and this was contributing to greater cellular uptake in the liver and hence greater toxicity of LMX (Mendelsohn et al., 1996; Pohland et al., 1994). Another hypothesis was that thrombocytopenia occurred because platelets have the highest requirement for ATP than any other cell of the body. It is delayed because of the long maturation time of megakaryocytes (which is probably further extended under conditions of purine shortage), and it may be irreversible because the polyglutamate forms of LMX turn over very slowly such that, once formed, they are effectively impossible to eliminate (Jackman, 1999). In an effort to reduce toxicity, second generation inhibitors were synthesized. LY309887 was designed to have lower FRβ affinity (Wang et al., 1992), reduced polyglutamylation (Mendelsohn et al., 1996) and a 9-fold increased affinity for GARFTase compared to LMX (Budman et al., 2001; Mendelsohn et al., 1999). Additionally, structure-based drug-design was used to design AG2034, which was based on the X-ray crystal structures of the *E. coli* GARFTase and of the GARFTase domain of the human enzyme. Like LY309887, preclinical enzyme inhibition studies showed that AG2034 was a potent inhibitor of GARFTase (Almassy et al., 1992; Boritzki et al., 1996). However, clinical evaluation of both these compounds demonstrated the same delayed, cumulative toxicity

as observed with LMX (Bissett et al., 2001; Boritzki et al., 1996; Budman et al., 2001; Kisliuk, 2003; Roberts et al., 2000b). Continued toxicity of these compounds, even with altered FR affinity, suggests that FR-mediated uptake in the liver is not a major determinant of toxicity and implies another transport-mediated process in the liver, most likely RFC (given the neutral pH microenvironment), that may be the true source of toxicity. Thus, GARFTase inhibitors with PCFT selectivity may have the potential of improving the efficacy and reducing the toxicity of antipurine antifolates in the clinic (Goldman et al., 2010).

GARFTase inhibitors block *de novo* purine synthesis, leading to a rapid decline in ATP and GTP pools (Beardsley et al., 1989; Boritzki et al., 1996; Chen et al., 1998; Pizzorno et al., 1991). Unlike TS and DHFR inhibitors, reduction of purine pools does not necessarily induce DNA strand breaks. There are two principle hypotheses as to how GARFTase inhibitors impact p53, cell cycle and cell death. The first proposed by Zhang et al. (1998a) states that reduction of ribonucleotide pools is sensed by p53, which then stabilizes and accumulates causing arrest at the G1 checkpoint and induction of cytostasis (Linke et al., 1996; Zhang et al., 1998a). Tumor cells lacking functional p53 or that have other defects in the G1 checkpoint are more sensitive to GARFTase inhibitors. Since 50% of human cancers lack a functional G1 checkpoint, GARFTase drugs may be selectively active towards these tumors while protecting normal cells with functional p53. Moran and colleagues demonstrated that the cytotoxic effects of agents that target *de novo* purine nucleotide biosynthesis are not dependent on p53 status since ribonucleotide depletion prevents full activation of p53. Due to low ATP and GTP pools, kinases cannot phosphorylate p53 leading to hypophosphorylated and hypoacetylated forms of p53. In these forms, p53 is capable of nuclear retention and binding to the p21 promoter, but remains in an inactive pre-initiation complex because of insufficient recruitment of chromatin-remodeling

complexes which prevent chromatin accessibility and transcriptional activation of the p21 gene. Lack of p21 induction prevents G1 arrest and allows for S-phase entrance of tumor cells; DNA replication in the face of low purine levels results in cytotoxicity to the cell regardless of p53 status (Bronder and Moran, 2002; Bronder and Moran, 2003). If these findings are accurate, characteristic growth inhibition by antipurine antifolates is not dependent on p53 status, thus increasing the potential of this drug to treat many different malignancies.

Another consideration involves the purine salvage pathway. In bone marrow mononuclear cells, physiologic levels of hypoxanthine inhibited *de novo* purine biosynthesis and the salvage pathway was preferentially used to synthesize purines (King et al., 1983). These findings may explain the low rates of *de novo* purine synthesis in bone marrow tissues and suggests that inhibitors of *de novo* purine synthesis will not be marrow toxic. Additionally, methylthioadenosine phosphorylase (MTAP) is an enzyme that releases adenine and methionine from methylthioadenosine formed during polyamine biosynthesis (Illei et al., 2003). Whereas MTAP has been reported to be abundantly expressed in normal tissues, in many solid tumors the MTAP gene is co-deleted with CDKN2A (encodes p16INK4A) (Illei et al., 2003). Thus, many solid tumors are deficient in purine salvage and functional purine salvage in normal tissues would theoretically protect cells from cell death caused by GARFTase inhibition, increasing tumor cell selectivity for GARFTase inhibitors (Bertino et al., 2011; Hori et al., 1996).

Recently, it was found that upon purine depletion, the human *de novo* purine biosynthetic enzymes colocalize in the cytoplasm to form a multienzyme complex called the “purinosome” (An et al., 2008). Purinosome formation is associated with an increased rate of purine biosynthesis. The formation of functional multienzyme complexes may produce efficient substrate channels that link the 10 catalytic active sites. Purinosomes are dynamically regulated

by inhibition of casein kinase 2 (CK2) (An et al., 2010b) and are spatially controlled by the matrix of microtubule filaments (An et al., 2010a). It will be important to determine the effect of *de novo* purine synthesis inhibitors on the formation and function of the purinosome. Interestingly, the trifunctional MTHFD1 which synthesizes 10-formylTHF through the ATP-dependent condensation of formate and THF is not associated with the purinosome (An et al., 2008; An et al., 2010b). Recently, methenylTHF synthase (MTHFS), which catalyzes the irreversible and ATP-dependent conversion of 5-formylTHF to 5,10-methenylTHF was found to enhance purine biosynthesis by delivering 10-formylTHF to the purinosome in a cell cycle and SUMO-dependent fashion (Field et al., 2011). Furthermore, MTHFS expression has been found to be elevated in some tumors, which enhances *de novo* purine biosynthesis and confers partial resistance to antifolate purine synthesis inhibitors (Field et al., 2009; Field et al., 2006). Thus, MTHFS may be a modifier of GARFTase inhibitor efficacy and determining MTHFS expression in malignancies may be an important predictor of antipurine antifolate drug activity. Because of its importance of MTHFS in *de novo* purine biosynthesis, inhibitors have been designed for potential use in cancer therapy (Wu et al., 2009).

1.5.3 Mulitargeted Antifolate.

In order to meet FDA requirements of purity, efforts were made to eliminate the synthesis of both R and S diastereomers of DDATHF by eliminating the chirality at the 6-position of LMX. One strategy replaced the 5-deazapteridine ring of LMX with a pyrrolo[2,3-*d*]pyrimidine ring, resulting in LY231514 (PMX; Alimta) (Figure 1.1) (Taylor, 1993; Taylor et al., 1992). This structural alteration converted the sp3 center at C6 to sp2 geometry. Cell culture end-product reversal and enzymology experiments indicated that this compound potently inhibited TS and had weak inhibition of DHFR, GARFTase and AICARFTase (Figure 1.2) (Shih et al., 1997;

Taylor et al., 1992). PMX is rapidly transported across the cell membrane by both RFC and PCFT (Wang et al., 2004; Westerhof et al., 1995; Zhao et al., 2008), is highly polyglutamylated (best known substrate of FPGS) (Shih et al., 1997; Taylor et al., 1992) and is very sensitive to the cellular folate status (Taylor et al., 1992; Zhao et al., 2001b). The basis for this latter finding involves the inhibitory effects of physiological folates in cells on the polyglutamylation of antifolates at the level of FPGS (Andreassi and Moran, 2002) and at the level of drug binding their target enzymes. Recently, it was discovered by Moran and colleagues that AICARFTase inhibition by PMX causes a marked accumulation of the purine synthesis intermediate 5-amino-4-imidazolecarboxamide ribotide (ZMP) (Racanelli et al., 2009). ZMP is an AMP mimetic that is an activator of AMP-activated protein kinase (AMPK). Activation of AMPK causes phosphorylation of AMPK target proteins involved in initiation of cap-dependent translation, lipid synthesis and energy metabolism. Two such proteins are the tuberous sclerosis complex 2 (TSC2) and raptor (component of mTORC1 complex). AMPK phosphorylation in response to PMX exposure and ZMP accumulation leads to inhibition of mTOR signaling in colon and lung cancer cells (Racanelli et al., 2009; Rothbart et al., 2010). PMX was found to act synergistically with sorafenib (a multi-kinase inhibitor) to enhance tumor killing via the promotion of a toxic form of autophagy that leads to activation of the intrinsic apoptosis pathway (Bareford et al., 2011). As mentioned in the introduction, PMX in combination with cisplatin has been approved for the treatment of malignant pleural mesothelioma (Hazarika et al., 2004) and NSCLC (Cohen et al., 2009). Other phase II clinical trials have been recently completed or are underway to test the efficacy of this compound in a wide range of malignancies (Adjei et al., 2010; Karapanagiotou et al., 2009; Katirtzoglou et al., 2010; Krug et al., 2009; Martin et al., 2009; Matulonis et al., 2008; Patel et al., 2009a; Patel et al., 2009b; Paz-Ares et al., 2010; Pippen et al.,

2010; Simon et al., 2008). It will be interesting to determine why PMX has significant activity against lung carcinomas, which is unusual for an antifolate.

1.5.4 Polyglutamylation of Antifolates.

The above-mentioned antifolates with the exception of PT523 are substrates for polyglutamylation by FPGS. Polyglutamation of antifolates leads to augmentation of pharmacological activity through their sustained inhibition of THF-dependent enzymes, reflecting increased affinities for target enzymes, and abilities to inhibit enzymes that are poorly inhibited by monoglutamate antifolate forms (Goldman and Zhao, 2002; Hughes et al., 1999; Mendelsohn, 1999). For example, the crystal structure of GARFTase shows that the surface of the protein near the folate binding loop is either neutral or positively charged and, therefore, would provide a suitable surface for interaction with a polyglutamate tail. This may explain the increased affinity of polyglutamylated drugs such as LMX for GARFTase (Dahms et al., 2005; Zhang et al., 2002). Similar explanations have been provided for other antifolates and intracellular targets such as TS (Allegra et al., 1985). However, inhibition of DHFR by MTX is not in itself enhanced by polyglutamylation (Goldman and Matherly, 1985; Matherly et al., 1987b). Another important consequence of polyglutamylation involves sustained inhibition of intracellular targets since long chain polyglutamates of antifolates are poor substrates for influx or efflux transporters. Therefore, antifolates are retained by cells at high concentrations even after extracellular drug levels have been reduced due to clearance (Goldman and Matherly, 1985; Matherly et al., 1987b). It is interesting to note that polyglutamylation is important for selectivity of antifolates for tumor cells. Polyglutamates of MTX have been reported to accumulate more in tumor cells than in the bone marrow or intestinal cells, such that the metabolic effects of antifolates in normal cells tend to be relatively transient (Fry et al., 1983;

Koizumi et al., 1985). Yet, the effect on normal tissues such as myelosuppression and mucositis is still the dose-limiting factor in antifolate treatment.

1.5.5 Transport as a Determinant of Selectivity and Resistance.

Transport of antifolates by RFC, PCFT and FR is a very important determinant of drug activity and tumor selectivity. Since RFC is ubiquitously expressed and functional at the neutral pH surrounding most normal tissues, transport of antifolates by RFC into proliferating normal tissues is thought to be the cause of many drug-induced toxicities. The specificities of antifolates differ for the various folate uptake mechanisms. RFC can transport all the classic antifolates including MTX, AMT, PDX, RTX, LMX, and PMX with high affinities (Figure 1.2) (Matherly et al., 2007). MTX can be transported by PCFT, albeit to a lower extent than RFC (Zhao et al., 2008). PMX has a higher affinity for PCFT than RFC at low pH and is the best known substrate for PCFT yet described (Zhao and Goldman, 2007). PT523 is not a transport substrate for PCFT (Figure 1.2) (Zhao and Goldman, 2007). As mentioned in this section, it has been observed that the same or better growth inhibition could be obtained from an analog that had reduced affinity for its enzyme target but had greater substrate affinity and therefore uptake by RFC. Examples include PDX compared with AMT, and RTX compared with CB3717. This highlights the importance of concentrative antifolate uptake to provide sufficient (unbound) intracellular drug to sustain maximal inhibition of enzyme targets and for the synthesis of polyglutamates. The significance of transport-mediated uptake can also be demonstrated in cases of antifolate resistance where loss of RFC expression causes cells to become resistant to antifolates that depend on RFC for cellular uptake (Assaraf, 2007; Matherly et al., 2007; Zhao and Goldman, 2003).

Impaired RFC function is an important mechanism of resistance to MTX (Hill et al., 1979; Niethammer and Jackson, 1975; Sirotnak et al., 1968; Sirotnak et al., 1981) and other antifolates *in vitro*, and it may be associated with clinical resistance to this agent in the treatment of ALL (Belkov et al., 1999; Gorlick et al., 1997; Levy et al., 2003; Zhang et al., 1998b), osteosarcoma (Guo et al., 1999; Ifergan et al., 2003; Yang et al., 2003) and colorectal cancer (Wettergren et al., 2005), as well as primary central nervous system lymphoma (Ferreri et al., 2004). Impaired transport of antifolates into tumor cells in preclinical and clinical studies has been associated with quantitative and/or qualitative alterations in RFC expression and/or transport activity (Assaraf, 2007; Matherly et al., 2007; Zhao and Goldman, 2003). RFC function can be lost by methylation of a CpG island in the promoter between exons B and A (Worm et al., 2001), genomic deletion (Chattopadhyay et al., 2006; Ding et al., 2001; Zhao et al., 2004c), single point mutations within the open reading frame, mutation of the ATG start codon, insertions and frameshifts, truncated proteins, deletions, mutations resulting in RFC instability, and loss of RFC alleles due to translocations (Assaraf, 2007; Ding et al., 2001; Matherly et al., 2007; Rothem et al., 2002; Wong et al., 1999; Zhao and Goldman, 2003; Zhao et al., 1999). Treatment of a L1210 murine leukemia cell line with mutagen (ethylmethanesulfonate) followed by selection with MTX using 5-CHO-THF in the growth medium produced a spectrum of RFC mutations (Assaraf, 2007; Zhao and Goldman, 2003; Zhao et al., 1999). Two RFC point mutations (V104M and S46N) that led to MTX resistance but preserved PMX and LMX growth inhibition were identified. The first mutation, V104M in the third TMD of RFC had markedly impaired transport of MTX and 5-CHO-THF. Despite the fact that the cellular THF-cofactor pool was substantially decreased, growth was sustained, consistent with the low levels of folate required for normal growth (Zhao et al., 2000b). Cells with this mutation had collateral

sensitivity to LMX due to partial maintenance of LMX transport and contraction of the folate pools. A second mutation, S46N did not alter the influx K_t for MTX and the natural folates (Zhao et al., 1998). Rather, it produced a marked (40-fold) decrease in the V_{max} for MTX but a lesser (~7–8-fold) decrease in the V_{max} for 5-CHO-THF. Sensitivity to PMX was partially preserved even though the THF-cofactor pools were similar to cells with wild-type RFC (Zhao et al., 2000a). The S46N mutation has also been identified in osteosarcoma patient samples from patients treated with MTX (Yang et al., 2003) and is therefore a clinically relevant mutation. Clinically, complete loss or functional alterations in RFC are rare since tumor cells need RFC-mediated transport of reduced folates to maintain tumor growth; therefore most clinically occurring point mutations are similar to S46NN which have marked loss of carrier affinity and/or mobility towards MTX, while preserving THF cofactor transport. Similarly, reductions in RFC expression are observed; for example approximately 65% of osteosarcoma samples have decreased RFC expression at biopsy and 50% have reduced RFC expression in recurrent or metastatic disease (Guo et al., 1999). It has been shown that reduced RFC expression can be caused by CpG island promoter hypermethylation and transcriptional silencing due to loss of function of transcription factors that regulate the expression of RFC (Worm et al., 2001).

In addition to impaired transport, antifolate resistance can arise from reduced polyglutamylation (Drake et al., 1996; Li et al., 1992; Liani et al., 2003; Mauritz et al., 2002; McCloskey et al., 1991; McGuire and Russell, 1998; Pizzorno et al., 1989; Pizzorno et al., 1988; Pizzorno et al., 1995; Zhao et al., 2000c), decreased affinity of the drug for its folate dependent intracellular target due to mutation (Albrecht et al., 1972; Flintoff and Essani, 1980; Goldie et al., 1980; Haber et al., 1981; Jackson et al., 1976; McIvor and Simonsen, 1990; Melera et al., 1984; Melera et al., 1988; Miyachi et al., 1995; Srimatkandada et al., 1989), increased expression of the

enzyme target so that more drug is needed for the same level of inhibition (eg. DHFR (Alt et al., 1978; Dolnick et al., 1979; Horns et al., 1984; Jackson and Harrap, 1973; Mini et al., 1985; Nunberg et al., 1978; Trent et al., 1984; White and Goldman, 1981) and TS (Drake et al., 1996; Freemantle et al., 1995; Jackman et al., 1995; Kitchens et al., 1999; O'Connor et al., 1992; Sigmond et al., 2003; Tong et al., 1998; Wang et al., 2001a)) and increased expression and function of high capacity efflux pumps, such as MRPs that remove the antifolate from cells (Assaraf, 2006). Many of the antifolates that came after AMT and MTX were designed in an effort to reduce toxicity observed clinically, increase tumor selectivity and to circumvent some of the antifolate resistance mechanisms. This dissertation will highlight drug discovery efforts to find novel antifolates that are selective for PCFT-mediated uptake and that inhibit GARFTase and *de novo* purine nucleotide synthesis as a way to avoid selectivity and resistance problems. These compounds will also be tested in cells that are MTX resistant due to RFC loss to determine the impact of RFC function on antifolates that depend on PCFT for uptake.

1.6 Hijacking the Acidic Tumor Microenvironment for Solid Tumor Targeting.

To maintain their rapid growth and proliferation, cancer cells have a higher need for energy and for biosynthesis of nucleotides than normal differentiated cells. This increased biosynthetic demand can be, in part, met by an altered metabolic program known as the Warburg effect or aerobic glycolysis in which cancer cells become highly glycolytic even in the presence of normal oxygen tension (Lunt and Vander Heiden, 2011). To avoid intracellular acidification, glycolytically-produced acid must be extruded from cells. This is achieved by increased expression and/or function of plasma membrane ion pumps and transporters such as H^+-ATPases or vacuolar ATPases (Hinton et al., 2009; Martinez-Zaguilan et al., 1993; Sennoune et al., 2004), the Na^+/H^+ exchanger (NHE1) of the SLA9A family (Chiang et al., 2008; Kumar et al., 2009;

McLean et al., 2000; Miraglia et al., 2005), the monocarboxylate-H^+ efflux symporter (MCT1 and MCT4) of the SLC9A family (Chiche et al., 2012; Kennedy and Dewhirst, 2010; Pinheiro et al., 2008a; Pinheiro et al., 2008b; Pinheiro et al., 2010), and the carbonic anhydrases CAIX and CAXII (Chiche et al., 2009; Ilie et al., 2011; Loncaster et al., 2001; Swietach et al., 2009; Wykoff et al., 2000), the Cl^-/HCO3$^-$ exchanger (CBE) (Alper, 2009) and Na^+/HCO_3^- cotransporter (NBC) (Boron et al., 2009). The increased activities of these transporters cause reversal of the normal intra-extracellular pH gradients, so that cancer cells produce significant acidification of the extracellular environment (acidic tumor microenvironment). Extracellular pH in tumor cells can be as low as ~6.7-7.1, while they maintain a normal or slightly alkaline intracellular pH of ≥7.4. This is in comparison to normal differentiated adult cells which maintain an intracellular pH of ~7.2 and an extracellular pH of ~7.4 (Busco et al., 2010; Gallagher et al., 2008; Gillies et al., 2002; Stuwe et al., 2007; Webb et al., 2011). Acidification of the tumor environment is exacerbated by limited removal of glycolytic waste products due to poor perfusion, which is affected by tumor size and abnormal vascularization (Webb et al., 2011). The resultant H^+- electrochemical gradient favors passive weak acid uptake by pH partition and, importantly, acts as a driving force for H^+-coupled solute transport at the cancer cell plasma membrane. Additionally, the decrease in extracellular pH increases the affinity and broadens substrate specificity of pH-dependent transporters (Leuthold et al., 2009; Nozawa et al., 2004; Qiu et al., 2006; Rubio-Aliaga et al., 2003).

The targeted drug strategy that uses selective uptake of therapeutics into the tumor cell by H^+-coupled transporters is novel but not unprecedented (Anderson and Thwaites, 2010). Aberrant H^+-coupled di/tripeptide (PepT1 and PepT2) transport has been characterized in tumor cells and overexpression may be useful for targeting a number of experimental and clinical

anticancer substrates to tumor cells, including the photodynamic therapy and imaging agent 5-aminolevulinic acid (Anderson et al., 2010) and the aminopeptidase inhibitor bestatin (Nakanishi et al., 2000). Prodrugs of floxuridine and cytarabine may also be transported by PepT1 (Sun et al., 2009). Additionally, the H^+-coupled amino acid transporter PAT1 and the pH dependent OATPs could also be used for mediating uptake of anti-cancer drugs. PAT1 can also transport 5-aminolevulinic acid (Anderson et al., 2010) and L-cycloserine (Anderson et al., 2004). Prominent low-pH transport activities have been observed for several organic anion transporting polypeptides (OATPs) (Leuthold et al., 2009); of these, only OATP1A2 is known to have MTX transport activity at low pH (Badagnani et al., 2006). Recently, OATP2B1 has been established as a low-affinity, but highly selective, low pH antifolate transporter demonstrating the critical role that pH, substrate, and substrate concentration can play in identifying the spectrum of activities of a transporter (Visentin et al., 2012).

This dissertation will focus on PCFT-mediated uptake of novel antifolates into the tumor cell by harnessing the proton gradient that exists in the tumor microenvironment as a therapeutic strategy.

CHAPTER 2

THE HUMAN PROTON-COUPLED FOLATE TRANSPORTER IS EXPRESSED AND FUNCTIONAL IN HUMAN SOLID TUMORS

2.1 Introduction.

The anionic nature of folates and antifolates precludes their diffusion across biological membranes. Therefore, three genetically distinct and functionally diverse transport systems are in place to facilitate uptake of these molecules into the cells of peripheral tissues. Two facilitative transporters, RFC and the newly discovered PCFT and two FR isoforms (α and β) mediate this uptake.

RFC is ubiquitously expressed in both normal and tumor tissues, with characteristic patterns of localization in intestine, hepatocytes, renal epithelial cells and choroid plexus, which suggest specialized roles in these tissues for folate homeostasis (Matherly and Goldman, 2003; Matherly et al., 2007; Zhao et al., 2009a). Indeed, given its widespread tissue expression, RFC is considered the major transport system for folates in mammalian cells and tissues.

FRα is predominantly expressed on the apical (luminal) surface of polarized epithelial cells where it is not in contact with circulating folate (Chancy et al., 2000). FRα is expressed in epithelial cells of the kidney, choroid plexus, retina, uterus, and placenta (Elnakat and Ratnam, 2004). Malignant tissue expression includes malignant pleural mesothelioma (Bueno et al., 2001) and adenocarcinomas of the cervix, uterus, and ovary (Elnakat and Ratnam, 2004). Importantly, FRα is overexpressed in up to 90% of ovarian cancers (Toffoli et al., 1997; Wu et al., 1999). Close associations were reported between FRα expression levels with grade and differentiation status of ovarian tumors (Buist et al., 1995; Garin-Chesa et al., 1993; Veggian et al., 1989; Wu et al., 1999). FRβ is expressed in the thymus, spleen, placenta, and CD34+ human hematopoietic cells and is needed for normal myelopoiesis (Pan et al., 2002; Reddy et al., 1999).

Both acute and chronic myelogenous leukemias express FRβ (Kamen and Smith, 2004; Salazar and Ratnam, 2007).

Human PCFT transcripts were reported to be highly expressed along the proximal jejunum, duodenum, kidney, liver, placenta, spleen and choroid plexus and, to a lesser extent, in the brain, testis and lung (Inoue et al., 2008; Qiu et al., 2006). Mouse PCFT transcripts were highly expressed in the duodenum, proximal jejunum, kidney, liver and to a lesser extent in the brain, skin, lung, stomach, and testis. Mouse PCFT protein was found on the apical brush-border membrane of the proximal jejunum and duodenum (Qiu et al., 2007). Direct evidence that this transporter is responsible for low-pH transport and intestinal folate absorption came from the discovery that homozygous mutations in the coding region of the PCFT gene leads to the rare autosomal recessive disorder HFM (Atabay et al., 2010; Borzutzky et al., 2009; Geller et al., 2002; Lasry et al., 2008; Mahadeo et al., 2010; Mahadeo et al., 2011; Meyer et al., 2010; Min et al., 2008; Qiu et al., 2006; Shin et al., 2011; Shin et al., 2010; Zhao et al., 2007). Loss of PCFT function leads to impaired intestinal folate absorption, resulting in severe folate deficiency, and impaired transport of folates across the choroid plexus into the central nervous system. Importantly this establishes the critical physiological functions of PCFT folate transport (Zhao et al., 2009a).

The discovery of PCFT may provide a novel transport route for antifolates into tumor cells. The ability of PCFT to utilize a proton gradient across the cell membrane to transport antifolates intracellularly may provide a new mechanism for tumor targeting, based on the acidic tumor microenvironments of solid tumors. To determine whether this approach is plausible, the therapeutic potential of PCFT as a means of selectively delivering antifolates into the tumor cell must be established. The expression of PCFT and how it compares to RFC and FR expression in

human malignancies is largely unestablished. In solid tumor cells, previous results have shown that MTX influx at pH 5.5 was equal to, or greater than, influx at pH 7.4 in 29 of 32 cell lines, including cell lines from the NCI60 cell line panel (Zhao et al., 2004b). However, it has yet to be established what the levels of PCFT are in these and other clinically relevant solid tumor cell lines. Further patterns of PCFT expression in tumor specimens have not been previously established. This chapter will focus on determining the level of PCFT expression in a wide range of solid tumor and leukemia cell lines. The expression of PCFT will be compared in tumor and normal tissues at the RNA, protein, and functional levels. Patterns of PCFT expression in both normal and tumor tissue will be compared to those for RFC and FR.

The findings presented in this chapter indeed establish that PCFT is expressed and functional in solid tumors and has restricted expression in normal tissues. Thus, PCFT could be used in conjunction with the acidic tumor microenvironment to efficiently deliver cytotoxic antifolates into the tumor cell.

2.2 Materials and Methods.

2.2.1 Chemicals and Reagents.

[3',5',7-^{3}H]MTX (20 Ci/mmol) was purchased from Moravek Biochemicals (Brea, CA). Both labeled and unlabeled MTX were purified by HPLC prior to use (Fry et al., 1982). Other chemicals were obtained from commercial sources in the highest available purities.

2.2.2 Cell Culture.

The sources and cell culture conditions for the panel of human solid tumor and leukemia cell lines used for real-time RT-PCR assays of transcript levels for RFC and PCFT are summarized in Table 2.1. HeLa R1-11-RFC6 and R1-11-PCFT4 cells were derived from RFC- and PCFT-null R1-11 cells by stable transfection with HA-tagged pZeoSV2(+)-RFC and

pZeoSV2(+)-PCFT constructs, respectively (Zhao et al., 2008), and were gifts of Dr. I. David Goldman (Albert Einstein School of Medicine, Bronx, NY).

2.2.3 Real-time RT-PCR Analysis of RFC and PCFT Transcripts.

2.2.3.1 Origene cDNA Arrays of Tumor and Normal Tissue.

To expand the transporter expression profiles in normal and malignant human tissues we measured the levels of PCFT and RFC transcripts in a wide range of human normal and tumor tissues. We used arrays of normalized cDNAs from either 48 pathologist-verified normal tissues (e.g., adrenal, small intestine, liver, lung, ovary, etc.; "Human Major Tissue qPCR Array", Origene HMRT102) or 96 normalized cDNAs from pathologist-verified solid tumors and paired normal tissues ("TissueScan Oncology qPCR Array", Origene CSRT101). Real-time RT-PCR was performed in a 384 well plate format on a Roche LightCycler 480 using Universal Probes (Roche, Indianapolis, IN) and gene-specific primers. Details are included in Table 2.1. Transcript levels for PCFT and RFC genes were normalized to those for glyceraldehyde-3-phosphate dehydrogenase (GAPDH) and transcripts were quantified using the delta Ct method.

2.2.3.2 Solid tumor and Leukemia Cell Lines.

RNAs were isolated from a large variety of human cell lines including solid tumors (n=57) and leukemias (n=27) (Table 2.2) using TRIzol reagent (Invitrogen). cDNAs were synthesized using the Superscript reverse transcriptase III kit (Invitrogen) and purified with the QIAquick PCR Purification Kit (Qiagen). PCFT, RFC and FRα transcript levels were measured by real-time RT-PCR, which was performed using Universal Probes (Roche, Indianapolis, IN) and gene-specific primers. Details are included in Table 2.1. Transcripts were normalized to GAPDH and quantified by constructing external standard curves for each gene of interest. Standard curves were made by using serial dilutions of linearized templates, prepared by

Table 2.1 Universal Probes and SYBR Green RT-PCR Primer Sequences of Human Genes.

	Gene	Primer Sequences	Probe	Size (bp)	Annealing (˚C)	GenBank Accession
Universal Probes	PCFT	Upper: 5'-CTCATCCCGGCTGTTCTG-3' Lower: 5'-CTGGAACTCGAGGTGAGGAT-3'	89	60	60	NM_080669
	RFC	Upper: 5'-CAGTTCCTCGTGCCCATC -3' Lower: 5'-GGCAAAGAACGTGTTGACC -3'	37	93	60	U19720
	GAPDH	Upper: 5'-CTCTGCTCCTCCTGTTCGAC-3' Lower: 5'-GCCCAATACGACCAAATCC-3'	Catalog # 05190541001	119	60	----
SYBR Green	PCFT	Upper: 5' -CCTCCGGCATCTTCAACTCACTCTA -3' Lower: 5'-CTCTGGGGAAACTGCTGGAACTC -3'		157	60	NM_080669
	RFC	Upper: 5' -GTGGAGAAGCAGGTGCCCGTGGAA -3' Lower: 5'-GGCAAAGAACGTGTTGACC -3'		174	64	U19720
	FRα	Upper: 5' -GACTGTGAGCAATGGTGGGAAGAT -3' Lower: 5'-TGTGGGGAAGTAGAGATGGAAAGGT -3'		141	60	AK223527
	GAPDH	Upper: 5' –AACGGGAAGCTTGTCATCAATGGAAA -3' Lower: 5' -CGTGACCTGCTCCCGCGTGAAGTT-3'		194	60	NM_002046

Table 2.2 Leukemia and solid tumor cell lines used for real-time PCR.			
CELL LINE	**DISEASE**	**ORIGIN**	**SOURCE**
U937	AML	Macrophage?	ATCC
CTS	AML M1	Peripheral blood	Fuse, A.
Kasumi-1	AML M2	Peripheral blood	ATCC
HL60	AML M2	Peripheral blood	ATCC
MV4-11	AML M5	Peripheral blood	ATCC
THP-1	AML M5	Peripheral blood	ATCC
AML-193	AML M5	Peripheral blood	ATCC
KG-1	AML M6	Bone marrow	ATCC
KG-1a	AML M6	Bone marrow	ATCC
K562[1]	CML	Bone marrow	ATCC
CMS	AML M7	Peripheral blood	Fuse, A.
MEG-01	CML	Bone marrow	ATCC
CMK	DS AML M7	Peripheral blood	DSMZ
CMY	DS AML M7	Bone marrow	Fuse, A.
697	BP-ALL	Bone marrow	DSMZ
Nalm6	BP-ALL	Peripheral blood	DSMZ
Uoc B4	BP-ALL	CSF	Findley, H.
REH	BP-ALL	Unknown	ATCC
CCRF-CEM[1,2]	T-cell ALL	Peripheral blood	ATCC
MOLT4[1]	T-cell ALL	Peripheral blood	DSMZ
MOLT3	T-cell ALL	Peripheral blood	DSMZ
HPB-ALL	T-cell ALL	Peripheral blood	DSMZ
TALL-1	T-cell ALL	Bone marrow	DSMZ
DND 41	T-cell ALL	Peripheral blood	DSMZ
ALL-SIL	T-cell ALL	Peripheral blood	DSMZ
Jurkat	T-cell ALL	Peripheral blood	ATCC
TE-85	Osteosarcoma	Bone	Peterson, W.D.
HTB166	Ewing's sarcoma	Bone	ATCC
MCF-7[1,2]	Adenocarcinoma	Breast	ATCC
MDA-MB231[1,2]	Adenocarcinoma	Breast	ATCC
MDA-MB435[1,2]	Adenocarcinoma/Melanoma	Breast/Skin?	ATCC
T-47D[1]	Ductal carcinoma	Breast	ATCC
KB	Adenocarcinoma	Cervix	ATCC
HeLa[2]	Adenocarcinoma	Cervix	ATCC
HCT-116[1,2]	Colorectal adenocarcinoma	Colon	ATCC
SW-620[1]	Colorectal adenocarcinoma	Colon	ATCC
HCT15[1,2]	Colorectal adenocarcinoma	Colon	ATCC
Caco-2	Colorectal adenocarcinoma	Colon	ATCC
BCPC-3	Adenocarcinoma	Pancreas	ATCC
UCVA-1	Adenocarcinoma	Pancreas	Peterson, W.D.
786-O[1,2]	Renal cell adenocarcinoma	Kidney	ATCC

ACHN[1,2]	Renal cell adenocarcinoma	Kidney	ATCC
IGROV-1[1]	Adenocarcinoma	Ovary	Ratnam, M.
OVCAR-3[1,2]	Adenocarcinoma	Ovary	ATCC
SKOV-3[1]	Adenocarcinoma	Ovary	ATCC
HepG2[2]	Hepatocellular carcinoma	Liver	ATCC
Hep3B[2]	Hepatocellular carcinoma	Liver	ATCC
Y79	Retinoblastoma	Eye, retina	ATCC
SK-MEL5[1,2]	Melanoma	Skin	ATCC
SK-MEL-28[1]	Melanoma	Skin	ATCC
HTB139	Rabdomyosarcoma	Muscle	Peterson, W.D.
SK-N-SH	Neuroblastoma	Brain	ATCC
SK-N-BE	Neuroblastoma	Brain	ATCC
SK-N-MC	Neuroepithelioma	Supraorbital area	ATCC
HT1080	Fibrosarcoma	Connective tissue	ATCC
PC-3[1,2]	Adenocarcinoma	Prostate	ATCC
DU-145[1,2]	Carcinoma	Prostate	ATCC
H1650	Bronchoalveolar adenocarcinoma	lung	ATCC
H2122	Adenocarcinoma/NSCLC	lung	ATCC
H2030	Adenocarcinoma/NSCLC	lung	ATCC
H1573	Adenocarcinoma	lung	ATCC
H1781	Bronchoalveolar adenocarcinoma	lung	ATCC
H3255	Adenocarcinoma/NSCLC	lung	Gazdar, A.F.
A549[1]	Carcinoma	lung	ATCC
CRL5807	Bronchioalveolar carcinoma /NSCLC	lung	ATCC
CRL5872	Adenocarcinoma/NSCLC	lung	ATCC
CRL5810[1,2]	Adenocarcinoma/NSCLC	lung	ATCC
CRL5800[1,2]	Adenocarcinoma/NSCLC	lung	ATCC
H596	Adenosquamous carcinoma	Lung	ATCC
NCI-H460[1,2]	Large-cell carcinoma	Lung	ATCC
H69	SCLC	Lung	ATCC
H446	SCLC	Lung	ATCC
H226[1]	Pleural mesothelioma	Pleura	ATCC
H2373	Pleural mesothelioma	Pleura	Pass, H.I.
H2452	Pleural mesothelioma	Pleura	Pass, H.I.
H2461	Pleural mesothelioma	Pleura	Pass, H.I.
H2591	Pleural mesothelioma	Pleura	Pass, H.I.
H2595	Pleural mesothelioma	Pleura	Pass, H.I.
H2714/HP-1	Pleural mesothelioma	Effusion	Pass, H.I.

1 – Cell lines of NCI60 cell line panel

2 – Cell lines used in the report of (Zhao et al., 2004b)

amplification from suitable cDNA templates, subcloned into a TA-cloning vector (PCR-Topo; Invitrogen), and restriction digested.

2.2.4 Determination of PCFT Protein Expression Levels.

To determine whether transcript levels correlate with increased protein levels, PCFT and RFC protein levels in solid tumor cell lines and tissues were measured. Our laboratory has made human PCFT and RFC-specific (Hou et al., 2011; Wong et al., 1998; Wong et al., 1999) polyclonal antibodies specific for a carboxyl-termini PCFT peptide (CKADPHLEFQQFPQSP) or RFC (PEDSLGAVGPASLEQRQS) peptide. For PCFT, polyclonal antibody services at Invitrogen injected the peptide into rabbits with a hapten-conjugated carrier, after which they collected the bleeds and tested antibody specificity by ELISA. The serum was purified using a peptide affinity column synthesized from Affi-Gel 10 (BioRad, Richmond, CA) and the specific peptide, using pH 2.5 sodium citrate to elute the antibody. Specificity was validated by peptide competition in both western blot and immunohistochemistry experiments.

2.2.4.1 Western Blot Analysis of Solid Tumor Cell Lines.

For characterizing PCFT protein expression in solid tumor cell lines, sucrose-enriched plasma membranes were prepared by differential centrifugation. Briefly, cells were suspended in 10 mM Tris-HCl, pH 7.0, containing X1 protease inhibitor cocktail tablets (Roche, Indianapolis, IN), and disrupted with a Parr nitrogen cavitator (500 psi, 20 min). The homogenate was spun at 600 x g to remove cell debris and nuclei; the supernatant was centrifuged at 200,000 x g in a Beckman 70Ti rotor for 90 min. The membrane pellet was suspended in 600 μL of 10 mM Tris-HCl, pH 7.0, containing the protease inhibitor cocktail, and layered on a discontinuous sucrose gradient (2 mL 60% and 2.5 mL 20% sucrose in a SW55Ti rotor). Centrifugation was for l h at 58,000 x g. The 20%-60% interface containing plasma membranes was removed, diluted

approximately 10-fold with 10 mM Tris-HCl pH 7.0 (containing proteolytic inhibitors), and again centrifuged at 200,000 x g for 60 min to pellet the membranes (Matherly et al., 1991). Proteins were quantified with Folin-phenol reagent (Lowry et al., 1951). Membrane proteins were electrophoresed on 7.5% polyacrylamide gels in the presence of SDS (Laemmli, 1970) and electroblotted onto polyvinylidene difluoride membranes (PVDF) (Pierce, Rockford, IL) (Matsudaira, 1987). Immunoreactive PCFT and RFC were detected on membranes with the PCFT or RFC-specific polyclonal antibodies described above. An IRDye800CW-conjugated goat anti-rabbit IgG (Rockland, Gilbertsville, PA) was used as a secondary antibody, and the membranes were scanned with the Odyssey® Imaging System. Densitometry used Odyssey software (v 1.2) for quantitating levels of PCFT protein. PCFT levels were normalized to Na^+/K^+ ATPase protein levels (mouse antibody from Novus Biologicals, Littleton, CO) on Westerns.

2.2.4.2 Immunohistochemistry of Tumor and Normal Tissue Panels.

PCFT and RFC-specific peptide antibodies were used with immunohistochemistry to profile tissue/cellular distributions and transporter levels in commercially available paraffin tissue panels (US Biomax) of normal (FDA995) and malignant tissues (BCN961) from ovary, breast, prostate, liver, etc. Specificity was established with normal IgG and (as warranted) the addition of blocking peptide to the antibody mix. Panels included malignant tissues from a wide range of tumor types and normal tissue types including some samples with established expression of PCFT such as the duodenum, kidney, and liver. Immunohistochemistry was performed in collaboration with Mr. Larry Tait from the Karmanos Cancer Institute Imaging Core Facility.

2.2.5 Transport of [^{3}H]MTX in Solid Tumor Cell Lines.

To determine the function of PCFT and RFC in the solid tumor cell lines, transport of 0.5 μM [^{3}H]MTX was assayed in cell monolayers over 5 min at 37°C in 4-(2-hydroxyethyl)-1-piperazineethanesulfonic acid (HEPES)-buffered saline (20 mM HEPES, 140 mM NaCl, 5 mM KCl, 2 mM $MgCl_2$, and 5 mM glucose) at pH 7.2 to determine RFC-mediated transport, or in 4-morphilinopropane sulfonic (MES)-buffered saline (20 mM MES, 140 mM NaCl, 5 mM KCl, 2 mM $MgCl_2$, and 5 mM glucose) at pH 5.5 for determining transport by PCFT (Zhao et al., 2004b). Some transport experiments were performed in the presence of 20 nM folic acid to rule out uptake by the folate receptor. At the end of the incubations, transport was quenched with ice-cold Dulbecco's phosphate-buffered saline (DPBS), cells were washed 3 times with ice-cold DPBS, and cellular proteins were solubilized with 0.5 N NaOH. Levels of drug uptake were expressed as pmol/mg protein, calculated from direct measurements of radioactivity and protein contents of cell homogenates. Radioactivity was measured with a scintillation counter (Model LS6500; Beckman-Coulter, Fullerton, CA) and proteins were quantified using Folin-phenol reagent (Lowry et al., 1951). MTX was frequently used to characterize RFC and PCFT-mediated transport because it is commercially available, it is not metabolized over short intervals, and because of the ease and accuracy of influx determinations and distinguishing between free and tightly bound drugs within cells.

2.3 Results

2.3.1 Expression of RFC and PCFT in Human Normal and Tumor Tissue.

In order to determine the potential of targeting PCFT for drug uptake it was important to establish the expression of PCFT at both the transcript and protein levels in human normal and tumor tissues. For normal tissues, transcript levels for RFC and PCFT were measured by real-time RT-PCR of normalized Origene cDNA arrays from 48 pathologist-verified normal human

tissues. PCFT is expressed in most normal tissues, albeit at low levels. We measured high levels of PCFT mRNA in highly metabolic tissues such as the duodenum, kidney, liver, and the adrenal and pituitary glands (Figure 2.1, Panel A). This corroborated expression patterns observed in mouse tissues (Qiu et al., 2006). For RFC, expression was ubiquitous with the highest levels in tissues of the liver, lung, placenta, ovary and retina, and low in the heart and muscle. These findings were similar to mRNA expression patterns described by Whetstine et al. (2002a) in human tissues measured by northern blotting. The levels of PCFT at the transcript level were validated by immunohistochemical detection of PCFT protein using US Biomax tissue arrays of FDA approved human normal tissue and a polyclonal PCFT antibody. As demonstrated by real-time RT-PCR, the levels of PCFT protein were high in the duodenum (Figure 2.1, Panel B) and kidney (Figure 2.1, Panel C). Staining was specific since the signal could be competed out with a PCFT-specific peptide (data not shown) or when the secondary antibody was not included (data not shown). Overall, PCFT transcript and protein expression is more limited than RFC expression in normal tissues. For tumor tissues, RFC and PCFT transcripts were measured by real-time RT-PCR of normalized Origene cDNA arrays from multiple human primary tumors. Significant, albeit variable levels of PCFT transcripts were detected in all tumors tested. The expression pattern of PCFT in tumor tissue was similar to levels found in normal tissue, with liver tumors showing the highest levels (Figure 2.2, Panel A). Expression of RFC was high in the liver and lung, similar to the normal tissue expression pattern. Interestingly, the level of RFC was higher in both breast and colon tumors compared to normal tissue (Figure 2.2, Panel B). The continued clinical use of classical antifolates, which are substrates for RFC-mediated uptake, including MTX in breast cancer and RTX in colon cancer, may reflect the tumor-specific expression of RFC in these tissues. Patterns of transporter expression in primary tumors were

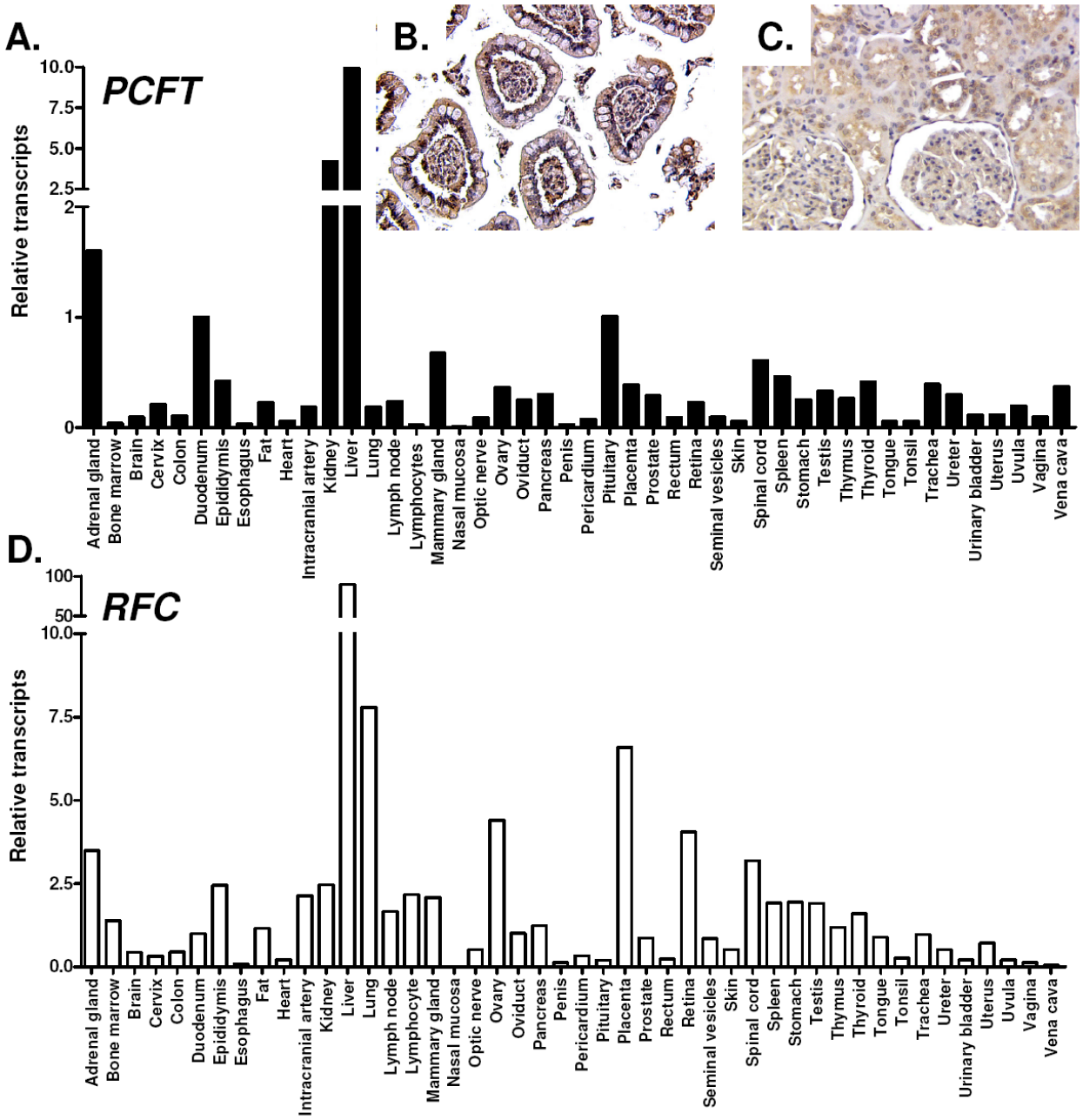

Figure 2.1 PCFT and RFC expression in human normal tissues. PCFT (*Panel A*) and RFC (*Panel D*) transcripts were measured using an Origene cDNA array of 48 pathologist-verified human normal tissue by real-time RT-PCR from total RNAs using a Roche480 Light-cycler and gene specific Universal probes and primers (Table 2.1). Transcript levels were normalized to GAPDH transcripts. Immunohistochemistry of US Biomax tissue arrays of human small intestine (*Panel B*) and kidney (*Panel C*) normal tissues stained with a polyclonal PCFT antibody. Experimental details are provided in the Materials and Methods.

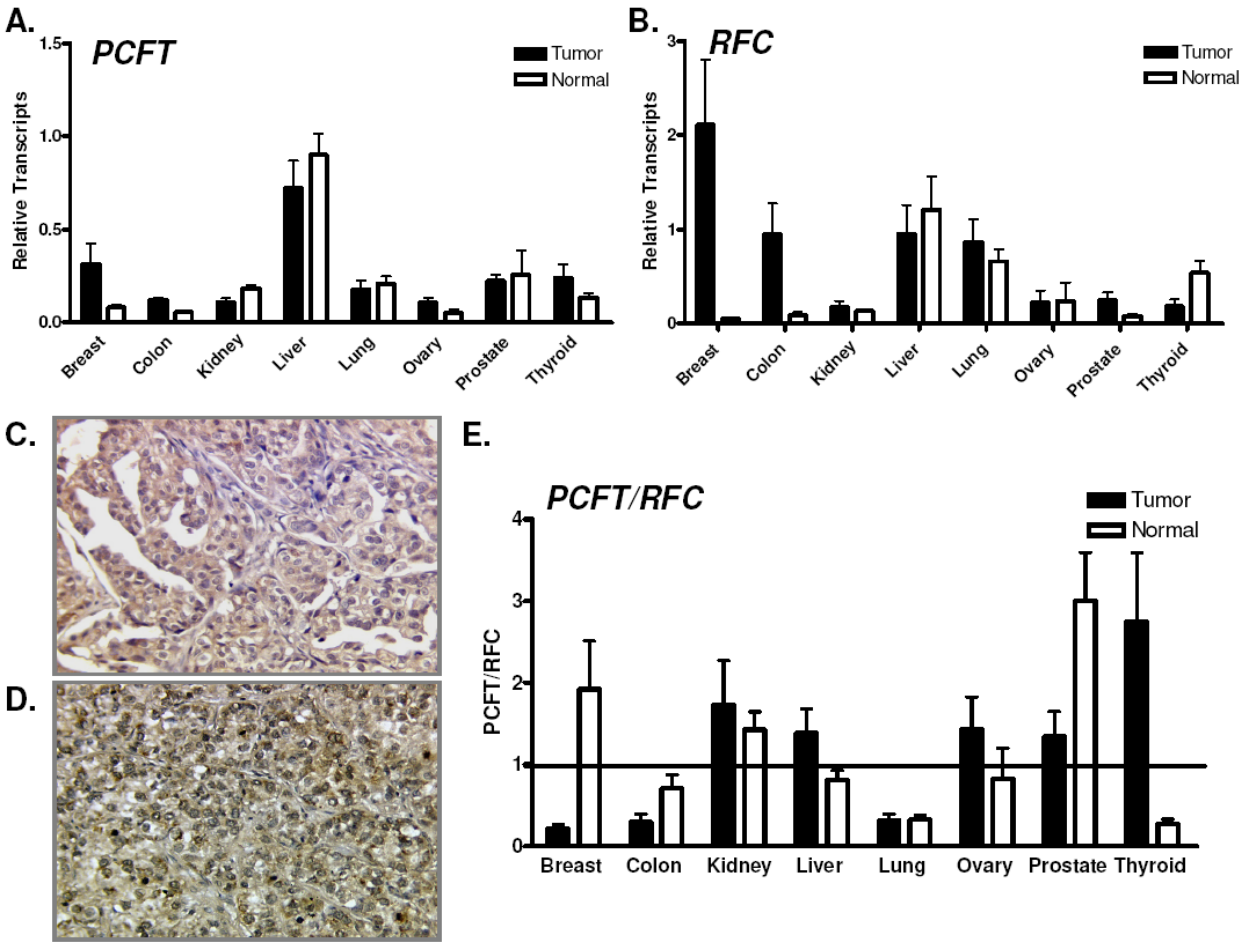

Figure 2.2 PCFT and RFC expression in human normal and tumor tissues. PCFT (*Panel A*) and RFC (*Panel B*) transcripts were measured in an Origene cDNA array of pathologist-verified, breast, colon, kidney, liver, lung, ovary, prostate and thyroid human tumor tissue (n=6) cDNAs compared to paired normal tissues from the same patient (n=3) by real-time RT-PCR from total RNAs using a Roche480 Light-cycler and gene specific Universal probes and primers (Table 2.1). Transcript levels were normalized to β-actin transcripts. Immunohistochemistry of US Biomax tissue arrays of human ovarian (*Panel C*) and liver (*Panel D*) tumors stained with a polyclonal PCFT antibody. *Panel E*, the ratio of PCFT to RFC transcript levels. Experimental details are provided in the Materials and Methods.

confirmed by immunohistochemistry of tissue arrays probed with transporter-specific antibodies. Tissue arrays contained multiple cancer and adjacent tissues, single core per case, 16 types of common organs and were pathologically confirmed (bladder, brain, breast, colon, esophagus, kidney, liver, lung, lymph node, ovary, pancreas, prostate, rectum, skin, stomach and uterine cervix). Similar to real-time RT-PCR, the levels of PCFT protein were high in the ovarian and liver tumors (Figure 2.2, Panel C and D; respectively) compared to IgG control (data not shown), again reflecting PCFT transcript levels obtained from real-time RT-PCR. For the most part, PCFT levels are similar in both normal and tumor tissues at both the transcript and protein level.

The ratios of PCFT to RFC transcript expression in human normal and tumor tissues were determined. Thyroid, ovarian and liver tumors had higher tumor PCFT/RFC ratios compared to normal tissues (Figure 2.2, Panel E). The ratio of PCFT to RFC expression and function may represent a more important indicator of which tumor types will benefit from PCFT-selective antifolates. Functional RFC could transport reduced folates into the cell which would compete with the antifolate for binding to folate-dependent enzymes, thereby reducing the cytotoxicity of antifolates that depend on PCFT for cellular uptake (see Chapter 5).

2.3.2 Expression and Function of RFC and PCFT in Human Solid Tumor and Leukemia Cell Lines.

Following reports of a low pH transport activity in solid tumor cells lines and to find a solid tumor cell line model for our PCFT-targeted therapeutics, we turned our attention to establishing an expression profile for PCFT compared to RFC and FRs in a number of cell lines derived from human solid tumors and leukemias (Table 2.2). Transcript levels for PCFT along with RFC and FRs α and β were measured by real-time RT-PCR and normalized to levels of GAPDH. Our results demonstrated significant levels of PCFT transcripts in the majority of

human solid tumor cell lines of different origins (e.g., breast, prostate, ovarian, etc.) (Figure 2.3, Panel A), and uniformly low PCFT transcript levels in human leukemias, including both ALL and AML (Figure 2.3, Panel C). PCFT levels were highest in Caco-2 (colorectal) SKOV3 (ovarian), HepG2 (hepatoma), HeLa (cervical), and T47D (breast) cancer cells. RFC transcripts were detected in all leukemia and solid tumor cell lines with the exception of MDA-MB-231 breast cancer cells (reported to express very low RFC (Worm et al., 2001)) (Figure 2.3, Panel B and D). High levels of FRα were detected in a small subset of ovarian, cervical, and breast cancer cell lines and modest FRα levels were measured in ALL (mostly T-cell) sublines (data not shown). FRβ transcripts were consistently low-to-undetectable in both solid tumors and leukemias, with the highest levels restricted to a small number of AML and T-cell ALLs (data not shown). The levels of human PCFT, RFC and FR transcripts in solid tumor and leukemia cell lines were published (Kugel Desmoulin et al., 2011). Real-time RT-PCR was repeated with SYBR green and gene-specific primers (Table 2.1), (experimental details are the same as in section 5.2.6) and identical results were obtained.

The level of PCFT and RFC protein expression was validated for ten solid tumor cell lines (HepG2, Hep3B, H596, CRL5810, H2595, HCT15, Caco-2, DU145, MDA-MB 321, SK-MEL5) and four control HeLa cell lines (R1-11-mock (no functional PCFT or RFC), R1-11-PCFT4 (R1-11-mock stably transfected with PCFT), HeLa (functional PCFT and RFC), R5 (HeLa cells that express PCFT but not RFC)) by isolating membrane fractions through differential centrifugation and sucrose gradients, followed by immunoblotting with PCFT and RFC-specific polyclonal antibodies. Relative PCFT and RFC protein levels paralleled levels of PCFT (Figure 2.4, Panel A) and RFC (Figure 2.4, Panel B) transcripts, as detected by real-time RT-PCR. There were some differences in protein sizes, which likely reflect post-translational

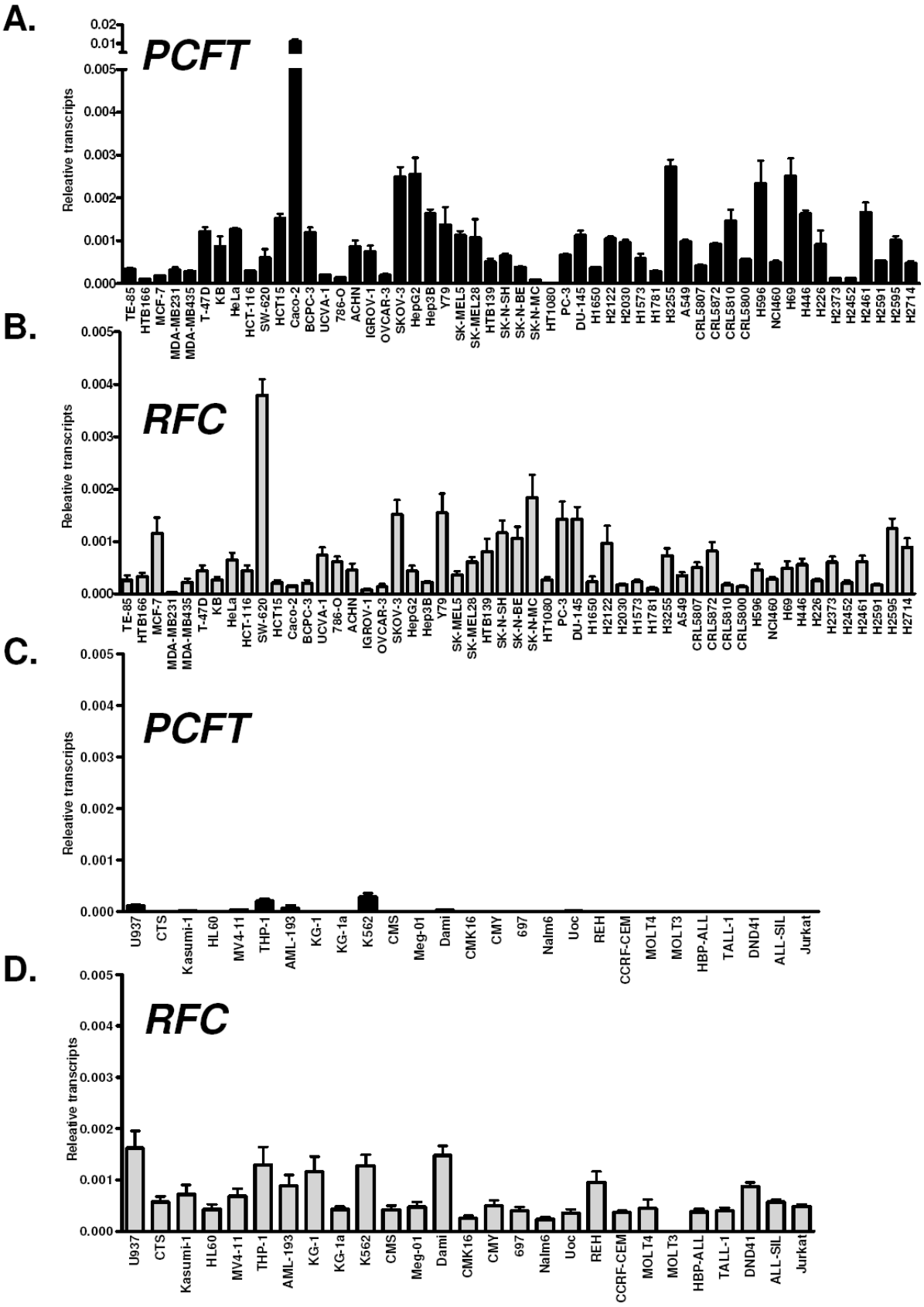

Figure 2.3 PCFT and RFC transcript expression in human solid tumor and leukemia cell lines. PCFT (*Panel A and C*) and RFC (*Panel B and D*) transcripts were measured in 53 human solid tumor (*Panels A and B*) and 27 leukemia (*Panels C and D*) cell lines by real-time RT-PCR from total RNAs using a Roche480 Light-cycler and gene specific Universal probes and primers (Table 2.1). Transcript levels were normalized to GAPDH transcripts. Experimental details are provided in the Materials and Methods. A table summarizing the characteristics of the 53 tumor and 27 leukemia cell lines is also included in Table 2.2.

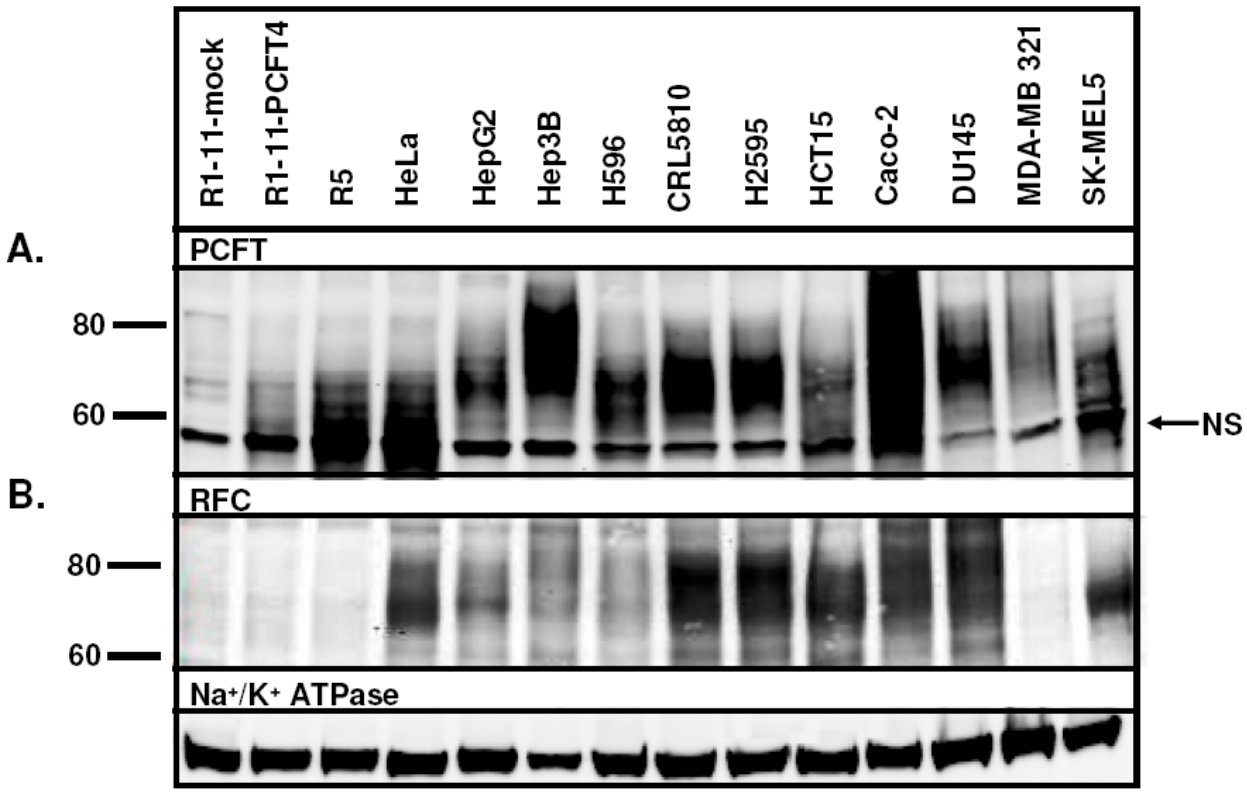

Figure 2.4 PCFT and RFC protein expression in human solid tumor cell lines. PCFT (*Panel A*) and RFC (*Panel B*). Pure membrane fractions were isolated using a Parr nitrogen cavitator at 500 psi for 20 min, differential centrifugation and sucrose gradients. Membrane proteins (25 µg) were electrophoresed on 7.5% denaturing polyacrylamide gels and immunoblotted with polyclonal PCFT and RFC antibodies. Na^+/K^+ ATPase protein levels were used as loading controls. The characteristics of the 14 tumor cell lines are included in Table 2.2. Non-specific (NS) band.

modifications (e.g., glycosylation (Unal et al., 2008; Wong et al., 1998)). Finally, functional validation of transporter expression in solid tumor cell lines was determined by transport of [^{3}H]MTX (Figure 2.5) at pH 5.5 for PCFT (Panel A), and at pH 7.2 for RFC (Panel B). Relative uptake of [^{3}H]MTX somewhat paralleled transcript and protein levels for PCFT. More modest levels of transport were detected at pH 7.2, although the correlation with RFC protein was inexact. The reason for this is unclear. pH 5.5 (PCFT) to pH 7.2 (RFC) transport ratios ranged from ~2- to ~9-fold (Figure 2.5, Panel C), demonstrating broad spectrum and high-level PCFT to RFC membrane transport in clinically relevant human tumor cell lines, as previously reported (Zhao et al., 2004b).

2.4 Discussion

Our findings have established the expression patterns and pH-specific transport for PCFT in human solid tumor cell lines, primary tumors and normal tissues. We found that expression of PCFT transcripts and protein in normal tissues is more limited than for the ubiquitously expressed RFC, with high levels in the liver, kidney, and small intestine. In addition, a wide range of human solid tumor tissues and cell lines expressed PCFT transcripts and protein, and PCFT expression generally correlated with pH-dependent transport function. Goldman and colleagues measured low pH transport of MTX into human tumor cell lines (Zhao et al., 2004b). Our comprehensive analysis of PCFT expression and function identified PCFT as the low pH folate transporter responsible of MTX uptake at acid pH in solid tumor cell lines. While RFC protein was likewise detected in most of the tumor cell lines, transport was only modestly reflected in levels of RFC protein, suggesting the existence of previously unrecognized posttranslational regulatory mechanisms for RFC and/or an unknown non-RFC transport process at neutral pH. Finally, we have found the expression of PCFT to be very low in the bone marrow,

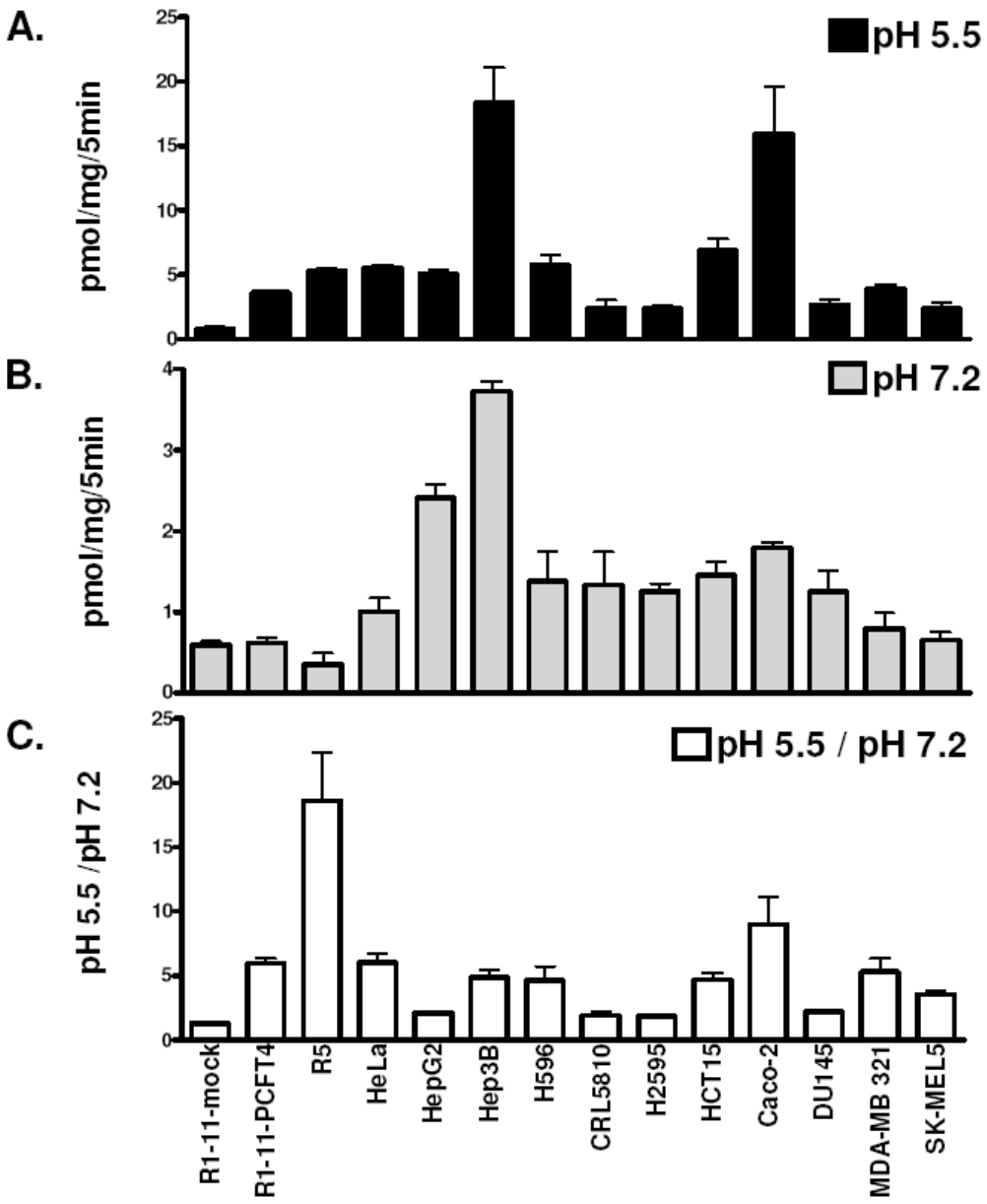

Figure 2.5 PCFT and RFC function in human solid tumor cell lines. Uptake of 0.5 μM [^{3}H]MTX was measured at 37˚C for 5 min in cell monolayers at pH 5.5 (MES-buffered saline) (*Panel A*) or pH 7.2 (HEPES-buffered saline) (*Panel B*), and internalized [^{3}H]drug was normalized to total protein. *Panel C*, the ratio of [^{3}H]MTX uptake at pH 5.5 / pH 7.2 in WT and R5 HeLa cells. A table summarizing the characteristics of the 14 tumor cell lines is included in Table 2.2.

which would suggest that PCFT-targeted therapeutics may be less marrow toxic compared to antifolates presently in clinical use that rely on RFC-mediated uptake at neutral pH. It will be important to test normal hematopoietic stem cells to assess the impact of PCFT-selective analogs on this cell fraction.

The importance of PCFT expression in normal tissues to the development of drug toxicities will depend on transport function of PCFT in these tissues. Even though PCFT-mediated transport is maximal at low pH, transport is also detected at pH 7.4 in human cells and *Xenopus* oocytes that express PCFT. This residual PCFT function at pH 7.4 is thought to be driven by increases in membrane potential. Whether the level of PCFT-mediated transport at pH 7.4 in normal tissues is sufficient to cause dose-limiting toxicity of antifolates selective for PCFT mediated uptake remains to be determined. Additionally, there are instances of a localized acidic environment created by Na^+/H^+ exchangers at the basolateral membranes of the choroid plexus (Segal, 2000) and hepatocyte (Horne, 1993) which may contribute to uptake and toxicity in normal tissues generally thought to be at neutral extracellular pH.

PCFT expression is not static, as it has been found to be modulated by promoter methylation, vitamin D3 and the NRF-1 transcription factor. Hypermethylation of the PCFT promoter was shown to be associated with low PCFT protein expression in CCRF-CEM and Jurkat T-cell leukemia cell lines (Gonen et al., 2008) and a MTX-resistant HeLa cell line (R1) (Diop-Bove et al., 2009) and could represent a mechanism of resistance against drugs that use PCFT as their primary means of cellular entry. Nutritional status could also affect PCFT expression, as VDR heterodimerizes with RXRα in response to vitamin D3 and binds a VDR response element in the PCFT promoter region (-1694/-1680), increasing expression of PCFT (Eloranta et al., 2009). Interestingly, mouse PCFT transcript levels increased ~13-fold in the

proximal small intestine in mice fed folate-deficient versus folate-replete diets, consistent with the critical role that PCFT plays in intestinal folate absorption (Qiu et al., 2007). Interestingly, PCFT mRNA expression directly correlated with NRF-1 transcript levels in these tissues and was dependent on folate status (C. Cherian, unpublished observation), reaffirming the likely importance of NRF-1 in PCFT transcriptional control (Gonen and Assaraf, 2010). Thus, dietary increases or decreases in folate and vitamin D3 levels could affect expression of PCFT in normal tissues and could impact antifolate toxicity. The extracellular pH surrounding a cell may also have an effect on PCFT expression. For instance, treatment of patients with proton pump inhibitors, which increase extracellular pH, leads to decreased PCFT expression and folate deficiency due to reduced folate uptake from the gut (Urquhart et al., 2010). Of course, transcriptional control is most likely not the only mechanism of PCFT regulation. PCFT protein expression may also be stimulus controlled, such that decreased extracellular folate or decreased extracellular pH may induce cycling of PCFT from intracellular compartments to the cell surface in order to facilitate folate uptake. Indeed, PCFT protein has not only been found on the cell surface but also in intracellular compartments (Kugel Desmoulin et al., 2010b; Qiu et al., 2006), and PCFT has been proposed to aid in the exit of (anti)folate from acidic endosomes (Zhao et al., 2009b). It may be possible that the presence of intracellular PCFT may have particular regulatory significance.

This chapter has established PCFT expression in many solid tumor cell lines, but whether the level of expression and function is enough to transport a cytotoxic dose of antifolates that use this mechanism is still unknown. There is some indication that PCFT may facilitate PMX uptake and cytotoxicity toward solid tumor cell lines that express moderate levels of PCFT. PMX is a transport substrate for both RFC and PCFT-mediated uptake and is the best known substrate for

PCFT (Zhao and Goldman, 2007). Upon loss of RFC expression, when PCFT was the sole mechanism of PMX transport, uptake by PCFT was sufficient to maintain PMX cytotoxicity (Chattopadhyay et al., 2006; Zhao et al., 2004c) (See Chapter 5). Uptake of cytotoxic antifolates by RFC not only precludes selectivity, since RFC, as shown in this chapter as well as by Whetstine et al. (2002a) is expressed and functional in human normal tissues. However, its ability to transport antifolates into tumor cells may be compromised due to reduced transport activity at acidic pHs characterizing the tumor microenvironment. This suggests that designing drugs with greater affinity for PCFT and not the RFC has the potential to increase tumor selectivity without loss of drug activity (Kugel Desmoulin et al., 2011; Kugel Desmoulin et al., 2010b; Wang et al., 2010; Wang et al., 2011) (see Chapters 3 and 4). Due to the low activity of RFC at acidic pHs, tumor cells may favor overexpression of H^+-coupled transporters, such as PCFT, in order to transport folates to meet their nutritional and metabolic requirements and to gain a competitive advantage in the acidic tumor microenvironment (Anderson and Thwaites, 2010). Hence, PCFT expression and function may increase in more advanced aggressive tumors, suggesting that antifolates selectively transported into tumor cells by PCFT would make better, more selective drugs that have the potential to improve therapy. Future studies should look at expression of PCFT with increasing tumor stage or grade.

To determine whether the therapeutic targeting of agents selective for PCFT uptake by utilizing tumor acidity to drive drug uptake will be successful, investigators will not only need to establish PCFT expression in tumors but also PCFT function. Further, the ability to measure tumor pH with accuracy, precision and high spatiotemporal resolution in experimental preclinical systems and in human beings will be very important for this therapeutic strategy (Zhang et al., 2010). Recent advances in optical imaging, PET radiotracers, and magnetic resonance

spectroscopy (MRS) and magnetic resonance imaging (MRI) have improved the ability to measure tumor pH. Optical techniques such as fluorescence ratio imaging spectroscopy and fluorescent lifetime imaging can be used to measure tumor pH. These methods use fluorescent probes that have varied fluorescent properties depending on local pH, which can be measured optically and converted to a pH distribution map. Positron emission tomography (PET)-based approaches use pH-sensitive PET radiotracers including the pH (low) insertion peptide (pHLIP) conjugated to ^{64}Cu (Vavere et al., 2009). pHLIP is a peptide that predominantly inserts across a lipid bilayer as a monomeric α-helix at an acidic extracellular environment but not at a normal physiological pH (Andreev et al., 2007; Fendos and Engelman, 2012). MRS methods are generally based on a difference in chemical shifts between pH-dependent and independent resonances; several isotopes have been evaluated for determination of tumor pH, such as ^{31}P-MRS and ^{1}H-MRS with some success. There are still some limitations in spatial and temporal resolution (Gillies and Morse, 2005). Hyperpolarized ^{13}C bicarbonate is a technique that uses ^{13}C MRI and is based on transferring the polarization of unpaired electrons to neighboring nuclei by microwave irradiation of the sample (Hu et al., 2008). Finally, an alternative approach uses MRI and relies on agitating the relaxivity of water with pH-dependent relaxation agents (Aime et al., 1999; Garcia-Martin et al., 2006; Zhang et al., 1999). With the improvement of *in vivo* pH measurements, it may be possible to target treatment to those tumors that are more acidic, thus focusing therapy on the population of patients that will most benefit from PCFT-selective agents.

CHAPTER 3

THE IDENTIFICATION OF NOVEL ANTIFOLATES WITH PCFT-SELECTIVE UPTAKE

3.1 Introduction.

The activities of RFC, PCFT and FR folate transport systems toward antifolate substrates in tissues and tumors reflect their relative expression levels, along with their specificities for different antifolates and transport kinetics. With this said, antifolates selective for RFC, which include all classical antifolates presently approved by the FDA, can be envisaged to possess *limited selectivity* toward tumors over normal proliferative tissues such as bone marrow since these tissues all express RFC (Chapter 2 and Whetstine et al. (2002a)). The therapeutic approach of rational folate analog design that is based on targeting delivery into cancer cells by exploiting the tumor-specific patterns of expression and/or function of PCFT and FR may lead to more tumor-selective therapeutics. This approach is not entirely unprecedented, as recent efforts have focused on targeting FR as a means of delivering cytotoxic antifolates into the tumor cell. For instance, ONX0801 (previously BGC945) which is selectively transported by FRs and inhibits TS as its primary target (Gibbs et al., 2005; Theti et al., 2003) has recently been licensed by Onyx Pharmaceuticals and is currently in Phase I in the United Kingdom. Another approach links a variety of lipid soluble drugs, structurally unrelated to folates, to folic acid via a covalent bond. The complex binds FR on the cell surface, is endocytosed, the bond is broken in the reducing environment of the endosome, and the drug diffuses out of the endosome to inactivate its intracellular target. Several such agents have been designed. BMS-753493 is a molecule born from collaboration between scientists at Endocyte Inc. and Bristol Myers Squibb. It represents a folic acid conjugate that was constructed with a semi-synthetic analog of Epothilone A (a microtubule inhibitor). BMS-753493 is currently being evaluated for safety and efficacy in Phase

II clinical trials sponsored by Bristol Myers Squibb. EC-145 (Endocyte) is a desacetylvinblastine monohydrazide – folic acid complex (Reddy et al., 2007). A randomized Phase II trial is near completion in which EC-145 with Doxil was compared to Doxil alone for the treatment of platinum-resistant ovarian cancers (Dosio et al., 2010). Farletuzumab is a humanized MoAb with high affinity for FRα. Preclinical studies have demonstrated that farletuzumab mediates robust antibody-dependent cellular cytotoxicity and complement-dependent cytotoxicity *in vitro*, inhibits tumor growth in ovarian tumor xenografts, and displays a safe toxicology profile in non human-primates (Kalli, 2007; Smith-Jones et al., 2008). Farletuzumab has shown clinical efficacy in early phase trials as single agent and combination therapy with minimal drug-specific toxicity (Spannuth et al., 2010). The Phase III development plan in ovarian cancer patients includes combination chemotherapy studies in both platinum-sensitive (recently launched) and platinum-resistant (planned) recurrent disease (Bellati et al., 2011).

Based on the clinical successes of PMX, and in an effort to design novel antifolates with specificities other than RFC, our lab formed collaborations with Dr. Aleem Gangjee's group from Duquesne University. This cooperation has resulted in several novel series of compounds based on the chemical structure of PMX. These include: (**i**) 6-substituted pyrrolo[2,3-*d*]pyrimidine benzoyl antifolates with carbon bridge length variations of 1- to 6-carbons, compounds **1-6**, respectively (Deng et al., 2008; Kugel Desmoulin et al., 2010b) (Figure 3.1, Panel A); (**ii**) 6-substituted thieno[2,3-*d*]pyrimidine benzoyl antifolates with bridge length variations from 2-8 carbon atoms, compounds **7-13**, respectively (Deng et al., 2009) (Figure 3.1, Panel B); (**iii**) 6-substituted pyrrolo[2,3-*d*]pyrimidine antifolates with a thienoyl replacement for the benzoyl moiety and bridge length variations from 1-6 carbons, compounds **14-19**, respectively (Kugel Desmoulin et al., 2011; Wang et al., 2010; Wang et al., 2011) (Figure 3.1,

Panel C); and the (**iv**) 6-substituted pyrrolo[2,3-*d*]pyrimidine thienoyl regioisomers with a 4-carbon bridge and different thienoyl ring substitutions (compounds **20-24**) (Wang et al., 2012) (Figure 3.1, Panel C).

The rationale behind the synthesis of the 6-substituted pyrrolo[2,3-*d*]pyrimidine benzoyl structures (group (i) above) (Figure 3.1, Panel A) is in part based on the finding that the 6-regio isomer of PMX (compound **2**) was inactive against the growth of tumor cells expressing RFC in culture (Shih, 1993). Gangjee et al. postulated that a possible reason for its inactivity in culture could be that transposing the 5-ethylene bridge to the 6-position forces the benzoyl glutamic acid side chain in an orientation different from that required for optimal enzyme interaction and antitumor activity (Gangjee et al., 2005; Gangjee et al., 2004). They therefore elongated the ethylene bridge between the heterocycle and *para*-aminobenzoate with 3 (compound **3**) or 4 (compound **4)** methylene groups to allow greater conformational flexibility. Compounds **3** and **4** were both modest inhibitors of proliferation with CCRF-CEM leukemia cells (express RFC but no PCFT or FR) in the presence of micromolar concentrations of folic acid (Gangjee et al., 2005; Gangjee et al., 2004). Our laboratory found that the 6-substituted pyrrolo[2,3-*d*]pyrimidine benzoyl analogs were characterized by potent and selective substrate activities for FRα and FRβ, and negligible substrate activity for RFC. Moreover, the intracellular enzyme target of the 6-substituted pyrrolo[2,3-*d*]pyrimidine benzoyl antifolates was identified as GARFTase, the first folate-dependent reaction in the *de novo* purine nucleotide biosynthesis pathway (Deng et al., 2008).

The synthesis of 6-substituted thieno[2,3-*d*]pyrimidine benzoyl antifolates with bridge length variations (from 2-8 carbon atoms; compounds **7-13** respectively) (group (ii), above) (Figure 3.1, Panel B) was pursued to try to find a more potent analog and to understand the

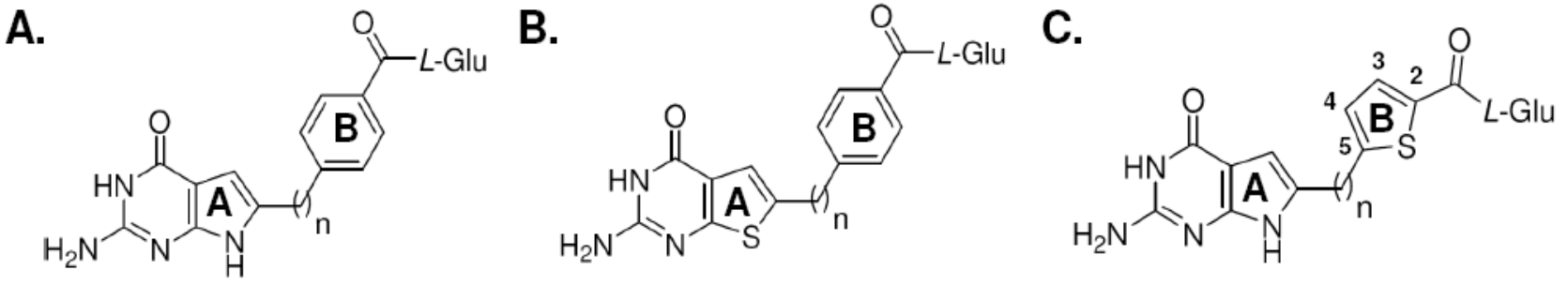

n=1 **1**
n=2 **2**
n=3 **3**
n=4 **4**
n=5 **5**
n=6 **6**

n=2 **7**
n=3 **8**
n=4 **9**
n=5 **10**
n=6 **11**
n=7 **12**
n=8 **13**

n=1 **14**
n=2 **15**
n=3 **16**
n=4 **17**
n=5 **18**
n=6 **19**

17 w/ 2,3 substitution **20**
17 w/ 4,5 substitution **21**
17 w/ 3,4 substitution **22**
17 w/ 3,5 substitution **23**
17 w/ 2,4 substitution **24**

Figure 3.1 Structures of novel antifolate drugs. *Panel A*, 6-substituted pyrrolo[2,3-*d*]pyrimidine benzoyl antifolates with carbon bridge length variations of 1- to 6-carbons, compounds **1-6**, respectively. *Panel B*, 6-substituted thieno[2,3-*d*]pyrimidine benzoyl antifolates with bridge length variations from 2-8 carbon atoms, compounds **7-13**, respectively. *Panel C*, 6-substituted pyrrolo[2,3-*d*]pyrimidine antifolates with a thienoyl replacement for the benzoyl moiety and bridge length variations from 1-6 carbons, compounds **14-19**, respectively, and 6-substituted pyrrolo[2,3-*d*]pyrimidine thienoyl regioisomers with a 4-carbon bridge (compound **17**) and different thienoyl ring substitutions, compounds **20-24**, respectively.

structural determinants of transport selectivity. Isosteric replacement of the pyrrolo ring with a thieno ring for this series provided an increase in ring size that more closely approximates the pteridine, 6-6 fused ring system of the natural cofactor. In addition, replacement of the NH of the pyrrole with an S also allows for comparison of the relative importance of a hydrogen bond donor (NH) with a hydrogen bond acceptor (S). Our laboratory found that the 6-substituted thieno[2,3-*d*]pyrimidine antifolate series was characterized by potent and selective substrate activities for FRα and FRβ, and negligible substrate activities for RFC. Furthermore, the 6-substituted thieno[2,3-*d*]pyrimidine antifolates were found to target both GARFTase and AICARFTase (Deng et al., 2009).

The rationale for the synthesis of 6-substituted pyrrolo[2,3-*d*]pyrimidines with a thienoyl replacement for the benzoyl moiety and bridge length variations from 1-6 carbons antifolates (compounds **14-19**, respectively) (group (iii) above) (Figure 3.1, Panel C) came from the discovery and biochemical evaluation of RTX. RTX was synthesized by replacing the para-aminobenzoate of ICI 198583 (a precursor analog of RTX) with a thiophene and a N10-methyl substituent. This modification reduced TS inhibition compared to earlier analogs but enhanced cellular uptake by RFC and polyglutamylation leading to more potent tumor growth inhibition both *in vitro* and *in vivo*. Therefore, the rationale was that combining the chemical structures of the 6-substituted PMX with different carbon bridge lengths with the thienoyl group of RTX might give a more potent novel antifolate.

As an alternative approach for decreasing the distance between the bicyclic pyrrolo[2,3-*d*]pyrimidine and the L-glutamate portions, we systematically assessed the effects on cell proliferation for an expanded series of pyrrolo[2,3-*d*]pyrimidine thienoyl regioisomers of **17** with a 4-carbon bridge and thienoyl ring substitutions, 2',3' (**20**), 4',5' (**21**), 3',4' (**22**), 3',5' (**23**), and

2',4' (**24**) (group (iv) above) (Figure 3.1, Panel C). In analogs **20**-**24**, the [1,2] substitution pattern on the thiophene forces the bicyclic scaffold and L-glutamate closer together than in the parent 3-atom bridge compound **16** which includes a [1,3] pattern on the thiophene ring.

This chapter will explore the potential of PCFT to selectively deliver cytotoxic antifolates for the chemotherapy of tumors. The transport activity profile for the earlier series of 6-substituted pyrrolo[2,3-*d*]pyrimidine benzoyl antifolates (Deng et al., 2008) and 6-substituted thieno[2,3-*d*]pyrimidine benzoyl antifolates (Deng et al., 2009) will be expanded to include PCFT and the transport selectivity of the other novel series will be established. The potent antiproliferative activities of these compounds, attributable to inhibition of GARFTase and *de novo* purine biosynthesis, will be characterized. The goal is to establish a structure-activity relationship for compounds that are selective for PCFT-mediated uptake, have no RFC substrate activity and cause cell death through GARFTase inhibition at doses that are pharmacologically feasible. The findings presented here will establish that PCFT is an efficient means of delivering cytotoxic antifolate drugs and suggest that PCFT provides a unique opportunity to selectively target solid tumors with cytotoxic antifolates that are not substrates for the ubiquitously expressed RFC.

3.2 Materials and Methods.

3.2.1 Chemicals and Reagents.

[3',5',7-^{3}H]MTX (20 Ci/mmol) and [^{3}H]PMX (3.7 Ci/mmol) were purchased from Moravek Biochemicals (Brea, CA). Unlabeled MTX and (6 R,S)-5-formyl tetrahydrofolate (5-CHO-THF) were provided by the Drug Development Branch, National Cancer Institute, Bethesda, MD. Both labeled and unlabeled MTX were purified by HPLC prior to use (Fry et al., 1982). The sources of the antifolate drugs were as follows. RTX [*N*-(5-[*N*-(3,4-dihydro-2-

methyl-4-oxyquinazolin-6-ylmethyl)-*N*-methyl-amino]-2-thenoyl)-L-glutamic acid] was obtained from AstraZeneca Pharmaceuticals (Maccesfield, Cheshire, England); LMX (5,10-dideaza-5,6,7,8-tetrahydrofolate) and PMX (Alimta) were from Eli Lilly and Co. (Indianapolis, IN); GW1843U89 [(*S*)-2-(5-(((1,2-dihydro-3-methyl-1-oxo-benzo(F) quinazolin-9-yl) methyl) amino)1-oxo-2-isoindolinyl) glutaric acid] was from the GlaxoWellcome-SmithKline Co. (Research Triangle Park, NC); and N^{alpha}-(4-amino-4-deoxypteroyl)-N^{delta}-hemiphthaloyl-L-ornithine (PT523) was a gift of Dr. Andre Rosowsky (Boston, MA). Restriction and modifying enzymes were purchased from Promega (Madison, WI). Other chemicals were obtained from commercial sources in the highest available purities. Synthesis and properties of the 6-substituted pyrrolo[2,3-*d*]pyrimidine benzoyl antifolate compounds **1-6** (1-6 methylene groups in the bridge region connecting the pyrrolo[2,3-*d*]pyrimidine moiety to *para*-aminobenzoate) were described (Deng et al., 2008; Kugel Desmoulin et al., 2010b). Synthesis and properties of the 6-substituted thieno[2,3-*d*]pyrimidine antifolate with bridge variations from 2-8 carbon atoms (compounds **7-13**) were described (Deng et al., 2009). Synthesis and properties of pyrrolo[2,3-*d*]pyrimidine thienoyl antifolate compounds **14-19** (1-6 methylene groups in the bridge region connecting the pyrrolo[2,3-*d*]pyrimidine moiety to *para*-aminobenzoate) were described (Kugel Desmoulin et al., 2011; Wang et al., 2010). Finally, synthesis and properties of 6-substituted pyrrolo[2,3-*d*]pyrimidine thienoyl regioisomers with a 4-carbon bridge and different thienoyl ring substitutions (compounds **20-24**) were described (Wang et al., 2012).

3.2.2 Cell Culture.

Novel antifolate preliminary screening was performed in sublines derived from PCFT-, RFC-, and FR-null MTXRIIOua^{R}2-4 (R2) Chinese hamster ovary (CHO) cells (Flintoff and Nagainis, 1983), a gift from Dr. Wayne Flintoff (University of Western Ontario, London,

Ontario, Canada). R2 cells were cultured in alpha-minimal essential media (MEM) supplemented with 10% bovine calf serum (Invitrogen, Carlsbad, CA), 100 units/mL penicillin, 100 µg/mL streptomycin, and 2 mM L-glutamine at 37˚C with 5% CO_2. PC43-10 and R2/PCFT4 cells are R2 cells stably transfected with human RFC (Wong et al., 1995) or human PCFT (Kugel Desmoulin et al., 2010b), respectively. Generation of R2/PCFT4 cells is described below. Both cell lines were cultured in complete alpha-MEM medium plus 1 mg/mL G418. Using LookOut™, a PCR-based *Mycoplasma* detection kit from Sigma Chemical Company (St. Louis, MO), cell lines were periodically determined to be free of *Mycoplasma*.

3.2.3 Preparation of a Myc-His6-tagged Human PCFT Construct and Generation of Stable Transfectants.

Total RNA from wild type HeLa cells was reverse transcribed and PCR amplified with EasyA proof-reading polymerase (Agilent Technologies, La Jolla, CA) using the following primers: 5'-AACTC **GGA TCC** gca cat gga ggg gag cgc gag cc-3'; and 5'–AACTC **GGT ACC** ggg gct ctg ggg aaa ctg ctg gaa ctc ga-3' (bold capitals designate the BamHI and KpnI restriction sites, respectively). The 1403 bp amplicon was subcloned into pCDNA3.1 (Invitrogen) in-frame with a Myc-His6 sequence inserted at the C-terminal amino acid 466 (hereafter designated $PCFT^{Myc\text{-}His6}$/pCDNA3.1). The construct was confirmed by automated DNA sequencing at the Wayne State University Sequencing Core.

R2 cells were transfected with $PCFT^{Myc\text{-}His6}$/pCDNA3.1 by electroporation (200 V, 1000 µF capacitance). After 24 h, the cells were cultured in the presence of G418 (1.5 mg/mL). Stable clones were selected by plating for individual colonies in the presence of 1.5 mg/mL G418. Colonies were isolated, expanded and screened for expression of $PCFT^{Myc\text{-}His6}$ protein by Western blotting and transport assays at pH 5.5 (see below). One clone (R2/PCFT4) was

selected for further study. Vector control R2 cells (R2/VC) transfected with empty pCDNA3.1 were also prepared and used as a negative control.

3.2.4 Gel Electrophoresis and Western Blotting.

For characterizing PCFT and RFC protein expression in R2/PCFT4 and PC43-10 cells, respectively, crude plasma membranes were prepared by differential centrifugation. Briefly, cells were suspended in 10 mM Tris-HCl, pH 7.0, containing X1 protease inhibitor cocktail tablets (Roche, Indianapolis, IN), and disrupted with a probe sonicator. The cell homogenate was centrifuged (600 x g, 10 min) to remove cell debris and nuclei; the supernatant was then centrifuged at 200,000 x g (48,000 rpm) in a Beckman TL100 ultracentrifuge for 30 min. The particulate fraction was solubilized in 10 mM Tris-HCl (pH 7) with 2% SDS in the presence of proteolytic inhibitors and proteins were quantified with Folin-phenol reagent (Lowry et al., 1951). Membrane proteins were electrophoresed on 7.5% polyacrylamide gels in the presence of SDS (Laemmli, 1970) and electroblotted onto PVDF (Pierce, Rockford, IL) (Matsudaira, 1987). $PCFT^{Myc\text{-}His6}$ protein was detected with monoclonal Myc-specific mouse antibody (Covance, Berkeley, CA) and secondary IRDye800CW-conjugated antibody (Rockland, Gilbertsville, PA). Detection of immunoreactive proteins used the Odyssey® Infrared Imaging System (LI-COR, Lincoln, NE).

3.2.5 Indirect Immunofluorescence and Confocal Microscopy.

For confocal microscopy, R2/PCFT4 and R2/VC CHO cells were plated in Lab-Tek®II chamber slides™ (Nalge Nunc International, Naperville, IL). Cells were fixed with 3.3% paraformaldehyde (in DPBS), permeabilized with 0.1% Triton X-100 (in PBS), and stained with monoclonal Myc-specific mouse antibody (Covance) and Alexa Fluor® 488 donkey anti-mouse IgG (H+L) secondary antibody (Molecular Probes, Eugene, OR). Slides were visualized with a

Zeiss laser scanning microscope 510 using a 63x water immersion lens, and exactly the same parameter setting for all samples. Confocal analysis was performed at the Imaging Core of the Karmanos Cancer Institute.

3.2.6 Transport Assays.

The expression and function of PCFT and RFC in R2/PCFT4, R2/VC, PC43-10 and R2 cell lines was validated by measuring pH-dependent transport of 0.5 μM [^{3}H]MTX over 2 min at 37°C in cell suspensions. Briefly, three days before transport experiments, cells grown in monolayers, under G418 selection, were transferred to Cytostir spinners and maintained in suspension at densities of 2-5 x 10^5 cells/mL. Cells were collected by centrifugation, washed with DPBS, and the cell pellets (~2 x 10^7 cells) were suspended in 2 mL of either [^{3}H]MTX containing HEPES-buffered saline (20 mM HEPES, 140 mM NaCl, 5 mM KCl, 2 mM $MgCl_2$, and 5 mM glucose) at pH 6.8 or 7.2, or in MES-buffered saline (20 mM MES, 140 mM NaCl, 5 mM KCl, 2 mM $MgCl_2$, and 5 mM glucose) at pH 5.5, 6.0, or 6.5 (Zhao et al., 2004b). At the end of the incubations, transport was quenched with ice-cold DPBS, cells were washed 3 times with ice-cold DPBS, and cellular proteins were solubilized with 0.5 N NaOH. Levels of drug uptake were expressed as pmol/mg protein, calculated from direct measurements of radioactivity and protein contents of the cell homogenates. Radioactivity was measured with a scintillation counter (Model LS6500; Beckman-Coulter, Fullerton, CA) and proteins were quantified using Folin-phenol reagent (Lowry et al., 1951).

To determine [^{3}H]MTX and [^{3}H]PMX kinetic constants for PCFT in R2/PCFT4 cells (K_t and V_{max}), transport rates were measured at pH 6.8 and pH 5.5, as described above, using substrate concentrations from 0.04 to 5.0 μM. K_t and V_{max} values were determined from Lineweaver-Burke plots. Inhibition of RFC transport by unlabeled antifolates (reflecting

transport by the carrier) was measured in PC43-10 cells over 2 min at 37°C in Hank's balanced salts solution (pH 7.2) with 0.5 μM [^{3}H]MTX and 10 μM inhibitor. For PCFT, inhibition of transport was determined from pH 5.5 to 7.2 in the above MES- and HEPES-buffered saline over 2 min at 37°C with 0.5 μM [^{3}H]MTX and 10 μM inhibitors. K_is for PCFT were calculated from Dixon analysis, by plotting reciprocal transport velocities measured over a range (1-5 μM) of inhibitor concentrations and 0.5 μM [^{3}H]MTX at pH 5.5 and pH 6.8. K_i values were calculated from the slopes, K_t and V_{max} values for MTX, and the concentration of [^{3}H]MTX, using the equation $K_i=K_t/(V_{max})(slope)(S)$.

3.2.7 Electrophysiology Experiments.

Electrophysiology experiments were performed in collaboration with Dr. Michael Romero (Mayo Clinic, Rochester, MN). *Xenopus* oocytes were used to assess currents associated with transport of the antifolate substrates. PCFT cRNA (50 nL of 0.5 μg/μL, i.e., 25 ng) or water (50 nL) was injected into stage V/VI oocytes and electrophysiological measurements were made 3-5 days later (Unal et al., 2009a). Oocytes were voltage clamped to -90 mV to maximize folate-induced currents, a technique that was previously utilized in studies on the divalent metal transporter, DMT1 (Gunshin et al., 1997; Mackenzie et al., 2006) and PCFT (Unal et al., 2009a). Oocyte solutions were adjusted to pH 5.5 using MES. During these experiments, oocytes were continuously superfused with solution (with and without antifolates as indicated) at 5 mL/min.

3.2.8 Proliferation and Colony-forming Assays.

For growth inhibition assays, R2/PCFT4 CHO cells were plated in 96 well culture dishes (2500 cells/well, respectively; total volume of 200 μL medium) with a broad concentration range of drugs. The drugs were dissolved in DMSO such that after dilution the DMSO concentration did not exceed 0.5%. The medium was folate-free RPMI 1640 (pH 7.2) supplemented with 10%

dialyzed fetal bovine serum (dFBS) (Invitrogen), 2 mM L-glutamine, 100 units/mL penicillin and 100 µg/mL streptomycin (hereafter referred to as complete folate-free RPMI 1640 media), containing 25 nM 5-CHO-THF. Cells were routinely incubated for up to 96 h, and metabolically active cells (a measure of cell viability) were assayed with CellTiter-Blue™ cell viability assay (Promega). Fluorescence was measured (590 nm emission, 560 nm excitation) with a Molecular Devices fluorescence plate reader. Data were exported from Softmax Pro software to an Excel spreadsheet for analysis and determinations of IC_{50}s, corresponding to drug concentrations that result in 50% loss of cell growth. In some experiments, the protective effects of adenosine (60 µM), thymidine (10 µM), and 5-amino-4-imidazolecarboxamide (AICA) (320 µM) were tested to validate the intracellular targeted pathways and enzymes for the cytotoxic antifolates. Growth inhibition assays for the PC43-10 CHO were routinely performed in regular RPMI 1640 (pH 7.2) supplemented with 10% dFBS (Invitrogen), 2 mM L-glutamine and 100 units/mL penicillin and 100 µg/mL streptomycin (hereafter referred to as complete RPMI 1640 media), although for a few experiments PC43-10 cells were cultured exactly as for the R2/PCFT4 cells. To follow changes in pH accompanying cell outgrowth, cells were seeded into T75 flasks, using the same media, cell number to volume ratio, and incubation times as for the cytotoxicity assays. Media pH values were measured daily with an Orion 2 Star benchtop pH meter.

For colony-forming assays, R2/PCFT4 cells (500 cells) were harvested in log-phase and plated into 60 mm dishes in complete folate-free RPMI 1640 medium, supplemented with 25 nM 5-CHO-THF and allowed to adhere for 48 h. For continuous drug exposures, R2/PCFT4 cells were then treated with increasing concentrations of drugs and colonies were allowed to outgrow for 10 days. At the end of the incubations, the dishes were rinsed with DPBS, 5% trichloroacetic acid (TCA), and borate buffer (10 mM, pH 8.8), followed by 1% methylene blue (in borate

buffer; 30 min). The dishes were again rinsed with borate buffer, and colonies were counted for calculating percent colony formation relative to the DMSO control.

To test the reversibility of compound **3** drug effects, as reflected in inhibition of colony formation over time, R2/PCFT4 cells were harvested in log phase and 500 cells were plated, allowed to adhere for 48 h, then cultured in the presence or absence of 1 μM antifolate compounds and thymidine (10 μM) plus adenosine (60 μM) for 2, 4, 8, 24, or 48 h, before rinsing with DPBS and adding medium with or without thymidine (10 μM) plus adenosine (60 μM). The dishes were incubated for 10 days, and colonies were counted, as described above, for calculating percent colony formation compared to control.

3.2.9 *In situ* Assays for GARFTase.

Incorporation of [^{14}C(U)]glycine into [^{14}C]formyl GAR as an *in situ* measure of endogenous GARFTase activity in R2/PCFT4 cells was performed using a modification of published methods (Beardsley et al., 1989; Deng et al., 2008). For these experiments, R2/PCFT4 cells were seeded in 5 mL of complete folate-free RPMI 1640 plus 25 nM 5-CHO-THF in T25 flasks at a density of 2 x 10^5 cells per flask. After 48 h, antifolate inhibitor or DMSO (control) was added to the culture medium and the cells were incubated for another 15 h after which the pH of the media was determined with an Orion 2 Star benchtop pH meter. Cells were washed twice with DPBS and resuspended in 5 mL folate-free, L-glutamine-free RPMI 1640 (Sigma) plus penicillin-streptomycin, 10% dFBS, 0.46 g/L $NaHCO_3$ and 1.21 g/L NaCl medium, with or without 0.5-100 nM antifolate and azaserine (4 μM final concentration), and incubated for 30 min. L-glutamine (2 mM final concentration) and [^{14}C]glycine (final specific activity, 0.1 mCi/L) were added, followed by incubation at 37^o C for 8 h, after which time cells were trypsinized and washed twice with ice-cold DPBS. Cell pellets were treated with 2 mL of 5%

TCA at 0° C. Cell debris was removed by centrifugation, samples were solubilized in 0.5 N NaOH and assayed for protein contents (Lowry et al., 1951). The supernatants were extracted twice with 2 mL of ice-cold ether to remove the TCA. The aqueous layer was passed through a 1 cm column of AG1x8 (chloride form), 100-200 mesh (BioRad), washed with 10 mL of 0.5 N formic acid, followed by 10 mL of 4 N formic acid, and eluted with 8 mL of 1 N HCl solution. The elutants were collected as 1 mL fractions and determined for radioactivity.

3.2.10 Determination of Intracellular ATP/GTP Levels.

For analysis of ATP and GTP levels following antifolate treatments, R2/PCFT4 cells were seeded in 10 mL of complete folate-free RPMI 1640 plus 25 nM 5-CHO-THF in T75 flasks at a density of 7 x 10^5 cells per flask. After 48 h, antifolates or DMSO (control) were added to the culture medium. After another 24 h, the cells were trypsinized and washed (2x) with ice-cold DPBS, with a final additional wash with ice-cold DPBS containing 1 mM EDTA. The final cell pellet (2-5 x 10^6 cells) was resuspended in 100 µL of 155 mM NaCl containing 1 mM EDTA and 100 µL of ice-cold 0.6 M TCA was added drop-wise while vortexing. Samples were incubated 10 min on ice with occasional mixing, and then centrifuged (14,000 rpm, 5 min). The supernatant was removed, whereas the protein pellet was solubilized in 0.2 mL of 0.5 N NaOH for protein determinations. Tri-n-octylamine (0.5 M) in trichlorotrifluoroethane (Freon) (1 mL) was added to the supernatant and the mixtures vortexed and incubated for 20 min on ice. Samples were centrifuged and the freon amine (lower) layer was discarded. One mL of methylene chloride was added to the upper layer, followed by mixing, incubation (ice, 10 min), centrifugation, and removal of the organic (lower) layer. Samples were stored at -80°C until analysis. Intracellular adenosine and guanosine triphosphates were measured by a modification of the HPLC method of Huang et al. (2003a). The chromatography system consisted of a Varian

9010 ternary gradient pump, a 9050 variable wavelength detector, and a Varian Star 5.3 data handling system. A 50 µL injection loop was used. The analytical column was a Waters Symmetry C_{18} (5 µm, 150 x 4.6 mm) equipped with a Waters Novapak phenyl pre-column (Waters, Milford, MA). The detection wavelength was set at 254 nm. The flow rate was 1 mL/min. The gradient elution was as follows: 0-30 min at 60% A/40% B; 30-50 min linear at 1%/min to 40% A/60% B; and 50-60 min at 40% A/60% B. Buffer A was comprised of 10 mM tetrabutylammonium hydroxide, 10 mM KH_2PO_4 and 0.25% methanol (MeOH); the pH was adjusted to 6.9 with 1 N H_3PO_4. Buffer B consisted of 5.6 mM tetrabutylammonium hydroxide, 50 mM KH_2PO_4 and 30% MeOH; the pH was adjusted to 7.0 with 1 N KOH. Both solutions were freshly prepared before each experiment and degassed. External standards were used for each assay to construct a standard curve from which cellular levels were calculated. Standards ranged from 0-75 µM for ATP and 0-30 µM for GTP in the initial mobile phase. Variations between standards were 5% or less. Extraction efficiencies were established by adding known amounts of ATP and GTP standards (200 and 50 µM, respectively) to a control sample prior to extraction.

3.3 Results.

3.3.1 Generation of PCFT Stable Transfectants in Transport-impaired CHO Cells.

As part of our larger drug discovery endeavor to establish pharmacophores for all the major folate transporters and to develop transporter-specific drugs, we previously generated novel sublines derived from the RFC, FR-, and PCFT-null MTXRIIOua^{R}2-4 CHO cells (hereafter, simply R2) that ectopically express human RFC protein (designated PC43-10; Figure 3.2, Panel A and E) (Wong et al., 1995) and human FRs (designated RT-16).

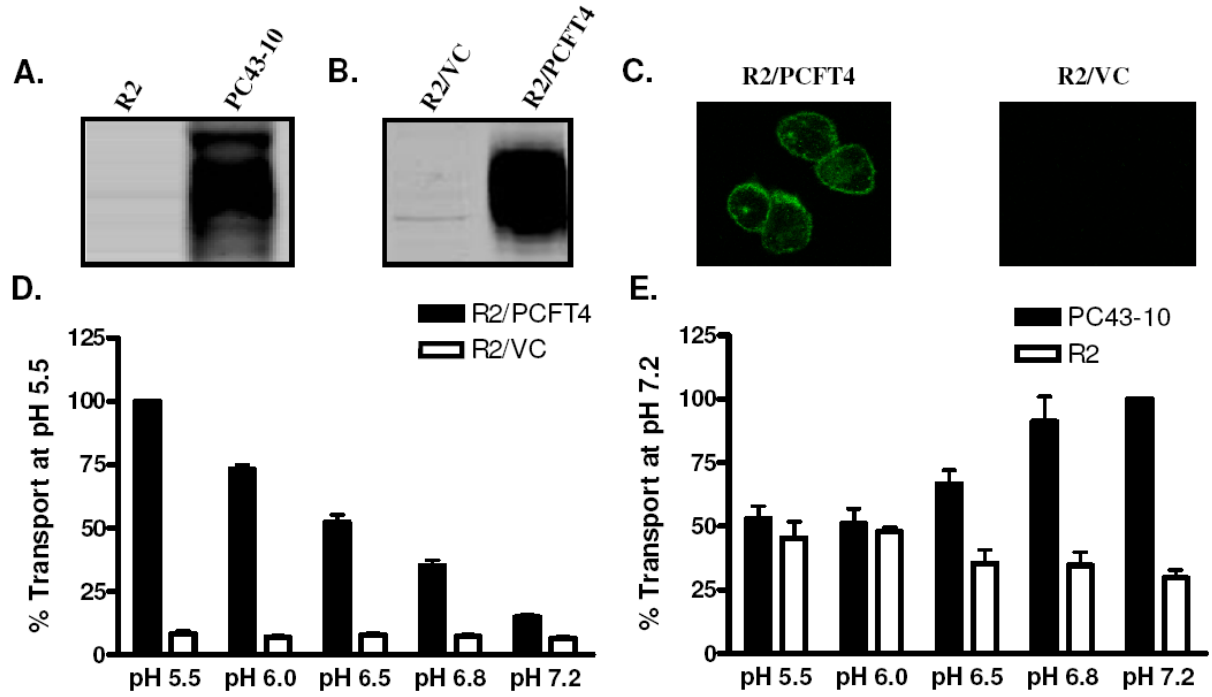

Figure 3.2 Characterization of PCFT protein expression, membrane localization and pH-dependent transport in R2/PCFT4 and R2/VC cells. *Panel A*, Western blot analysis of RFC in PC43-10 and R2 cells. *Panel B*, human PCFTMyc-His6 in R2/PCFT4 and R2/VC cells. Membrane fractions (10 µg) were analyzed by SDS-PAGE and immunoblotting with human RFC and PCFT polyclonal antibody. *Panel C*, Immunofluorescence of R2/PCFT4 and R2/VC cells. Cells were fixed with paraformaldehyde, permeabilized with Triton X-100, stained with anti-myc antibody and visualized using confocal microscopy. *Panel D*, PCFT transport activity in R2/PCFT4 and R2/VC cells was assessed by measuring uptake of 0.5 µM [^{3}H]MTX at 37˚C for 2 min at pH 5.5 or 6.0 in MES-buffered saline, and at 6.5, 6.8, or 7.2 in HEPES-buffered saline. Internalized [^{3}H]MTX was normalized to total protein and expressed as a percent of the transport activity at pH 5.5. *Panel E*, RFC transport activity in PC43-10 and R2 cells was determined by measuring uptake of 0.5 µM [^{3}H]MTX at 37˚C for 2 min at pH 5.5 or 6.0 in MES-buffered saline, and at 6.5, 6.8, or 7.2 in HEPES-buffered saline. As above, internalized [^{3}H]MTX was normalized to total cellular protein and expressed as percent transport at pH 7.2. Transport results are presented as mean values ± standard errors from 6 experiments.

More recently, we generated another R2 subline (R2/PCFT4) that expressed human PCFT (Deng et al., 2009; Kugel Desmoulin et al., 2010b). R2/PCFT4 cells were made by electroporating R2 CHO cells with a Myc-His6-tagged human PCFT ($PCFT^{Myc\text{-}His6}$) cDNA construct. Stable transfectants were selected with G418. Clones were isolated, expanded, and screened by Western blotting. The clonal R2/PCFT4 subline was established that expressed a high level of $PCFT^{Myc\text{-}His6}$ protein (Figure 3.2, Panel B).

By indirect immunofluorescence staining with Myc-specific antibody and Alexa Fluor488-tagged secondary antibody, $PCFT^{Myc\text{-}His6}$ protein was targeted predominantly to the cell surface of R2/PCFT4 cells with some intracellular staining compared to R2/VC (Figure 3.2, Panel C). Expression of $PCFT^{Myc\text{-}His6}$ protein was accompanied by substantial [^{3}H]MTX transport at pH 5.5 during 2 min over the low level measured in vector control R2/VC cells (Figure 3.2, Panel D). Transport at pH 7.2 was ~14% of that at pH 5.5 and at pH 6.8 transport increased to ~35% of that at pH 5.5. For RFC-expressing PC43-10 cells, [^{3}H]MTX transport was active at pH 7.2 as reported (Wong et al., 1995), then fell with decreasing pH and was essentially indistinguishable from the residual low level in R2 cells at pH 5.5 (Figure 3.2, Panel E).

We measured the kinetics for [^{3}H]MTX and [^{3}H]PMX transport in R2/PCFT4 cells over a range of concentrations at pH 5.5 and pH 6.8. Data were analyzed by Lineweaver-Burke plots and are summarized in Table 3.2. Results for MTX showed a 16-fold decrease in K_t and a 2.3-fold increase in V_{max} when the pH was decreased from 6.8 to 5.5, whereas for PMX, the K_t and V_{max} changed 3.7-fold and 4.6-fold respectively. V_{max}/K_t values, a reflection of overall transport efficiency, were calculated for [^{3}H]MTX and [^{3}H]PMX and were 37-, 17-fold higher, respectively, at pH 5.5 than at pH 6.8.

Table 3.1 Growth inhibition by antifolate drugs toward PCFT- and RFC stable R2 CHO and HeLa transfectants. Growth inhibition was measured by a fluorescence (Cell Titer-Blue™)-based assay after 96 h of exposure to a range of inhibitor concentrations. Results are presented as 50% inhibitory concentrations (IC_{50}s) (in nMolar) ± standard errors from >3 experiments. ND, not determined.

Drug	R2/PCFT4	R2/VC	PC43-10	R2	R1-11-RFC6	R1-11-PCFT4
MTX	120.5 ± 16.8	>1000	12 ± 1.1	216 ± 9	35.7±7.1	218.2 (15.1)
GW1843U89	>1000	>1000	11 ± 3.3	>1000	ND	ND
LMX	38.6 ± 5.0	>1000	12 ± 2.3	>1000	36.1±9.9	278.3±26.2
PMX	13.2 ± 2.4	974.0 ± 18.1	138 ± 13	894 ± 93	81.7±5.5	59.3±7.4
PT523	>1000	>1000	1.53 ± 0.16	>1000	3.19±0.4	>1000
RTX	99.5 ± 11.4	>1000	6.3 ± 1.3	>1000	ND	ND
1	>1000	>1000	>1000	>1000	ND	ND
2	>1000	>1000	>1000	>1000	ND	ND
3	23.0 ± 3.3	>1000	648.6 ± 38.1	>1000	>1000	155.0±12.9
4	212.9 ± 28.0	>1000	>1000	>1000	ND	ND
5	>1000	>1000	>1000	>1000	ND	ND
6	>1000	>1000	>1000	>1000	ND	ND
7	>1000	>1000	>1000	>1000	ND	ND
8	>1000	>1000	>1000	>1000	ND	ND
9	>1000	>1000	>1000	>1000	ND	ND
10	>1000	>1000	>1000	>1000	ND	ND
11	>1000	>1000	>1000	>1000	ND	ND
12	>1000	>1000	>1000	>1000	ND	ND
13	>1000	>1000	>1000	>1000	ND	ND

Table 3.1 Growth inhibition by antifolate drugs toward PCFT- and RFC stable R2 CHO and HeLa transfectants. Growth inhibition was measured by a fluorescence (Cell Titer-Blue™)-based assay after 96 h of exposure to a range of inhibitor concentrations. Results are presented as 50% inhibitory concentrations (IC_{50}s) (in nMolar) ± standard errors from >3 experiments. ND, not determined.

Drug	R2/PCFT4	R2/VC	PC43-10	R2	R1-11-RFC6	R1-11-PCFT4
14	291 ± 71	>1000	>1000	>1000	ND	ND
15	135 ± 18	>1000	>1000	>1000	ND	ND
16	3.34 ± 0.26	288 ± 12	101.0 ± 16.6	273.5 ± 49.1	>1000	28.2 ± 7.0
17	43.4 ± 4.1	>1000	>1000	>1000	>1000	99.2 ± 20.2
18	101.4 ± 17.9	>1000	>1000	>1000	ND	ND
19	>1000	>1000	>1000	>1000	ND	ND
20	>1000	>1000	>1000	>1000	ND	ND
21	>1000	>1000	>1000	>1000	ND	ND
22	>1000	>1000	>1000	>1000	ND	ND
23	41.5 ± 13.09	>1000	>1000	>1000	ND	ND
24	63.8 ± 16.23	>1000	>1000	>1000	ND	ND

Table 3.2. Kinetic constants for PCFT - CHO. Kinetic constants for MTX (K_t and V_{max}) and PMX (K_t and V_{max}) were determined with [^{3}H]MTX and [^{3}H]PMX respectively, and calculated from Lineweaver Burke plots with R2/PCFT4 cells. K_i values were determined by Dixon plots with [^{3}H]MTX as substrate and a range of inhibitor concentrations in R2/PCFT4 cells. Results are presented as mean values ± standard errors from 3 experiments.

Substrate	Parameter	pH 5.5	pH 6.8
MTX	K_t (μM)	0.280 ± 0.022	4.52 ± 0.19
	V_{max} (pmol/mg/min)	31.23 ± 4.31	13.72 ± 2.26
	V_{max}/ K_t	111.5	3.0
PMX	K_t (μM)	0.15 ± 0.03	0.56 ± 0.12
	V_{max} (pmol/mg/min)	32.32 ± 6.49	7.06 ± 1.39
	V_{max}/ K_t	215.5	12.6
Compound **3**	K_i (μM)	0.223 ± 0.017	4.07 ± 0.339
Compound **16**	K_i (μM)	0.1278 ± 0.0054	1.816 ± 0.0704
Compound **17**	K_i (μM)	0.132 ± 0.009	1.954 ± 0.024
Compound **18**	K_i (μM)	0.100 ± 0.012	2.234 ± 0.203
Compound **23**	K_i (μM)	0.386 ± 0.095	28.12 ± 5.31
Compound **24**	K_i (μM)	0.424 ± 0.112	30.70 ± 8.53
PMX	K_i (μM)	0.0960 ± 0.012	1.54 ± 0.17
LMX	K_i (μM)	0.249 ± 0.013	12.30 ± 0.96

Thus, as previously reported, transport by PCFT shows extraordinary pH dependence with the greatest activity at acidic pH. Further, the impact of pH on kinetic parameters for PCFT membrane transport varies with different transport substrates (Zhao et al., 2009a).

3.3.2 Chemosensitivities to Classical Antifolate Inhibitors and Identification of Novel Antifolates with PCFT Selectivity over RFC.

We screened R2/PCFT4 and PC43-10 cells for growth inhibition in the continuous presence of established antifolates including MTX, GW1843U89, LMX, PMX, PT523 and RTX. Growth inhibition results for PC43-10 were compared to those for R2 cells and R2/PCFT4 results were compared to R2 cells transfected with empty pCDNA3.1 vector (R2/VC) (Deng et al., 2009; Kugel Desmoulin et al., 2010b) (Table 3.1). Assays were performed at pH 7.2 in complete RPMI 1640 (for RFC-expressing PC43-10 and R2), or in complete folate-free RPMI 1640 supplemented with 25 nM 5-CHO-THF (for R2/PCFT4 and R2/VC cells). For most of the antifolates, drug sensitivities, as reflected in decreased IC_{50}s for inhibition of growth over 96 h, were increased in both R2/PCFT4 and PC43-10 cells over respective controls (Table 3.1). With RFC-expressing PC43-10 CHO cells, sensitivities to the classical antifolates were significantly increased (from 6.5-fold for PMX to >159-fold for RTX) over R2 cells. Likewise, R2/PCFT4 cells were sensitive to the classical inhibitors (>8.3- to 74-fold, compared to negative controls). Neither GW1843U89 nor PT523 showed any activity toward R2/PCFT4 cells. Since PCFT is optimally active at acidic pHs (Figure 3.2, Panel D), we measured the changes in media pH during the interval of drug exposure. Over 96 h, the pH of the media decreased linearly and reached pH 6.7 to 6.9 by day 4 (data not shown). Thus, at extracellular pHs approximating those associated with solid tumor microenvironments, several of these classical agents appeared to be substrates for PCFT in R2/PCFT4 cells, as reflected in patterns of growth inhibition. PT523 and

GW1843U89 were completely selective toward RFC over PCFT. Only PMX showed any indication of selective activity toward PCFT over RFC, (i.e., 74-fold increased activity for R2/PCFT4 cells versus 6.5-fold for the PC43-10 cells, compared to respective negative controls). However, this was incomplete; i.e., PMX was appreciably active toward both PCFT- and RFC-expressing cells.

Initial testing of the 6-substituted pyrrolo[2,3-*d*]pyrimidine benzoyl antifolate series as inhibitors of growth in the isogenic CHO sublines, revealed that compounds **1**, **2**, and **4-6** were all completely inert toward PC43-10 cells, establishing a lack of RFC transport activity for this series (Table 3.1). The 3-carbon analog of this series, compound **3**, showed a low level activity toward PC43-10 cells. Compounds **3** and **4** were active toward PCFT-expressing R2/PCFT4 cells, and **3** was more potent than **4** by ~9-fold (IC_{50}s of ~23 and ~213 nM, respectively). Conversely, compounds **1**, **2**, **5**, and **6** were completely inactive (Table 3.1). This result with compounds **3** and **4** is the first identification of an antifolate with selectivity for PCFT-mediated uptake with no or very little substrate activity for RFC (Deng et al., 2008; Kugel Desmoulin et al., 2010b).

The 6-substituted thieno[2,3-*d*]pyrimidine benzoyl antifolate series exhibited a different substrate specificity than compounds **3** and **4** when growth inhibition was measured in the CHO sublines. Compounds **8** and **9** were characterized by potent and selective substrate activities for FRα and FRβ (**8 = 9 > 10 > 11**) (data not shown) and negligible substrate activities for both RFC and PCFT (Table 3.1) (Deng et al., 2009; Kugel Desmoulin et al., 2010b). The most potent analogs of the series, compounds **8** and **9**, with 3- and 4-methylene groups in the bridge region, respectively, showed activities similar to those for the most active classical inhibitors, LMX and RTX, toward FR-expressing cells, but were somewhat more active than either PMX or MTX.

The finding of FR- but not PCFT selectivity for this series is particularly interesting given the report of possible direct functional coupling between these transport systems (Zhao et al., 2009b). Our results with 6-substituted thieno[2,3-*d*]pyrimidine benzoyl antifolate substrates for FR establish that, should FR-PCFT coupling occur, this must not be obligatory.

Growth Inhibition of the 6-substituted pyrrolo[2,3-*d*]pyrimidine thienoyl antifolate series in the isogenic CHO cell line panel found that while **14**, **15** and **17**-**19** were inert toward RFC-expressing PC43-10 cells and R2 cells up to 1000 nM drug, compound **16** showed evidence of a non-FR, non-PCFT cellular uptake process at higher drug concentrations (seemingly in part mediated by RFC and also by a non-RFC uptake mechanism), although substantial FR- and PCFT-selectivity over RFC (as reflected in relative IC_{50}s) was nonetheless preserved (Table 3.1). Of the pyrrolo[2,3-*d*]pyrimidine thienoyl antifolates, **16** (3-carbon bridge) and **17** (4-carbon bridge) are the most potent agents toward PCFT-expressing R2/PCFT4 cells. Compounds **16**, **17** and **18** showed a high level of PCFT-targeted activity, for PCFT-expressing R2/PCFT4 cells with IC_{50}s of 3.34, 43 and 101 nM, respectively (Table 3.1). Activity substantially declined for compounds **14** and **15** with 1- and 2-carbon bridge lengths, respectively, and compound **19** was completely inert. Compound **16** was more active than the classic agents and was likewise more so than compound **17**. This was most impressively reflected in the ~11-fold decrease in IC_{50} (~3 nM) toward PCFT-expressing R2/PCFT4 cells with **16** compared to **17** (Kugel Desmoulin et al., 2011; Wang et al., 2010; Wang et al., 2011).

Finally, 6-substituted pyrrolo[2,3-*d*]pyrimidine thienoyl regioisomers with 4-carbon bridge lengths and with contiguous thiophene substitutions [2’3’ (**20**); 4’5’ (**21**); 3’4’(**22**)] were completely inactive toward the RFC- and PCFT-expressing CHO sublines (Table 3.1). Compounds **23** and **24** were likewise inert toward PC43-10 cells, although both compounds

inhibited proliferation of R2/PCFT4 cells (IC_{50}s of 41.5 and 63.8 nM for **23** and **24**, respectively), essentially equivalent to compound **17** (IC_{50} of 43.4 nM) (Table 3.1). This establishes cellular uptake of compounds **23** and **24** by PCFT. Drug sensitivities for **23** and **24** with R2/PCFT4 cells exceeded those for MTX and RTX, and were comparable to those for LMX. However, **23** and **24** were less potent than PMX (~3- and ~5-fold, respectively) and **16** (~12- and ~19-fold, respectively). None of the 6-substituted pyrrolo[2,3-*d*]pyrimidine regioisomers (**17** and **20**-**24**) had any impact on proliferation of R2 or R2/VC cells (Wang et al., 2012).

Since nucleoside salvage mechanisms circumvent biosynthetic requirements for reduced folates and growth inhibitory effects of classical antifolates such as MTX, we tested excess adenosine and thymidine for their capacities to abolish the growth inhibitory effects of the most potent analogs (compounds **3**, **16** and **17**). Results were compared to those for PMX, reported to act as an inhibitor of both purine nucleotide biosynthesis primarily at TS and AICARFTase and less so at GARFTase (Racanelli et al., 2009; Shih and Thornton, 1999), and for LMX, an established inhibitor of GARFTase (Beardsley et al., 1989; Mendelsohn et al., 1999; Moran et al., 1989). Whereas thymidine (10 μM) also protected R2/PCFT4 cells from the growth inhibitory effects of low concentrations (<50 nM) of PMX, at higher PMX concentrations, protection was incomplete with thymidine either in the presence or absence of AICA (320 μM) (Figure 3.3, Panel A), which is metabolized to AICAR (circumvents drug effects at GARFTase). Adenosine (60 μM) could not circumvent effects of PMX. However, growth inhibition by PMX was completely reversed by adenosine combined with thymidine. Analogous results were previously described for nucleoside protection from the inhibitory effects of PMX for CCRF-CEM cells (Racanelli et al., 2009). In contrast, for LMX and compounds **3**, **16** and **17**

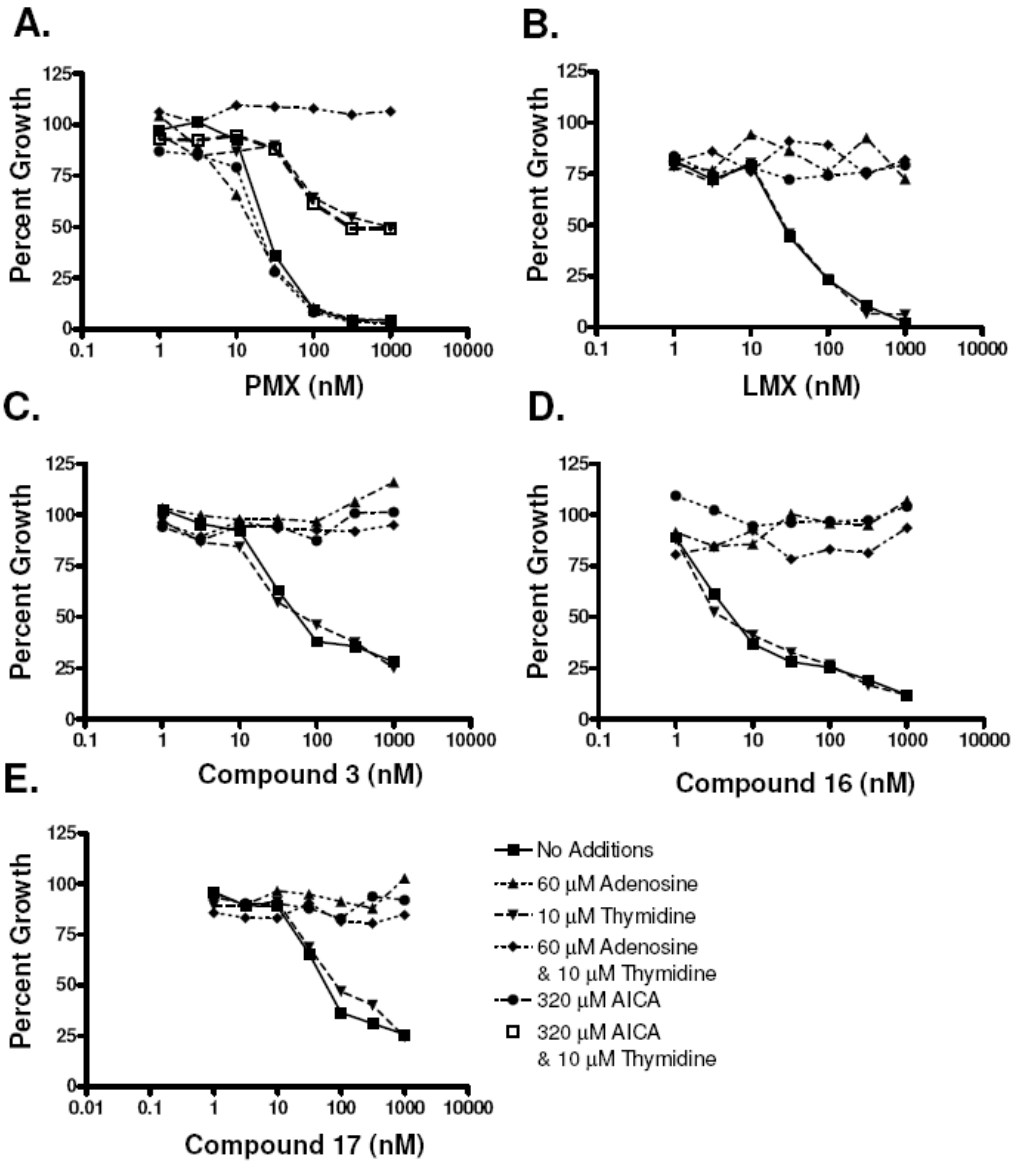

Figure 3.3 Protection of R2/PCFT4 cells from growth inhibition by PMX, compounds 3, 16 and 17 in the presence of nucleosides and 5-amino-4-imidazole (AICA). Proliferation inhibition was measured for R2/PCFT4 cells over a range of concentrations of PMX (*Panel A*), LMX (*Panel B*), **3** (*Panel C*), **16** (*Panel D*) or **17** (*Panel E*), as shown, in complete folate-free RPMI 1640 with 25 nM 5-CHO-THF, in the presence or absence of adenosine (60 µM) or thymidine (10 µM), or AICA (320 nM). Cell densities were measured with CellTiter-Blue™ fluorescence dye and a fluorescence plate reader. Results were normalized to cell density in the absence of drug. Results shown are representative data of experiments performed in triplicate.

(Figure 3.3, Panels B-D), growth inhibition was abolished by either adenosine or AICA alone. These results establish *de novo* purine nucleotide biosynthesis as the targeted pathway for compounds **3**, **16** and **17** and GARFTase as the principal intracellular enzyme target, analogous to LMX (Beardsley et al., 1989).

Cytotoxicity assays were extended to include colony-forming assays. Colony-forming assays were performed in which R2/PCFT4 cells were continuously exposed to a range of concentrations of compounds **3, 16, 17**, PMX, or LMX for 10 days (Figure 3.4, Panels A-E). Colonies were scored by counting visible colonies after 10 days and are presented as a percent of the vehicle control. Composite results are presented as mean values ± standard errors from 3 experiments (Panel E). As an inhibitor of colony-formation, compounds **3** (Panel B)**, 16** (Panel C) and **17** (Panel D) gave IC_{50}s of 17.14 $\pm$ 0.74 nM (SEM), 1.41 $\pm$ 0.03 nM and 27.17 $\pm$ 2.89 nM, respectively, whereas IC_{50}s for PMX (Panel A) and LMX were 4.94 $\pm$ 0.48 nM and 29.70 $\pm$ 0.59 nM, respectively.

To establish the time-dependent requirements for loss of clonogenicity upon exposure to compound **3**, LMX, or PMX, R2/PCFT4 cells were exposed to the drugs (each at 1 μM) for different times (2, 4, 8, 24, 48, and 72 h), after which drug was removed and cells were incubated in the presence or absence of adenosine (60 μM) and thymidine (10 μM). A parallel incubation was performed in which cells were treated with drugs and nucleosides, after which drugs were removed and cells incubated in the presence of adenosine and thymidine. Colonies were counted after 10 days, with results compared to those for the untreated vehicle (DMSO) control. Nucleoside protection, both during and after drug treatments, completely protected R2/PCFT4 cells from loss of colony formation. When cells were treated during the initial incubation with antifolates *without nucleoside protection*, colony formation was significantly inhibited whether

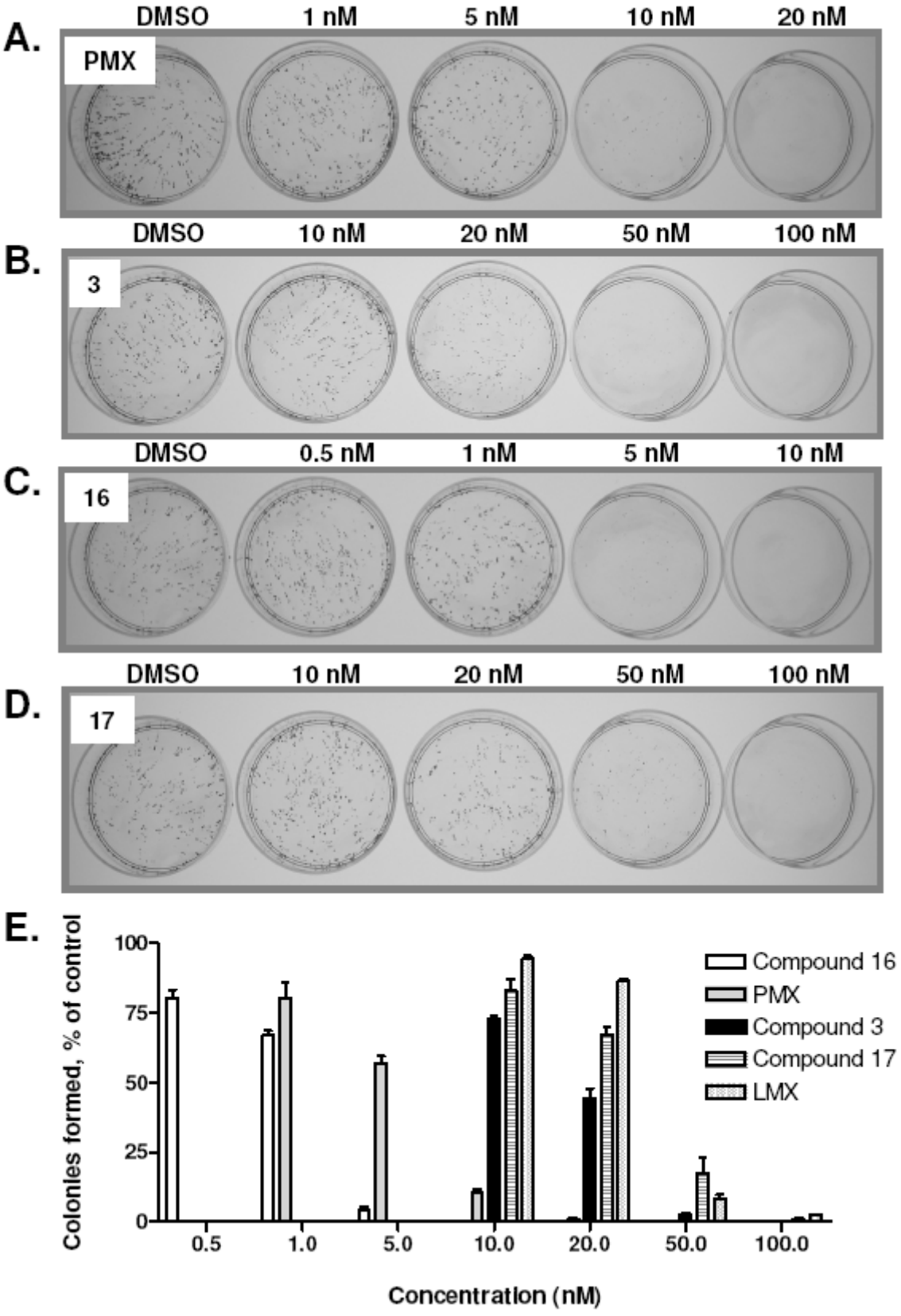

Figure 3.4 Inhibition of colony formation. R2/PCFT4 cells were plated into 60 mm dishes at a density of 500 cells per dish in the presence or absence of different concentrations of PMX (*Panel A*), **3** (*Panel B*), **16** (*Panel C*) or **17** (*Panel D*) from 1 to 100 nM. Colonies were scored by counting visible colonies after 10 days and are presented as a percent of the vehicle control. Results are presented as mean values ± standard errors from 3 experiments (*Panel E*).

or not nucleosides were included after the drug was removed (Figure 3.5). The difference between these two conditions established a time-requirement for *irreversible* drug effects resulting in loss of clonogenicity and ranged from greater than 4 h for PMX (Figure 3.5, Panel A) and compound **3** (Panel C), to greater than 8 h for LMX (Panel B). For all drugs thereafter, there was a progressive diminution of the protective effects such that by 48-72 h, loss of colony formation was essentially complete. For compound **3** treatments, a visual representation of the stained colonies has been included to demonstrate the time-dependent irreversible drug effects (Panel D).

3.3.3 PCFT-selective Transport Characteristics for Compounds 3, 16 and 17.

Growth inhibition results (Table 3.1) strongly suggested selective membrane transport by PCFT and not RFC for compounds **3, 16** and **17**. For further confirmation, we tested these compounds (10 μM) as direct competitors for inhibition of PCFT-mediated uptake of [^{3}H]MTX (0.5 μM) in R2/PCFT4 cells from pH 5.5 to 7.2, and compared the results to those for PMX and PT523, established RFC substrates. A parallel experiment was performed with PC43-10 cells to assess the inhibitory effects of compounds **3, 16** and **17** (10 μM) on RFC-mediated [^{3}H]MTX uptake (at pH 7.2), compared to other established RFC transport substrates. As shown in (Figure 3.6, Panel A), with R2/PCFT4 cells, compounds **3, 16** and **17** were potent inhibitors of PCFT transport, only slightly less so than PMX and with substantially increased potencies at pH values less than 7.2. As expected (Zhao and Goldman, 2007), PT523 did not inhibit [^{3}H]MTX uptake at any pH for R2/PCFT4 cells. For RFC-expressing PC43-10 cells at pH 7.2, PT523, PMX, RTX, LMX, and 5-CHO-THF all potently inhibited [^{3}H]MTX transport (Figure 3.6, Panel B). However, compounds **3, 16** and **17** were *essentially inert* as inhibitors of RFC.

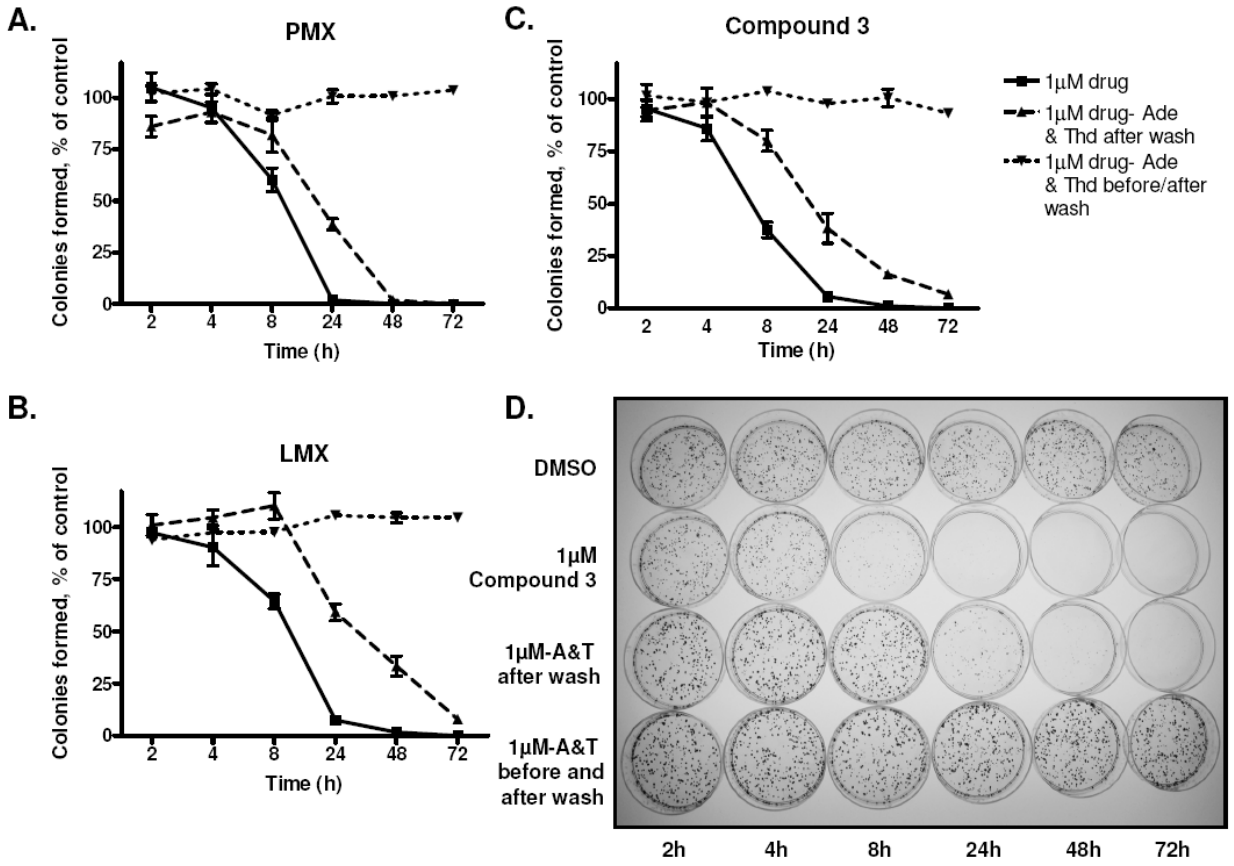

Figure 3.5 Time dependence for loss of clonogenicity in R2/PCFT4 cells treated with PMX, LMX and compound 3. R2/PCFT4 cells were plated into 60 mm dishes at 500 cells per dish and allowed to adhere for 48 h, after which cells were treated with or without 1 μM drug in the presence or absence of adenosine (60 μM) and thymidine (10 μM) for 2, 4, 8, 24 and 48 h. Following drug treatment, cells were washed with DPBS and resuspended with drug-free media with or without adenosine (60 μM) and thymidine (10 μM) protection. Colonies were enumerated after 10 days and results are presented as a percent of vehicle control. *Panel A*, PMX. *Panel B*, LMX. *Panel C*, Compound **3**. *Panel D*, Representative image of dishes that were counted to produce *Panel C*. Results are presented as mean values ± standard errors from 3 experiments. Abbreviations: Ade, adenosine; Thd, thymidine.

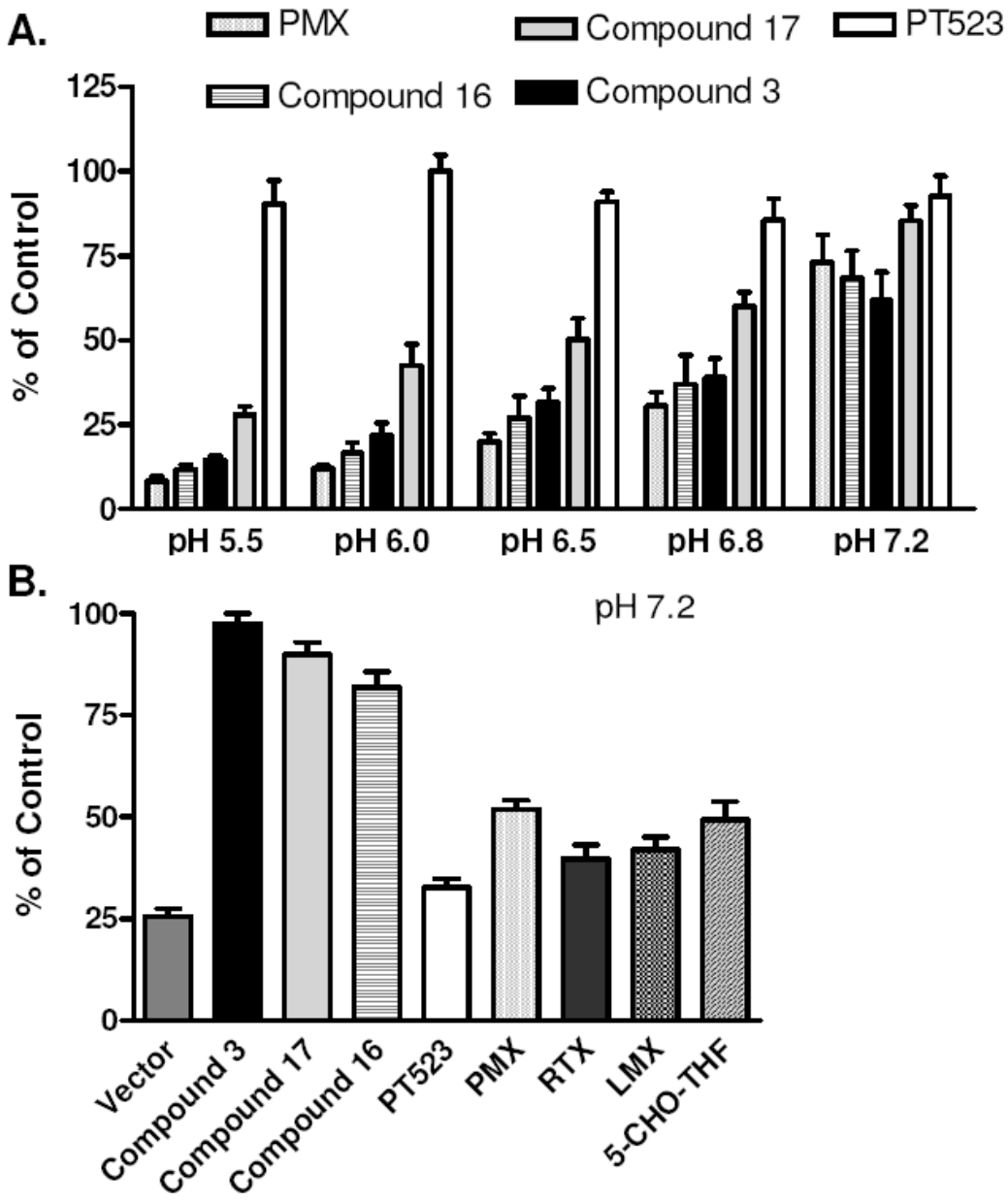

Figure 3.6 Competitive inhibition of PCFT and RFC transport of [^{3}H]MTX. *Panel A*, R2/PCFT4 cells ectopically expressing PCFT but no FR or RFC were assayed for [^{3}H]MTX transport in the presence of 10 µM PMX, compounds **3**, **16**, **17** and PT523 at pH 5.5-7.2. *Panel B*, R2 cells (vector) expressing no RFC, PCFT or FR and PC43-10 cells expressing RFC but no PCFT or FR were assayed for [^{3}H]MTX transport in the presence of 10 µM compounds **3**, **16**, **17**, PT523, PMX, RTX, LMX, or 5-CHO-THF at pH 7.2. Results are presented as mean values ± standard errors from >3 experiments.

We used Dixon analysis at pH 5.5 and pH 6.8 with R2/PCFT4 cells and [^{3}H]MTX to calculate K_is for PCFT competitors including compounds **3, 16, 17**, PMX and LMX (Table 3.2). Transport of 0.5 μM [^{3}H]MTX was measured over a range of inhibitor concentrations. The relative affinities of our lead compounds to PCFT were similar to PMX and are as follows: PMX < **17** < **16** < **3** < LMX. K_i values increase 14-18 fold at pH 6.8 for all compounds except LMX which had a 50-fold increased K_i at pH 6.8. For PMX, the K_is closely approximated the K_ts recorded with [^{3}H]PMX.

To confirm that compounds **3, 16,** and **17** are transported by PCFT, electrophysiological studies were performed in *Xenopus* oocytes injected with PCFT cRNA. Uptake was assessed in oocytes clamped to -90 mV at a bath pH of 5.5. A substrate concentration of 5 μM was used, which is saturating for 5-CHO-THF and PMX. These experiments show that the currents induced by compounds **3, 16** and **17** were comparable to that produced by 5-CHO-THF (Figure 3.7).

3.3.4 Identification of *de novo* Purine Nucleotide Biosynthesis and GARFTase as Primary Cellular Targets for Compounds 3, 16 and 17.

Our protection studies further identified *de novo* purine nucleotide biosynthesis as the primary targeted pathway following PCFT transport of the 6-substituted pyrrolo[2,3-*d*]pyrimidine –benzoyl (**3**) and –thienoyl antifolates (**16** and **17**). To confirm the inhibition of purine nucleotide biosynthesis by compounds **3, 16** and **17**, we measured ATP and GTP pools by HPLC in R2/PCFT4 cells for compounds **3**, **16** and **17**. For compound **3,** cells were treated with increasing concentrations for 24 h and results were compared to those of LMX; results are shown as a percentage of control ATP and GTP levels (Figure 3.8, Panel A). Additionally, cells were treated with 1 μM of **16** and **17** for 24 h at pH 6.8, and results were compared to those for LMX and PMX (both at 1 μM) (Figure 3.8, Panel B). GTP and ATP pools

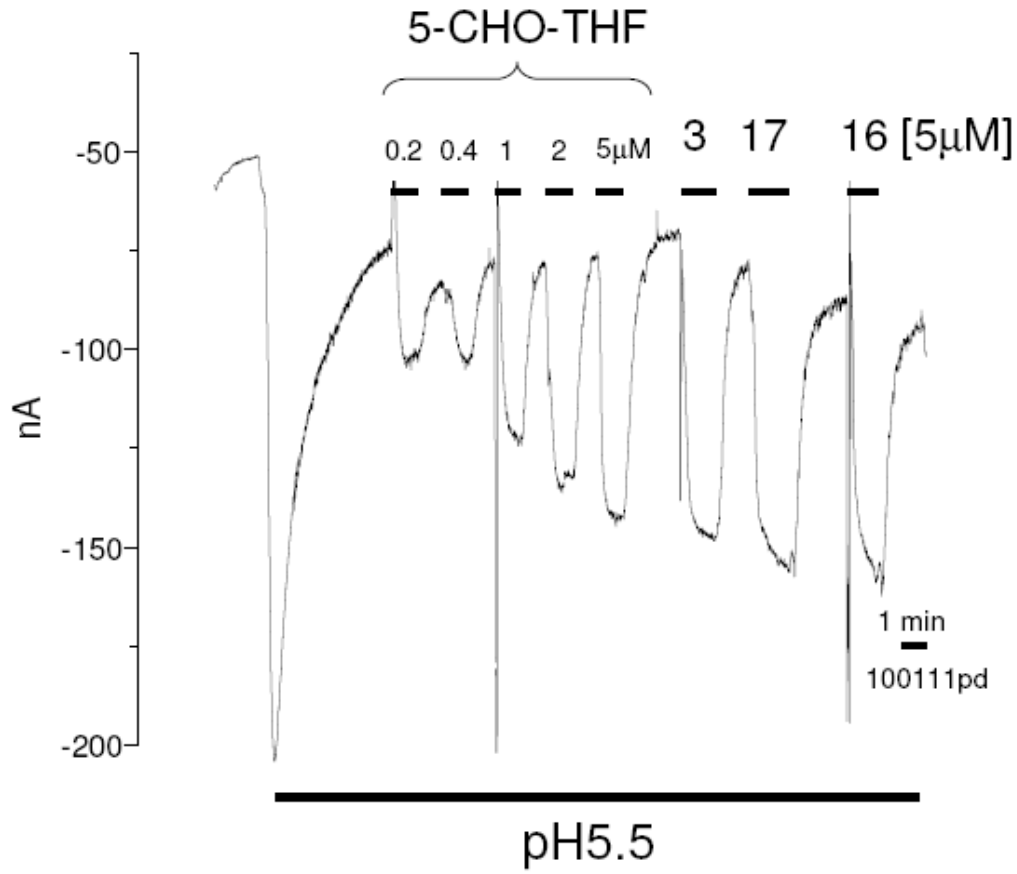

Figure 3.7 Electrophysiology studies of antifolate transport by PCFT in *Xenopus* oocytes. Substrate-induced currents (nA) were recorded in individual oocytes injected with wild type PCFT and voltage clamped to a holding potential (*V*h) of -90 mV. Oocytes were perfused with ND90 solution at pH 5.5 with 5-CHO-THF followed by compounds **3**, **17** and **16**. For all substrates, concentrations were maintained at a level of 5 μM.

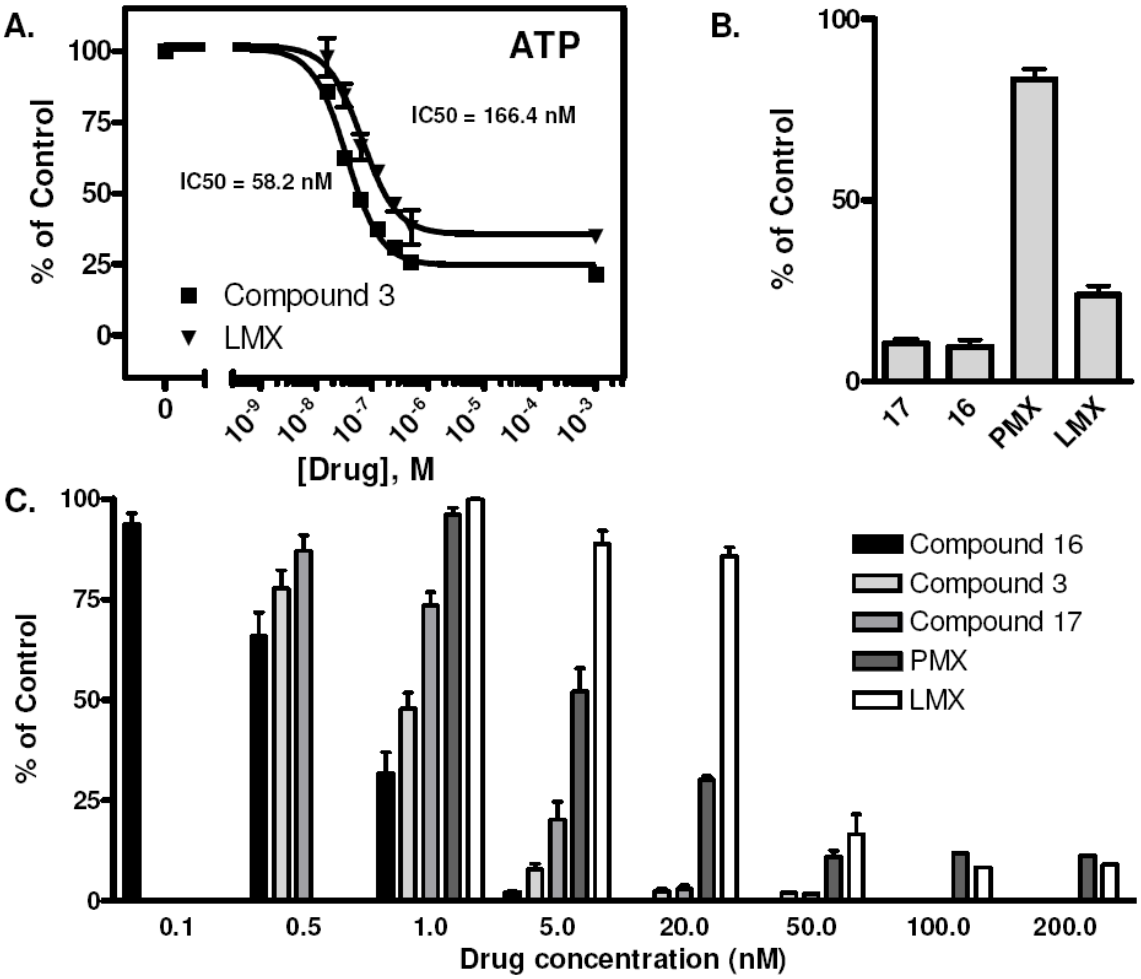

Figure 3.8 Intracellular ATP levels and *in situ* GARFTase inhibition in R2/PCFT4 cells treated with compounds 3, 16, 17, LMX, and PMX. *Panel A*, for analysis of ATP levels, cells were treated with various concentrations of compounds **3** or LMX for 24 h. Nucleotides were extracted and ATP pools were determined by a modification of the HPLC method of Huang et al. (2003a). Details are provided in the Materials and Methods. *Panel B*, R2/PCFT4 cells were treated with 1 μM **17**, **16**, PMX, or LMX, or solvent (0.5% DMSO for **3**, **16** and **17**, H_2O for PMX and LMX) for 24 h. Cells were washed, and nucleotides were extracted and analyzed by HPLC. Results are shown for percentage control ATP after the drug treatments. *Panel C*, GARFTase activity and inhibition were evaluated *in situ* with R2/PCFT4 cells. Accumulation of [^{14}C]formyl GAR from [^{14}C]glycine was measured in R2/PCFT4 cells treated with the antifolates. The production of [^{14}C]formyl GAR was calculated as a percent of vehicle control over a range of antifolate concentrations. Results are presented as the mean values (standard errors from 3 experiments. Methodologic details are described in the Experimental Procedures section. IC_{50}s were as follows: 0.97 nM, **3**; 0.69 nM, **16**; 1.96 nM, **17**; 31.5 nM LMX; and 7.3 nM, PMX.

were severely depleted (approximately 50 and 75%, respectively) during a 24 h exposure of R2/PCFT4 cells to 1 μM of either compound **3** or LMX. For ATP pools, IC_{50} values of 58 and 166 nM were measured for compound **3** and LMX, respectively (Figure 3.8, Panel A). For GTP pools, IC_{50} values were 441 and 579 nM, respectively (data not shown). Treatment of R2/PCFT4 cells with either 1 μM **16** or **17** for 24 h resulted in profound depletion of ATP pools (90%), which exceeded the decrease resulting from treatment with LMX (76%). PMX treatment, on the other hand only minimally impacted ATP pools (17%) (Figure 3.8, Panel B). Similar results were reported by Chen et al. (1998).

To confirm GARFTase inhibition and to provide a metabolic "read-out" for PCFT transport of compounds **3, 16** and **17** in R2/PCFT4 cells, we used an *in situ* assay for GARFTase. GARFTase catalyzes formylation of the glycine-derived nitrogen of GAR, producing formyl GAR with 10-formyl THF as the one-carbon donor. The *in situ* GARFTase assay measures incorporation of [^{14}C]glycine into [^{14}C]formyl GAR in the presence of azaserine (4 μM) (Beardsley et al., 1989; Deng et al., 2008). Modifications were made in the original protocol to measure GARFTase inhibition under pH conditions which permitted PCFT transport. Briefly, R2/PCFT4 cells were cultured for 48 h in complete folate-free media supplemented with 25 nM 5-CHO-THF. The 48 h incubation allowed the cells to adhere and the pH of the culture media to decrease to ~6.9 accompanying cell growth. Cells were then treated for 15 h with or without a range of concentrations of compounds **3, 16** and **17**, or with PMX or LMX, after which cells were washed, resuspended in complete L-glutamine- and folate-free medium with or without drug and then treated with azaserine for 30 min, after which L-glutamine and [^{14}C]glycine were added. After an additional 8 h, cells were washed, proteins were precipitated with TCA, and the

supernatants were ether-extracted and fractionated on anion exchange columns so that [^{14}C]formyl GAR could be measured and IC_{50}s calculated.

Our results demonstrate that PMX, LMX, and compounds **3, 16** and **17** all inhibited [^{14}C]formyl GAR accumulation in R2/PCFT4 cells at ~pH 6.9 when PCFT is the *sole* mode of antifolate drug delivery (Figure 3.8, Panel C). Compound **16** was by far the most potent of these drugs with an impressive IC_{50} for GARFTase inhibition of 0.69 nM. Relative drug sensitivities for the other lead compounds and classic antifolates were as follows, IC_{50}s (in nM) are in parentheses: **3** (0.97) > **17** (1.96) > PMX (7.3) > LMX (31.5). The most potent inhibitors were compounds **3** and **16**, suggesting that the chain length of the bridge region is an important determinant of GARFTase inhibition regardless of whether the compound is a pyrrolo[2,3-*d*]pyrimidine –benzoyl or –thienoyl. GARFTase inhibition is the ultimate determinant of growth inhibition, with the IC_{50}s following the same trend, **16 > 3** > **17** (Table 3.1).

3.4 Discussion.

Chemotherapy activity of classic antifolates has traditionally been interpreted in terms of their active membrane transport into tumors by RFC (Matherly et al., 2007). Furthermore, impaired membrane transport due to loss or mutations of RFC was reported to result in antifolate resistance (Assaraf, 2007; Matherly et al., 2007; Zhao and Goldman, 2003). However, after reports of a novel low-pH transporter termed PCFT (Nakai et al., 2007; Qiu et al., 2006; Zhao and Goldman, 2007) and the recognition that PCFT is expressed and functional in human solid tumors (Chapter 2) and can efficiently transport cytotoxic antifolates, such as MTX, at pH values approximating those of solid tumors (Chapter 2), it becomes necessary to examine the possibility that PCFT could represent an important mode of chemotherapy drug transport.

Because most cultured cells endogenously express more than one folate transport system (Chapter 2), to explore the role of PCFT in delivery of cytotoxic antifolates, we engineered the R2/PCFT4 CHO subline from PCFT-, RFC-, and FR-null R2 cells to express PCFT without either RFC or FRs. R2/PCFT4 cells exhibited optimal transport activity at acidic over neutral pHs, reflecting high-affinity transport of substrates with decreasing pH. The impact of pH on transport by PCFT was substantially different between (anti)folate substrates. By growth inhibition assays, R2/PCFT4 cells were sensitive to classic antifolates, including MTX, RTX, PMX, and LMX, suggesting their membrane transport by PCFT; PMX was the most active transport substrate and neither GW1843U89 nor PT523 was growth inhibitory. Although PCFT exhibits limited transport at neutral pH typical of culture media, transport of these cytotoxic antifolates by PCFT was enhanced by the progressively decreasing pH that accompanies cell outgrowth. PMX is a 5-substituted pyrrolo[2,3-*d*]pyrimidine benzoyl analog and is the best substrate previously described for PCFT (Zhao and Goldman, 2007). Because PMX was a potent inhibitor of R2/PCFT4 cell growth, we compared the growth inhibitory effects of a number of structurally related 6-substituted pyrrolo or thieno[2,3-*d*]pyrimidine benzoyl or thienoyl antifolates with bridge lengths from one to eight methylenes (depending on the drug series) as inhibitors of R2/PCFT4 cell proliferation.

The 6-substituted pyrrolo[2,3-*d*]pyrimidine with a –benzoyl B ring and three methylenes (compound **3**) or a -thienoyl B ring and three or four methylenes (compounds **16** and **17,** respectively) were potent inhibitors of R2/PCFT4 cell growth or clonogenicity. Additionally, these compounds were essentially inert toward RFC-expressing PC43-10 cells, thus establishing these analogs as our lead compounds for future studies. It is noteworthy that compounds **3, 16** and **17** all selectively inhibited transport of [^{3}H]MTX by PCFT with potencies only slightly less

than that for PMX, as reflected in K_i values, and with nearly identical pH dependencies. After microinjection of PCFT cRNA into *X. laevis* oocytes, perfusion with a saturating concentration of compounds **3**, **16** and **17** elicited a current, confirming that these compounds are electrogenically transported by PCFT. Collectively, these results establish that the cytotoxic 6-substituted pyrrolo[2,3-*d*]pyrimidine –benzoyl compound **3** and –thienoyl compounds **16** and **17** are *bona fide* transport substrates for PCFT, essentially on par with PMX. However, unlike PMX, compounds **3**, **16,** and **17** have nominal transport activity with RFC.

Compound **3** was previously reported to be cytotoxic toward cells that express high levels of FRα, reflecting inhibition of GARFTase, the trifunctional enzyme that catalyzes the second, third, and fifth reactions of *de novo* purine nucleotide biosynthesis, including the first folate-dependent step (Deng et al., 2008). Consistent with primary inhibition of GARFTase after transport by PCFT, both adenosine and AICA protected R2/PCFT4 cells from growth inhibition by compounds **3**, **16** and **17**. By an *in situ* GARFTase assay, which measures [^{14}C]glycine incorporation into formyl GAR, compounds **3**, **16** and **17** were disproportionately inhibitory, with IC_{50} values less than 1 nM, far lower than the IC_{50} for LMX. Although PMX is primarily an inhibitor of TS and was recently reported to inhibit AICARFTase in CCRF-CEM cells (Racanelli et al., 2009), in R2/PCFT4 CHO cells, appreciable GARFTase inhibition was detected, albeit less than that for compounds **3**, **16** and **17**.

These results describe the first PCFT-selective antifolates and establish that PCFT is a surprisingly efficient means of cytotoxic drug delivery. The much higher concentrations of compounds **3**, **16** and **17** needed to inhibit colony formation and cell proliferation, or to significantly suppress ATP/GTP pools versus those required to inhibit GARFTase in cells, must reflect the nature of the enzyme target and requirement for sustained inhibition of GARFTase

and *de novo* purine biosynthesis for cell killing. Indeed, sustained exposures to GARFTase inhibitors were required to irreversibly inhibit colony formation of R2/PCFT4 cells, although an analogous time-dependence was obtained with PMX. Similar results were previously reported when comparing effects on clonogenicity of GARFTase inhibition by LMX versus TS inhibition by RTX in WiDr colonic carcinoma cells (Smith et al., 1993). The higher concentrations of LMX over compound **3** needed to inhibit GARFTase in cells relative to those required to manifest cytotoxicity provide further evidence that GARFTase inhibition is not limiting to cell killing. The decreased GARFTase inhibition for LMX in R2/PCFT4 cells probably reflects its reduced transport by PCFT compared with compound **3**, although factors such as differences in the extent of polyglutamate synthesis may also contribute. High-level substrate activity was previously reported for compound **3** for human FPGS (Gangjee et al., 2004); however compounds **16** and **17** have not been directly tested. The delay in irreversible drug effects upon inhibition of GARFTase may reflect salvage of purines generated from breakdown of nucleic acids (Bronder and Moran, 2002; Smith et al., 1993). Accordingly, the delay for irreversible cell death by GARFTase inhibitors may be substantially shortened in cells that have defects in purine salvage, increasing dependence on *de novo* purine synthesis. For instance, deletions of MTAP have been described in human malignancies, including ~70% of pleural mesotheliomas (Illei et al., 2003) and 38% of NSCLC (Schmid et al., 1998). On this basis, GARFTase inhibitors such as compounds **3**, **16**, and **17** may show far greater potencies in MTAP-deficient tumors, especially if there are high levels of PCFT.

It will be interesting to determine whether the ATP depletion caused by GARFTase inhibitors will lead to an increase in NRF-1, upregulation of PCFT transcription and enhanced

activity of the drug in tumor cells. Conversely, there could be an upregulation of *de novo* purine biosynthesis enzyme expression and subsequent resistance to GARFTase inhibitors.

Finally, the present results, combined with earlier studies of 6-substituted pyrrolo- and thieno[2,3-*d*]pyrimidine antifolates (Deng et al., 2009; Wang et al., 2010) begin to establish a structure activity relationship for PCFT-selective antifolates and shed light on the impact of both aromatic ring systems and the length of the bridge domain on transport by PCFT versus other folate transporters. Thus, antifolates with thieno[2,3-*d*]pyrimidine and benzoyl rings (designated A and B rings, respectively) (Figure 3.1) are effective transport substrates for FRs but not for RFC or PCFT, with optimal activity for the 3- and 4-carbon bridge analogs (Deng et al., 2009). Replacement of the thieno[2,3-*d*]pyrimidine A ring with a pyrrolo[2,3-*d*]pyrimidine system favors binding and transport by both PCFT and FRs, regardless of whether the B ring is a benzoyl (**3**) or thiophene (**16** and **17**). For the pyrrolo[2,3-*d*]pyrimidine -benzoyl and -thienoyl series, decreasing the bridge lengths between the bicyclic scaffold and L-glutamate from 8- to 4-carbons (**4** and **17**) substantially increased the antiproliferative activities of the analogs, reflecting transport by PCFT. Further decreasing the bridge length of these compounds from 4- to 3-carbons (**3** and **16**) increased drug potencies; however, this appeared to be accompanied by some loss of absolute transporter specificity for PCFT over RFC. Decreasing the bridge length to 1- or 2-carbons caused complete loss of activity.

In conclusion, we document PCFT-selective transport over RFC for the potent 6 substituted pyrrolo[2,3-*d*]pyrimidine -benzoyl and -thienoyl antifolate series, particularly compounds **3**, **16** and **17**. Our results strongly suggest the therapeutic potential of PCFT for targeting drugs to tumors. The notion of PCFT drug targeting is appealing given the acidic pH optimum for this system and the low pH microenvironment of many solid tumors (Anderson and

Thwaites, 2010; Helmlinger et al., 1997; Webb et al., 2011). For drugs such as compounds **3, 16** and **17** which exhibit PCFT selectivity over RFC, tumor selectivity would be enhanced because transport by PCFT would be extensive under the low pH conditions in solid tumors yet should be limited at neutral pH typical of most normal tissues. This would result in significantly lower toxicity. Although compounds **3**, **16** and **17** are also cytotoxic toward FR-expressing cells (Deng et al., 2008), given the frequent association of FRs with malignant cells (Chapter 2) (Elnakat and Ratnam, 2004), this may serve to broaden potential therapeutic applications of this drug platform. Our drug discovery efforts are currently focused toward identifying PCFT-specific agents without transport by FR or RFC to test this. Validation of these concepts will undoubtedly depend on establishing cytotoxicity of **3**, **16** and **17** in human solid tumor cell lines with endogenous levels of PCFT (~10 fold lower than levels found in R2/PCFT4 cells) delivered at pHs that resemble the solid tumor microenvironment (pH 6.8), determining whether these novel analogs are polyglutamylated and establishing their affinities for FPGS, identifying the effects of the analogs on the cell cycle and the mechanisms of cell death. Further, it will be important to establish *in vivo* activity of the drugs against transplanted tumors that express PCFT as the sole means of drug delivery and also determining the impact of functional RFC on the pharmacology of these drugs. These questions will be studied in Chapters 4 and 5 of this dissertation.

CHAPTER 4

SOLID TUMOR TARGETING BY PCFT-MEDIATED UPTAKE OF NOVEL ANTIFOLATES

4.1 Introduction.

PCFT transport function may be enhanced in many solid tumors by the acidic pH of the tumor microenvironment, which has been reported to reach as low as pH 6.2 to 6.8 (Helmlinger et al., 1997; Webb et al., 2011). Intracellular pH is normally alkaline, which creates a substantial transmembrane pH gradient directed *intra*cellularly (Fais et al., 2007). Clearly, harnessing this proton-motive gradient to transport cytotoxic antifolates into tumor cells by PCFT offers a uniquely attractive mechanism of therapeutic targeting solid tumors. Importantly, as described in Chapter 2, PCFT is expressed and is functional in a wide range of human solid tumor cell lines. PCFT expression was confirmed in primary human tumors. For tumor targeting of cytotoxic drugs via FR or PCFT, ideally, therapeutic agents are specifically transported by FRs and/or PCFT and not by RFC (Deng et al., 2008; Deng et al., 2009; Gibbs et al., 2005; Hilgenbrink and Low, 2005; Kugel Desmoulin et al., 2010b; Salazar and Ratnam, 2007; Wang et al., 2010). This strategy is necessary because antifolate membrane transport by RFC precludes tumor selectivity, in that RFC is expressed in both normal and tumor cells, and RFC transport is optimal at neutral pH characterizing most normal tissues (Matherly et al., 2007; Zhao and Goldman, 2003). Indeed, a major obstacle in implementing this approach has been a lack of FR- or PCFT-selective agents, since all of the clinically useful antifolates with significant FR- and PCFT substrate activity (e.g., MTX and PMX) are also transported by RFC (Matherly et al., 2007). In Chapter 3, we described a novel 6-substituted pyrrolo[2,3-*d*]pyrimidine antifolate with a thienoyl-for-benzoyl B ring replacement and a bridge length of four carbons (compound **17**) (Figure 3.1, Panel C) (Kugel Desmoulin et al., 2011; Wang et al., 2010). Cellular uptake of compound **17** by FRα and PCFT

was substantial in the absence of its membrane transport by RFC, resulting in potent antitumor activity *in vitro* because of its inhibition of GARFTase in *de novo* purine nucleotide biosynthesis.

This chapter will focus on directly testing the capacity of PCFT to deliver a cytotoxic dose of compound **17** under conditions relevant to the solid tumor microenvironment. Characteristics of drug transport, polyglutamylation, GARFTase inhibition, ATP levels, cell cycle analysis and mechanism of cell death will be evaluated in human solid tumor cell lines that have modest endogenous levels of PCFT. Drug treatments will be studied at pHs that are similar to those surrounding many solid tumors (pH 6.8), or performed *in vivo* where a true acidic tumor microenvironment can be created by the growing tumor (Raghunand et al., 1999). This chapter describes such experiments with compound **17** to establish the feasibility of selectively targeting chemotherapy to human solid tumors based upon drug membrane transport by PCFT. The majority of this work has been published (Kugel Desmoulin et al., 2011).

4.2 Materials and Methods.

4.2.1 Chemicals and Reagents.

[3',5',7-^{3}H]MTX (20 Ci/mmol), [^{3}H]PMX (2.5 Ci/mmol), and custom-radiolabeled [^{3}H]compound **17** (1.3 Ci/mmol) were purchased from Moravek Biochemicals (Brea, CA). (6*R*,*S*)-5-formyl tetrahydrofolate (5-CHO-THF) was provided by the Drug Development Branch, National Cancer Institute (Bethesda, MD). PMX [*N*-(4-[2-(2-amino-3,4-dihydro-4-oxo-7H-pyrrolo[2,3-*d*]pyrimidin-5-yl)ethyl] benzoyl)-L-glutamic acid] (Alimta) was provided by Eli Lilly and Co. (Indianapolis, IN). Synthesis and properties of the 6-substituted pyrrolo[2,3-*d*]pyrimidine thienoyl antifolate compound **17** were described previously (Kugel Desmoulin et al., 2011; Wang et al., 2010). Other chemicals were obtained from commercial sources in the highest available purities.

4.2.2 Cell Culture.

To determine the efficacies of the novel antifolates in human solid tumor cell lines, RFC-/PCFT-null HeLa (R1-11) sublines were obtained from Dr. I. David Goldman (Albert Einstein School of Medicine, Bronx, NY). R1-11-RFC6 and R1-11-PCFT4 cells were derived from R1-11 cells by stable transfection with HA-tagged pZeoSV2(+)-RFC and pZeoSV2(+)-PCFT constructs, respectively. Cells were maintained in regular RPMI 1640 medium supplemented with 10% fetal bovine serum (Invitrogen, Carlsbad, CA), 100 units/mL penicillin, 100 µg/mL streptomycin, 2 mM L-glutamine and 0.1 mg/mL zeocin (Invitrogen, Carlsbad, CA) at 37˚C with 5% CO_2. Characteristics of the HeLa sublines were described previously (Zhao et al., 2008). Additionally, HepG2 cells were purchased from ATCC and were routinely grown in Eagle's MEM (Invitrogen, Carlsbad, CA) supplemented with 10% fetal bovine serum (Thermo Fisher Scientific, Waltham, MA), 100 units/mL penicillin, 100 µg/mL streptomycin and 2 mM L-glutamine.

4.2.3 Real-time RT-PCR Analysis of RFC, FRα, and PCFT Transcripts.

For characterizing human PCFT, RFC and FRα transcript levels, RNAs were isolated using TRIzol reagent (Invitrogen, Carlsbad, CA) according to the manufacturers instructions, from the HepG2 human hepatocellular carcinoma cell line, the IGROV1 human ovarian adenocarcinoma cell line, engineered R1-11 HeLa sublines (R1-11 mock, R1-11-RFC6, and R1-11-PCFT4) and *in vivo* HepG2 tumor samples (see section 4.2.10 for trial information). For isolation of RNA from HepG2 tumor *xenografts*, dry ice was used to ensure that the snap-frozen tumors remained cold to prevent RNase degradation of tumor RNA. Tumors were cut into thin sections using an ice cold razor blade. Tumor fragments were transferred into a microcentrifuge tube containing 1 mL TRIzol (Invitrogen) and quickly homogenized using a Kontes pellet pestle motor and

RNAase-free pellet pestle (Sigma-Aldrich, St. Louis, MO). The tumor fragments, resuspended in TRIzol (Invitrogen), were vortexed, pelleted by microcentrifugation and homogenized until all solid tumor fragments were solubilized. The remaining protocol for RNA isolation was the same as above. cDNAs for all samples were synthesized using random hexamers, RNase inhibitor, and MuLV reverse transcriptase and purified with the QIAquick PCR Purification Kit (Qiagen). Real-time RT-PCR was performed on a Roche LightCycler 1.2 (Roche, Indianapolis, IN) with gene-specific primers (Table 2.1) and FastStart DNA Master SYBR Green I enzyme reaction mix (Roche), as described (Ge et al., 2007). Transcript levels for human PCFT, RFC and FRα were normalized to those for GAPDH. External standard curves were constructed for each gene of interest using serial dilutions of linearized templates, prepared by amplification from suitable cDNA templates, subcloning into a TA-cloning vector (PCR-Topo; Invitrogen), and restriction digestions.

4.2.4 Proliferation and Colony-forming Assays.

For growth inhibition assays, R1-11-PCFT4, R1-11-RFC6 HeLa, and HepG2 cells were cultured in complete folate-free RPMI 1640 medium, pH 7.2, supplemented with 25 nM 5-CHO-THF, for at least 2 weeks prior to the experiment (folate-depleted). Cells were plated in 96-well culture dishes (5000 cells/well; 200 μL/well) in the above medium with a broad concentration range of drugs (depending on the compound, drug dilutions were in DMSO or water with appropriate vehicle controls); cells were incubated for up to 96 h at 37°C in a CO_2 incubator. Metabolically active cells (a measure of cell viability) were assayed with CellTiter-Blue™ cell viability assay (Promega, Madison, WI) and a fluorescent plate reader (emission at 590 nm, excitation at 560 nm) for determining IC_{50} values, corresponding to drug concentrations that result in 50% loss of cell growth. For colony-forming assays, folate-depleted R1-11-PCFT4 cells

(500 cells) in log-phase were plated into 60-mm dishes in complete folate-free RPMI 1640 medium, pH 7.2, supplemented with 25 nM 5-CHO-THF and allowed to adhere for 48 h. Cells were then treated with compound **17** or PMX in the above media, supplemented with 25 mM PIPES and 25 mM HEPES (complete buffered folate-free RPMI 1640 medium) to maintain the pH at 6.8. After 16, 24, or 48 h, cells were rinsed with DPBS, and then incubated in drug-free, complete folate-free RPMI 1640 medium, supplemented with 25 nM 5-CHO-THF, pH 7.2. Cells were allowed to outgrow for 12 days, at which time the dishes were rinsed with DPBS, 5% TCA, and borate buffer (10 mM, pH 8.8), followed by 1% methylene blue (in borate buffer). The dishes were again rinsed with borate buffer, and colonies were counted for calculating percentage colony formation relative to the DMSO controls.

4.2.5 Transport Assays.

For comparison of PCFT transport activities in R2/PCFT4 and R1-11-PCFT4 cells, PCFT transport activities in R2/VC, R2/PCFT4, R1-11-mock and R1-11-PCFT4 cells were assessed in cell monolayers by measuring uptake of 0.5 μM [^{3}H]MTX at 37˚C for 5 min at pH 7.2 in HEPES-buffered saline (20 mM HEPES, 140 mM NaCl, 5 mM KCl, 2 mM $MgCl_2$, and 5 mM glucose), or at pH 5.5 in MES-buffered saline (20 mM MES, 140 mM NaCl, 5 mM KCl, 2 mM $MgCl_2$, and 5 mM glucose) (Zhao et al., 2004b). To determine the pH-dependent transport of [^{3}H]compound **17** and [^{3}H]PMX (both at 0.25 μM) in R1-11-PCFT4, R1-11-mock, and HepG2 cells, uptake was assayed at 37°C in cell monolayers over 2 to 30 min at 37°C in complete buffered folate-free RPMI 1640 (pH 5.5, 6.8, and 7.2). At the end of the incubations, transport was quenched with ice-cold DPBS, cells were washed three times with ice-cold DPBS, and cellular proteins were solubilized with 0.5 N NaOH. Levels of drug uptake were expressed as picomoles per milligram of protein, calculated from direct measurements of radioactivity and

protein contents of cell homogenates. Proteins were quantified using Folin-phenol reagent (Lowry et al., 1951). For PCFT transport kinetic analyses, R1-11-PCFT4 cells were grown in suspension using spinner flasks at densities of 2 to 5 X 10^5 cells/mL. Cells were collected by centrifugation, washed with DPBS, and suspended (at 1.5 X 10^7 cells) in 2 mL of transport buffer (below) for cellular uptake assays. To determine [^{3}H]compound **17** and [^{3}H]PMX kinetic constants for PCFT (K_t and V_{max}), initial uptake rates were measured at 37°C over 2 min in HEPES-buffered saline at pH 6.8, or in MES-buffered saline at pH 5.5 (Zhao et al., 2004b), using substrate concentrations from 0.04 to 5 μM. K_t and V_{max} values were determined from Lineweaver-Burk plots.

4.2.6 HPLC Analysis of Polyglutamyl Derivatives of Compound 17 and PMX.

Folate-depleted R1-11-PCFT4 and HepG2 cells were grown in complete folate-free RPMI 1640 medium, supplemented with 25 nM 5-CHO-THF. Cells were washed with DPBS and incubated in complete buffered folate-free RPMI 1640 medium, pH 6.8, with 1 μM [^{3}H]compound **17** or [^{3}H]PMX at 37°C in the presence of 60 μM adenosine, or 60 μM adenosine plus 10 μM thymidine, respectively. After 16 h, cells were washed three times with ice-cold DPBS, then scraped mechanically into 5 mL of ice cold DPBS, pelleted, and flash-frozen. The cell pellets were resuspended into 0.5 mL of 50 mM sodium phosphate buffer, pH 6.0, and 100 mM 2-mercaptoethanol, including unlabeled compound **17** (or PMX) and MTX–diglutamate, –triglutamate, and –tetraglutamate standards (Schircks Laboratories, Jona, Switzerland) (50 μM each). A portion (50 μL) was used to determine total [^{3}H]compound **17** or PMX (in picomoles per milligram of protein). Proteins were measured by the Bio-Rad protein assay (Bio-Rad Laboratories, Richmond, CA). The remaining extract was boiled (10 min), the supernatant containing radiolabeled compound **17** (or PMX) and its metabolites was centrifuged, then (250

μL) injected into a Waters 4 μm Nova-Pak C-18 column (3.9 X 150 mm) with a Nova-Pak 4 μm C-18 guard column. A Varian 9012 ternary gradient-programmable pump was used for gradient development, and a 9050 Varian UV/Vis detector set to 313 nm was used for detection of compound **17**, PMX, or MTX polyglutamate standards. HPLC analysis involved a binary gradient. Mobile phase A consisted of 100 mM sodium acetate at pH 5.5; mobile phase B consisted of 100% acetonitrile. The flow rate was set at 1.6 mL/min. The gradient consisted of 100% A from 0 to 5 min, then 85% A/15% B from 5 to 27.5 min. Fractions were mechanically collected every min for the first 10 min and then every 10 s for the duration of the run. Radioactivity of the fractions was measured with a scintillation counter. Intracellular levels of radiolabeled compounds are expressed as picomoles per milligram of protein, based on calculated percentages in the peaks from the HPLC chromatogram and total picomoles per milligram of cellular [^{3}H]antifolate. To confirm the identities of the early-eluting peaks as polyglutamate metabolites of compound **17**, samples were hydrolyzed to their parent drug forms by an overnight treatment at 32°C with a preparation of partially purified chicken pancreas conjugase in 0.5 mL of 0.1 M sodium borate, pH 7.8, containing 10 mM 2-mercaptoethanol (Matherly et al., 1985). Samples were deproteinized by boiling (5 min), then analyzed by HPLC.

4.2.7 *In situ* GARFTase Enzyme Inhibition Assay.

Incorporation of [^{14}C(U)]glycine into [^{14}C]formyl GAR as an *in situ* measure of endogenous GARFTase activity in folate-depleted R1-11-PCFT4 cells at pH 6.8 was performed using a modification of published methods (Beardsley et al., 1989; Deng et al., 2008; Kugel Desmoulin et al., 2010b). For these experiments, R1-11-PCFT4 cells were seeded in 5 mL of complete folate-free RPMI 1640 medium plus 25 nM 5-CHO-THF in 60 mm dishes and allowed to adhere overnight. Cells were washed twice with DPBS and resuspended in 5 mL of complete

buffered folate-free RPMI 1640 medium, pH 6.8, and 25 nM 5-CHO-THF. Antifolate inhibitor or an equivalent amount of vehicle (e.g., DMSO) ("control") was added to the culture medium, and the cells were incubated for another 16 h. Cells were washed twice with DPBS and resuspended in 5 mL of complete folate-free, L-glutamine-free RPMI 1640 medium/10% dFBS plus 25 mM PIPES/25 mM HEPES, pH 6.8, and 25 nM 5-CHO-THF, with or without 0.5 to 100 nM antifolate and azaserine (final concentration, 4 μM), and incubated for 30 min. L-Glutamine (final concentration, 2 mM) and [^{14}C]glycine (final specific activity, 0.1 mCi/L) were added, followed by incubation at 37°C for 8 h, after which time cells were washed three times with ice-cold DPBS and trypsinized. Cell pellets were suspended in 2 mL of 5% TCA at 0°C. Cell debris was removed by centrifugation; samples were solubilized in 0.5 N NaOH and assayed for protein contents (Lowry et al., 1951). The supernatants were extracted twice with 2 mL of ice-cold ether. The aqueous layer was passed through a 1 cm column of AG1x8 (chloride form, 100–200 mesh) (BioRad Laboratories, Hercules, CA), washed with 10 mL of 0.5 N formic acid, followed by 10 mL of 4 N formic acid, and eluted with 8 mL of 1 N HCl solution. The elutants were collected as 1 mL fractions and determined for radioactivity.

4.2.8 Determination of Intracellular ATP levels.

For analysis of ATP levels after antifolate treatments, R1-11-PCFT4 cells were seeded in 10 mL of complete buffered folate-free RPMI 1640 medium, pH 6.8, and 25 nM 5-CHO-THF. After 24 h, 10 μM compound **17** or DMSO (final concentration, 0.5%) (control) was added to the culture medium. Cells were incubated for an additional 24 to 72 h, after which they were trypsinized and washed twice with ice-cold DPBS. Nucleotides were extracted and ATP levels quantitated by HPLC exactly as described in Chapter 3 (Kugel Desmoulin et al., 2010b).

4.2.9 Assessment of Apoptosis and Cell Cycle Distribution.

R1-11-PCFT4 cells were treated with 10 μM compound **17** for 48 h at pH 6.8 in complete buffered folate-free RPMI 1640 medium, pH 6.8, and 25 nM 5-CHO-THF. Cells were trypsinized, pelleted, and washed once with ice-cold DPBS. Samples were divided so that the cell cycle profile and apoptosis analysis could be performed on the same sample. The amount of apoptosis was measured by staining cells with fluorescein isothiocyanate (FITC)-conjugated annexin V and propidium iodide (PI) with the apoptotic cells determined using the CELL LAB ApoScreen Annexin V-FITC Apoptosis Kit (Beckman Coulter, Fullerton, CA), as recommended by the manufacturer. Cells were analyzed for the presence of viable (annexin $V^-$and PI^-), early apoptotic (annexin $V^+$and PI^-), and late apoptotic/necrotic (annexin V^+ and PI^-) cells by flow cytometry. To determine compound **17** concentration-dependent effects on cell cycle progression, R1-11-PCFT4 cells (10^6) were treated with 0, 0.5, 1, 5, and 10 μM compound **17** in complete buffered folate-free RPMI 1640 medium, pH 6.8, and 25 nM 5-CHO-THF for 48 h. Cells (10^6) were fixed in ethanol (at least 1 h), then stained by resuspension in 0.5 mL of DPBS containing 50 μg/mL PI and 100 μg/mL RNase type I-A (Sigma Aldrich, St. Louis, MO). The cells were analyzed by flow cytometry for determining the percentage of cells in each phase of the cell cycle. Flow cytometry was performed at the Karmanos Cancer Institute Imaging and Cytometry Core using the BD FACSCanto II operated with BD FACSDiva software (v6.0) (BD Biosciences, San Jose, CA). In each experiment, 2 $X10^4$ cells were assessed for apoptosis and cell cycle distribution. Data were analyzed with the FlowJo software (ver. 7.6.1; Tree Star, Inc, Ashland, OR).

4.2.10 *In vivo* Efficacy Study of Compound 17 in HepG2 Xenografts.

Cultured HepG2 human hepatoma tumor cells were implanted subcutaneously (~10^7 cells/flank) to establish a solid tumor xenograft model in female ICR SCID mice (National

Institutes of Health DCT/DTP Animal Production Program, Frederick, MD). For the efficacy study, mice were 8 weeks old on day 0 (tumor implant) with an average body weight of 17.6 g. Mice were provided food and water *ad libitum*. Study mice were maintained on either a folate deficient diet (Harlan-Teklad, Madison, WI) or a folate-replete diet (autoclavable mouse breeder diet) starting 16 days before subcutaneous tumor implant to ensure serum folate levels would approximate those of humans. Folate serum levels were determined before tumor implantation and after the study with a *Lactobacillus casei* bioassay (Varela-Moreiras and Selhub, 1992). The animals were pooled and implanted bilaterally subcutaneously with 30- to 60-mg tumor fragments by a 12-gauge trocar and again pooled before unselective distribution to the various treatment and control groups. Chemotherapy was begun 4 days after tumor implantation, when the number of cells was relatively small (10^7–10^8 cells; before the established limit of palpation). Tumors were measured with a caliper two or three times weekly. Mice were sacrificed when the cumulative tumor burden reached 1500 mg. Tumor weights were estimated from two dimensional measurements [i.e., tumor mass (in milligrams) = $(ab^2)/2$, where a and b are the tumor length and width in millimeters, respectively]. For calculation of end points, both tumors on each mouse were added together, and the total mass per mouse was used. The following quantitative end points were used to assess antitumor activities: 1) T/C and $T - C$ (tumor growth delay) [where T is the median time in days required for the treatment group tumors to reach a predetermined size (e.g., 500 mg) and C is the median time in days for the control group tumors to reach the same size; tumor free survivors are excluded from these calculations]; and 2) calculation of tumor cell kill [$\log_{10}$ cell kill total (gross) = $(T - C)/(3.32)(T\text{d})$, where $(T - C)$ is the tumor growth delay, as described above, and Td is the tumor volume doubling time in days, estimated from the best fit straight line from a log-linear growth plot of control group tumors in

exponential growth (100- to 800-mg range)]. With the exception of the xenograft model, these methods are essentially identical to those described previously (Wang et al., 2010).

4.3 Results.

4.3.1 Effects of Compound 17 on Cell Growth Inhibition and Colony Formation in HeLa and HepG2 Human Tumor Sublines.

In Chapter 3, studies established that the novel pyrrolo[2,3-*d*]pyrimidine thienoyl antifolate compound **17** (Figure 3.1 and Table 3.1) was a potent (nanomolar) inhibitor of proliferation of a R2/PCFT4 CHO subline engineered to express PCFT in the absence of other folate transporters (RFC and FRs) and to inhibit [^{3}H]MTX transport by PCFT (Figure 3.6, Panel A). Conversely, the data strongly suggested that compound **17** was not transported by RFC in a CHO subline similarly engineered to exclusively express human RFC. To begin to establish the therapeutic potential of PCFT as a selective approach for chemotherapy drug delivery to human solid tumors, we used isogenic HeLa sublines derived by stable transfections of RFC- and PCFT-null R1-11 HeLa cells, designated R1-11-PCFT4 (express physiologic levels of PCFT in the absence of RFC, as measured by real-time RT-PCR) and R1-11-RFC6 (engineered to express RFC without PCFT), (Zhao et al., 2008) (Figure 4.1, Panel A and B). Low levels of FRα were detected in all the R1-11 sublines (Panel C). As a tumor prototype with endogenous PCFT expression, we used HepG2 cells established from our tumor cell line screen to express significant levels of PCFT and RFC (Figure 2.3, Panels A and B) without FRα (expression levels for PCFT and RFC in HepG2 cells are compared with those for the R1-11 sublines in Figure 4.1, Panel A-C). We measured inhibition of cell proliferation by compound **17** and results were compared with those for PMX. PMX inhibited cell growth in both the R1-11-PCFT4 and R1-11-RFC6 lines with IC_{50} values (mean ± S.E.M.) of 59.3 ± 7.37 and 81.7 ± 5.49 nM, respectively

(Figure 4.2, Panel A), demonstrating its lack of specificity for PCFT over RFC despite its high PCFT substrate activity (Kugel Desmoulin et al., 2010b; Zhao et al., 2008). Conversely, compound **17** inhibited cell growth in R1-11-PCFT4 cells (IC_{50}, 99.2 ± 20.2 nM) but not R1-11-RFC6 (Figure 4.2, Panel B), indicating selective PCFT transport. The decreased (~2-fold) sensitivity in the R1-11-PCFT4 cells versus R2/PCFT4 CHO cells (Table 3.1) probably reflects differences (~10-fold) in PCFT transport activity at pH 5.5 between these engineered sublines (Figure 4.1, Panel D). In HepG2 cells, both PMX (IC_{50}, 40.63 ± 4.52 nM) and compound **17** (IC_{50}, 227.50 ± 8.98 nM) were growth inhibitory (data not shown). The decreased sensitivity to compound **17** for HepG2 cells compared with R1-11-PCFT4 cells probably reflects the presence of RFC in HepG2 cells. Although not active for transport with compound **17**, RFC still transports folates and elevates intracellular folate pools, resulting in decreased cytotoxic drug effects on this basis (see Chapter 5). Proliferation assays were extended to include colony-forming assays, in which R1-11-PCFT4 cells were exposed to a range of concentrations (1–10 μM) of PMX (Figure 4.2, Panel C) or compound **17** (Panel D) for 16, 24, or 48 h. Drug exposures were performed at pH 6.8, after which drugs were removed and colonies allowed to outgrow for 12 days. As an inhibitor of colony formation, PMX and compound **17** showed both concentration- and time-dependence, although this effect was more pronounced for compound **17,** and PMX was more active at 16 h for the lower drug concentrations. Despite the latter activity, the maximum extent of inhibition after 48 h at 10 μM drug was greater for compound **17** (95%) than for PMX (87%). Collectively, these results demonstrate that compound **17**, like PMX, is cytotoxic toward cells that express PCFT, and under acidic conditions (pH 6.8) achievable in solid tumors. Unlike PMX, compound **17** is selectively active toward cells expressing PCFT and is inactive toward cells expressing exclusively RFC.

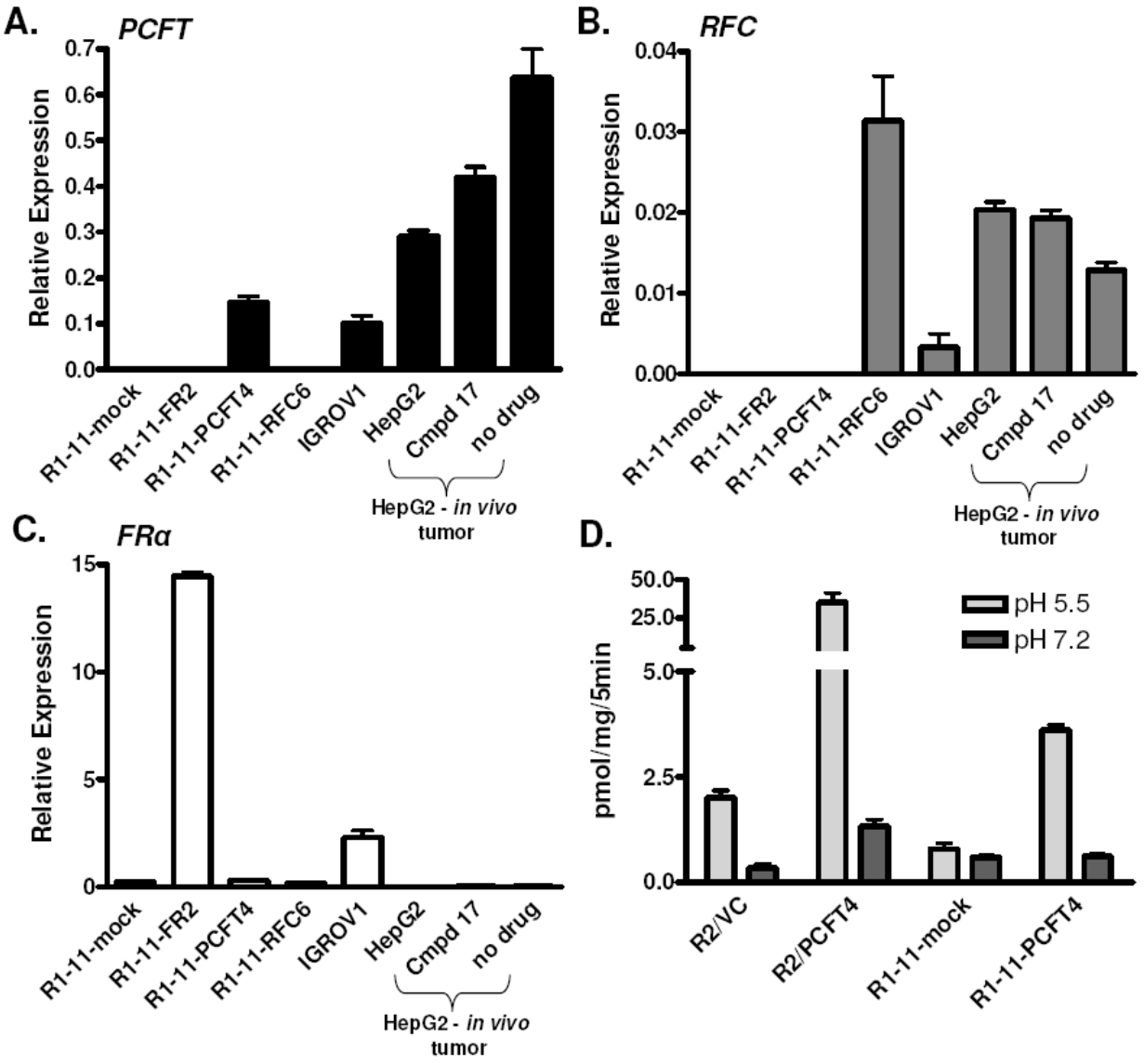

Figure 4.1 Characterization of folate transporter expression in solid tumor, HeLa, CHO sublines and HepG2 *in vivo* tumor samples. RT-PCR was used to measure: *Panel A*, PCFT; *Panel B*, RFC; and *Panel C*, FRα transcript levels. The cell lines included R1-11 sublines, IGROV1 and HepG2 cells and HepG2 tumors from the *in vivo* efficacy trial treated with compound **17** or untreated. RNAs were isolated using TRIzol reagent, cDNAs were synthesized using random hexamers and RT-PCR was performed using SYBR green and gene-specific primers (primer sequences are reported in Table 2.1). Transcript levels were normalized to GAPDH. *Panel D*, PCFT transport activities in R2/VC, R2/PCFT4, R1-11-mock and R1-11-PCFT4 cells were assessed in cell monolayers by measuring uptake of 0.5 μM [^{3}H]MTX at 37˚C for 5 min at pH 5.5 or 7.2 in MES-buffered saline, and at 7.2 in HEPES-buffered saline. Internalized [^{3}H]MTX was normalized to total protein.

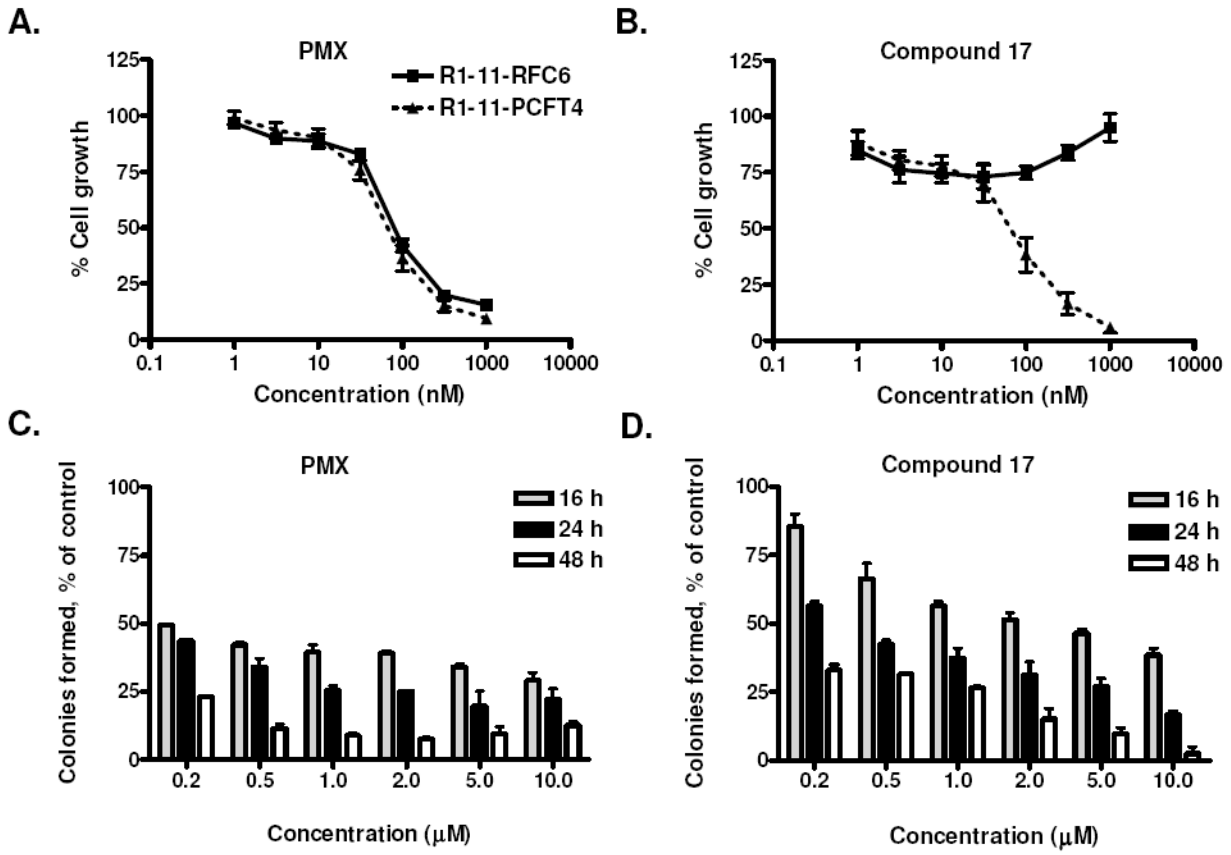

Figure 4.2 Compound 17 and PMX growth inhibition and inhibition of colony formation in R1-11 sublines. *Panels A and B*, Growth inhibition curves for folate-depleted R1-11-PCFT4 and -RFC6 cells treated with PMX (*Panel A*) or compound **17** (*Panel B*) for 96 h are shown. *Panels C and D*, R1-11-PCFT4 cells were plated in 60 mm dishes at a density of 500 cells per dish and allowed to adhere overnight. Cells were treated at pH 6.8 in the presence or absence of different concentrations of PMX (*Panel C*) or compound **17** (*Panel D*) from 0 to 10 μM for 16, 24 and 48 h, followed by removal of drug. Plates were scored by counting visible colonies after 12 days (by staining with methylene blue) and presented as a percent of vehicle control.

4.3.2 Transport Characteristics for [^{3}H]Compound 17 in HeLa R1-11-PCFT4 and HepG2 Cells.

To directly measure PCFT membrane transport of the cytotoxic antifolates into HeLa R1-11-PCFT4 and HepG2 cells, we used radiolabeled compound **17** and PMX. For R1-11-PCFT4 cells, uptake of [^{3}H]compound **17** (0.25 μM) was time- and pH dependent with maximum drug accumulation at pH 5.5 (Figure 4.3, Panels A–C). Uptake in R1-11-PCFT4 cells exceeded that of its PCFT-null isogenic counterpart (R1-11-mock transfectant), unequivocally establishing transport of compound **17** by PCFT. A modest time-dependent uptake in the PCFT null R1-11-mock transfected subline was particularly obvious at 30 min and probably reflects the presence of low levels of FR in these cells (Figure 4.1, Panel C).

We compared the uptake of [^{3}H]PMX with that of [^{3}H]compound **17** in HepG2 cells (Figure 4.3, Panel D and E). For compound **17**, pH-dependent uptake in HepG2 cells showed a profile (despite the ~2-fold increased net uptake) similar to that of R1-11-PCFT4 HeLa cells. Net uptake of [^{3}H]PMX exceeded that of [^{3}H]compound **17** in HepG2 cells by ~50 to 100% and showed a greater uptake fraction at neutral pH, most likely due to the presence of RFC in HepG2 cells (Figure 4.1, Panel B).

We measured transport kinetics over 2 min for [^{3}H]compound **17** and [^{3}H]PMX in R1-11-PCFT4 cells using a range of drug concentrations at pH 5.5 and 6.8 (Table 4.1). The data show nearly identical *K*t values for compound **17** and PMX at pH 5.5 and only modest (within ~40%) differences in V_{max}. Increases in both K_t (increased ~300- to 400-fold, respectively, compared with values at pH 5.5) and V_{max} values (~70% increased) were observed at pH 6.8. V_{max} /K_t ratios for compound **17** and PMX were similar (within ~2-fold) at both pH 5.5 and pH

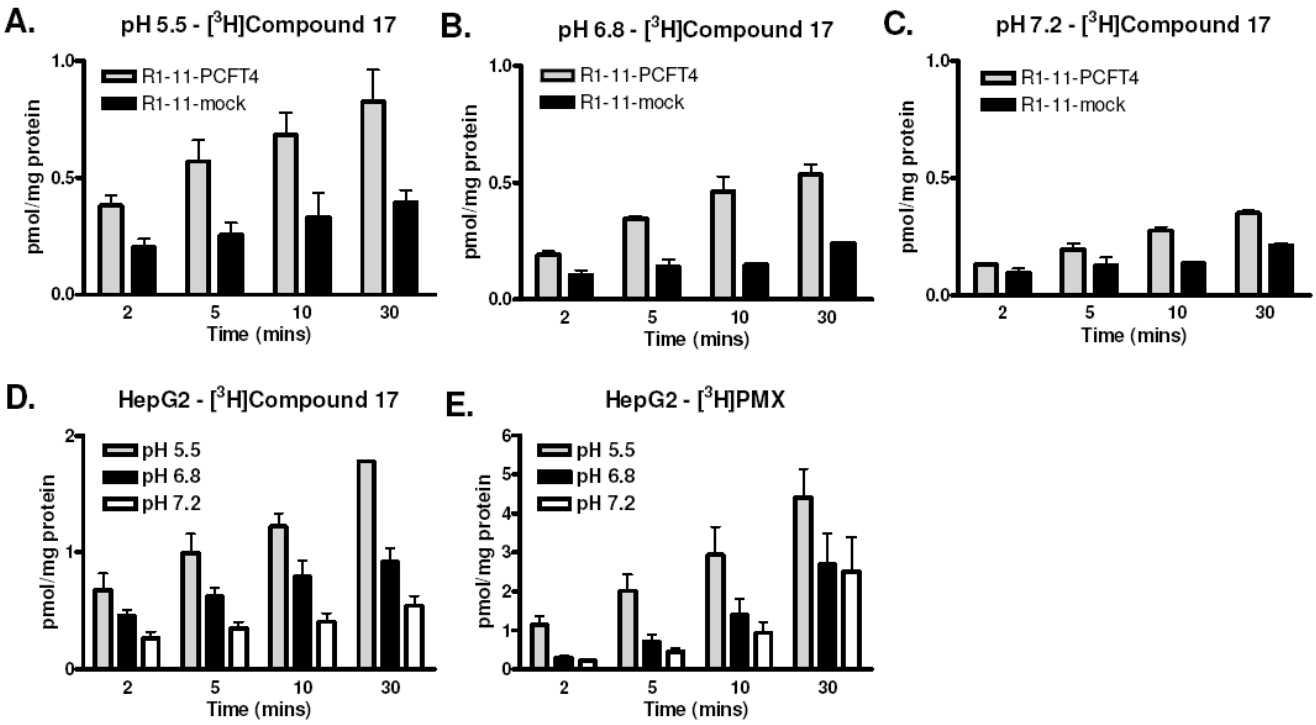

Figure 4.3 pH- and time-dependent transport of compound 17 and PMX into R1-11-PCFT4 and HepG2 cells. *Panels A-D*, Direct PCFT transport activity of compound **17** and *Panel E*, PMX in R1-11-PCFT4 (*A-C*) and HepG2 (*D and E*) cells was assessed by measuring uptake of 0.25 μM [^{3}H]compound **17** or [^{3}H]PMX over 2-30 min at 37°C in complete folate-free RPMI 1640 (pH 5.5, 6.8 and 7.2), supplemented with 10% dFBS, and 25 mM HEPES/25 mM PIPES. Internalized [^{3}H]compound **17** and [^{3}H]PMX were normalized to total protein and expressed as pmol/mg protein.

Table 4.1 Kinetic constants for PCFT – R1-11-PCFT4. Kinetic constants for PMX (K_t and V_{max}) and compound **17** (K_t and V_{max}) were determined with [^{3}H]PMX and [^{3}H]compound **17**, respectively, and calculated from Lineweaver Burke plots with R1-11-PCFT4 cells. Results are presented as mean values ± standard errors from 3 experiments.

Substrate	Parameter	pH 5.5	pH 6.8
PMX	K_t (μM)	0.03 ± 0.003	4.43 ± 0.253
	V_{max} (pmol/mg/min)	1.27 ± 0.023	2.18 ± 0.317
	V_{max}/ K_t	42.3	0.49
Compound **17**	K_t (μM)	0.02 ± 0.013	5.91 ± 1.36
	V_{max} (pmol/mg/min)	1.76 ± 0.154	3.08 ± 0.451
	V_{max}/ K_t	88	0.52

6.8. These results establish that for both R1-11-PCFT4 and HepG2 cells, compound **17** is an excellent substrate for PCFT, essentially equivalent to PMX.

4.3.3 Polyglutamylation of Compound 17 in R1-11-PCFT4 and HepG2 Cells.

Polyglutamylation of classic antifolates is a critical factor in drug activity, because these conjugated drug forms are retained within cells and they typically inhibit folate-dependent enzyme targets to a greater extent than their nonpolyglutamyl forms (Goldman and Matherly, 1985; Shane, 1989). To assess the extent of this metabolism for compound **17** in R1-11-PCFT4 and HepG2 cells, cells were treated with 1 μM [^{3}H]compound **17** for 16 h at pH 6.8 in the presence of adenosine (60 μM). For HepG2 cells, parallel incubations were performed with [^{3}H]PMX [in presence of thymidine (10 μM) and adenosine (60 μM)]. ^{3}H-labeled metabolites were extracted and analyzed by reversed-phase HPLC. Figure 4.4 shows HPLC chromatographs for compound **17** (Panel A) and PMX (Panel B) in HepG2 cells. Up to five polyglutamyl (PG) metabolites of [^{3}H]compound **17** and [^{3}H]PMX ($PG_{2–6}$) were resolved by HPLC. The identities of the peaks were confirmed by comparing elution times with those for MTX polyglutamyl standards and by treatment with chicken pancreas conjugase which reverted the majority of the polyglutamyl metabolites to the parental drug. The distributions of the individual compound **17** and PMX drug forms in R1-11-PCFT4 and HepG2 cells are summarized in Table 4.2. Although there were differences in the relative amounts of total intracellular compound **17** between the R1-11-PCFT4 and HepG2 sublines (as expected from the transport results in Figure 4.3), in both cases, compound **17** was predominantly polyglutamylated (64 and 84% of the total intracellular drug, respectively). For HepG2 cells, the increased accumulation of [^{3}H]compound **17** over that of R1-11-PCFT4 cells was reflected in the polyglutamate levels. Analogous results were obtained with [^{3}H]PMX in HepG2 cells, although the net extent of drug uptake and metabolism

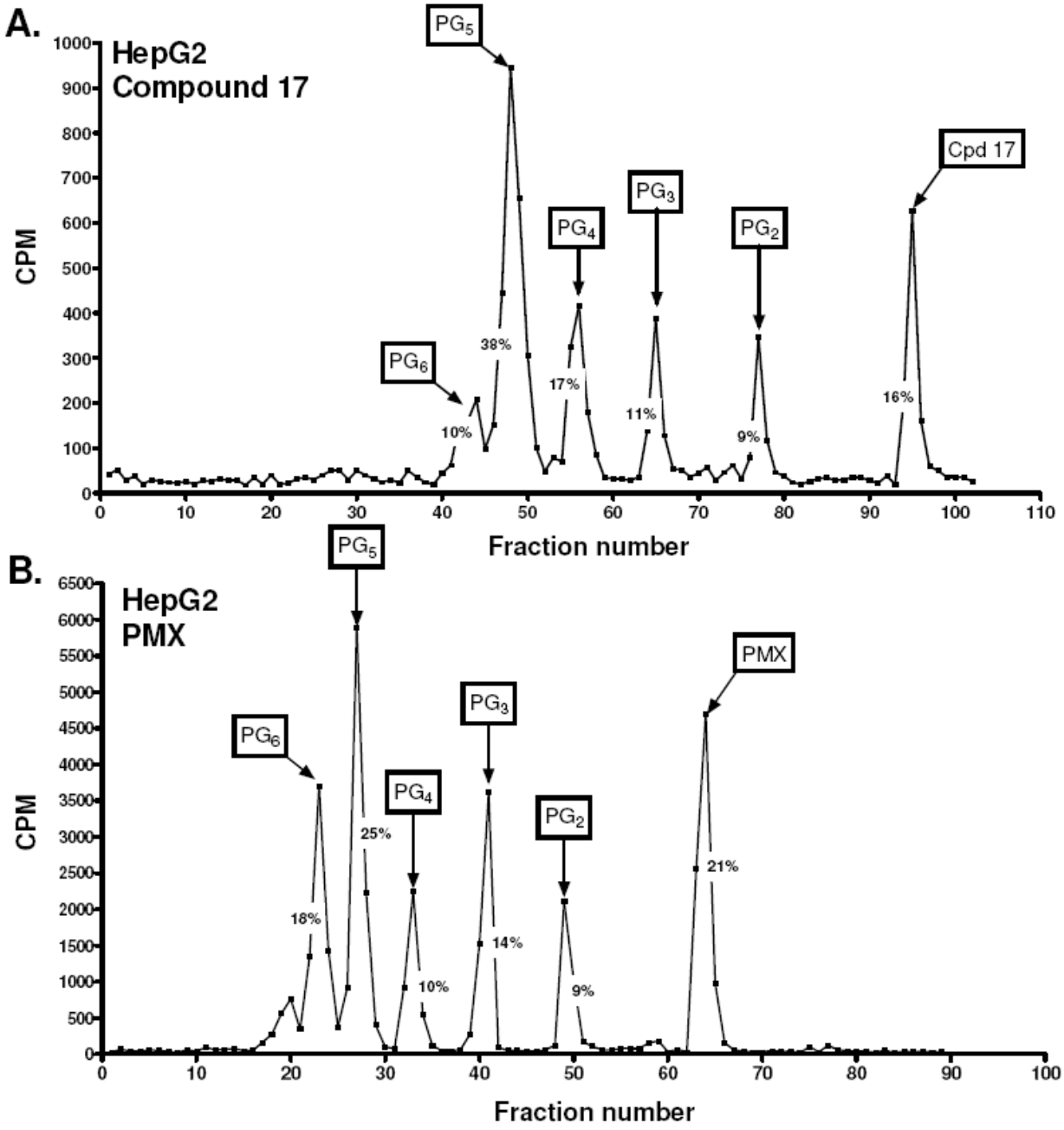

Figure 4.4 HPLC analysis of polyglutamyl derivatives of compound 17 in HepG2 cells at pH 6.8. HepG2 cells were treated with 1 µM [^{3}H]compound **17** (*Panel A*) and 1 µM [^{3}H]PMX (*Panel B*) at pH 6.8 in the presence of adenosine (60 µM) for 16 h. Polyglutamates were extracted by boiling in 50 mM phosphate buffer (pH 6.0) containing 100 mM 2-mercaptoethanol and separated on a 5 µm Spherisorb C-18 ODS-2 column (4.6 mm x 250mm) with a Nova-Pak 4 µm C-18 guard column. Fractions were collected and radioactivity was measured. Percent monoglutamate and polyglutamate (PG_{2-6}) drug forms were determined by chromatographic analysis and the total intracellular radiolabel calculated in units of pmol/mg protein (Table 4.2).

Table 4.2 Distribution of compound 17 and PMX polyglutamates in R1-11-PCFT4 and HepG2 cells. Cells were incubated for 16 h with 1 μM [^{3}H]compound **17** or [^{3}H]PMX. Drug accumulations and HPLC analysis of [^{3}H] polyglutamate metabolites were performed as described in Materials and Methods.

Metabolites	Compound 17		PMX
	R1-11-PCFT4 (pmol/mg)	HepG2 (pmol/mg)	HepG2 (pmol/mg)
Total Drug	5.8	12.8	41.6
PG_6	0	1.3 (10%)	7.4 (18%)
PG_5	1.4 (23%)	4.9 (38%)	10.3 (25%)
PG_4	0.78 (14%)	2.2 (17%)	4.1 (10%)
PG_3	1.0 (18%)	1.5 (12%)	5.8 (14%)
PG_2	0.48 (8%)	1.2 (9%)	3.7 (9%)
$PG_1^{\#}$	2.1 (36%)	2.1 (16%)	8.8 (21%)

 # Parent (unmetabolized) drug.

of [^{3}H]PMX was elevated over that of [^{3}H]compound **17**. Collectively, these results establish that, like PMX, compound **17** is an excellent substrate for polyglutamylation under conditions (pH 6.8) that favor its membrane transport by PCFT.

4.3.4 Validation of GARFTase and *De novo* Purine Nucleotide Biosynthesis as the Primary Cellular Targets for Compound 17 in R1-11-PCFT4 Cells.

In Chapter 3 the principal intracellular target of compound **17** was established in PCFT-expressing CHO cells as GARFTase, the first folate-dependent enzyme in *de novo* purine nucleotide biosynthesis (Wang et al., 2010). To confirm this result in R1-11-PCFT4 HeLa cells under acidic conditions (pH 6.8) that favor PCFT transport, we used an *in situ* metabolic assay that quantifies incorporation of [^{14}C]glycine into [^{14}C]formyl GAR as a measure of GARFTase inhibition. Results were compared with those of PMX, an established GARFTase inhibitor, along with its documented effects on TS (Chattopadhyay et al., 2007) and AICARFTase (Racanelli et al., 2009) (Figure 4.5, Panel A). IC_{50} values for GARFTase inhibition in R1-11-PCFT4 cells by compound **17** and PMX were 43.6 and 69.7 nM, respectively. Although the IC_{50} for GARFTase inhibition by compound **17** closely approximated the IC_{50} for growth inhibition of R1-11-PCFT4 cells (Table 3.1), GARFTase inhibition by PMX was incomplete up to 5 μM. Analogous results were described for PMX with PCFT-expressing CHO cells (R2/PCFT4) (Chapter 3) (Kugel Desmoulin et al., 2010b) and with CCRF-CEM cells by Moran and coworkers (Racanelli et al., 2009). To confirm that potent inhibition of GARFTase in R1-11-PCFT4 cells by compound **17** also results in decreased ATP pools, we measured intracellular ATP levels in cells treated with 10 μM compound **17** for 16, 24 and 48 h under conditions (pH 6.8) analogous to those used for our clonogenicity studies (Figure 4.2, Panel D). Compound **17** caused a time-dependent and concentration-dependent decrease in cellular ATP levels, such that treatment for 48 h led to an

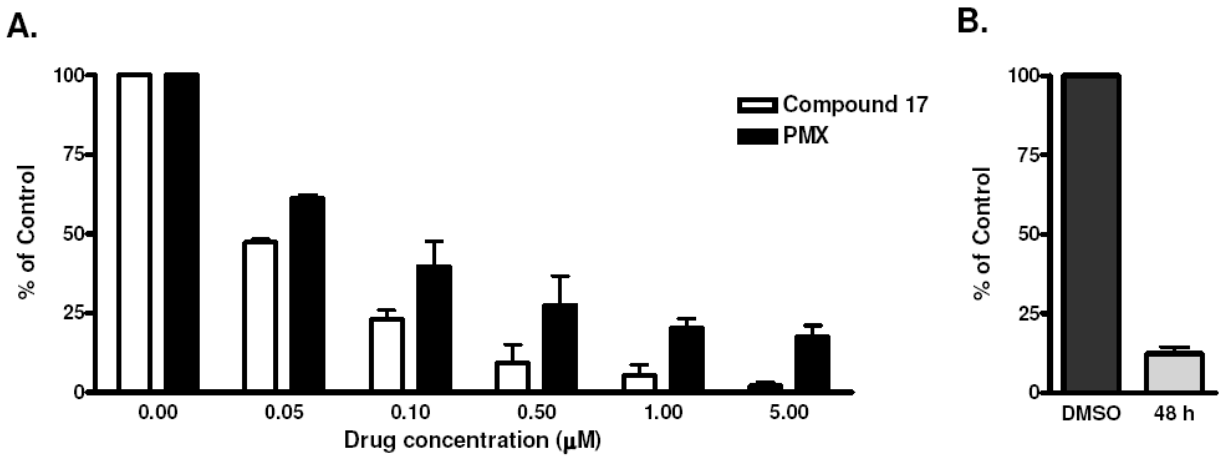

Figure 4.5 *in situ* GARFTase inhibition and intracellular ATP levels in R1-11-PCFT4 cells treated with compound 17 and PMX. *Panel A,* GARFTase activity and inhibition were evaluated *in situ* with R1-11-PCFT4 cells. R1-11-PCFT4 cells were treated with drug for 16 h at pH 6.8 in complete buffered folate-free RPMI 1640 supplemented with 25 nM 5-CHO-THF before incubating in the presence of 4 μM azaserine for 30 min, followed by [^{14}C]glycine and L-glutamine treatment. After 8 h, radioactive metabolites were extracted and fractionated on 1 cm columns of AG1x8(Cl-) and the fractions were collected and radioactivity measured. Accumulation of [^{14}C]formyl GAR was calculated as a percent of vehicle control over a range of antifolate concentrations. *Panel B,* For analysis of ATP levels, cells were treated with 10 μM compound **17** or left untreated (DMSO) for 48 h at pH 6.8. Nucleotides were extracted and ATP pools were determined by a modification of the HPLC method of Huang et al. (2003a), as previously described (Kugel Desmoulin et al., 2010b). Details are provided in the Materials and Methods.

88% decrease in ATP pools (Figure 4.5, Panel B). These results demonstrate that PCFT-delivery of compound **17** is an efficient mode of drug uptake that effects a potent inhibition of GARFTase and ATP depletion in R1-11-PCFT4 cells.

4.3.5 Effect of Compound 17 on Cell Cycle Progression and Apoptosis Induction in R1-11-PCFT4 Cells.

To determine the impact of GARFTase inhibition and ATP depletion on cell-cycle progression, we treated R1-11-PCFT4 cells with compound **17** (10 μM) for 48 h at pH 6.8, along with a vehicle control. Cells were fixed, stained with PI, and analyzed for cell cycle distribution by flow cytometry. Treatment with 10 μM compound **17** caused an accumulation of cells in S-phase such that 38.9% of cells were in S-phase, compared with 16.8% of the control (Figure 4.6, Panel A and B). When a range of concentrations (0.5, 1, 5, and 10 μM) of compound **17** were tested for their abilities to induce S-phase accumulation, we found that maximal arrest was achieved at 1 μM. Because treatment with compound **17** (10 μM, 48 h at pH 6.8) causes loss of clonogenicity in R1-11-PCFT4 cells (Figure 4.2, Panel D) and a modest increase in the sub-G1 fraction (Figure 4.6, Panel A and B), we were interested in measuring apoptosis under these same conditions using annexin V/PI staining. Results were compared with those for R1-11-PCFT4 cells treated with etoposide (5 μM) and with a no-drug control. Whereas etoposide strongly induced apoptosis (12.2% early apoptotic and 22.3% late apoptotic/necrotic) compared with the negative controls (2.9 and 10.3%, respectively), compound **17** was less apoptotic (8.4 and 15.7%, respectively) (Figure 4.6, Panel C). These results are consistent with previous reports that GARFTase inhibitors are distinctly cytotoxic, yet modestly apoptotic (Deng et al., 2008; Smith et al., 1993).

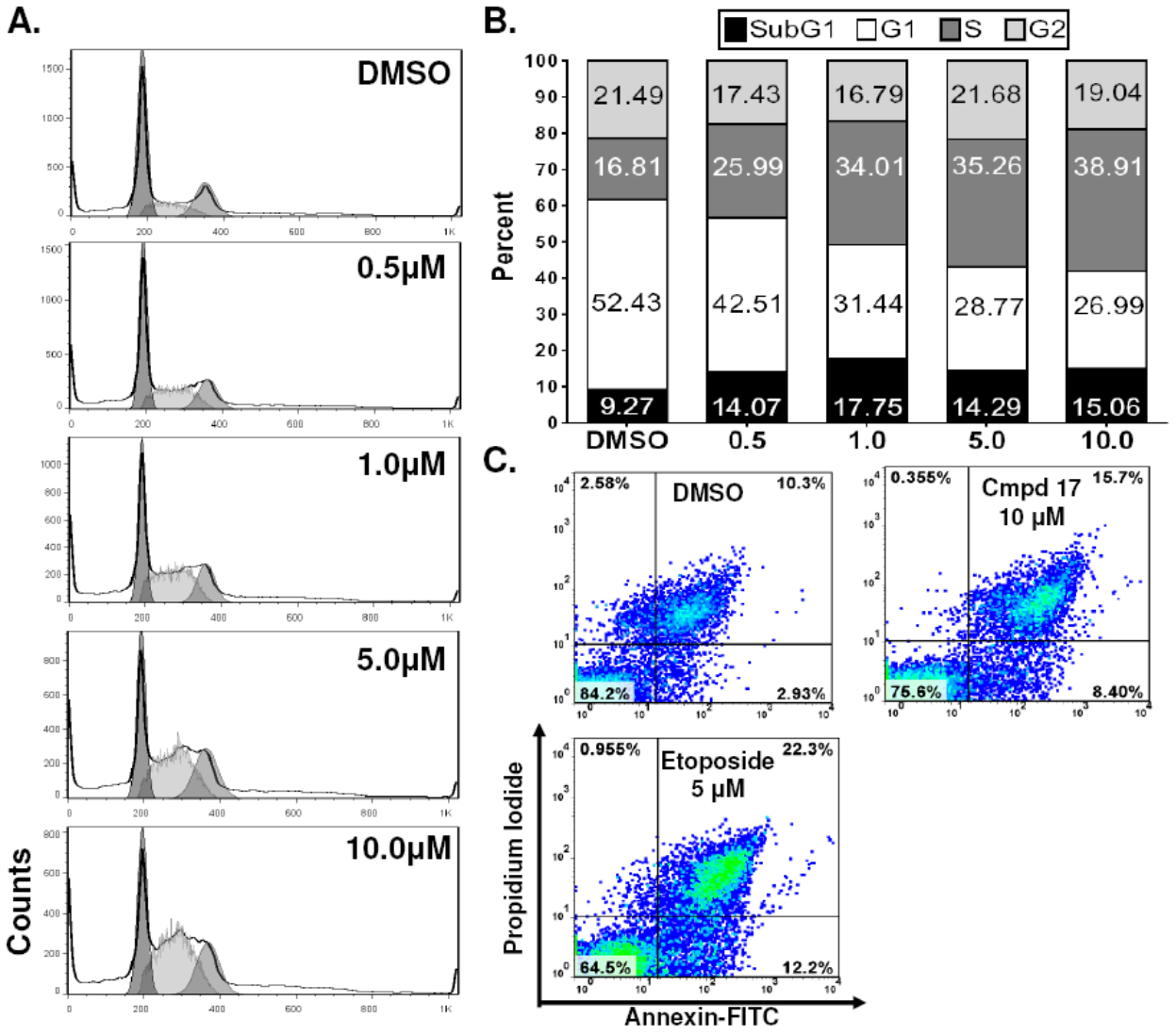

Figure 4.6 Compound 17 treatment induces an S-phase accumulation, accompanied by a modest level of apoptosis in R1-11-PCFT4 cells. *Panel A*, Representative cell cycle profiles were determined in R1-11-PCFT4 cells treated with a range of concentrations of compound **17** for 48 h by measuring the cellular DNA content with PI staining and flow cytometry. SubG1 (apoptotic fraction) (white trace), G1 (dark grey trace), S (light grey trace), and G2 (grey trace). *Panel B*, The percentages of cells in each phase of the cell cycle (G1, S, and G2), including those in the subG1 fraction for all concentrations of compound **17**. *Panel C*, Pseudo-color dot plots show the flow cytometric analysis of cells stained with annexin V-FITC and PI. The percentages of viable cells (annexin V-/PI-), early apoptotic cells (annexin V+/PI-), and late apoptotic/necrotic cells (annexin V+/PI+) are noted. As a positive control, cells were treated with 5 μM etoposide for 48 h at pH 6.8 to induce apoptosis.

4.3.6 *In vivo* Efficacy Study of Compound 17 Against HepG2 Xenografts.

As proof of concept that *in vivo* antitumor efficacy can result from tumor targeting of compound **17** via its transport by PCFT, an *in vivo* efficacy trial was performed with 8-week-old female ICR SCID mice implanted with subcutaneous HepG2 tumors that express PCFT and RFC but not FRα (Figure 4.1, Panel A). Mice were maintained *ad libitum* on folate-deficient or standard folate-replete diets. Serum folate concentrations were measured in mice after 14 days on the folate-deficient diet by an *L. casei* bioassay; the value was 90.2 nM (median) [range, 79.2–120.7 nM (n = 3)]. This value slightly exceeds serum folate levels (31 and 35 nM, respectively) reported previously in humans (Ganji and Kafai, 2009). With the standard diet, by comparison, serum folate was 715.2 nM (median) [range, 652.8–742.8 nM (n = 3)]. For the trial, control and drug treatment groups were nonselectively randomized (five mice per group); compound **17** was administered intravenously on a schedule of every 4 days for three treatments (180 mg/kg per injection) on days 4, 8, and 12 after implantation (total dose 540 mg/kg). Results were compared with those for paclitaxel (Taxol; every 2 days for six treatments, 7.5 mg/kg per injection). Mice were weighed daily and tumors were measured 2 to 3 times per week. For the mice maintained on the folate-deficient diet, appreciable antitumor activity was recorded with compound **17** (T/C of 0% on day 21; $T - C$ = 13 days; 1.4 gross log kill) (Table 4.3), exceeding that for paclitaxel (T/C = 16%; 0.8 gross log kill). Antitumor drug efficacy for **17** was completely abolished (99% T/C) for the standard folate-replete diet. The treatment regimen was well tolerated with dose-limiting symptoms manifesting as reversible body weight loss for mice maintained on the folate-deficient diet. Results for the *in vivo* efficacy experiment shown in Figure 4.7 are summarized in Table 4.3. Tumor samples treated with compound **17** and untreated controls were harvested, RNA was extracted and PCFT, RFC and FRα transcripts were measured.

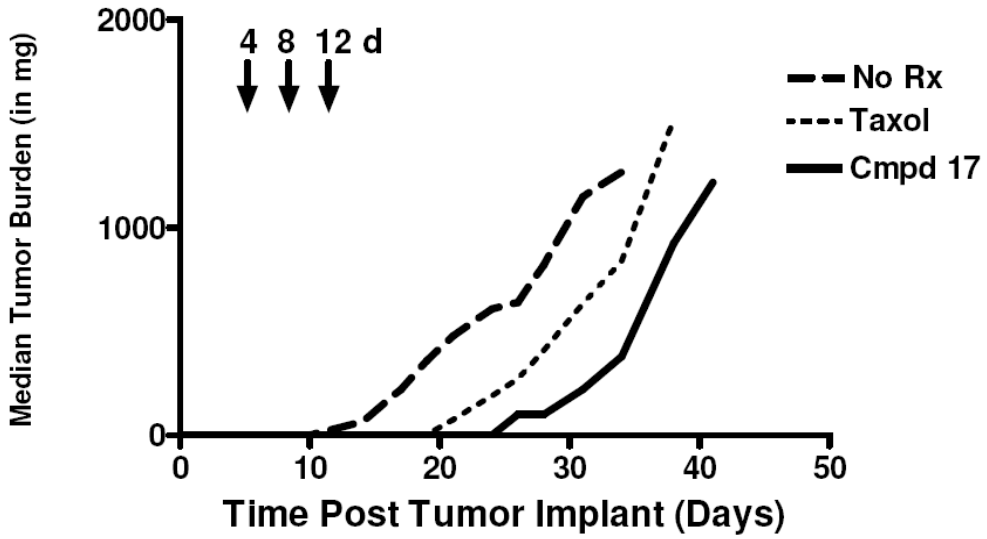

Figure 4.7 *in vivo* efficacy trial of compound 17 in HepG2 xenografts. Female ICR SCID mice were maintained on a folate-deficient diet *ad libitum*. Human HepG2 tumors were implanted bilaterally and mice were non-selectively randomized into 5 mice/group. Compound **17** [dissolved in 5% ethanol (v/v), 1% Tween-80 (v/v), 0.5% $NaHCO_3$] was administered on a Q4dx3 schedule intravenously on days 4, 8, and 12 (indicated with arrows) at 180 mg/kg/injection. Taxol (dissolved in water) was administered on a Q2dx6 schedule (7.5 mg/kg/injection) beginning on day 4. Mice were observed and weighed daily; tumors were measured twice per week. For the mice maintained on the folate-deficient diet and treated with compound **17**, appreciable antitumor activity was recorded (T/C=0%; T-C=13 days; 1.4 gross log kill).

Table 4.3 Antitumor efficacy evaluation of compound 17 and taxol against early stage human HepG2 in female SCID mice (under folate deficient and standard folate replete diet conditions)

Treatment	Drug Route	Schedule (Start on day 4)	Total Dosage mg/kg	Drug Deaths	Median Tumor Burden in mg on day 21 (range)	T/C mass %	Tumor Free on day 28	Median Time to 500 mg in days (range)	Tumor Growth Delay (days)	Log Kill	Activity Rating
No Rx (Folate deficient)	—	—	—	—	477 (0-752)	—	0/5	22 (20-41)	—	—	—
Compound 17	IV	Q4dx3	540	0/5	0 (0-875)	0	0/5	35 (18-38)	13	1.4	++
Taxol	IV	Q2dx6	45	0/5	75 (0-234)	16	0/5	29 (27-33)	7	0.8	+
Treatment	**Drug Route**	**Schedule (Start on day 4)**	**Total Dose mg/kg**	**Drug Deaths**	**Median Tumor Burden in mg on day 21 (range)**	**T/C mass %**	**Tumor Free on day 31**	**Median Time to 500 mg in days (range)**	**Tumor Growth Delay (days)**	**Log Kill**	**Activity Rating**
No Rx (STD diet)	—	—	—	—	548 (207-740)	—	0/5	21 (20-31)	—	—	—
Compound 17	IV	Q4dx3	540	0/5	546 (448-881)	99	0/5	21 (18-22)	NA	None	–
Taxol	IV	Q2dx6	45	0/5	0 (0-88)	0	0/5	31 (30-39)	10	1.1	+

The NCR SCID mice were implanted bilaterally subcutaneously with 30-60 mg tumor fragments by a 12-gauge trocar on day 0. Chemotherapy was started on day 4 after tumor implantation, when the number of cells was relatively small (10^7 – 10^8 cells). A T/C= 0 indicates very high antitumor activity. The conversion of log tumor cell kill (LK) to activity rating is as follows: >2.8 LK = ++++ (highly active); 2.0 - 2.8 LK = +++; 1.3 – 1.9 LK = ++; 0.7 – 1.2 LK = +; <0.7 = — (inactive). + = positive + for LK but negative for T/C.

In vivo passage of HepG2 cells did not change the expression of RFC (Figure 4.1, Panel B) or FRα (Panel C) transcripts; PCFT (Panel A) on the other hand increased expression in the *in vivo* environment in both treated and untreated tumor samples, suggesting that tumor cells expressing PCFT may be selected for *in* vivo or that the acidic environment may have induced PCFT expression. The results of the *in vivo* efficacy trial demonstrate potent antitumor activity for compound **17** toward subcutaneously engrafted HepG2 tumors associated with significant transport by PCFT and a lack of membrane transport by RFC.

4.4 Discussion.

This chapter significantly expands upon previous results (Chapter 3) (Anderson and Thwaites, 2010; Kugel Desmoulin et al., 2010b; Zhao and Goldman, 2007) suggesting that PCFT may be therapeutically exploitable for treating solid tumors. We further show that the novel 6-substituted pyrrolo[2,3-*d*]pyrimidine thienoyl antifolate compound **17** can be selectively transported by PCFT in a pH- and time-dependent manner. The tumor models employed, R1-11-PCFT4 HeLa and HepG2 cells, express similar levels of PCFT, although they differ in the presence of RFC and FRα. The premise behind our drug discovery efforts, exemplified by compound **17**, is that membrane transport of cytotoxic antifolates is a critical determinant of antitumor drug selectivity. Compound **17** is not transported by the ubiquitously expressed RFC (Wang et al., 2010). This is particularly important because drugs such as compound **17** that target FRα and/or PCFT, yet are not substrates for RFC, have the potential to selectively target tumor cells and decrease toxicity to normal tissues. This is a substantial advantage over chemotherapy drugs currently in use; indeed, pursuing the development of these novel antifolates could yield a new class of clinically relevant antitumor agents. Our previous work used engineered CHO models (Chapter 3), as well as KB (nasopharyngeal) and IGROV1 (ovarian) human tumor cells

that express FRα and/or PCFT to deliver cytotoxic antifolates, including compound **17**, that are not substrates for RFC (Deng et al., 2008; Deng et al., 2009; Kugel Desmoulin et al., 2011; Wang et al., 2010).

The present report significantly expands upon this concept by demonstrating exclusive transport of compound **17** by PCFT into human tumor cell lines at pH values characterizing the tumor microenvironment. For R1-11-PCFT4 and HepG2 cells, after its internalization at pH 6.8, compound **17** was extensively polyglutamylated, such that the predominant metabolite was the pentaglutamate form (compound **17** conjugated to 4 glutamate residues). Moreover, compound **17** potently inhibited GARFTase, leading to R1-11-PCFT4 HeLa cell death *in vitro* and HepG2 tumor growth delay *in vivo*.

Expression of PCFT transcripts and protein in normal human tissues is more restrictive than for RFC, high PCFT levels being observed in the liver, kidney, and small intestine and very low levels in the bone marrow and colon (Chapter 2 and Kugel Desmoulin et al. (2010a)). This pattern of PCFT transcripts was also generally observed in mouse tissues (Qiu et al., 2007). Our finding that PCFT transcripts are low in human bone marrow is particularly significant and suggests that PCFT-targeted therapeutics may be less marrow toxic than antifolates presently in clinical use. The microenvironments for most normal tissues probably exhibit a neutral pH (Martin and Jain, 1994), such that even if PCFT is present, the electrochemical proton gradient is reduced, leading to less accumulation of PCFT substrates such as compound **17**. Conversely, RFC would exhibit a far greater activity under these conditions. This, when combined with the greater capacity of RFC to transport reduced folates across the cell membrane compared with PCFT (Zhao et al., 2008), would result in elevated levels of cellular folates in normal tissues. The increased availability of reduced folates would result in competition with internalized

antifolates for polyglutamylation and/or for binding to intracellular drug targets (e.g., GARFTase), thus protecting normal cells from drug cytotoxicity. Likewise, for PCFT-targeted agents in solid tumors, if sufficient RFC were present, enough transport of folates might occur even at slightly acidic pH values to decrease drug efficacy on this basis. This implies that the ratio of PCFT to RFC in tumors is critical to antitumor activities of PCFT-selective cytotoxic antifolates and that MTX-resistant tumors that have substantially lost RFC function may be exquisitely sensitive to the effects of PCFT selective drugs such as compounds **16** and **17** (Chapter 5). Thus, for compound **17** and related agents, tumor selectivity is not only reliant upon differential PCFT levels between normal tissues and solid tumors but is also affected by interstitial pH and activity of RFC.

It is interesting that under nearly the same conditions, the IC_{50} for GARFTase inhibition in R1-11-PCFT4 cells by the *in situ* GARFTase assay is virtually identical to the IC_{50} for inhibition of cell proliferation. This result differs somewhat from our previous finding with an analogous 6-substituted pyrrolo[2,3 *d*]pyrimidine benozyl antifolate compound **3** in CHO cells for which the IC_{50} for GARFTase inhibition was substantially lower, suggesting that sustained GARFTase inhibition was necessary to manifest as cytotoxicity (Chapter 3 and Kugel Desmoulin et al. (2010b)). This quantitative difference may reflect differences in the size of purine pools between the human and hamster sublines such that R1-11-PCFT4 HeLa cells would be more sensitive to the inhibition of GARFTase. Of course, other factors could also contribute. For instance, differences in drug polyglutamylation and polyglutamate turnover could result in disparate potencies for sustained GARFTase inhibition in different cell lines. Finally, our studies with compound **17** assess the impact of GARFTase inhibition on ATP levels and the mechanism(s) of tumor cell death.

Treatment of R1-11-PCFT4 cells with compound **17** substantially reduced ATP levels and caused S-phase accumulation. Apoptosis resulting from compound **17** was reduced compared with etoposide. This could (at least in part) reflect the requirement of ATP for apoptosis, because ATP levels must be maintained above a minimal level for apoptosis induction (Tsujimoto, 1997).

In conclusion, our *in vitro* studies suggest the feasibility of using PCFT and the acidic tumor microenvironment to selectively deliver a novel PCFT-targeted antifolate to human solid tumors endogenously expressing modest levels of PCFT. Our *in vivo* results with HepG2 tumor cells that express only PCFT and RFC provide compelling proof-of-principle validation and rationale for developing drugs whose transport by PCFT, but not RFC, allows for GARFTase inhibition.

CHAPTER 5

THE IMPACT OF RFC FUNCTION ON THE ACTIVITY OF ANTIFOLATES SELECTIVELY TRANSPORTED BY PCFT

5.1 Introduction.

Classic antifolates such as MTX and PMX, like folate cofactors, have minimal lipid solubility and therefore require specific transport mechanisms to enter tumor cells. There are three primary folate transporters, including RFC, PCFT and FRα (Assaraf, 2007; Goldman et al., 2010). RFC is the predominant transport route for the major circulating folate, 5-methylTHF, and (6S) 5-CHO-THF in mammalian cells and tissues. RFC also mediates cellular uptake of MTX and is essential to MTX antitumor activity (Matherly et al., 2007). Impaired RFC function is a major mechanism of MTX resistance in cultured tumor cells selected *in vitro* (Matherly et al., 2007; Zhao and Goldman, 2003) and in murine leukemia cells *in vivo* (Sirotnak et al., 1981). Loss of RFC function in clinical specimens has also been reported (Gorlick et al., 1997; Guo et al., 1999; Yang et al., 2003). RFC transport of cytotoxic antifolates can also be undesirable since RFC is ubiquitously expressed and exhibits a high level of activity at the physiological pH of most normal tissues (Matherly et al., 2007). Thus, transport of antifolates by RFC could easily preclude tumor selectivity and cause toxicity to normal tissues.

The novel 6-substituted pyrrolo[2,3-*d*]pyrimidine thienoyl antifolates with 3- (compound **16**) or 4- (compound **17**) carbon bridge lengths (Chapters 3 and 4; Figure 3.1, Panel C) represent an entirely new class of antitumor agents that exhibit a lack of significant membrane transport by RFC (Chapters 3 and 4) (Kugel Desmoulin et al., 2011; Wang et al., 2010; Wang et al., 2011). Cellular uptake of compounds **16** and **17** by PCFT and FRα is efficient and offers a promising new strategy for tumor targeting. (Anderson and Thwaites, 2010). Since PCFT functions optimally at acidic pHs (Qiu et al., 2006; Umapathy et al., 2007; Zhao et al., 2008), transport of

16 and **17** by this mechanism may lead to enhanced tumor selectivity owing to the acidic microenvironments of many solid tumors (Anderson and Thwaites, 2010; Helmlinger et al., 1997; Webb et al., 2011). Following internalization, compound **17** is metabolized to polyglutamates (Chapter 4) (Kugel Desmoulin et al., 2011), although this has not been previously confirmed for compound **16**. Both **16** and **17** inhibit *de novo* purine nucleotide synthesis by targeting the first folate-dependent enzyme, GARFTase, causing a dramatic drop in purine nucleotide pools (Chapters 3 and 4) (Kugel Desmoulin et al., 2011; Wang et al., 2010; Wang et al., 2011). In the case of compound **17**, treatment results in S-phase accumulation and cell death, in part by a non-apoptotic mechanism (Kugel Desmoulin et al., 2011). Not surprisingly, compounds **16** and **17** are potent inhibitors of tumor cell proliferation both *in vitro* and *in vivo* (Chapters 3 and 4) (Kugel Desmoulin et al., 2011; Wang et al., 2010; Wang et al., 2011).

For agents such as PMX that are excellent substrates for both RFC and PCFT, loss of RFC has limited impact on overall activity , since PMX uptake is maintained by PCFT (Zhao et al., 2004c; Zhao et al., 2008). Paradoxically, RFC loss has been shown to enhance antitumor activity (i.e., collateral sensitivity) of PMX via decreased intracellular THF cofactor pools (Chattopadhyay et al., 2007; Chattopadhyay et al., 2006; Zhao et al., 2004c). This response to RFC loss can be further impacted by the type and amount of extracellular folate (Chattopadhyay et al., 2006; Zhao et al., 2004b; Zhao et al., 2004c).

An analogous effect may exist for PCFT-selective substrates such as compounds **16** and **17** (Kugel Desmoulin et al., 2011), although this has never been systematically tested. In this chapter, the complex interplay between RFC and extracellular reduced folates is examined. Specifically, we investigate the mechanistic ramifications of loss of RFC function toward *in vitro*

and *in vivo* antitumor efficacies of these novel PCFT-targeted antifolates, including the impact on their membrane transport, polyglutamylation, and GARFTase inhibition. The results strongly imply that levels of RFC transport in tumors are a critical determinant of drug efficacy for this novel class of PCFT-selective antitumor agents.

5.2 Materials and Methods.

5.2.1 Chemicals and Reagents.

[3',5',7-^{3}H]MTX (20 Ci/mmol), [^{3}H]PMX (2.5 Ci/mmol), [3',5',7,9-^{3}H(N)](6S)5-formyl tetrahydrofolate (5-CHO-THF) (16.6 Ci/mmol), and custom-radiolabeled [^{3}H]compound **16** (16 Ci/mmol) and [^{3}H]compound **17** (1.3 Ci/mmol) were purchased from Moravek Biochemicals (Brea, CA). Unlabeled MTX and (6R,S) 5-CHO-THF were provided by the Drug Development Branch, National Cancer Institute, Bethesda, MD. Sources of the antifolate drugs were as follows. LMX (5,10-dideaza-5,6,7,8-tetrahydrofolate) and PMX [N-(4-[2-(2-amino-3,4-dihydro-4-oxo-7H-pyrrolo[2,3-*d*]pyrimidin-5-yl)ethyl] benzoyl)(4)-L-glutamic acid] (Alimta) were from Eli Lilly and Co. (Indianapolis, IN); RTX [*N*-(5-[*N*-(3,4-dihydro-2-methyl-4-oxyquinazolin-6-ylmethyl)-*N*-methyl-amino]-2-thenoyl)-L-glutamic acid] was obtained from AstraZeneca Pharmaceuticals (Maccesfield, Cheshire, England); and N^{alpha}-(4-amino-4-deoxypteroyl)-N^{delta}-hemiphthaloyl-L-ornithine (PT523) was a gift of Dr. Andre Rosowsky (Boston, MA). Restriction and modifying enzymes were purchased from Promega (Madison, WI). Other chemicals were obtained from commercial sources in the highest available purities. Synthesis and properties of the 6-substituted pyrrolo[2,3-*d*]pyrimidine thienoyl antifolate compounds **16** and **17** were previously described (Wang et al., 2010; Wang et al., 2011).

5.2.2 Cell Culture.

HeLa cells were purchased from ATCC (Manassas, VA). RFC-null R5 HeLa cells in which RFC is deleted from the genome were selected by high dose MTX and ethylmethanesulfonate treatments (Zhao et al., 2004b). R1-11-mock and R1-11-PCFT4 HeLa cells were derived from RFC- and PCFT-null R1-11 cells by stable transfection with pZeoSV2(+) vector only, or HA-tagged pZeoSV2(+)-PCFT constructs, respectively. Characteristics of the R1-11 HeLa sublines were previously described by Zhao et al. (2008) and Chapter 4). The R5 and R1-11 sublines were gifts from Dr. I. David Goldman (Albert Einstein School of Medicine, Bronx, NY). All cell lines were maintained in regular RPMI 1640 supplemented with 10% fetal bovine serum (Invitrogen, Carlsbad, CA), 100 units/mL penicillin, 100 µg/mL streptomycin, and 2 mM L-glutamine at 37˚C with 5% CO_2. For many experiments, cells were maintained at physiologic folate levels for at least two weeks prior to the experiment. These details are listed in the individual sections.

5.2.3 Preparation of the RFC^{HA}/pZeoSV2 Construct and Generation of Stable RFC Transfectants.

Full length human RFC was subcloned using BamHI and Xho1 restriction enzymes into pZeoSV2(+) (Invitrogen) in-frame with an HA sequence inserted at the C-terminus (hereafter, designated RFC^{HA}/pZeoSV2). The plasmid was transformed into XL10-Gold ultracompetent cells (Agilent) and selected using low salt (<90 mM) LB agar plates containing 25 µg/mL Zeocin. Plasmids were isolated and the WT RFC construct was confirmed by automated DNA sequencing by Genewiz Corp. (South Plainfield, NJ).

R5 cells were transfected with pZeoSV2 vector control or RFC^{HA}/pZeoSV2 WT with Lipofectamine 2000 and opti-MEM (Invitrogen). After 24 h, the cells were cultured in the presence of zeocin (0.1 mg/mL). Stable clones were selected by plating for individual colonies in

the presence of 0.1 mg/mL zeocin. Colonies were isolated, expanded and screened for expression of RFC^{HA} protein by real-time RT-PCR, Western blotting and transport assays at pH 7.2 (see below). A representative clone (R5-RFC2) was selected for further study. R5 cells transfected with empty pZeoSV2 (R5-mock) were also prepared and used as a negative experimental control. R5-RFC2 and R5-mock cells were cultured in regular RPMI 1640 supplemented with 10% fetal bovine serum (Invitrogen, Carlsbad, CA), 100 units/mL penicillin, 100 µg/mL streptomycin, and 2 mM L-glutamine with 0.1 mg/mL zeocin.

5.2.4 Gel Electrophoresis and Western Blotting.

To characterize PCFT and RFC protein levels in the assorted solid tumor cell lines and the R5-RFC transfectants, sucrose gradient-enriched plasma membranes were prepared, exactly as described in Chapter 2 (Matherly et al., 1991). Proteins were quantified with Folin-phenol reagent (Lowry et al., 1951). Membrane proteins were electrophoresed on 7.5% polyacrylamide gels in the presence of SDS (Laemmli, 1970) and electroblotted onto PVDF membranes (Pierce, Rockford, IL) (Matsudaira, 1987). For the solid tumor cell lines and RFC clones, immunoreactive human PCFT and human RFC proteins were detected on PVDF membranes with the PCFT or RFC-specific polyclonal antibodies described in Chapter 2. An IRDye800CW-conjugated goat anti-rabbit IgG (Rockland, Gilbertsville, PA) secondary antibody was used. For detection of HA-tagged proteins ($R5\text{-}RFC^{HA}$) HA-specific mouse monoclonal antibody (Covance, Emeryville, CA) and an IRDye800CW-conjugated goat anti-mouse IgG (Rockland, Gilbertsville, PA) secondary antibody were used. Membranes were scanned with the Odyssey® Imaging System. PCFT and RFC levels were normalized to Na^+/K^+ ATPase protein levels (mouse antibody from Novus Biologicals, Littleton, CO).

5.2.5 Transport Assays.

To measure the pH-dependent uptake of [^{3}H]compound **16**, [^{3}H]compound **17**, [^{3}H]PMX and [^{3}H]MTX (0.5 μM) in WT and R5 HeLa cells, drug uptake was assayed at 37^o C in cell monolayers in 60 mm dishes over 2 min at 37°C in 2 mL "anion-free" HEPES-sucrose-Mg^{+2} buffer (20 mM HEPES, 235 mM sucrose, pH adjusted to 7.14 with MgO) (AFB) (Wong et al., 1997) or in MES-buffered saline (20 mM MES, 140 mM NaCl, 5 mM KCl, 2 mM $MgCl_2$, and 5 mM glucose) at pH 5.5. In either case, transport fluxes were stopped by aspirating the incubation buffer and quenching with excess (>5 mL) ice-cold DPBS, followed by 3 washes with ice-cold DPBS. Cellular proteins were solubilized with 0.5 N NaOH and quantified using Folin-phenol reagent (Lowry et al., 1951). Levels of drug uptake were expressed as pmol/mg protein, calculated from direct measurements of radioactivity with a Beckman Model LS6500 liquid scintillation counter (Beckman-Coulter, Fullerton, CA) and protein contents of the cell homogenates.

5.2.6 Real-time RT-PCR Analysis of RFC, FR*α*, and PCFT Transcripts.

RNAs were isolated from HeLa, R5 and R5-RFC2 cells using TRIzol reagent (Invitrogen). cDNAs were synthesized using random hexamers, RNase inhibitor, and MuLV reverse transcriptase and purified with the QIAquick PCR Purification Kit (Qiagen). Real-time RT-PCR was performed on a Roche LightCycler 2.1 (Roche, Indianapolis, IN) with gene-specific primers and FastStart DNA Master SYBR Green I enzyme reaction mix (Roche), as described (Ge et al., 2007). Primers are included in Table 2.1. Transcript levels for RFC were normalized to those for GAPDH. External standard curves were constructed for each gene of interest using serial dilutions of linearized templates, prepared by amplification from suitable cDNA templates, subcloning into a TA-cloning vector (PCR-Topo; Invitrogen), and restriction digestions.

5.2.7 Cell Proliferation Assays.

For cell proliferation assays, WT and R5 HeLa sublines were cultured in folate-free RPMI 1640 (pH 7.2), supplemented with 10% dialyzed fetal bovine serum (dFBS), 2 mM L-glutamine and 100 units/mL penicillin 100 µg/mL streptomycin (hereafter, designated complete folate-free RPMI 1640 medium), containing 25 nM 5-CHO-THF, for at least 2 weeks prior to experiment. For assays of drug inhibitions, the cells were plated in 96 well culture dishes (5000 cells/well; 200 µL/well) in the above medium with a broad concentration range of drugs (depending on the compound, drug dilutions were in DMSO or water with appropriate vehicle controls); cells were incubated for up to 96 h at 37^{o}C in a CO_2 incubator. Metabolically active cells (a measure of cell viability) were assayed with CellTiter-Blue™ cell viability assays (Promega, Madison, WI) with a fluorescent plate reader (590 nm emission, 560 nm excitation) for determining IC_{50}s, corresponding to drug concentrations that result in 50% loss of cell growth. To test the impact of extracellular folates on the collateral sensitivities of **16** and **17** in R5 and HeLa cells, some growth inhibition experiments included increasing concentrations (25, 100, 1000 nM) of 5-CHO-THF.

5.2.8 Accumulation of [^{3}H]5-CHO-THF.

WT and R5 HeLa sublines were cultured in complete folate-free RMPI 1640 supplemented with 0.06 mM adenosine and 0.01 mM thymidine for five days prior to the experiment. Cells were treated with 0, 25, 100 and 1000 nM [^{3}H]5-CHO-THF (since [^{3}H] (6S)5-CHO-THF was diluted with non-radioactive (6R,S)5-CHO-THF for these experiments, the actual concentration of (6S) stereoisomer was 12.5, 50, 500 nM, respectively) for four days, followed by 3 washes with ice-cold DPBS. 0.06 mM adenosine and 0.01 mM thymidine was added to control dishes that had no [^{3}H]5-CHO-THF to maintain cell viability. Cellular proteins were

solubilized with 0.5 N NaOH and quantified using Folin-phenol reagent (Lowry et al., 1951). Total cellular [^{3}H]5-CHO-THF accumulations were expressed as pmol/mg protein, calculated from direct measurements of radioactivity and protein contents of cell homogenates. Since [^{3}H](6S)5-CHO-THF was diluted with unlabeled (6R,S)5-CHO-THF, as noted above, for purposes of calculating intracellular folate metabolites only the unlabeled (6S) isomer was considered. To measure the impact of the PCFT-targeted therapeutics **16** and **17** on [^{3}H]5-CHO-THF accumulations, some experiments analyzed the uptake of 25 nM [^{3}H]5-CHO-THF in the presence of increasing concentrations (0-1000 nM) of compounds **16** and **17** in complete folate-free RPMI 1640 supplemented with 0.06 mM adenosine.

5.2.9 Measurement of Compound 16 and Compound 17 Polyglutamylation.

Folate-depleted HeLa and R5 cells were plated in complete folate-free RPMI 1640 medium, supplemented with 25 nM 5-CHO-THF, and allowed to adhere overnight. Cells were washed with DPBS and incubated in the same media, supplemented with 25 mM PIPES/25 mM HEPES (pH 6.8), 0.06 mM adenosine and 1 μM [^{3}H]compound **16** or [^{3}H]compound **17.** After 16 h, cells were washed three times with ice-cold DPBS and scraped mechanically into 5 mL of ice-cold DPBS, pelleted (1500 rpm) and flash frozen. Polyglutamyl and unmetabolized drug forms were extracted and drug levels quantified by HPLC exactly as previously described in Chapter 4 and by Kugel Desmoulin et al. (2011). Cellular proteins were precipitated with ice-cold TCA. The TCA precipitates were solubilized in 0.5 N NaOH before quantifying with Folin-phenol reagent (Lowry et al., 1951).

5.2.10 *In vivo* Efficacy Study of Compounds 16 and 17 in HeLa and R5 Xenografts.

Cultured WT and R5 HeLa tumor cells were implanted subcutaneously (~ 10^7 cells/flank) to establish a solid tumor xenograft model in female ICR SCID mice (National Institutes of Health

DCT/DTP Animal Production Program, Frederick, MD). The mice were supplied food and water *ad libitum.* Study mice were maintained on a folate-deficient diet (Harlan-Teklad; Product ID: TD.00434) starting 18 days before subcutaneous tumor implant to ensure serum folate levels would approximate those of humans prior to the start of therapy (Kugel Desmoulin et al., 2011; Wang et al., 2010; Wang et al., 2011). This design is analogous to those previously published by others (Alati et al., 1996; Gibbs et al., 2005). Individual mouse body weights for each experiment were within 2 g, and all mice were 19 g (WT) or 19.5 g (R5) HeLa at the start of therapy.

For the efficacy trial, the experimental animals were pooled and implanted bilaterally subcutaneously with 30-60 mg tumor fragments using a 12-gauge trocar as described in Chapter 4 for the HepG2 *in vivo* tumor model (Figure 4.7) and chemotherapy began on day 3 post tumor implantation, when the number of cells was relatively small (between 10^7-10^8 cells; below the established limit of palpation). An organic solvent (ethanol, 5% v/v), carrier (Tween-80, 1% v/v) and sodium bicarbonate (0.5% v/v) was used to effect water solubilization of compounds **16** and **17.** Injection volumes were 0.2 mL IV, pH adjusted to 7.0. Tumors were measured with a caliper two to three times weekly. Mice were sacrificed when the cumulative tumor burden reached 1500 mg. Tumor weights were estimated as described previously (Chapter 4). Experimental parameters as qualitative and quantitative end points to assess antitumor activities include T/C and T-C (tumor growth delay) [where T is the median time in days required for the treatment group tumors to reach a predetermined size (e.g., 500 mg) and C is the median time in days for the control group tumors to reach the same size; tumor-free survivors are excluded from these calculations], and tumor cell kill [$\log_{10}$ cell kill total (gross) = (T - C)/(3.32)(Td), where (T – C) is the tumor growth delay, as described above, and Td is the tumor volume doubling time in days, estimated from the best fit straight line from a log-linear growth plot of control group

tumors in exponential growth (100-800 mg range)]. For comparison of antitumor activity with standard agents and comparisons of activity between tumors, the $\log_{10}$ kill values were converted to an arbitrary activity rating (Corbett et al., 1998; Corbett et al., 1997; Polin et al., 2011; Polin et al., 1997). For duration of treatment between 5 - 20 days: >2.8 $\log_{10}$ kill (Highly active ++++); 2.0-2.8 (+++); 1.3-1.9 (++); 0.7-1.2 (+); <0.7 (Inactive; –). Both tumor studies (WT and R5 HeLa cells) used 4 mice per group. The day of tumor implant was day 0. With the exception of the xenograft model, these methods are essentially identical to those described previously in Chapter 4 (Kugel Desmoulin et al., 2011; Wang et al., 2010).

5.3 Results.

5.3.1 PCFT Transport of [^{3}H]Compound 16 in R1-11-PCFT4 HeLa Cells.

The expression of high levels of PCFT in diverse human tumor cell lines (Chapter 2) gives credence to the notion that folate-based cytotoxins with specificity for PCFT over RFC membrane transport could be used for chemotherapy of human solid tumors. We found that the novel 6-substituted pyrrolo[2,3-*d*]pyrimidine thienoyl antifolates **16** and **17** (Figure 3.1) were potent (nM) inhibitors of cell proliferation in cells engineered to express PCFT in the absence of RFC or FRs (Kugel Desmoulin et al., 2011; Wang et al., 2010; Wang et al., 2011) (Table 3.1), suggesting that **16** and **17** are substrates for PCFT-mediated cellular uptake (Chapter 3). This was extended to human HepG2 human hepatoma cells endogenously expressing PCFT without FRs (Chapter 4) (Kugel Desmoulin et al., 2011). In engineered cell lines, compounds **16** and **17** appeared to be poorly transported by RFC (Chapter 3 and 4) (Kugel Desmoulin et al., 2011; Wang et al., 2010; Wang et al., 2011). Both analogs induced current at -90 mV and pH 5.5 in *Xenopus* oocytes microinjected with PCFT cRNAs, and both were competitive inhibitors of [^{3}H]MTX transport in PCFT transfectants from pH 5.5 to pH 6.8 (Chapter 3) (Kugel Desmoulin

et al., 2011; Wang et al., 2011). Transport of [^{3}H]compound **17** by PCFT was directly demonstrated in R1-11-PCFT4 HeLa cells (Chapter 4) (Kugel Desmoulin et al., 2011).

By analogy, to confirm PCFT transport of compound **16**, R1-11-PCFT4 cells were incubated with [^{3}H]compound **16** (0.5 μM, 5 min, 37 ˚C) at pH 5.5 and pH 6.8 in the presence and absence of unlabeled compound **17** (10 μM) as a competitive inhibitor. Transport was detected at a ~4-fold higher level at pH 5.5 than at pH 6.8, and at either pH uptake was substantially abolished in the presence of unlabeled compound **17** (Figure 5.1). These results establish that compound **16**, like its 4-carbon analog, compound **17**, is a *bona fide* substrate for membrane transport by PCFT.

5.3.2 Transport and Membrane Expression of PCFT and RFC in WT and R5 HeLa Sublines.

While compounds **16** and **17** are not RFC transport substrates, levels of RFC could nonetheless markedly impact the anti-proliferative effects of these agents, *via* expansion or contraction of intracellular THF cofactor pools. This could be further impacted by varying concentrations of extracellular THF cofactors. Thus, RFC levels or ratios of PCFT to RFC transport might effectively predict anti-tumor potencies of these prototypical PCFT-targeted antifolates (Figure 2.2, Panel E and Figure 2.5, Panel C).

To explore this concept, we used WT and R5 HeLa cells which express comparable levels of PCFT with or without RFC at the protein (Figure 5.2, Panel A) and transcript levels Figure 5.2, Panel B). R5 cells are resistant to MTX (Figure 5.4, Panel A) because of a genomic deletion that results in loss of RFC (Zhao et al., 2004a). MTX resistance is completely reversible

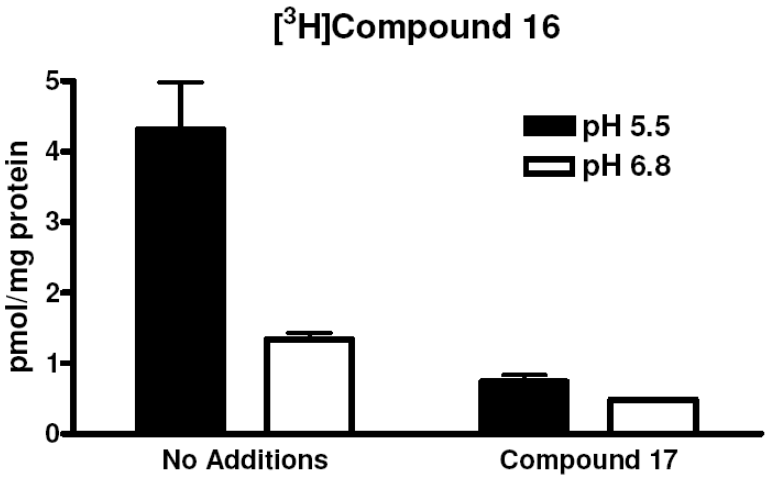

Figure 5.1 PCFT transport activity of compound 16 in R1-11-PCFT4 HeLa cells. Uptake of [^{3}H]compound **16** (0.5 μM) was measured at 37˚C for 5 min at pH 5.5 (MES-buffered saline) and 6.8 (HEPES-buffered saline) in the presence or absence of unlabeled compound **17** (10μM). Internalized [^{3}H]compound **16** was normalized to total protein. Details are provided in Materials and Methods. Results are shown for mean values ± SEMs for 3 independent experiments.

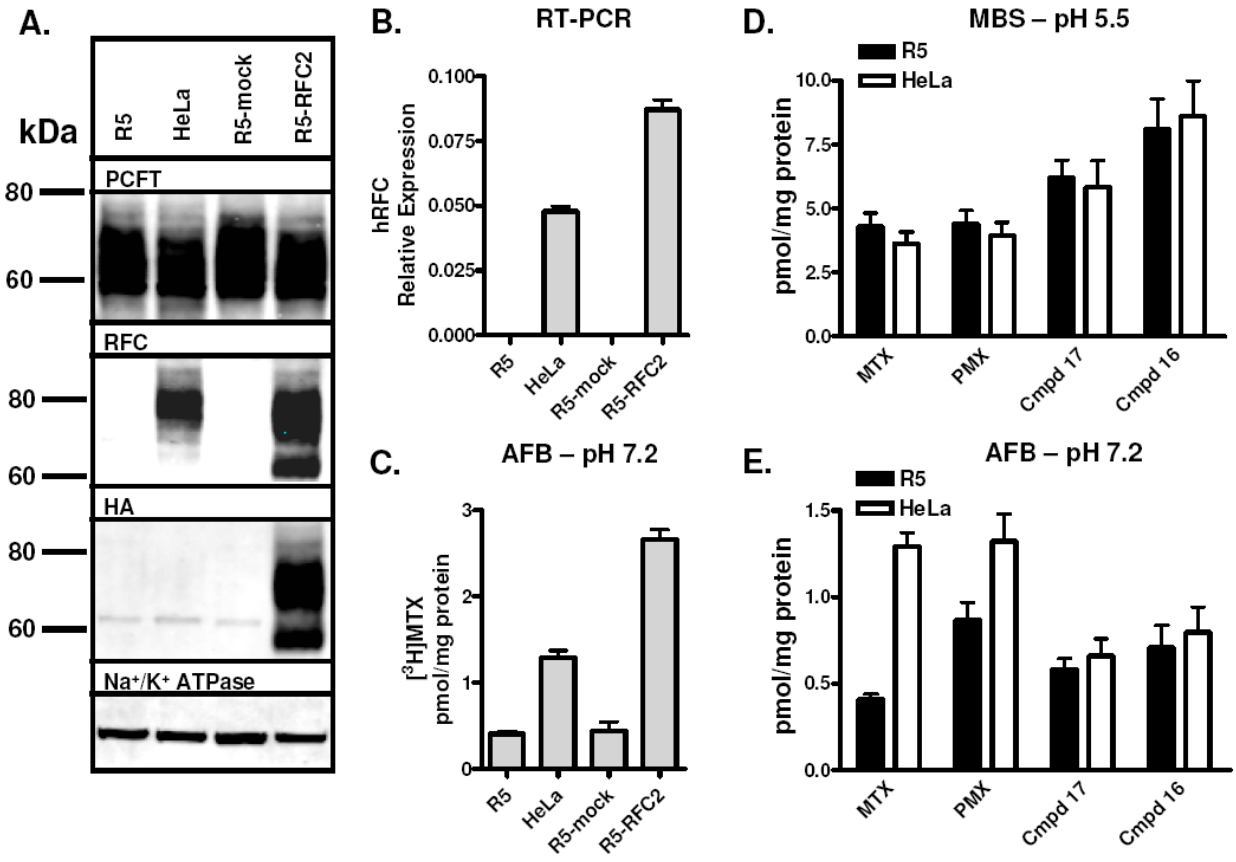

Figure 5.2 Characterization of WT and R5 HeLa sublines. *Panel A*, Western blots of sucrose gradient purified membrane fractions (25 μg) using human polyclonal PCFT and RFC and monoclonal HA antibodies to detect WT and HA-tagged proteins (R5-RFC^{HA}). *Panel B*, RT-PCR was used to measure RFC transcript levels in WT and R5 HeLa sublines, RNA was isolated using TRIzol reagent, cDNA was synthesized using random hexamers and RT-PCR was performed using SYBR green and gene-specific primers (primer sequences are reported in Table 2.1) and transcript levels were normalized to GAPDH. *Panel C*, the uptake of [^{3}H]MTX was measured at 37˚C for 2 min in WT and R5 HeLa monolayers at pH 7.2 (Anion-free buffer). Uptake of 0.5 μM [^{3}H]MTX, [^{3}H]PMX, [^{3}H]compound **17** and [^{3}H]compound **16** was measured at 37˚C for 2 min in WT and R5 HeLa cell monolayers at pH 5.5 in MES-buffered saline (*Panel D*) and pH 7.2 (Anion-free buffer) (*Panel E*). Internalized [^{3}H]drug was normalized to total protein. The data in *panels D and E* represent mean values ± SEMs for 3 independent experiments. While there were slight differences in initial rates of uptake for compounds **16** and **17** in *panel D*, these were not statistically significant ($p>0.1$).

upon transfection with WT RFC (R5-RFC2 cells), which restores RFC transport (Figure 5.2, Panel C); confirming that loss of RFC transport is causal to the resistant phenotype.

While [^{3}H]MTX (0.5 μM) transport at pH 5.5 was nearly identical for WT and R5 HeLa cells at pH 5.5 (Figure 5.2, Panel D), MTX uptake in R5 cells in Anion-free buffer at pH 7.2 was decreased ~3-fold compared to WT cells (Figure 5.2, Panel E), consistent with the loss of RFC. pH 5.5 (PCFT) to pH 7.2 (RFC) MTX transport ratios for R5 and HeLa cells were ~11- and ~3-fold, respectively (Figure 2.5, Panel C). Transport was also measured for [^{3}H]compounds **16** and **17** (both at 0.5 μM; 2 min, 37^o C) and for [^{3}H]PMX at pH 5.5 and pH 7.2. Results were compared to those for [^{3}H]MTX. For all compounds and both cell lines, transport by PCFT over RFC clearly predominated, as uptake showed a characteristic pH dependence for PCFT with the highest levels at pH 5.5. While there were differences in cellular uptake of the various analogs at pH 5.5 with **16** > **17** > PMX~MTX, there were no obvious differences in net membrane transport of the individual analogs between WT HeLa and R5 cell lines (Figure 5.2, Panels D and E).

5.3.3 Impact of RFC and Extracellular Folate on Antitumor Activities of Compounds 16 and 17.

5-CHO-THF is poorly transported by PCFT at neutral pH and is less effective in supporting proliferation of PCFT-expressing cells (without RFC) than RFC-expressing cells (without PCFT) (Zhao et al., 2008). Thus, the loss of RFC in R5 cells would be predicted to impact THF cofactor requirements for cell proliferation and to contract intracellular pools of reduced folates derived from 5-CHO-THF, compared to those in WT HeLa cells (Chattopadhyay et al., 2006; Zhao et al., 2004b). This response may be exacerbated in the presence of high affinity PCFT-selective substrates which could further restrict the modest levels of THF cofactor uptake via PCFT through direct competition.

To examine these possibilities, folate-depleted WT, R5 and R5-RFC2 cells were cultured in 25, 100, or 1000 nM [^{3}H]5-CHO-THF [corresponding to 12.5, 50, or 500 nM of the active (6S) stereoisomer] for 96 h in order to determine cellular accumulation of [^{3}H]THF metabolites. During sustained culture, the media pH decreases to ~6.8 (Kugel Desmoulin et al., 2010b) and was accompanied by a dose-dependent accumulations of [^{3}H]5-CHO-THF (Figure 5.3, Panel A). At 25 nM extracellular [^{3}H]5-CHO-THF, R5 HeLa cells experienced a 31.6% decreased net accumulation of [^{3}H]5-CHO-THF compared to WT cells ($p<0.05$), and a 49.6% decrease compared to R5-RFC2 cells ($p<0.005$).

We measured proliferation for WT HeLa and R5 cells grown in 25 nM 5-CHO-THF in the presence of antifolates (over a range of concentrations up to 1000 nM), including PCFT-selective compounds **16** and **17**, for comparison with MTX, LMX, RTX and PMX, classic antifolates which are transported by both RFC and PCFT (Goldman et al., 2010; Kugel Desmoulin et al., 2011; Kugel Desmoulin et al., 2010b), and with PT523, which is transported by RFC but not PCFT (Kugel Desmoulin et al., 2011; Kugel Desmoulin et al., 2010b; Zhao and Goldman, 2007). Cytotoxicity and transport inhibition experiments have demonstrated that MTX, PDX, RTX, and LMX can be transported by PCFT, albeit to a lower extent than RFC. Similar to published results (Zhao et al., 2004c), R5 (and R5 mock-transfectant) cells were substantially resistant to PT523 compared to WT (>213-fold) and R5-RFC2 (>303-fold) cells (Figure 5.4, Panel A and Table 5.1). Further, compared to WT HeLa cells, R5 cells were 1.4-, 4.6-, 6.5-, 13.28- and >213-fold resistant to PMX, MTX, LMX, RTX and PT523, respectively. Thus, the greater the affinity of the antifolate for RFC, the more its cytotoxicity is reduced by RFC loss, especially if the drug has a lower selectivity for PCFT over RFC. For PMX, WT and R5 cells showed similar sensitivities (IC_{50}s of 48.3 and 66.1 nM, respectively). Notably, RFC-

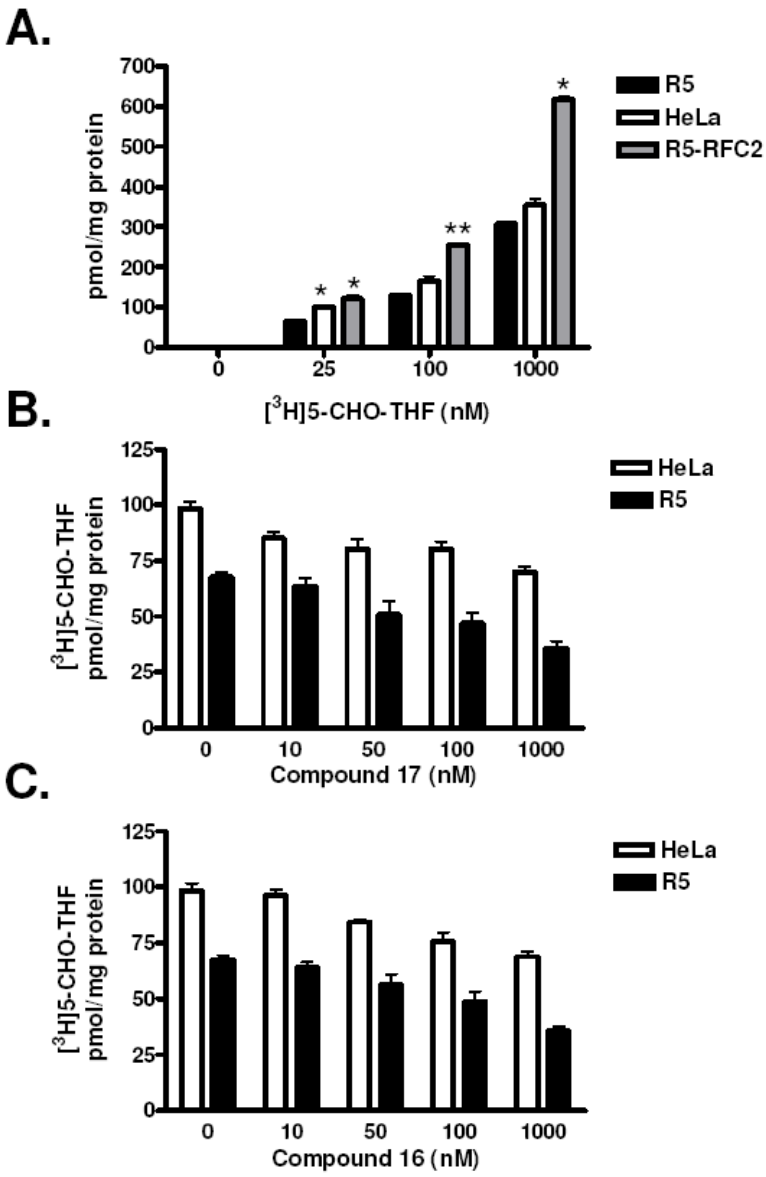

Figure 5.3 [^{3}H]5-CHO-THF accumulation in WT and R5 HeLa sublines. Folate depleted R5 HeLa sublines were treated with increasing concentrations of [^{3}H]5-CHO-THF (0-1000nM) for 96 h in the absence (*Panel A*) or presence (0-1000nM) of unlabeled compound **17** (*Panel B*) or compound **16** (*Panel C*). Internalized [^{3}H]5-CHO-THF was normalized to total protein. The data in *panel A* summarize the results as mean values $\pm$ SEMs for 3 independent experiments. For each 5-CHO-THF concentration, statistically significant differences were calculated between WT HeLa or R5-RFC2 cells and R5 cells and are noted with * ($p<0.05$) and ** ($p<0.005$). For *panels B and C*, both R5 and HeLa cells showed decreased total folate metabolites derived from [^{3}H]5-CHO-THF, accompanying treatment with increased concentrations of compounds **17** or **16** (results as mean values $\pm$ SEMs for 3-5 independent experiments). This difference was somewhat greater for R5 cells over WT HeLa cells (52.9% versus 72.9% and 52.7% versus 71.1%, respectively). Statistical analyses were performed and for compound **16**, the difference between the two sublines was statistically significant ($p=0.006$), although statistical significance was not quite reached for compound **17** ($p=0.078$).

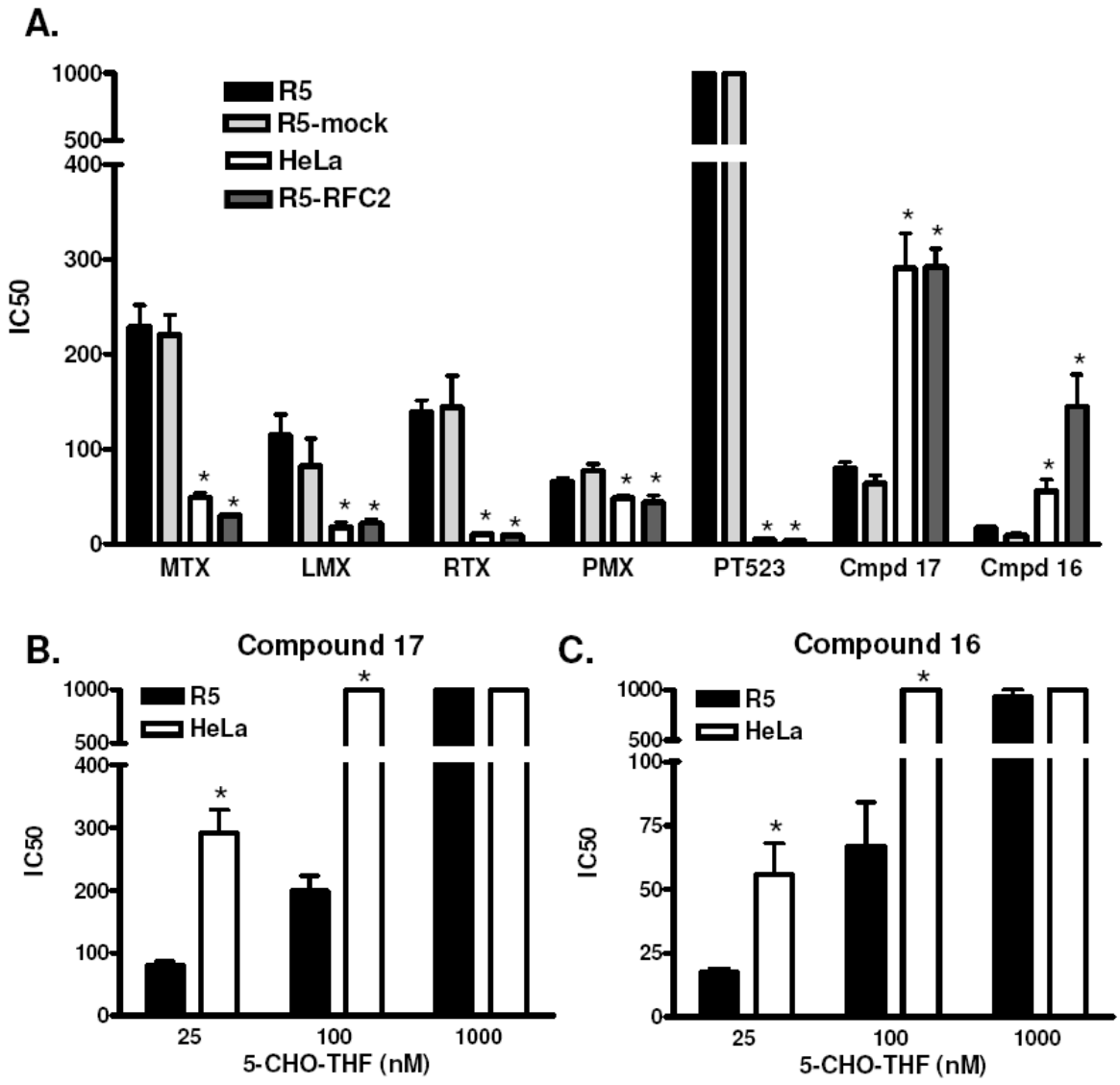

Figure 5.4 Growth inhibition by antifolate drugs toward WT and R5 HeLa sublines. (*Panel A*) Growth inhibitions were measured by a fluorescence (CellTiter-Blue™)-based assay after 96 h of exposure of folate-depleted WT and R5 HeLa sublines to a range of inhibitor concentrations. Results are presented as 50% inhibitory concentrations (IC_{50}s) as mean IC_{50} values ± SEMs from 5-12 independent experiments. IC_{50} values are summarized in Table 5.1. Statistically significant differences between results for WT HeLa or R5-RFC2 cells and those for R5 cells are noted with a * ($p<0.01$). For compound **17** (*Panel B*) and compound **16** (*Panel C*), growth inhibition experiments were performed in the presence of increasing concentrations (25-1000 nM) of extracellular 5-CHO-THF. Results are summarized as mean IC_{50} values ± SEMs from 3-11 independent experiments. Statistically significant differences between results for WT HeLa and those for R5 cells are noted with a * ($p<0.005$).

Table 5.1 Growth inhibition by antifolate drugs toward WT and R5 HeLa sublines. Growth inhibition was measured by a fluorescence (CellTiter-Blue™)-based assay after 96 h of exposure of folate depleted WT and R5 HeLa sublines to a range of inhibitor concentrations. Results are presented as 50% inhibitory concentrations (IC_{50}s) ± standard error means (SEM) from more than six experiments.

Antifolate	R5	R5-mock	HeLa	R5-RFC2
MTX	229.5 (22.5)	220.8 (21.0)	49.4 (4.8)	30.3 (1.38)
LMX	114.4 (22.5)	82.3 (28.5)	17.5 (5.5)	22.1 (3.8)
RTX	138.8 (13.0)	143.9 (33.3)	10.5 (1.0)	8.5 (1.7)
PMX	66.1 (3.6)	77.1 (7.4)	48.3 (3.3)	43.9 (7.4)
PT523	>1000	>1000	4.7 (0.45)	3.3 (0.48)
Compound 17	80.1 (6.1)	63.9 (8.8)	290.6 (37.1)	292.3 (19.2)
Compound 16	17.4 (1.7)	9.3 (2.1)	55.8 (12.2)	144.7 (34.0)

deficient R5 cells were *more sensitive* to the PCFT-specific antifolates **16** and **17** than were WT HeLa cells (3.6- and 3.2-fold, respectively) and the R5-RFC2 transfected cells (3.6- and 8.3-fold, respectively). While differences in growth inhibitions between R5 and WT HeLa cells for **16** and **17** were preserved at 100 nM 5-CHO-THF (4.3- and 15-fold, respectively), the effects of both drugs were abolished when the concentration of 5-CHO-THF was increased to 1000 nM (Figure 5.4, Panels B and C).

Since compounds **16** and **17** are high affinity substrates for PCFT (Kugel Desmoulin et al., 2011; Wang et al., 2010; Wang et al., 2011), we hypothesized that these drugs compete with [^{3}H]5-CHO-THF for PCFT-mediated uptake, leading to a more severe contraction of the cellular folate pool in R5 cells compared to WT cells than in their absence. Indeed, both compounds **16** and **17** affected a striking dose-dependent decrease in net accumulation of [^{3}H]5-CHO-THF which were greater in RFC-null R5 cells than in WT HeLa cells. At 1000 nM compound **17**, levels of [^{3}H]5-CHO-THF accumulation in R5 and WT HeLa cells were 52.9% and 72.9%, respectively, of levels without drug; for compound **16**, the corresponding values were 52.7% and 71.1%, respectively (Figure 5.3, Panels B and C).

Collectively, these results establish that loss of RFC contributes to a contraction of cellular folate pools, which is exacerbated in the presence of the PCFT-selective analogs compounds **16** and **17**. Importantly, decreased intracellular folates were accompanied by markedly increased antiproliferative effects of compounds **16** and **17**.

5.3.4 Polyglutamylation of Compounds 16 and 17 in WT and R5 HeLa Cells.

Analogous to physiologic folates and other classic antifolate drugs such as MTX (Goldman and Matherly, 1985; Shane, 1989), compound **17** is metabolized to polyglutamates (Chapter 4 and Kugel Desmoulin et al. (2011)), catalyzed by FPGS. Polyglutamylation of

compound **16** has not been previously assessed. For classic antifolates, polyglutamylation is critical to drug activity since polyglutamates are retained in cells and typically inhibit folate-dependent enzyme targets more than their non-polyglutamyl forms (Stokstad, 1990). As polyglutamylation of antifolate drugs by FPGS can be regulated by elevated extra- and intracellular folates (Shane, 1989), it seemed possible that the impact of RFC and cellular THF cofactors on the anti-proliferative effects of compounds **16** and **17** (Figure 5.4, Panel A and Table 5.1) may be partly explained in this manner.

To assess this possibility, HeLa and R5 cells were incubated with 1 μM [^{3}H]compound **16** or [^{3}H]compound **17** for 16 h at pH 6.8 in the presence of 25 nM 5-CHO-THF and 0.06 mM adenosine. Total cellular radiolabeled drug levels were quantitated and tritiated parent drug and PGs were extracted and analyzed by reverse-phase HPLC as described in Chapter 4. At least four polyglutamyl metabolites (PG_{2-5}) of [^{3}H]compound **17** and five metabolites for [^{3}H]compound **16** (PG_{2-6}) were resolved by HPLC. Migrations were compared to those for non-polyglutamyl **16** or **17**, and to MTX and MTX polyglutamate standards. Further, samples were treated in parallel with conjugase (Kugel Desmoulin et al., 2011), which reverted the majority of the polyglutamyl metabolites to the parental drug (data not shown). Results are summarized in Figure 5.5 (Panels A and B). HPLC chromatograms for the compound **16** in WT HeLa and R5 cells are shown in Figure 5.5 (Panels C and D). For R5 and WT cells, there was a 7-8-fold greater accumulation of total and polyglutamyl [^{3}H]compound **16** than [^{3}H]compound **17**. WT and R5 cells accumulated similar levels of total **16** and **17** drug forms, although there were slight differences in relative accumulations of individual PGs between the cell lines. This difference was most obvious for the longest chain-length PGs (PG_5 and PG_6) and appears to be somewhat greater for **17** than **16**.

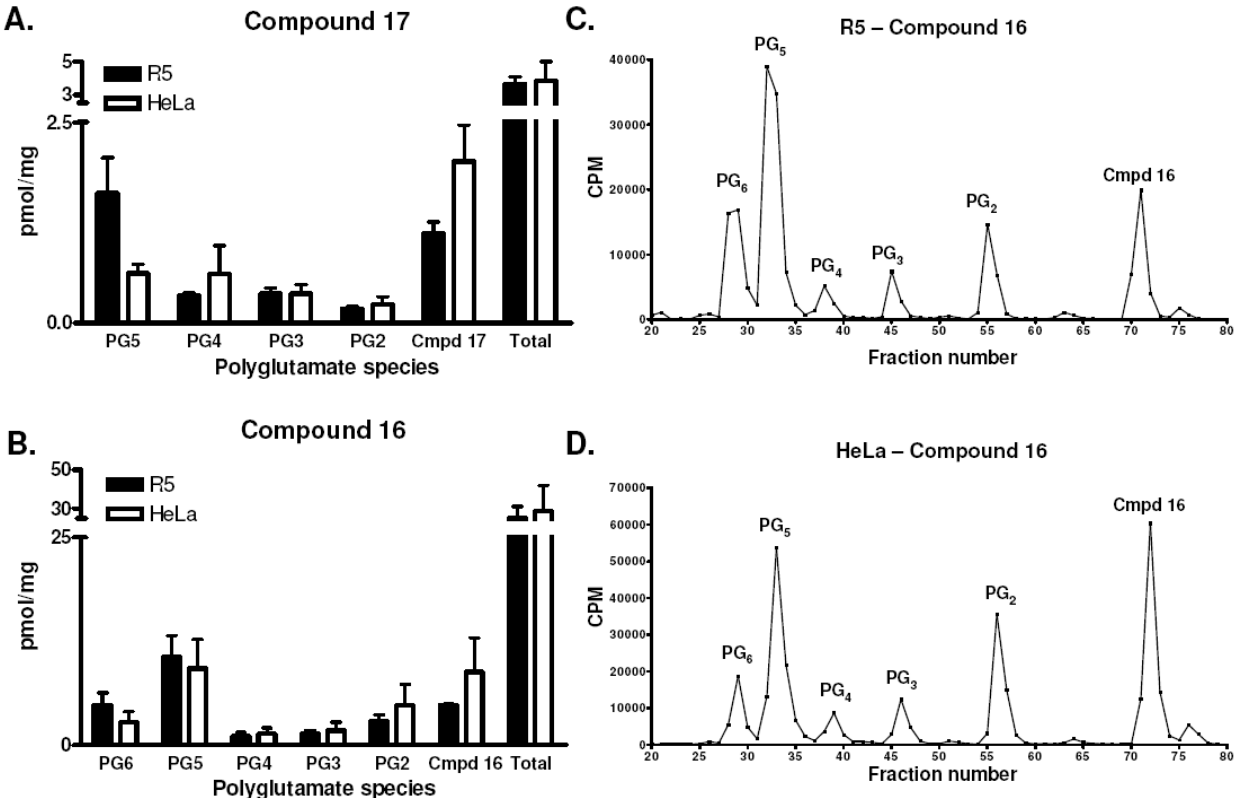

Figure 5.5 HPLC analysis of polyglutamyl derivatives of compound 17 and 16 in WT and R5 HeLa cells at pH 6.8. Folate depleted WT and R5 HeLa cells were treated with 1 µM [3H]compound **17** (*Panel A*) and **16** (*Panel B*) at pH 6.8 in the presence of adenosine (0.06 mM) and 25 nM 5-CHO-THF for 16 h. Polyglutamate drug forms were extracted and analyzed as described in Materials and Methods. Percent monoglutamate and polyglutamate drug forms were determined by chromatographic analysis and the total intracellular radiolabel calculated in units of pmol/mg protein. Results are presented as average values plus/minus ranges for two independent experiments. *Panels C and D*, show representative HPLC chromatograms for R5 and HeLa cells treated with compound **16**.

These results establish that: (i) compounds **16** and **17** are both excellent substrates for polyglutamylation under conditions (pH 6.8) that favor their membrane transport by PCFT; (ii) net drug accumulation and polyglutamylation of compound **16** far exceeds that for compound **17**; and (iii) expression of functional RFC exerts only a modest effect on net polyglutamate synthesis of compounds **16** and **17**.

5.3.5 *In vivo* Efficacy Study of Compounds 16 and 17 Against HeLa and R5 Xenografts.

To extend our *in vitro* cell proliferation studies *in vivo*, we performed *in vivo* antitumor efficacy studies with 8 week old female ICR SCID mice implanted with subcutaneous R5 or WT HeLa cells.

Mice were maintained *ad libitum* on a folate-deficient diet which decreases serum folates to levels approximating those seen in humans (Kugel Desmoulin et al., 2011; Wang et al., 2010; Wang et al., 2011). For the drug trial, control and drug treatment groups were non-selectively randomized (four mice/group); compounds **17** or **16** were administered intravenously (180 and 32 mg/kg per injection, respectively) on days 3, 7, 14 and 18 post-implantation. Mice were weighed daily and tumors were measured 2-3 times per week. As reported for other tumor models (Kugel Desmoulin et al., 2011; Wang et al., 2011), compounds **17** and **16** showed substantial efficacy toward R5 and WT HeLa xenografts (Table 5.2). Both compound **17** and compound **16** showed greater efficacy toward R5 cells (0% T/C, (T-C (tumor growth delay) = 23 days, 3.3 gross log kill, ++++ activity for compound **17**; 3% T/C, T-C = 17.5 days, 2.5 gross log kill, +++ activity for compound **16**) than toward WT HeLa cells (6% T/C, T-C = 13 days, 1.9 gross log kill, ++ activity for compound **17**; 7% T/C, T-C=13 days, 1.9 gross log kill, ++ activity for compound **16**). The treatment regimens with compounds **16** and **17** were well tolerated with

Table 5.2 Antitumor efficacy evaluation of compound 17 and 16 against early stage human R5 and HeLa in female SCID mice (under folate deficient conditions)

Tumor	Agent	Total dose (mg/kg)	Drug Deaths	Median tumor mass in mg (range) on day 21	T/C (%)	T-C (days)	Gross Log_{10} kill	Activity rating
R5	No Rx	–	NA	1054 (916 – 1272)	–	–	–	–
	Compound 17	720	0/4	0 (all zeroes)	0	23	3.3	++++
	Compound 16	128	0/4	32 (0 – 75)	3	17.5	2.5	+++
HeLa	No Rx	–	NA	1009 (847 – 1701)	–	–	–	–
	Compound 17	720	0/4	63 (0 – 247)	6	13	1.9	++
	Compound 16	128	0/4	69 (0 – 189)	7	13	1.9	++

The 8-week old female NCR SCID mice were implanted bilaterally subcutaneously with 30-60 mg tumor fragments by a 12-gauge trocar on day 0. Chemotherapy was started on day 3 after tumor implantation, when the number of cells was relatively small (10^7 – 10^8 cells). A *T/C* = 0 indicates very high antitumor activity. The conversion of log10 tumor cell kill to activity rating is as follows: >2.8 log10 kill (highly active ++++); 2.0 - 2.8 (+++); 1.3 – 1.9 (++); 0.7 – 1.2 (+); <0.7 (Inactive –). Day 0 = day of implant

dose-limiting symptoms manifesting as reversible body weight loss (nadirs sustained for body weight loss.

The results of the *in vivo* efficacy trial provide proof-of-principal confirmation of our *in vitro* findings that the antitumor effects of both compounds **16** and **17** are greater in RFC-deficient R5 cells than in WT HeLa cells. Interestingly, the impact of loss of RFC is greater with compound **17** than compound **16** *in vivo*.

5.4 Discussion.

In this chapter, we significantly expanded upon previous reports (Kugel Desmoulin et al., 2011; Kugel Desmoulin et al., 2010b; Wang et al., 2010; Wang et al., 2011; Zhao and Goldman, 2007) that PCFT may be therapeutically exploitable for treating solid tumors, reflecting unique patterns of PCFT expression and transport activity at pHs approximating the tumor microenvironment (Chapters 2-4).

We demonstrated that functional loss of RFC in R5 cells caused a contraction of total cellular THF cofactor pools derived from 5-CHO-THF which enhanced the antitumor activities of both compounds **16** and **17** compared to WT cells. Importantly, reduction of total cellular folate pools in R5 cells was exacerbated in the presence of compounds **16** and **17**, through direct competition at PCFT, which further restricted cellular uptake of exogenous 5-CHO-THF. Efficacies of compounds **16** and **17** were also increased toward R5 tumors compared to WT tumors transplanted into SCID mice with serum folate concentrations approximating those achieved in humans.

There is ample precedent for an impact of extra- and intracellular folate pools on antifolate drug efficacy. Indeed, this is the premise of leucovorin rescue from MTX toxicity (Matherly et al., 1987a) or of low-dose folic acid protection from LMX *in vivo* toxicity (Roberts et al., 2000a),

whereby elevated extra- and intracellular folates compete at multiple levels to reverse drug activity (Zhao et al., 2001a). *In vitro* studies in assorted cell line models have extended these findings to both classic (PMX, LMX) and non-classic (trimetrexate) antifolates, which inhibit a range of cellular targets (DHFR, TS, and GARFTase) (Goldman et al., 2010; Tse and Moran, 1998; Zhao et al., 2001a). Further, effects on antifolate drug activities are enhanced by decreased intracellular folates resulting from a RFC genomic deletion (Chattopadhyay et al., 2006; Zhao et al., 2004b; Zhao et al., 2004c) or RFC mutations (Zhao et al., 2000a). Similarly antifolate activities are reduced by increased intracellular folates resulting from impaired efflux of folic acid by MRP1 (Assaraf and Goldman, 1997) or enhanced folic acid influx by a mutant RFC (Tse et al., 1998; Tse and Moran, 1998).

Regardless of the underlying mechanism and intracellular drug target involved, markedly decreased total intracellular THF pools can result in collateral sensitivities to antifolates, often in the face of substantially decreased levels of drug uptake (Chattopadhyay et al., 2006; Zhao et al., 2000b; Zhao et al., 2004c). This could reflect inhibitory effects on antifolate polyglutamylation (with consequent impact on drug retention and inhibition of folate-dependent enzyme targets) due to competitive feedback inhibition at FPGS by high levels of THF cofactor PGs (Shane, 1989). Additionally, FPGS activity has been found to increase in response to decreased extra- and intracellular folates (Gates et al., 1996). There can also be direct competitive interactions between polyglutamyl folates and antifolates that interfere with drug binding and inhibition at their enzyme targets, as documented for MTX and other classic antifolates (Matherly et al., 1983). Changes in drug efflux are also possible, as ABC transporter (ABCG2, ABCC1) levels and/or intracellular distributions have been described in response to folate deprivation (Ifergan et al., 2005).

In the present study, we found that transport of compounds **16** and **17** by PCFT was virtually identical between the RFC-deficient R5 and WT HeLa cell lines. By analogy with other classical antifolates (Mendelsohn et al., 1999; Shih and Thornton, 1999), the increased accumulation of long chain polyglutamyl forms of compounds **16** and **17** observed in the R5 subline might be expected to result in increased inhibition of intracellular GARFTase and *de novo* purine nucleotide biosynthesis (Kugel Desmoulin et al., 2011; Wang et al., 2010; Wang et al., 2011). However, even though total and polyglutamyl accumulations of compounds **16** and **17** during sustained drug exposures were similar between WT and R5 cells; there were slight differences in distributions of compounds **16** and **17** polyglutamates between the lines. This difference was greatest for the longest chain length PGs (PG_5 and PG_6) and appeared to be somewhat greater for compound **17** than **16**.

The results provide proof-of-principal evidence that RFC levels and function are critical determinants of *in vitro* antitumor activities and *in vivo* efficacies of PCFT-targeted antifolates that are not themselves substrates for RFC. It is this lack of RFC transport which should confer tumor selectivity and decreased toxicity to normal tissues for this novel class of agents. Tumor selectivity would be enhanced by substantial levels of PCFT protein in solid tumors and by acidic pHs characterizing the tumor microenvironment which favor PCFT over RFC transport (Kugel Desmoulin et al., 2011). Conversely, at neutral pHs characterizing most normal tissues, RFC transport of reduced folates would be increased, resulting in elevated levels of THF cofactors within cells which further protect from untoward drug effects. Of course, in tumors with sufficiently high RFC levels, uptake of THF cofactors by this process may still occur even at somewhat acidic pHs. Accordingly, any decrease in RFC function would serve to augment the inherent antitumor selectivity and increase sensitivities to PCFT-selective antifolates.

CONCLUSIONS

The goal of this dissertation research was to determine the therapeutic potential of using PCFT-mediated membrane transport to selectively deliver novel cytotoxic antifolates into tumor cells. To establish the feasibility of this approach the expression and function of PCFT in normal and tumor tissues was determined and compared to RFC levels (Chapter 2). Additionally, novel antifolates with selective uptake by PCFT were identified and characterized *in vitro* and *in vivo* to evaluate their preclinical antitumor efficacies (Chapters 3 and 4). Finally, the influence of RFC-mediated folate uptake on drug efficacy was determined for these novel PCFT-selective antifolates (Chapter 5).

The comprehensive analysis of PCFT expression and function in human normal and tumor tissue established for the first time that PCFT is present in tumor tissue and is functional at the acidic pH surrounding most solid tumors. There were significant levels of PCFT transcripts in the majority of human solid tumor tissues and cell lines of different origins (e.g., breast, prostate, ovarian, etc.), and uniformly low PCFT transcript levels in human leukemias, including both ALL and AML. PCFT levels were highest in Caco-2 (colorectal) SKOV3 (ovarian), HepG2 (hepatoma), HeLa (cervical), and T47D (breast) cancer cells. In human normal tissues, PCFT expression was detected in the small intestine, kidney, liver, and the adrenal gland. When compared to the ubiquitously expressed RFC, the presence of PCFT was more limited. This suggests, based on PCFT expression patterns, antifolates preferentially using PCFT and not RFC as a means of drug entry into tumor cells may be less toxic compared to antifolates presently used in cancer therapy.

The rational drug design and screening of novel 6-substituted pyrrolo[2,3-*d*]pyrimidine benzoyl (compound **3**) or thienoyl (compounds **16** and **17**) analogs identified the first antifolates

that are selective for PCFT-mediated uptake and have no appreciable transport by RFC. The novel antifolates were identified and characterized in multiple engineered cell lines that express PCFT alone (R2/PCFT4 CHO and R1-11-PCFT4 HeLa sublines), or RFC alone (PC43-10 CHO and R1-11-RFC6 HeLa sublines), to determine selectivity, as well as solid tumor cell lines such as HeLa and HepG2 that express both PCFT and RFC to determine therapeutic potential. The PCFT-mediated uptake of the novel antifolates was very efficient and led to growth inhibition in all cells tested expressing PCFT.

When further characterized these analogs were found to be directly transported by PCFT in a pH- and time-dependent manner, where uptake was enhanced at acidic pHs that are relevant to the solid tumor microenvironment. Once internalized the novel antifolate compounds were polyglutamylated and up to five or six polyglutamyl metabolites were identified. The principle intracellular folate-dependent enzyme target for compounds **3**, **16** and **17** was GARFTase, a key *de novo* purine nucleotide biosynthesis enzyme. This was determined by both nucleoside protection and an *in situ* GARFTase assay. Inhibition of GARFTase led to a dose- and time-dependent decrease in ATP and GTP levels, which caused an S-phase accumulation and irreversible cell death as measured by discontinuous colony formation. The mechanism of cell death was partially through apoptosis and partially through an unidentified process that remains to be elucidated.

RFC function had a large impact on the cytotoxicity of analogs selective for PCFT-mediated uptake. While the novel compounds are not RFC transport substrates, levels of RFC nonetheless markedly impacted the anti-proliferative effects of these agents, via expansion or contraction of intracellular THF cofactor pools. Loss of RFC, which occurs in clinical cases of *de novo* and acquired resistance to the classic antifolates, leads to enhanced sensitivity to

antifolates selective for PCFT-mediated uptake. This was due to contraction of reduced folate pools and enhanced polyglutamylation of the novel drugs presumably leading to better GARFTase inhibition.

The *in vitro* cytotoxicity of compounds **16** and **17** has been recapitulated *in vivo* in subcutaneous HepG2 and HeLa xenografts in which PCFT was the predominant mode of drug uptake. Treatment with compound **16** led to potent tumor growth delay of HepG2 tumors, providing compelling proof-of-principle validation that PCFT is an efficient mechanism of drug delivery. Additionally, subcutaneous HeLa tumors that lacked RFC function were exquisitely more sensitive to PCFT-targeted drugs compared to wild-type HeLa tumors that expressed functional RFC. These data suggests that drugs selective for PCFT may be useful in tumors with antifolate resistance due to lack of RFC function. Importantly, RFC levels or ratios of PCFT to RFC transport might effectively predict anti-tumor potencies of these novel PCFT-selective antifolates.

The evidence in this dissertation of widespread PCFT expression in human solid tumors paired with the discovery of novel antifolates selective for PCFT-mediated uptake offers exciting new therapeutic possibilities to selectively deliver novel antifolate drugs to tumors by exploiting the acidic tumor microenvironment. Data presented here suggests that PCFT is a surprisingly efficient means of delivering antifolates into a tumor cell both *in vitro* and *in vivo* and there is a strong rationale for developing drugs whose transport by PCFT, but not RFC, allows for GARFTase inhibition.

REFERENCES

Abramson J, Smirnova I, Kasho V, Verner G, Kaback HR and Iwata S (2003) Structure and mechanism of the lactose permease of Escherichia coli. *Science* **301**(5633): 610-615.

Adjei AA, Mandrekar SJ, Dy GK, Molina JR, Gandara DR, Ziegler KL, Stella PJ, Rowland KM, Jr., Schild SE and Zinner RG (2010) Phase II trial of pemetrexed plus bevacizumab for second-line therapy of patients with advanced non-small-cell lung cancer: NCCTG and SWOG study N0426. *Journal of clinical oncology : official journal of the American Society of Clinical Oncology* **28**(4): 614-619.

Aime S, Geninatti Crich S, Botta M, Giovenzana G, Palmisano G and Sisti M (1999) A macromolecular Gd(III) complex as pH-responsive relaxometric probe for MRI applications. *Chemical Communications*(16): 1577-1578.

Alati T, Worzalla JF, Shih C, Bewley JR, Lewis S, Moran RG and Grindey GB (1996) Augmentation of the therapeutic activity of lometrexol -(6-R)5,10-dideazatetrahydrofolate- by oral folic acid. *Cancer Res* **56**(10): 2331-2335.

Albrecht AM, Biedler JL and Hutchison DJ (1972) Two different species of dihydrofolate reductase in mammalian cells differentially resistant to amethopterin and methasquin. *Cancer Res* **32**(7): 1539-1546.

Allegra CJ, Chabner BA, Drake JC, Lutz R, Rodbard D and Jolivet J (1985) Enhanced inhibition of thymidylate synthase by methotrexate polyglutamates. *J Biol Chem* **260**(17): 9720-9726.

Almassy RJ, Janson CA, Kan CC and Hostomska Z (1992) Structures of apo and complexed Escherichia coli glycinamide ribonucleotide transformylase. *Proceedings of the National Academy of Sciences of the United States of America* **89**(13): 6114-6118.

Alper SL (2009) Molecular physiology and genetics of Na+-independent SLC4 anion exchangers. *The Journal of experimental biology* **212**(Pt 11): 1672-1683.

Alt FW, Kellems RE, Bertino JR and Schimke RT (1978) Selective multiplication of dihydrofolate reductase genes in methotrexate-resistant variants of cultured murine cells. *J Biol Chem* **253**(5): 1357-1370.

An S, Deng Y, Tomsho JW, Kyoung M and Benkovic SJ (2010a) Microtubule-assisted mechanism for functional metabolic macromolecular complex formation. *Proceedings of the National Academy of Sciences of the United States of America* **107**(29): 12872-12876.

An S, Kumar R, Sheets ED and Benkovic SJ (2008) Reversible compartmentalization of de novo purine biosynthetic complexes in living cells. *Science* **320**(5872): 103-106.

An S, Kyoung M, Allen JJ, Shokat KM and Benkovic SJ (2010b) Dynamic regulation of a metabolic multi-enzyme complex by protein kinase CK2. *J Biol Chem* **285**(15): 11093-11099.

Anderson CM, Grenade DS, Boll M, Foltz M, Wake KA, Kennedy DJ, Munck LK, Miyauchi S, Taylor PM, Campbell FC, Munck BG, Daniel H, Ganapathy V and Thwaites DT (2004) H+/amino acid transporter 1 (PAT1) is the imino acid carrier: An intestinal nutrient/drug transporter in human and rat. *Gastroenterology* **127**(5): 1410-1422.

Anderson CM, Jevons M, Thangaraju M, Edwards N, Conlon NJ, Woods S, Ganapathy V and Thwaites DT (2010) Transport of the photodynamic therapy agent 5-aminolevulinic acid by distinct H+-coupled nutrient carriers coexpressed in the small intestine. *J Pharmacol Exp Ther* **332**(1): 220-228.

Anderson CM and Thwaites DT (2010) Hijacking solute carriers for proton-coupled drug transport. *Physiology (Bethesda, Md)* **25**(6): 364-377.

Andreassi JL, 2nd and Moran RG (2002) Mouse folylpoly-gamma-glutamate synthetase isoforms respond differently to feedback inhibition by folylpolyglutamate cofactors. *Biochemistry* **41**(1): 226-235.

Andreev OA, Dupuy AD, Segala M, Sandugu S, Serra DA, Chichester CO, Engelman DM and Reshetnyak YK (2007) Mechanism and uses of a membrane peptide that targets tumors and other acidic tissues in vivo. *Proceedings of the National Academy of Sciences of the United States of America* **104**(19): 7893-7898.

Anguera MC, Field MS, Perry C, Ghandour H, Chiang EP, Selhub J, Shane B and Stover PJ (2006) Regulation of folate-mediated one-carbon metabolism by 10-formyltetrahydrofolate dehydrogenase. *J Biol Chem* **281**(27): 18335-18342.

Assaraf YG (2006) The role of multidrug resistance efflux transporters in antifolate resistance and folate homeostasis. *Drug resistance updates : reviews and commentaries in antimicrobial and anticancer chemotherapy* **9**(4-5): 227-246.

Assaraf YG (2007) Molecular basis of antifolate resistance. *Cancer Metastasis Rev* **26**(1): 153-181.

Assaraf YG and Goldman ID (1997) Loss of folic acid exporter function with markedly augmented folate accumulation in lipophilic antifolate-resistant mammalian cells. *J Biol Chem* **272**(28): 17460-17466.

Atabay B, Turker M, Ozer EA, Mahadeo K, Diop-Bove N and Goldman ID (2010) Mutation of the proton-coupled folate transporter gene (PCFT-SLC46A1) in Turkish siblings with hereditary folate malabsorption. *Pediatr Hematol Oncol* **27**(8): 614-619.

Azzoli CG, Krug LM, Gomez J, Miller VA, Kris MG, Ginsberg MS, Henry R, Jones J, Tyson L, Dunne M, Pizzo B, Farmer A, Venkatraman E, Steffen R and Sirotnak FM (2007) A

phase 1 study of pralatrexate in combination with paclitaxel or docetaxel in patients with advanced solid tumors. *Clin Cancer Res* **13**(9): 2692-2698.

Badagnani I, Castro RA, Taylor TR, Brett CM, Huang CC, Stryke D, Kawamoto M, Johns SJ, Ferrin TE, Carlson EJ, Burchard EG and Giacomini KM (2006) Interaction of methotrexate with organic-anion transporting polypeptide 1A2 and its genetic variants. *J Pharmacol Exp Ther* **318**(2): 521-529.

Baldwin SW, Tse A, Gossett LS, Taylor EC, Rosowsky A, Shih C and Moran RG (1991) Structural features of 5,10-dideaza-5,6,7,8-tetrahydrofolate that determine inhibition of mammalian glycinamide ribonucleotide formyltransferase. *Biochemistry* **30**(7): 1997-2006.

Bareford MD, Park MA, Yacoub A, Hamed HA, Tang Y, Cruickshanks N, Eulitt P, Hubbard N, Tye G, Burow ME, Fisher PB, Moran RG, Nephew KP, Grant S and Dent P (2011) Sorafenib enhances pemetrexed cytotoxicity through an autophagy-dependent mechanism in cancer cells. *Cancer Res* **71**(14): 4955-4967.

Barlowe CK and Appling DR (1988) In vitro evidence for the involvement of mitochondrial folate metabolism in the supply of cytoplasmic one-carbon units. *BioFactors (Oxford, England)* **1**(2): 171-176.

Barlowe CK and Appling DR (1990) Molecular genetic analysis of Saccharomyces cerevisiae C1-tetrahydrofolate synthase mutants reveals a noncatalytic function of the ADE3 gene product and an additional folate-dependent enzyme. *Mol Cell Biol* **10**(11): 5679-5687.

Beardsley GP, Moroson BA, Taylor EC and Moran RG (1989) A new folate antimetabolite, 5,10-dideaza-5,6,7,8-tetrahydrofolate is a potent inhibitor of de novo purine synthesis. *J Biol Chem* **264**(1): 328-333.

Beinart GA, Gonzalez-Angulo AM, Broglio K, Frye D, Walters R, Holmes FA, Gunale S, Booser D, Rosenthal J, Dhingra K, Young JA and Hortobagyi GN (2007) Phase II trial of 10-EDAM in the treatment of metastatic breast cancer. *Cancer Chemother Pharmacol* **60**(1): 61-67.

Belkov VM, Krynetski EY, Schuetz JD, Yanishevski Y, Masson E, Mathew S, Raimondi S, Pui CH, Relling MV and Evans WE (1999) Reduced folate carrier expression in acute lymphoblastic leukemia: a mechanism for ploidy but not lineage differences in methotrexate accumulation. *Blood* **93**(5): 1643-1650.

Bellati F, Napoletano C, Gasparri ML, Visconti V, Zizzari IG, Ruscito I, Caccetta J, Rughetti A, Benedetti-Panici P and Nuti M (2011) Monoclonal antibodies in gynecological cancer: a critical point of view. *Clinical & developmental immunology* **2011**: 890758.

Benigni R, Calcagnile A, Dogliotti E, Falcone E and Giuliani A (1983) DNA repair induction by cytostatic drugs in proliferating and quiescent MRC-5 cells. *Teratog Carcinog Mutagen* **3**(6): 481-490.

Bertino JR, Waud WR, Parker WB and Lubin M (2011) Targeting tumors that lack methylthioadenosine phosphorylase (MTAP) activity: current strategies. *Cancer biology & therapy* **11**(7): 627-632.

Bissett D, McLeod HL, Sheedy B, Collier M, Pithavala Y, Paradiso L, Pitsiladis M and Cassidy J (2001) Phase I dose-escalation and pharmacokinetic study of a novel folate analogue AG2034. *Br J Cancer* **84**(3): 308-312.

Bolusani S, Young BA, Cole NA, Tibbetts AS, Momb J, Bryant JD, Solmonson A and Appling DR (2011) Mammalian MTHFD2L encodes a mitochondrial methylenetetrahydrofolate dehydrogenase isozyme expressed in adult tissues. *J Biol Chem* **286**(7): 5166-5174.

Boritzki TJ, Barlett CA, Zhang C and Howland EF (1996) AG2034: a novel inhibitor of glycinamide ribonucleotide formyltransferase. *Investigational new drugs* **14**(3): 295-303.

Boron WF, Chen L and Parker MD (2009) Modular structure of sodium-coupled bicarbonate transporters. *The Journal of experimental biology* **212**(Pt 11): 1697-1706.

Borzutzky A, Crompton B, Bergmann AK, Giliani S, Baxi S, Martin M, Neufeld EJ and Notarangelo LD (2009) Reversible severe combined immunodeficiency phenotype secondary to a mutation of the proton-coupled folate transporter. *Clin Immunol* **133**(3): 287-294.

Brayton KA, Chen Z, Zhou G, Nagy PL, Gavalas A, Trent JM, Deaven LL, Dixon JE and Zalkin H (1994) Two genes for de novo purine nucleotide synthesis on human chromosome 4 are closely linked and divergently transcribed. *J Biol Chem* **269**(7): 5313-5321.

Bronder JL and Moran RG (2002) Antifolates targeting purine synthesis allow entry of tumor cells into S phase regardless of p53 function. *Cancer Res* **62**(18): 5236-5241.

Bronder JL and Moran RG (2003) A defect in the p53 response pathway induced by de novo purine synthesis inhibition. *J Biol Chem* **278**(49): 48861-48871.

Budman DR, Johnson R, Barile B, Bowsher RR, Vinciguerra V, Allen SL, Kolitz J, Ernest CS, 2nd, Kreis W, Zervos P and Walling J (2001) Phase I and pharmacokinetic study of LY309887: a specific inhibitor of purine biosynthesis. *Cancer Chemother Pharmacol* **47**(6): 525-531.

Bueno R, Appasani K, Mercer H, Lester S and Sugarbaker D (2001) The alpha folate receptor is highly activated in malignant pleural mesothelioma. *J Thorac Cardiovasc Surg* **121**(2): 225-233.

Buist MR, Molthoff CF, Kenemans P and Meijer CJ (1995) Distribution of OV-TL 3 and MOv18 in normal and malignant ovarian tissue. *Journal of clinical pathology* **48**(7): 631-636.

Busco G, Cardone RA, Greco MR, Bellizzi A, Colella M, Antelmi E, Mancini MT, Dell'Aquila ME, Casavola V, Paradiso A and Reshkin SJ (2010) NHE1 promotes invadopodial ECM proteolysis through acidification of the peri-invadopodial space. *FASEB J* **24**(10): 3903-3915.

Calvert AH, Alison DL, Harland SJ, Robinson BA, Jackman AL, Jones TR, Newell DR, Siddik ZH, Wiltshaw E, McElwain TJ and et al. (1986) A phase I evaluation of the quinazoline antifolate thymidylate synthase inhibitor, N10-propargyl-5,8-dideazafolic acid, CB3717. *Journal of clinical oncology : official journal of the American Society of Clinical Oncology* **4**(8): 1245-1252.

Calvert AH, Jones TR, Dady PJ, Grzelakowska-Sztabert B, Paine RM, Taylor GA and Harrap KR (1980) Quinazoline antifolates with dual biochemical loci of action. Biochemical and biological studies directed towards overcoming methotrexate resistance. *Eur J Cancer* **16**(5): 713-722.

Cao W and Matherly LH (2004) Analysis of the membrane topology for transmembrane domains 7-12 of the human reduced folate carrier by scanning cysteine accessibility methods. *Biochem J* **378**(Pt 1): 201-206.

Cario H, Bode H, Debatin KM, Opladen T and Schwarz K (2009) Congenital null mutations of the FOLR1 gene: a progressive neurologic disease and its treatment. *Neurology* **73**(24): 2127-2129.

Chancy CD, Kekuda R, Huang W, Prasad PD, Kuhnel JM, Sirotnak FM, Roon P, Ganapathy V and Smith SB (2000) Expression and differential polarization of the reduced-folate transporter-1 and the folate receptor alpha in mammalian retinal pigment epithelium. *J Biol Chem* **275**(27): 20676-20684.

Chang CM, Yu CC, Lu HT, Chou YF and Huang RFS (2007) Folate deprivation promotes mitochondrial oxidative decay: DNA large deletions, cytochrome c oxidase dysfunction, membrane depolarization and superoxide overproduction in rat liver. *British Journal of Nutrition* **97**(5): 855-863.

Chattopadhyay S, Moran RG and Goldman ID (2007) Pemetrexed: biochemical and cellular pharmacology, mechanisms, and clinical applications. *Mol Cancer Ther* **6**(2): 404-417.

Chattopadhyay S, Zhao R, Krupenko SA, Krupenko N and Goldman ID (2006) The inverse relationship between reduced folate carrier function and pemetrexed activity in a human colon cancer cell line. *Mol Cancer Ther* **5**(2): 438-449.

Chen S, Nagy PL and Zalkin H (1997) Role of NRF-1 in bidirectional transcription of the human GPAT-AIRC purine biosynthesis locus. *Nucleic acids research* **25**(9): 1809-1816.

Chen VJ, Bewley JR, Andis SL, Schultz RM, Iversen PW, Shih C, Mendelsohn LG, Seitz DE and Tonkinson JL (1998) Preclinical cellular pharmacology of LY231514 (MTA): a comparison with methotrexate, LY309887 and raltitrexed for their effects on intracellular folate and nucleoside triphosphate pools in CCRF-CEM cells. *Br J Cancer* **78 Suppl 3**: 27-34.

Chiang Y, Chou CY, Hsu KF, Huang YF and Shen MR (2008) EGF upregulates Na+/H+ exchanger NHE1 by post-translational regulation that is important for cervical cancer cell invasiveness. *Journal of cellular physiology* **214**(3): 810-819.

Chiche J, Ilc K, Laferriere J, Trottier E, Dayan F, Mazure NM, Brahimi-Horn MC and Pouyssegur J (2009) Hypoxia-inducible carbonic anhydrase IX and XII promote tumor cell growth by counteracting acidosis through the regulation of the intracellular pH. *Cancer Res* **69**(1): 358-368.

Chiche J, Le Fur Y, Vilmen C, Frassineti F, Daniel L, Halestrap AP, Cozzone PJ, Pouyssegur J and Lutz NW (2012) In vivo pH in metabolic-defective Ras-transformed fibroblast tumors: key role of the monocarboxylate transporter, MCT4, for inducing an alkaline intracellular pH. *Int J Cancer* **130**(7): 1511-1520.

Christopherson RI, Lyons SD and Wilson PK (2002) Inhibitors of de novo nucleotide biosynthesis as drugs. *Accounts of chemical research* **35**(11): 961-971.

Chu E, Callender MA, Farrell MP and Schmitz JC (2003) Thymidylate synthase inhibitors as anticancer agents: from bench to bedside. *Cancer Chemother Pharmacol* **52 Suppl 1**: S80-89.

Cohen MH, Justice R and Pazdur R (2009) Approval summary: pemetrexed in the initial treatment of advanced/metastatic non-small cell lung cancer. *Oncologist* **14**(9): 930-935.

Corbett TH, LoRusso P, Demchick L, Simpson C, Pugh S, White K, Kushner J, Polin L, Meyer J, Czarnecki J, Heilbrun L, Horwitz JP, Gross JL, Behrens CH, Harrison BA, McRipley RJ and Trainor G (1998) Preclinical antitumor efficacy of analogs of XK469: sodium-(2-[4-(7-chloro-2-quinoxalinyloxy)phenoxy]propionate. *Investigational new drugs* **16**(2): 129-139.

Corbett TH, Valeriote FA, Demchik L, Lowichik N, Polin L, Panchapor C, Pugh S, White K, Kushner J, Rake J, Wentland M, Golakoti T, Hetzel C, Ogino J, Patterson G and Moore R (1997) Discovery of cryptophycin-1 and BCN-183577: examples of strategies and

problems in the detection of antitumor activity in mice. *Investigational new drugs* **15**(3): 207-218.

Dahl NK, Jiang L, Chernova MN, Stuart-Tilley AK, Shmukler BE and Alper SL (2003) Deficient HCO3- transport in an AE1 mutant with normal Cl- transport can be rescued by carbonic anhydrase II presented on an adjacent AE1 protomer. *J Biol Chem* **278**(45): 44949-44958.

Dahms TE, Sainz G, Giroux EL, Caperelli CA and Smith JL (2005) The apo and ternary complex structures of a chemotherapeutic target: human glycinamide ribonucleotide transformylase. *Biochemistry* **44**(29): 9841-9850.

Davis SR, Stacpoole PW, Williamson J, Kick LS, Quinlivan EP, Coats BS, Shane B, Bailey LB and Gregory JF, 3rd (2004) Tracer-derived total and folate-dependent homocysteine remethylation and synthesis rates in humans indicate that serine is the main one-carbon donor. *American journal of physiology Endocrinology and metabolism* **286**(2): E272-279.

DeGraw JI, Colwell WT, Piper JR and Sirotnak FM (1993) Synthesis and antitumor activity of 10-propargyl-10-deazaaminopterin. *J Med Chem* **36**(15): 2228-2231.

Deng Y, Wang Y, Cherian C, Hou Z, Buck SA, Matherly LH and Gangjee A (2008) Synthesis and discovery of high affinity folate receptor-specific glycinamide ribonucleotide formyltransferase inhibitors with antitumor activity. *J Med Chem* **51**(16): 5052-5063.

Deng Y, Zhou X, Kugel Desmoulin S, Wu J, Cherian C, Hou Z, Matherly LH and Gangjee A (2009) Synthesis and biological activity of a novel series of 6-substituted thieno[2,3-d]pyrimidine antifolate inhibitors of purine biosynthesis with selectivity for high affinity folate receptors over the reduced folate carrier and proton-coupled folate transporter for cellular entry. *J Med Chem* **52**(9): 2940-2951.

Denkert C, Budczies J, Weichert W, Wohlgemuth G, Scholz M, Kind T, Niesporek S, Noske A, Buckendahl A, Dietel M and Fiehn O (2008) Metabolite profiling of human colon carcinoma--deregulation of TCA cycle and amino acid turnover. *Molecular cancer* **7**: 72.

Ding BC, Witt TL, Hukku B, Heng H, Zhang L and Matherly LH (2001) Association of deletions and translocation of the reduced folate carrier gene with profound loss of gene expression in methotrexate-resistant K562 human erythroleukemia cells. *Biochem Pharmacol* **61**(6): 665-675.

Diop-Bove NK, Wu J, Zhao R, Locker J and Goldman ID (2009) Hypermethylation of the human proton-coupled folate transporter (SLC46A1) minimal transcriptional regulatory region in an antifolate-resistant HeLa cell line. *Mol Cancer Ther* **8**(8): 2424-2431.

Dolnick BJ, Berenson RJ, Bertino JR, Kaufman RJ, Nunberg JH and Schimke RT (1979) Correlation of dihydrofolate reductase elevation with gene amplification in a homogeneously staining chromosomal region in L5178Y cells. *The Journal of cell biology* **83**(2 Pt 1): 394-402.

Dosio F, Milla P and Cattel L (2010) EC-145, a folate-targeted Vinca alkaloid conjugate for the potential treatment of folate receptor-expressing cancers. *Curr Opin Investig Drugs* **11**(12): 1424-1433.

Drake JC, Allegra CJ, Moran RG and Johnston PG (1996) Resistance to tomudex (ZD1694): multifactorial in human breast and colon carcinoma cell lines. *Biochem Pharmacol* **51**(10): 1349-1355.

Duan P, Wu J and You G (2011) Mutational analysis of the role of GXXXG motif in the function of human organic anion transporter 1 (hOAT1). *International journal of biochemistry and molecular biology* **2**(1): 1-7.

Elnakat H and Ratnam M (2004) Distribution, functionality and gene regulation of folate receptor isoforms: implications in targeted therapy. *Adv Drug Deliv Rev* **56**(8): 1067-1084.

Eloranta JJ, Zair ZM, Hiller C, Hausler S, Stieger B and Kullak-Ublick GA (2009) Vitamin D3 and its nuclear receptor increase the expression and activity of the human proton-coupled folate transporter. *Mol Pharmacol* **76**(5): 1062-1071.

Elwood PC (1989) Molecular cloning and characterization of the human folate-binding protein cDNA from placenta and malignant tissue culture (KB) cells. *J Biol Chem* **264**(25): 14893-14901.

Fairbanks LD, Bofill M, Ruckemann K and Simmonds HA (1995) Importance of ribonucleotide availability to proliferating T-lymphocytes from healthy humans. Disproportionate expansion of pyrimidine pools and contrasting effects of de novo synthesis inhibitors. *J Biol Chem* **270**(50): 29682-29689.

Fais S, De Milito A, You H and Qin W (2007) Targeting vacuolar H+-ATPases as a new strategy against cancer. *Cancer Res* **67**(22): 10627-10630.

Farber S (1949) Some observations on the effect of folic acid antagonists on acute leukemia and other forms of incurable cancer. *Blood* **4**(2): 160-167.

Farber S, Cutler EC, Hawkins JW, Harrison JH, Peirce EC, 2nd and Lenz GG (1947) The Action of Pteroylglutamic Conjugates on Man. *Science* **106**(2764): 619-621.

Farber S and Diamond LK (1948) Temporary remissions in acute leukemia in children produced by folic acid antagonist, 4-aminopteroyl-glutamic acid. *N Engl J Med* **238**(23): 787-793.

Fei YJ, Liu W, Prasad PD, Kekuda R, Oblak TG, Ganapathy V and Leibach FH (1997) Identification of the histidyl residue obligatory for the catalytic activity of the human H+/peptide cotransporters PEPT1 and PEPT2. *Biochemistry* **36**(2): 452-460.

Fendos J and Engelman D (2012) pHLIP and Acidity as a Universal Biomarker for Cancer. *The Yale journal of biology and medicine* **85**(1): 29-35.

Ferguson PL and Flintoff WF (1999) Topological and functional analysis of the human reduced folate carrier by hemagglutinin epitope insertion. *J Biol Chem* **274**(23): 16269-16278.

Ferreri AJ, Dell'Oro S, Capello D, Ponzoni M, Iuzzolino P, Rossi D, Pasini F, Ambrosetti A, Orvieto E, Ferrarese F, Arrigoni G, Foppoli M, Reni M and Gaidano G (2004) Aberrant methylation in the promoter region of the reduced folate carrier gene is a potential mechanism of resistance to methotrexate in primary central nervous system lymphomas. *British journal of haematology* **126**(5): 657-664.

Field MS, Anderson DD and Stover PJ (2011) Mthfs is an Essential Gene in Mice and a Component of the Purinosome. *Frontiers in genetics* **2**: 36.

Field MS, Anguera MC, Page R and Stover PJ (2009) 5,10-Methenyltetrahydrofolate synthetase activity is increased in tumors and modifies the efficacy of antipurine LY309887. *Arch Biochem Biophys* **481**(2): 145-150.

Field MS, Szebenyi DM and Stover PJ (2006) Regulation of de novo purine biosynthesis by methenyltetrahydrofolate synthetase in neuroblastoma. *J Biol Chem* **281**(7): 4215-4221.

Flatley RM, Payton SG, Taub JW and Matherly LH (2004) Primary acute lymphoblastic leukemia cells use a novel promoter and 5'noncoding exon for the human reduced folate carrier that encodes a modified carrier translated from an upstream translational start. *Clin Cancer Res* **10**(15): 5111-5122.

Flintoff WF and Essani K (1980) Methotrexate-resistant Chinese hamster ovary cells contain a dihydrofolate reductase with an altered affinity for methotrexate. *Biochemistry* **19**(18): 4321-4327.

Flintoff WF and Nagainis CR (1983) Transport of methotrexate in Chinese hamster ovary cells: a mutant defective in methotrexate uptake and cell binding. *Arch Biochem Biophys* **223**(2): 433-440.

Freemantle SJ, Jackman AL, Kelland LR, Calvert AH and Lunec J (1995) Molecular characterisation of two cell lines selected for resistance to the folate-based thymidylate synthase inhibitor, ZD1694. *Br J Cancer* **71**(5): 925-930.

Friedkin M and Roberts D (1956) Conversion of uracil deoxyriboside to thymidine of deoxyribonucleic acid. *J Biol Chem* **220**(2): 653-660.

Fry DW, Anderson LA, Borst M and Goldman ID (1983) Analysis of the role of membrane transport and polyglutamation of methotrexate in gut and the Ehrlich tumor in vivo as factors in drug sensitivity and selectivity. *Cancer Res* **43**(3): 1087-1092.

Fry DW, Yalowich JC and Goldman ID (1982) Rapid formation of poly-gamma-glutamyl derivatives of methotrexate and their association with dihydrofolate reductase as assessed by high pressure liquid chromatography in the Ehrlich ascites tumor cell in vitro. *J Biol Chem* **257**(4): 1890-1896.

Gallagher FA, Kettunen MI, Day SE, Hu DE, Ardenkjaer-Larsen JH, Zandt R, Jensen PR, Karlsson M, Golman K, Lerche MH and Brindle KM (2008) Magnetic resonance imaging of pH in vivo using hyperpolarized 13C-labelled bicarbonate. *Nature* **453**(7197): 940-943.

Gangjee A, Zeng Y, McGuire JJ and Kisliuk RL (2005) Synthesis of classical, four-carbon bridged 5-substituted furo[2,3-d]pyrimidine and 6-substituted pyrrolo[2,3-d]pyrimidine analogues as antifolates. *J Med Chem* **48**(16): 5329-5336.

Gangjee A, Zeng Y, McGuire JJ, Mehraein F and Kisliuk RL (2004) Synthesis of classical, three-carbon-bridged 5-substituted furo[2,3-d]pyrimidine and 6-substituted pyrrolo[2,3-d]pyrimidine analogues as antifolates. *J Med Chem* **47**(27): 6893-6901.

Ganji V and Kafai MR (2009) Demographic, lifestyle, and health characteristics and serum B vitamin status are determinants of plasma total homocysteine concentration in the post-folic acid fortification period, 1999-2004. *J Nutr* **139**(2): 345-352.

Garcia-Martin ML, Martinez GV, Raghunand N, Sherry AD, Zhang S and Gillies RJ (2006) High resolution pH(e) imaging of rat glioma using pH-dependent relaxivity. *Magnetic resonance in medicine : official journal of the Society of Magnetic Resonance in Medicine / Society of Magnetic Resonance in Medicine* **55**(2): 309-315.

Garcia-Martinez LF and Appling DR (1993) Characterization of the folate-dependent mitochondrial oxidation of carbon 3 of serine. *Biochemistry* **32**(17): 4671-4676.

Garin-Chesa P, Campbell I, Saigo PE, Lewis JL, Jr., Old LJ and Rettig WJ (1993) Trophoblast and ovarian cancer antigen LK26. Sensitivity and specificity in immunopathology and molecular identification as a folate-binding protein. *The American journal of pathology* **142**(2): 557-567.

Gates SB, Worzalla JF, Shih C, Grindey GB and Mendelsohn LG (1996) Dietary folate and folylpolyglutamate synthetase activity in normal and neoplastic murine tissues and human tumor xenografts. *Biochem Pharmacol* **52**(9): 1477-1479.

Ge Y, Haska CL, LaFiura K, Devidas M, Linda SB, Liu M, Thomas R, Taub JW and Matherly LH (2007) Prognostic role of the reduced folate carrier, the major membrane transporter for methotrexate, in childhood acute lymphoblastic leukemia: a report from the Children's Oncology Group. *Clin Cancer Res* **13**(2 Pt 1): 451-457.

Geller J, Kronn D, Jayabose S and Sandoval C (2002) Hereditary folate malabsorption: family report and review of the literature. *Medicine (Baltimore)* **81**(1): 51-68.

Gibbs DD, Theti DS, Wood N, Green M, Raynaud F, Valenti M, Forster MD, Mitchell F, Bavetsias V, Henderson E and Jackman AL (2005) BGC 945, a novel tumor-selective thymidylate synthase inhibitor targeted to alpha-folate receptor-overexpressing tumors. *Cancer Res* **65**(24): 11721-11728.

Gibson W, Bisset GM, Marsham PR, Kelland LR, Judson IR and Jackman AL (1993) The measurement of polyglutamate metabolites of the thymidylate synthase inhibitor, ICI D1694, in mouse and human cultured cells. *Biochem Pharmacol* **45**(4): 863-869.

Gillies RJ and Morse DL (2005) In vivo magnetic resonance spectroscopy in cancer. *Annual review of biomedical engineering* **7**: 287-326.

Gillies RJ, Raghunand N, Karczmar GS and Bhujwalla ZM (2002) MRI of the tumor microenvironment. *Journal of magnetic resonance imaging : JMRI* **16**(4): 430-450.

Goldie JH, Krystal G, Hartley D, Gudauskas G and Dedhar S (1980) A methotrexate insensitive variant of folate reductase present in two lines of methotrexate-resistant L5178Y cells. *Eur J Cancer* **16**(12): 1539-1546.

Goldin A, Venditti JM, Humphreys SR, Dennis D, Mantel N and Greenhouse SW (1955) A quantitative comparison of the antileukemic effectiveness of two folic acid antagonists in mice. *Journal of the National Cancer Institute* **15**(6): 1657-1664.

Goldman ID, Chattopadhyay S, Zhao R and Moran R (2010) The antifolates: evolution, new agents in the clinic, and how targeting delivery via specific membrane transporters is driving the development of a next generation of folate analogs. *Curr Opin Investig Drugs* **11**(12): 1409-1423.

Goldman ID, Lichtenstein NS and Oliverio VT (1968) Carrier-mediated transport of the folic acid analogue, methotrexate, in the L1210 leukemia cell. *J Biol Chem* **243**(19): 5007-5017.

Goldman ID and Matherly LH (1985) The cellular pharmacology of methotrexate. *Pharmacol Ther* **28**(1): 77-102.

Goldman ID and Zhao R (2002) Molecular, biochemical, and cellular pharmacology of pemetrexed. *Semin Oncol* **29**(6 Suppl 18): 3-17.

Gonen N and Assaraf YG (2010) The obligatory intestinal folate transporter PCFT (SLC46A1) is regulated by nuclear respiratory factor 1. *J Biol Chem* **285**(44): 33602-33613.

Gonen N, Bram EE and Assaraf YG (2008) PCFT/SLC46A1 promoter methylation and restoration of gene expression in human leukemia cells. *Biochem Biophys Res Commun* **376**(4): 787-792.

Gorlick R, Goker E, Trippett T, Steinherz P, Elisseyeff Y, Mazumdar M, Flintoff WF and Bertino JR (1997) Defective transport is a common mechanism of acquired methotrexate resistance in acute lymphocytic leukemia and is associated with decreased reduced folate carrier expression. *Blood* **89**(3): 1013-1018.

Gralla RJ (1995) Edatrexate studies in non-small cell lung cancer. *Lung Cancer* **12 Suppl 1**: S187-191.

Gregory JF, 3rd, Cuskelly GJ, Shane B, Toth JP, Baumgartner TG and Stacpoole PW (2000) Primed, constant infusion with [2H3]serine allows in vivo kinetic measurement of serine turnover, homocysteine remethylation, and transsulfuration processes in human one-carbon metabolism. *The American journal of clinical nutrition* **72**(6): 1535-1541.

Gunshin H, Mackenzie B, Berger UV, Gunshin Y, Romero MF, Boron WF, Nussberger S, Gollan JL and Hediger MA (1997) Cloning and characterization of a mammalian proton-coupled metal-ion transporter. *Nature* **388**(6641): 482-488.

Guo W, Healey JH, Meyers PA, Ladanyi M, Huvos AG, Bertino JR and Gorlick R (1999) Mechanisms of methotrexate resistance in osteosarcoma. *Clin Cancer Res* **5**(3): 621-627.

Haber DA, Beverley SM, Kiely ML and Schimke RT (1981) Properties of an altered dihydrofolate reductase encoded by amplified genes in cultured mouse fibroblasts. *J Biol Chem* **256**(18): 9501-9510.

Hartman SC and Buchanan JM (1959a) The biosynthesis of the purines. *Ergebnisse der Physiologie, biologischen Chemie und experimentellen Pharmakologie* **50**: 75-121.

Hartman SC and Buchanan JM (1959b) Biosynthesis of the purines. XXVI. The identification of the formyl donors of the transformylation reactions. *J Biol Chem* **234**(7): 1812-1816.

Hatch FT, Larrabee AR, Cathou RE and Buchanan JM (1961) Enzymatic synthesis of the methyl group of methionine. I. Identification of the enzymes and cofactors involved in the system isolated from Escherichia coli. *J Biol Chem* **236**: 1095-1101.

Hazarika M, White RM, Johnson JR and Pazdur R (2004) FDA drug approval summaries: pemetrexed (Alimta). *Oncologist* **9**(5): 482-488.

Helmlinger G, Yuan F, Dellian M and Jain RK (1997) Interstitial pH and pO2 gradients in solid tumors in vivo: high-resolution measurements reveal a lack of correlation. *Nat Med* **3**(2): 177-182.

Herbig K, Chiang EP, Lee LR, Hills J, Shane B and Stover PJ (2002) Cytoplasmic serine hydroxymethyltransferase mediates competition between folate-dependent deoxyribonucleotide and S-adenosylmethionine biosyntheses. *J Biol Chem* **277**(41): 38381-38389.

Hickman RK and Levy SB (1988) Evidence that TET protein functions as a multimer in the inner membrane of Escherichia coli. *J Bacteriol* **170**(4): 1715-1720.

Hilgenbrink AR and Low PS (2005) Folate receptor-mediated drug targeting: from therapeutics to diagnostics. *J Pharm Sci* **94**(10): 2135-2146.

Hill BT, Bailey BD, White JC and Goldman ID (1979) Characteristics of transport of 4-amino antifolates and folate compounds by two lines of L5178Y lymphoblasts, one with impaired transport of methotrexate. *Cancer Res* **39**(7 Pt 1): 2440-2446.

Hinton A, Sennoune SR, Bond S, Fang M, Reuveni M, Sahagian GG, Jay D, Martinez-Zaguilan R and Forgac M (2009) Function of a subunit isoforms of the V-ATPase in pH homeostasis and in vitro invasion of MDA-MB231 human breast cancer cells. *J Biol Chem* **284**(24): 16400-16408.

Hori H, Tran P, Carrera CJ, Hori Y, Rosenbach MD, Carson DA and Nobori T (1996) Methylthioadenosine phosphorylase cDNA transfection alters sensitivity to depletion of purine and methionine in A549 lung cancer cells. *Cancer Res* **56**(24): 5653-5658.

Horne DW (1993) Transport of folates and antifolates in liver. *Proc Soc Exp Biol Med* **202**(4): 385-391.

Horns RC, Jr., Dower WJ and Schimke RT (1984) Gene amplification in a leukemic patient treated with methotrexate. *Journal of clinical oncology : official journal of the American Society of Clinical Oncology* **2**(1): 2-7.

Hou Z, Kugel Desmoulin S, Etnyre E, Olive M, Hsiung B, Cherian C, Wloszczynski PA, Moin K and Matherly LH (2011) Identification and functional impact of homo-oligomers of the human proton-coupled folate transporter. *J Biol Chem*.

Hou Z and Matherly LH (2009) Oligomeric structure of the human reduced folate carrier: identification of homo-oligomers and dominant-negative effects on carrier expression and function. *J Biol Chem* **284**(5): 3285-3293.

Hou Z, Stapels SE, Haska CL and Matherly LH (2005) Localization of a substrate binding domain of the human reduced folate carrier to transmembrane domain 11 by radioaffinity labeling and cysteine-substituted accessibility methods. *J Biol Chem* **280**(43): 36206-36213.

Hou Z, Wu J, Ye J, Cherian C and Matherly LH (2010) Substrate-specific binding and conformational changes involving Ser313 and transmembrane domain 8 of the human reduced folate carrier, as determined by site-directed mutagenesis and protein cross-linking. *Biochem J* **430**(2): 265-274.

Hou Z, Ye J, Haska CL and Matherly LH (2006) Transmembrane domains 4, 5, 7, 8, and 10 of the human reduced folate carrier are important structural or functional components of the transmembrane channel for folate substrates. *J Biol Chem* **281**(44): 33588-33596.

Hovi T, Smyth JF, Allison AC and Williams SC (1976) Role of adenosine deaminase in lymphocyte proliferation. *Clinical and experimental immunology* **23**(3): 395-403.

Howell SB, Mansfield SJ and Taetle R (1981) Thymidine and hypoxanthine requirements of normal and malignant human cells for protection against methotrexate cytotoxicity. *Cancer Res* **41**(3): 945-950.

Hu S, Lustig M, Chen AP, Crane J, Kerr A, Kelley DA, Hurd R, Kurhanewicz J, Nelson SJ, Pauly JM and Vigneron DB (2008) Compressed sensing for resolution enhancement of hyperpolarized 13C flyback 3D-MRSI. *J Magn Reson* **192**(2): 258-264.

Huang D, Zhang Y and Chen X (2003a) Analysis of intracellular nucleoside triphosphate levels in normal and tumor cell lines by high-performance liquid chromatography. *J Chromatogr B Analyt Technol Biomed Life Sci* **784**(1): 101-109.

Huang Y, Lemieux MJ, Song J, Auer M and Wang DN (2003b) Structure and mechanism of the glycerol-3-phosphate transporter from Escherichia coli. *Science* **301**(5633): 616-620.

Hughes LR, Stephens TC, Boyle FT and Jackman AL (1999) Raltitrexed (Tomudex), a Highly Polyglutamatable Antifolate Thymidylate Synthase Inhibitor, in *Anticancer Drug Development Guide: Antifolate Drugs in Cancer Therapy* (Jackman AL ed) pp 147-165, Humana Press, Inc., Totowa, NJ.

Hum DW, Bell AW, Rozen R and MacKenzie RE (1988) Primary structure of a human trifunctional enzyme. Isolation of a cDNA encoding methylenetetrahydrofolate dehydrogenase-methenyltetrahydrofolate cyclohydrolase-formyltetrahydrofolate synthetase. *J Biol Chem* **263**(31): 15946-15950.

Humphreys GK and Greenberg DM (1958) Studies on the conversion of deoxyuridylic acid to thymidylic acid by a soluble extract from rat thymus. *Archives of biochemistry and biophysics* **78**(2): 275-287.

Ifergan I, Jansen G and Assaraf YG (2005) Cytoplasmic confinement of breast cancer resistance protein (BCRP/ABCG2) as a novel mechanism of adaptation to short-term folate deprivation. *Mol Pharmacol* **67**(4): 1349-1359.

Ifergan I, Meller I, Issakov J and Assaraf YG (2003) Reduced folate carrier protein expression in osteosarcoma: implications for the prediction of tumor chemosensitivity. *Cancer* **98**(9): 1958-1966.

Ilie MI, Hofman V, Ortholan C, Ammadi RE, Bonnetaud C, Havet K, Venissac N, Mouroux J, Mazure NM, Pouyssegur J and Hofman P (2011) Overexpression of carbonic anhydrase XII in tissues from resectable non-small cell lung cancers is a biomarker of good prognosis. *Int J Cancer* **128**(7): 1614-1623.

Illei PB, Rusch VW, Zakowski MF and Ladanyi M (2003) Homozygous deletion of CDKN2A and codeletion of the methylthioadenosine phosphorylase gene in the majority of pleural mesotheliomas. *Clin Cancer Res* **9**(6): 2108-2113.

Inoue K, Nakai Y, Ueda S, Kamigaso S, Ohta KY, Hatakeyama M, Hayashi Y, Otagiri M and Yuasa H (2008) Functional characterization of PCFT/HCP1 as the molecular entity of the carrier-mediated intestinal folate transport system in the rat model. *Am J Physiol Gastrointest Liver Physiol* **294**(3): G660-668.

Jackman AL (1999) Past and Future Perspectives, in *Anticancer Drug Development Guide: Antifolate Drugs in Cancer Therapy* (Jackman AL ed) pp 1-12, Humana Press Inc., Totowa, NJ.

Jackman AL, Boyle FT and Harrap KR (1996) Tomudex (ZD1694): from concept to care, a programme in rational drug discovery. *Investigational new drugs* **14**(3): 305-316.

Jackman AL and Calvert AH (1995) Folate-based thymidylate synthase inhibitors as anticancer drugs. *Annals of oncology : official journal of the European Society for Medical Oncology / ESMO* **6**(9): 871-881.

Jackman AL, Farrugia DC, Gibson W, Kimbell R, Harrap KR, Stephens TC, Azab M and Boyle FT (1995) ZD1694 (Tomudex): a new thymidylate synthase inhibitor with activity in colorectal cancer. *Eur J Cancer* **31A**(7-8): 1277-1282.

Jackman AL, Gibson W, Brown M, Kimbell R and Boyle FT (1993) The role of the reduced-folate carrier and metabolism to intracellular polyglutamates for the activity of ICI D1694. *Advances in experimental medicine and biology* **339**: 265-276.

Jackman AL, Marsham PR, Moran RG, Kimbell R, O'Connor BM, Hughes LR and Calvert AH (1991a) Thymidylate synthase inhibitors: the in vitro activity of a series of heterocyclic benzoyl ring modified 2-desamino-2-methyl-N10-substituted-5,8-dideazafolates. *Advances in enzyme regulation* **31**: 13-27.

Jackman AL, Newell DR, Gibson W, Jodrell DI, Taylor GA, Bishop JA, Hughes LR and Calvert AH (1991b) The biochemical pharmacology of the thymidylate synthase inhibitor, 2-desamino-2-methyl-N10-propargyl-5,8-dideazafolic acid (ICI 198583). *Biochem Pharmacol* **42**(10): 1885-1895.

Jackman AL, Taylor GA, Gibson W, Kimbell R, Brown M, Calvert AH, Judson IR and Hughes LR (1991c) ICI D1694, a quinazoline antifolate thymidylate synthase inhibitor that is a potent inhibitor of L1210 tumor cell growth in vitro and in vivo: a new agent for clinical study. *Cancer Res* **51**(20): 5579-5586.

Jackson RC and Harkrader RJ (1981) The contributions of de-novo and salvage pathways of nucleotide biosynthesis in normal and malignant cells, in *Nucleosides and Cancer Treatment* (Tattersall MHN and Fox RM eds) pp 18-31, Academic Press, Sydney.

Jackson RC and Harrap KR (1973) Studies with a mathematical model of folate metabolism. *Arch Biochem Biophys* **158**(2): 827-841.

Jackson RC, Hart LI and Harrap KR (1976) Intrinsic resistance to methotrexate of cultured mammalian cells in relation to the inhibition kinetics of their dihydrololate reductases. *Cancer Res* **36**(6): 1991-1997.

Jolivet J, Cowan KH, Curt GA, Clendeninn NJ and Chabner BA (1983) The pharmacology and clinical use of methotrexate. *N Engl J Med* **309**(18): 1094-1104.

Jones TR, Calvert AH, Jackman AL, Brown SJ, Jones M and Harrap KR (1981) A potent antitumour quinazoline inhibitor of thymidylate synthetase: synthesis, biological properties and therapeutic results in mice. *Eur J Cancer* **17**(1): 11-19.

Kalli KR (2007) MORAb-003, a fully humanized monoclonal antibody against the folate receptor alpha, for the potential treatment of epithelial ovarian cancer. *Curr Opin Investig Drugs* **8**(12): 1067-1073.

Kamen BA and Smith AK (2004) A review of folate receptor alpha cycling and 5-methyltetrahydrofolate accumulation with an emphasis on cell models in vitro. *Adv Drug Deliv Rev* **56**(8): 1085-1097.

Kamen BA, Wang MT, Streckfuss AJ, Peryea X and Anderson RG (1988) Delivery of folates to the cytoplasm of MA104 cells is mediated by a surface membrane receptor that recycles. *J Biol Chem* **263**(27): 13602-13609.

Karapanagiotou EM, Boura PG, Papamichalis G, Konstantinou M, Sepsas E, Chamalakis G, Simsiris P, Gkiozos I and Syrigos KN (2009) Carboplatin-pemetrexed adjuvant chemotherapy in resected non-small cell lung cancer (NSCLC): a phase II study. *Anticancer Res* **29**(10): 4297-4301.

Kastanos EK, Woldman YY and Appling DR (1997) Role of mitochondrial and cytoplasmic serine hydroxymethyltransferase isozymes in de novo purine synthesis in Saccharomyces cerevisiae. *Biochemistry* **36**(48): 14956-14964.

Katirtzoglou N, Gkiozos I, Makrilia N, Tsaroucha E, Rapti A, Stratakos G, Fountzilas G and Syrigos KN (2010) Carboplatin plus pemetrexed as first-line treatment of patients with malignant pleural mesothelioma: a phase II study. *Clinical lung cancer* **11**(1): 30-35.

Kennedy KM and Dewhirst MW (2010) Tumor metabolism of lactate: the influence and therapeutic potential for MCT and CD147 regulation. *Future Oncol* **6**(1): 127-148.

King ME, Honeysett JM and Howell SB (1983) Regulation of de novo purine synthesis in human bone marrow mononuclear cells by hypoxanthine. *J Clin Invest* **72**(3): 965-970.

Kisliuk RL (2003) Deaza analogs of folic acid as antitumor agents. *Current pharmaceutical design* **9**(31): 2615-2625.

Kitchens ME, Forsthoefel AM, Barbour KW, Spencer HT and Berger FG (1999) Mechanisms of acquired resistance to thymidylate synthase inhibitors: the role of enzyme stability. *Mol Pharmacol* **56**(5): 1063-1070.

Koizumi S, Curt GA, Fine RL, Griffin JD and Chabner BA (1985) Formation of methotrexate polyglutamates in purified myeloid precursor cells from normal human bone marrow. *J Clin Invest* **75**(3): 1008-1014.

Kondo M, Yamaoka T, Honda S, Miwa Y, Katashima R, Moritani M, Yoshimoto K, Hayashi Y and Itakura M (2000) The rate of cell growth is regulated by purine biosynthesis via ATP production and G(1) to S phase transition. *Journal of biochemistry* **128**(1): 57-64.

Krug LM, Pass HI, Rusch VW, Kindler HL, Sugarbaker DJ, Rosenzweig KE, Flores R, Friedberg JS, Pisters K, Monberg M, Obasaju CK and Vogelzang NJ (2009) Multicenter phase II trial of neoadjuvant pemetrexed plus cisplatin followed by extrapleural pneumonectomy and radiation for malignant pleural mesothelioma. *Journal of clinical oncology : official journal of the American Society of Clinical Oncology* **27**(18): 3007-3013.

Kugel Desmoulin S, Wang L, Hales E, Polin L, White K, Kushner J, Stout M, Hou Z, Cherian C, Gangjee A and Matherly LH (2011) Therapeutic targeting of a novel 6-substituted pyrrolo [2,3-d]pyrimidine thienoyl antifolate to human solid tumors based on selective uptake by the proton-coupled folate transporter. *Mol Pharmacol* **80**(6): 1096-1107.

Kugel Desmoulin S, Wang Y, Tait L, Hou Z, Cherian C, Gangjee A and Matherly LH (2010a) Expression profiling of the major folate facilitative transporters in human tumors and normal tissues. *Abstracts, American Association for Cancer Research* **51**: 1103.

Kugel Desmoulin S, Wang Y, Wu J, Stout M, Hou Z, Fulterer A, Chang MH, Romero MF, Cherian C, Gangjee A and Matherly LH (2010b) Targeting the proton-coupled folate transporter for selective delivery of 6-substituted pyrrolo[2,3-d]pyrimidine antifolate inhibitors of de novo purine biosynthesis in the chemotherapy of solid tumors. *Mol Pharmacol* **78**(4): 577-587.

Kumar AP, Quake AL, Chang MK, Zhou T, Lim KS, Singh R, Hewitt RE, Salto-Tellez M, Pervaiz S and Clement MV (2009) Repression of NHE1 expression by PPARgamma

activation is a potential new approach for specific inhibition of the growth of tumor cells in vitro and in vivo. *Cancer Res* **69**(22): 8636-8644.

Lacey SW, Sanders JM, Rothberg KG, Anderson RG and Kamen BA (1989) Complementary DNA for the folate binding protein correctly predicts anchoring to the membrane by glycosyl-phosphatidylinositol. *J Clin Invest* **84**(2): 715-720.

Laemmli UK (1970) Cleavage of structural proteins during the assembly of the head of bacteriophage T4. *Nature* **227**(5259): 680-685.

Lam-Yuk-Tseung S, Govoni G, Forbes J and Gros P (2003) Iron transport by Nramp2/DMT1: pH regulation of transport by 2 histidines in transmembrane domain 6. *Blood* **101**(9): 3699-3707.

Lasry I, Berman B, Straussberg R, Sofer Y, Bessler H, Sharkia M, Glaser F, Jansen G, Drori S and Assaraf YG (2008) A novel loss-of-function mutation in the proton-coupled folate transporter from a patient with hereditary folate malabsorption reveals that Arg 113 is crucial for function. *Blood* **112**(5): 2055-2061.

LeLeiko NS, Bronstein AD, Baliga BS and Munro HN (1983) De novo purine nucleotide synthesis in the rat small and large intestine: effect of dietary protein and purines. *Journal of pediatric gastroenterology and nutrition* **2**(2): 313-319.

Leuthold S, Hagenbuch B, Mohebbi N, Wagner CA, Meier PJ and Stieger B (2009) Mechanisms of pH-gradient driven transport mediated by organic anion polypeptide transporters. *Am J Physiol Cell Physiol* **296**(3): C570-582.

Levy AS, Sather HN, Steinherz PG, Sowers R, La M, Moscow JA, Gaynon PS, Uckun FM, Bertino JR and Gorlick R (2003) Reduced folate carrier and dihydrofolate reductase

expression in acute lymphocytic leukemia may predict outcome: a Children's Cancer Group Study. *Journal of pediatric hematology/oncology* **25**(9): 688-695.

Li WW, Lin JT, Schweitzer BI, Tong WP, Niedzwiecki D and Bertino JR (1992) Intrinsic resistance to methotrexate in human soft tissue sarcoma cell lines. *Cancer Res* **52**(14): 3908-3913.

Liani E, Rothem L, Bunni MA, Smith CA, Jansen G and Assaraf YG (2003) Loss of folylpoly-gamma-glutamate synthetase activity is a dominant mechanism of resistance to polyglutamylation-dependent novel antifolates in multiple human leukemia sublines. *Int J Cancer* **103**(5): 587-599.

Linke SP, Clarkin KC, Di Leonardo A, Tsou A and Wahl GM (1996) A reversible, p53-dependent G0/G1 cell cycle arrest induced by ribonucleotide depletion in the absence of detectable DNA damage. *Genes & development* **10**(8): 934-947.

Liu M, Ge Y, Cabelof DC, Aboukameel A, Heydari AR, Mohammad R and Matherly LH (2005) Structure and regulation of the murine reduced folate carrier gene: identification of four noncoding exons and promoters and regulation by dietary folates. *J Biol Chem* **280**(7): 5588-5597.

Liu M, Whetstine JR, Payton SG, Ge Y, Flatley RM and Matherly LH (2004) Roles of USF, Ikaros and Sp proteins in the transcriptional regulation of the human reduced folate carrier B promoter. *Biochem J* **383**(Pt 2): 249-257.

Liu XY and Matherly LH (2002) Analysis of membrane topology of the human reduced folate carrier protein by hemagglutinin epitope insertion and scanning glycosylation insertion mutagenesis. *Biochim Biophys Acta* **1564**(2): 333-342.

Loncaster JA, Harris AL, Davidson SE, Logue JP, Hunter RD, Wycoff CC, Pastorek J, Ratcliffe PJ, Stratford IJ and West CM (2001) Carbonic anhydrase (CA IX) expression, a potential new intrinsic marker of hypoxia: correlations with tumor oxygen measurements and prognosis in locally advanced carcinoma of the cervix. *Cancer Res* **61**(17): 6394-6399.

Lorico A, Toffoli G, Boiocchi M, Erba E, Broggini M, Rappa G and D'Incalci M (1988) Accumulation of DNA strand breaks in cells exposed to methotrexate or N10-propargyl-5,8-dideazafolic acid. *Cancer Res* **48**(8): 2036-2041.

Lowry OH, Rosebrough NJ, Farr AL and Randall RJ (1951) Protein measurement with the Folin phenol reagent. *J Biol Chem* **193**(1): 265-275.

Lu SC (2000) S-Adenosylmethionine. *The international journal of biochemistry & cell biology* **32**(4): 391-395.

Lunt SY and Vander Heiden MG (2011) Aerobic glycolysis: meeting the metabolic requirements of cell proliferation. *Annual review of cell and developmental biology* **27**: 441-464.

MacFarlane AJ, Liu X, Perry CA, Flodby P, Allen RH, Stabler SP and Stover PJ (2008) Cytoplasmic serine hydroxymethyltransferase regulates the metabolic partitioning of methylenetetrahydrofolate but is not essential in mice. *J Biol Chem* **283**(38): 25846-25853.

Mackenzie B, Ujwal ML, Chang MH, Romero MF and Hediger MA (2006) Divalent metal-ion transporter DMT1 mediates both H+ -coupled Fe2+ transport and uncoupled fluxes. *Pflugers Arch* **451**(4): 544-558.

Mackinnon AM and Deller DJ (1973) Purine nucleotide biosynthesis in gastrointestinal mucosa. *Biochimica et Biophysica Acta (BBA) - Nucleic Acids and Protein Synthesis* **319**(1): 1-4.

Mahadeo K, Diop-Bove N, Shin D, Unal ES, Teo J, Zhao R, Chang MH, Fulterer A, Romero MF and Goldman ID (2010) Properties of the Arg376 residue of the proton-coupled folate transporter (PCFT-SLC46A1) and a glutamine mutant causing hereditary folate malabsorption. *Am J Physiol Cell Physiol* **299**(5): C1153-1161.

Mahadeo KM, Diop-Bove N, Ramirez SI, Cadilla CL, Rivera E, Martin M, Lerner NB, DiAntonio L, Duva S, Santiago-Borrero PJ and Goldman ID (2011) Prevalence of a loss-of-function mutation in the proton-coupled folate transporter gene (PCFT-SLC46A1) causing hereditary folate malabsorption in Puerto Rico. *J Pediatr* **159**(4): 623-627 e621.

Marchi E, Paoluzzi L, Scotto L, Seshan VE, Zain JM, Zinzani PL and O'Connor OA (2010) Pralatrexate is synergistic with the proteasome inhibitor bortezomib in in vitro and in vivo models of T-cell lymphoid malignancies. *Clin Cancer Res* **16**(14): 3648-3658.

Martin GR and Jain RK (1994) Noninvasive measurement of interstitial pH profiles in normal and neoplastic tissue using fluorescence ratio imaging microscopy. *Cancer Res* **54**(21): 5670-5674.

Martin M, Blasinska-Morawiec M, Salas JF, Falcon S, Rolski J, Ferrari BL, Gulyas S, Liu Y and Benhadji KA (2009) A multicenter, single-arm phase II study of pemetrexed plus doxorubicin administered every 21 days in patients with advanced breast cancer. *Clinical breast cancer* **9**(3): 155-160.

Martinez-Zaguilan R, Lynch RM, Martinez GM and Gillies RJ (1993) Vacuolar-type H(+)-ATPases are functionally expressed in plasma membranes of human tumor cells. *The American journal of physiology* **265**(4 Pt 1): C1015-1029.

Matherly LH, Barlowe CK, Phillips VM and Goldman ID (1987a) The effects on 4-aminoantifolates on 5-formyltetrahydrofolate metabolism in L1210 cells. A biochemical basis of the selectivity of leucovorin rescue. *J Biol Chem* **262**(2): 710-717.

Matherly LH, Czajkowski CA and Angeles SM (1991) Identification of a highly glycosylated methotrexate membrane carrier in K562 human erythroleukemia cells up-regulated for tetrahydrofolate cofactor and methotrexate transport. *Cancer Res* **51**(13): 3420-3426.

Matherly LH, Fry DW and Goldman ID (1983) Role of methotrexate polyglutamylation and cellular energy metabolism in inhibition of methotrexate binding to dihydrofolate reductase by 5-formyltetrahydrofolate in Ehrlich ascites tumor cells in vitro. *Cancer Res* **43**(6): 2694-2699.

Matherly LH and Goldman DI (2003) Membrane transport of folates. *Vitam Horm* **66**: 403-456.

Matherly LH, Hou Z and Deng Y (2007) Human reduced folate carrier: translation of basic biology to cancer etiology and therapy. *Cancer Metastasis Rev* **26**(1): 111-128.

Matherly LH, Seither RL and Goldman ID (1987b) Metabolism of the diaminoantifolates: biosynthesis and pharmacology of the 7-hydroxyl and polyglutamyl metabolites of methotrexate and related antifolates. *Pharmacol Ther* **35**(1-2): 27-56.

Matherly LH, Voss MK, Anderson LA, Fry DW and Goldman ID (1985) Enhanced polyglutamylation of aminopterin relative to methotrexate in the Ehrlich ascites tumor cell in vitro. *Cancer Res* **45**(3): 1073-1078.

Matsudaira P (1987) Sequence from picomole quantities of proteins electroblotted onto polyvinylidene difluoride membranes. *J Biol Chem* **262**(21): 10035-10038.

Matsui SI, Arredondo MA, Wrzosek C and Rustum YM (1996) DNA damage and p53 induction do not cause ZD1694-induced cell cycle arrest in human colon carcinoma cells. *Cancer Res* **56**(20): 4715-4723.

Matulonis UA, Horowitz NS, Campos SM, Lee H, Lee J, Krasner CN, Berlin S, Roche MR, Duska LR, Pereira L, Kendall D and Penson RT (2008) Phase II study of carboplatin and pemetrexed for the treatment of platinum-sensitive recurrent ovarian cancer. *Journal of clinical oncology : official journal of the American Society of Clinical Oncology* **26**(35): 5761-5766.

Mauritz R, Peters GJ, Priest DG, Assaraf YG, Drori S, Kathmann I, Noordhuis P, Bunni MA, Rosowsky A, Schornagel JH, Pinedo HM and Jansen G (2002) Multiple mechanisms of resistance to methotrexate and novel antifolates in human CCRF-CEM leukemia cells and their implications for folate homeostasis. *Biochem Pharmacol* **63**(2): 105-115.

McCloskey DE, McGuire JJ, Russell CA, Rowan BG, Bertino JR, Pizzorno G and Mini E (1991) Decreased folylpolyglutamate synthetase activity as a mechanism of methotrexate resistance in CCRF-CEM human leukemia sublines. *J Biol Chem* **266**(10): 6181-6187.

McDougall BM and Blakley R (1960) Mechanism of the action of thymidylate synthetase. *Nature* **188**: 944.

McGuire JJ and Russell CA (1998) Folylpolyglutamate synthetase expression in antifolate-sensitive and -resistant human cell lines. *Oncology research* **10**(4): 193-200.

McIvor RS and Simonsen CC (1990) Isolation and characterization of a variant dihydrofolate reductase cDNA from methotrexate-resistant murine L5178Y cells. *Nucleic acids research* **18**(23): 7025-7032.

McLean LA, Roscoe J, Jorgensen NK, Gorin FA and Cala PM (2000) Malignant gliomas display altered pH regulation by NHE1 compared with nontransformed astrocytes. *Am J Physiol Cell Physiol* **278**(4): C676-688.

Mejia NR and MacKenzie RE (1985) NAD-dependent methylenetetrahydrofolate dehydrogenase is expressed by immortal cells. *J Biol Chem* **260**(27): 14616-14620.

Melera PW, Davide JP, Hession CA and Scotto KW (1984) Phenotypic expression in Escherichia coli and nucleotide sequence of two Chinese hamster lung cell cDNAs encoding different dihydrofolate reductases. *Mol Cell Biol* **4**(1): 38-48.

Melera PW, Davide JP and Oen H (1988) Antifolate-resistant Chinese hamster cells. Molecular basis for the biochemical and structural heterogeneity among dihydrofolate reductases produced by drug-sensitive and drug-resistant cell lines. *J Biol Chem* **263**(4): 1978-1990.

Mendelsohn G, Worzalla, J.F., Walling, J.M. (1999) Preclinical and clinical evaluation of the glycinamide ribonucleotidee formytransferase inhibitors Lometrexol and LY309887, in *Anticancer Development Guide: Antifolate Drugs in Cancer Therapy* (Jackman A ed) pp 261-280, Humana Press Inc., Totowa,NJ.

Mendelsohn LG, Gates SB, Habeck LL, Shackelford KA, Worzalla J, Shih C and Grindey GB (1996) The role of dietary folate in modulation of folate receptor expression, folylpolyglutamate synthetase activity and the efficacy and toxicity of lometrexol. *Advances in enzyme regulation* **36**: 365-381.

Mendelsohn LG, Worzalla JF and Walling JM (1999) Preclinical and Clinical Evaluation of the Glycinamide Ribonucleotide Formyltransferase Inhibitors Lometrexol and LY309887, in *Anticancer Drug Development Guide: Antifolate Drugs in Cancer Therapy* (Jackman AL ed) pp 261-280, Humana Press, Inc., Totowa, NJ.

Metzner L, Natho K, Zebisch K, Dorn M, Bosse-Doenecke E, Ganapathy V and Brandsch M (2008) Mutational analysis of histidine residues in the human proton-coupled amino acid transporter PAT1. *Biochim Biophys Acta* **1778**(4): 1042-1050.

Meyer E, Kurian MA, Pasha S, Trembath RC, Cole T and Maher ER (2010) A novel PCFT gene mutation (p.Cys66LeufsX99) causing hereditary folate malabsorption. *Mol Genet Metab* **99**(3): 325-328.

Min SH, Oh SY, Karp GI, Poncz M, Zhao R and Goldman ID (2008) The clinical course and genetic defect in the PCFT gene in a 27-year-old woman with hereditary folate malabsorption. *J Pediatr* **153**(3): 435-437.

Mini E, Srimatkandada S, Medina WD, Moroson BA, Carman MD and Bertino JR (1985) Molecular and karyological analysis of methotrexate-resistant and -sensitive human leukemic CCRF-CEM cells. *Cancer Res* **45**(1): 317-324.

Miraglia E, Viarisio D, Riganti C, Costamagna C, Ghigo D and Bosia A (2005) Na+/H+ exchanger activity is increased in doxorubicin-resistant human colon cancer cells and its modulation modifies the sensitivity of the cells to doxorubicin. *Int J Cancer* **115**(6): 924-929.

Miyachi H, Takemura Y, Kobayashi H and Ando Y (1995) Expression of variant dihydrofolate reductase with decreased binding affinity to antifolates in MOLT-3 human leukemia cell lines resistant to trimetrexate. *Cancer letters* **88**(1): 93-99.

Monahan BPA, C.J. (2001) Antifolates in *Cancer Chemotherapy and Biotherapy* (D.L. CBAL ed) pp 109-148, Lippincott-Raven, Philadelphia.

Moran RG, Baldwin SW, Taylor EC and Shih C (1989) The 6S- and 6R-diastereomers of 5, 10-dideaza-5, 6, 7, 8-tetrahydrofolate are equiactive inhibitors of de novo purine synthesis. *J Biol Chem* **264**(35): 21047-21051.

Murray AW (1971) The biological significance of purine salvage. *Annual review of biochemistry* **40**: 811-826.

Nakai Y, Inoue K, Abe N, Hatakeyama M, Ohta KY, Otagiri M, Hayashi Y and Yuasa H (2007) Functional characterization of human proton-coupled folate transporter/heme carrier protein 1 heterologously expressed in mammalian cells as a folate transporter. *J Pharmacol Exp Ther* **322**(2): 469-476.

Nakanishi T, Tamai I, Takaki A and Tsuji A (2000) Cancer cell-targeted drug delivery utilizing oligopeptide transport activity. *Int J Cancer* **88**(2): 274-280.

Niethammer D and Jackson RC (1975) Changes of molecular properties associated with the development of resistance against methotrexate in human lymphoblastoid cells. *Eur J Cancer* **11**(12): 845-854.

Nozawa T, Imai K, Nezu J, Tsuji A and Tamai I (2004) Functional characterization of pH-sensitive organic anion transporting polypeptide OATP-B in human. *J Pharmacol Exp Ther* **308**(2): 438-445.

Nunberg JH, Kaufman RJ, Schimke RT, Urlaub G and Chasin LA (1978) Amplified dihydrofolate reductase genes are localized to a homogeneously staining region of a single chromosome in a methotrexate-resistant Chinese hamster ovary cell line. *Proceedings of the National Academy of Sciences of the United States of America* **75**(11): 5553-5556.

O'Connor BM, Jackman AL, Crossley PH, Freemantle SE, Lunec J and Calvert AH (1992) Human lymphoblastoid cells with acquired resistance to C2-desamino-C2-methyl-N10-propargyl-5,8-dideazafolic acid: a novel folate-based thymidylate synthase inhibitor. *Cancer Res* **52**(5): 1137-1143.

Pan XQ, Zheng X, Shi G, Wang H, Ratnam M and Lee RJ (2002) Strategy for the treatment of acute myelogenous leukemia based on folate receptor beta-targeted liposomal doxorubicin combined with receptor induction using all-trans retinoic acid. *Blood* **100**(2): 594-602.

Pasternack LB, Laude DA, Jr. and Appling DR (1994) 13C NMR analysis of intercompartmental flow of one-carbon units into choline and purines in Saccharomyces cerevisiae. *Biochemistry* **33**(1): 74-82.

Pasternack LB, Littlepage LE, Laude DA, Jr. and Appling DR (1996) 13C NMR analysis of the use of alternative donors to the tetrahydrofolate-dependent one-carbon pools in Saccharomyces cerevisiae. *Arch Biochem Biophys* **326**(1): 158-165.

Patel H, Pietro ED and MacKenzie RE (2003) Mammalian fibroblasts lacking mitochondrial NAD+-dependent methylenetetrahydrofolate dehydrogenase-cyclohydrolase are glycine auxotrophs. *J Biol Chem* **278**(21): 19436-19441.

Patel JD, Bonomi P, Socinski MA, Govindan R, Hong S, Obasaju C, Pennella EJ, Girvan AC and Guba SC (2009a) Treatment rationale and study design for the pointbreak study: a randomized, open-label phase III study of pemetrexed/carboplatin/bevacizumab followed by maintenance pemetrexed/bevacizumab versus paclitaxel/carboplatin/bevacizumab followed by maintenance bevacizumab in patients with stage IIIB or IV nonsquamous non-small-cell lung cancer. *Clinical lung cancer* **10**(4): 252-256.

Patel JD, Hensing TA, Rademaker A, Hart EM, Blum MG, Milton DT and Bonomi PD (2009b) Phase II study of pemetrexed and carboplatin plus bevacizumab with maintenance pemetrexed and bevacizumab as first-line therapy for nonsquamous non-small-cell lung cancer. *Journal of clinical oncology : official journal of the American Society of Clinical Oncology* **27**(20): 3284-3289.

Paukert JL, Williams GR and Rabinowitz JC (1977) Formyl-methenyl-methylenetetrahydrofolate synthetase (combined); correlation of enzymic activities with limited proteolytic degradation of the protein from yeast. *Biochem Biophys Res Commun* **77**(1): 147-154.

Payton SG, Haska CL, Flatley RM, Ge Y and Matherly LH (2007) Effects of 5' untranslated region diversity on the posttranscriptional regulation of the human reduced folate carrier. *Biochim Biophys Acta* **1769**(2): 131-138.

Payton SG, Liu M, Ge Y and Matherly LH (2005a) Transcriptional regulation of the human reduced folate carrier A1/A2 promoter: Identification of critical roles for the USF and GATA families of transcription factors. *Biochim Biophys Acta* **1731**(2): 115-124.

Payton SG, Whetstine JR, Ge Y and Matherly LH (2005b) Transcriptional regulation of the human reduced folate carrier promoter C: synergistic transactivation by Sp1 and C/EBP beta and identification of a downstream repressor. *Biochim Biophys Acta* **1727**(1): 45-57.

Paz-Ares LG, Altug S, Vaury AT, Jaime JC, Russo F and Visseren-Grul C (2010) Treatment rationale and study design for a phase III, double-blind, placebo-controlled study of maintenance pemetrexed plus best supportive care versus best supportive care immediately following induction treatment with pemetrexed plus cisplatin for advanced nonsquamous non-small cell lung cancer. *BMC cancer* **10**: 85.

Phear EA and Greenberg DM (1957) The Methylation of Deoxyuridine1. *Journal of the American Chemical Society* **79**(14): 3737-3741.

Pinheiro C, Longatto-Filho A, Ferreira L, Pereira SM, Etlinger D, Moreira MA, Jube LF, Queiroz GS, Schmitt F and Baltazar F (2008a) Increasing expression of monocarboxylate transporters 1 and 4 along progression to invasive cervical carcinoma. *International journal of gynecological pathology : official journal of the International Society of Gynecological Pathologists* **27**(4): 568-574.

Pinheiro C, Longatto-Filho A, Scapulatempo C, Ferreira L, Martins S, Pellerin L, Rodrigues M, Alves VA, Schmitt F and Baltazar F (2008b) Increased expression of monocarboxylate transporters 1, 2, and 4 in colorectal carcinomas. *Virchows Archiv : an international journal of pathology* **452**(2): 139-146.

Pinheiro C, Reis RM, Ricardo S, Longatto-Filho A, Schmitt F and Baltazar F (2010) Expression of monocarboxylate transporters 1, 2, and 4 in human tumours and their association with CD147 and CD44. *Journal of biomedicine & biotechnology* **2010**: 427694.

Pippen J, Elias AD, Neubauer M, Stokoe C, Vaughn LG, Wang Y, Orlando M, Shonukan O, Muscato J, O'Shaughnessy JA and Gralow J (2010) A phase II trial of pemetrexed and gemcitabine in patients with metastatic breast cancer who have received prior taxane therapy. *Clinical breast cancer* **10**(2): 148-153.

Pizzorno G, Chang YM, McGuire JJ and Bertino JR (1989) Inherent resistance of human squamous carcinoma cell lines to methotrexate as a result of decreased polyglutamylation of this drug. *Cancer Res* **49**(19): 5275-5280.

Pizzorno G, Mini E, Coronnello M, McGuire JJ, Moroson BA, Cashmore AR, Dreyer RN, Lin JT, Mazzei T, Periti P and et al. (1988) Impaired polyglutamylation of methotrexate as a

cause of resistance in CCRF-CEM cells after short-term, high-dose treatment with this drug. *Cancer Res* **48**(8): 2149-2155.

Pizzorno G, Moroson BA, Cashmore AR and Beardsley GP (1991) (6R)-5,10-Dideaza-5,6,7,8-tetrahydrofolic acid effects on nucleotide metabolism in CCRF-CEM human T-lymphoblast leukemia cells. *Cancer Res* **51**(9): 2291-2295.

Pizzorno G, Moroson BA, Cashmore AR, Russello O, Mayer JR, Galivan J, Bunni MA, Priest DG and Beardsley GP (1995) Multifactorial resistance to 5,10-dideazatetrahydrofolic acid in cell lines derived from human lymphoblastic leukemia CCRF-CEM. *Cancer Res* **55**(3): 566-573.

Pohland RC, Alati T, Lantz RJ and Grindey GB (1994) Whole-body autoradiographic disposition and plasma pharmacokinetics of 5,10-dideazatetrahydrofolic acid in mice fed folic acid-deficient or regular diets. *J Pharm Sci* **83**(10): 1396-1399.

Polgar O, Ierano C, Tamaki A, Stanley B, Ward Y, Xia D, Tarasova N, Robey RW and Bates SE (2010) Mutational analysis of threonine 402 adjacent to the GXXXG dimerization motif in transmembrane segment 1 of ABCG2. *Biochemistry* **49**(10): 2235-2245.

Polin L, Corbett TH, Roberts BJ, Lawson AJ, Leopold WR, White K, Kushner J, Hazeldine S, Moore R, Rake J and Horwitz JP (2011) Transplantable Syngeneic Rodent Tumors: Solid Tumors in Mice

Tumor Models in Cancer Research, (Teicher BA ed) pp 43-78, Humana Press.

Polin L, Valeriote F, White K, Panchapor C, Pugh S, Knight J, LoRusso P, Hussain M, Liversidge E, Peltier N, Golakoti T, Patterson G, Moore R and Corbett TH (1997) Treatment of human prostate tumors PC-3 and TSU-PR1 with standard and investigational agents in SCID mice. *Investigational new drugs* **15**(2): 99-108.

Prasannan P, Pike S, Peng K, Shane B and Appling DR (2003) Human mitochondrial C1-tetrahydrofolate synthase: gene structure, tissue distribution of the mRNA, and immunolocalization in Chinese hamster ovary calls. *J Biol Chem* **278**(44): 43178-43187.

Pui CH and Evans WE (2006) Treatment of acute lymphoblastic leukemia. *N Engl J Med* **354**(2): 166-178.

Qiu A, Jansen M, Sakaris A, Min SH, Chattopadhyay S, Tsai E, Sandoval C, Zhao R, Akabas MH and Goldman ID (2006) Identification of an intestinal folate transporter and the molecular basis for hereditary folate malabsorption. *Cell* **127**(5): 917-928.

Qiu A, Min SH, Jansen M, Malhotra U, Tsai E, Cabelof DC, Matherly LH, Zhao R, Akabas MH and Goldman ID (2007) Rodent intestinal folate transporters (SLC46A1): secondary structure, functional properties, and response to dietary folate restriction. *Am J Physiol Cell Physiol* **293**(5): C1669-1678.

Quinlivan EP, Davis SR, Shelnutt KP, Henderson GN, Ghandour H, Shane B, Selhub J, Bailey LB, Stacpoole PW and Gregory JF, 3rd (2005) Methylenetetrahydrofolate reductase 677C->T polymorphism and folate status affect one-carbon incorporation into human DNA deoxynucleosides. *J Nutr* **135**(3): 389-396.

Racanelli AC, Rothbart SB, Heyer CL and Moran RG (2009) Therapeutics by cytotoxic metabolite accumulation: pemetrexed causes ZMP accumulation, AMPK activation, and mammalian target of rapamycin inhibition. *Cancer Res* **69**(13): 5467-5474.

Raghunand N, Altbach MI, van Sluis R, Baggett B, Taylor CW, Bhujwalla ZM and Gillies RJ (1999) Plasmalemmal pH-gradients in drug-sensitive and drug-resistant MCF-7 human breast carcinoma xenografts measured by 31P magnetic resonance spectroscopy. *Biochem Pharmacol* **57**(3): 309-312.

Ragoussis J, Senger G, Trowsdale J and Campbell IG (1992) Genomic organization of the human folate receptor genes on chromosome 11q13. *Genomics* **14**(2): 423-430.

Ratnam M, Marquardt H, Duhring JL and Freisheim JH (1989) Homologous membrane folate binding proteins in human placenta: cloning and sequence of a cDNA. *Biochemistry* **28**(20): 8249-8254.

Ray MS, Muggia FM, Leichman CG, Grunberg SM, Nelson RL, Dyke RW and Moran RG (1993) Phase I study of (6R)-5,10-dideazatetrahydrofolate: a folate antimetabolite inhibitory to de novo purine synthesis. *Journal of the National Cancer Institute* **85**(14): 1154-1159.

Reddy JA, Dorton R, Westrick E, Dawson A, Smith T, Xu LC, Vetzel M, Kleindl P, Vlahov IR and Leamon CP (2007) Preclinical evaluation of EC145, a folate-vinca alkaloid conjugate. *Cancer Res* **67**(9): 4434-4442.

Reddy JA, Haneline LS, Srour EF, Antony AC, Clapp DW and Low PS (1999) Expression and functional characterization of the beta-isoform of the folate receptor on CD34(+) cells. *Blood* **93**(11): 3940-3948.

Rijnboutt S, Jansen G, Posthuma G, Hynes JB, Schornagel JH and Strous GJ (1996) Endocytosis of GPI-linked membrane folate receptor-alpha. *The Journal of cell biology* **132**(1-2): 35-47.

Roberts JD, Poplin EA, Tombes MB, Kyle B, Spicer DV, Grant S, Synold T and Moran R (2000a) Weekly lometrexol with daily oral folic acid is appropriate for phase II evaluation. *Cancer Chemother Pharmacol* **45**(2): 103-110.

Roberts JD, Shibata S, Spicer DV, McLeod HL, Tombes MB, Kyle B, Carroll M, Sheedy B, Collier MA, Pithavala YK, Paradiso LJ and Clendeninn NJ (2000b) Phase I study of

AG2034, a targeted GARFT inhibitor, administered once every 3 weeks. *Cancer Chemother Pharmacol* **45**(5): 423-427.

Roberts SJ, Petropavlovskaja M, Chung KN, Knight CB and Elwood PC (1998) Role of individual N-linked glycosylation sites in the function and intracellular transport of the human alpha folate receptor. *Arch Biochem Biophys* **351**(2): 227-235.

Ross JF, Chaudhuri PK and Ratnam M (1994) Differential regulation of folate receptor isoforms in normal and malignant tissues in vivo and in established cell lines. Physiologic and clinical implications. *Cancer* **73**(9): 2432-2443.

Ross JF, Wang H, Behm FG, Mathew P, Wu M, Booth R and Ratnam M (1999) Folate receptor type beta is a neutrophilic lineage marker and is differentially expressed in myeloid leukemia. *Cancer* **85**(2): 348-357.

Rothbart SB, Racanelli AC and Moran RG (2010) Pemetrexed indirectly activates the metabolic kinase AMPK in human carcinomas. *Cancer Res* **70**(24): 10299-10309.

Rothem L, Ifergan I, Kaufman Y, Priest DG, Jansen G and Assaraf YG (2002) Resistance to multiple novel antifolates is mediated via defective drug transport resulting from clustered mutations in the reduced folate carrier gene in human leukaemia cell lines. *Biochem J* **367**(Pt 3): 741-750.

Rubio-Aliaga I, Frey I, Boll M, Groneberg DA, Eichinger HM, Balling R and Daniel H (2003) Targeted disruption of the peptide transporter Pept2 gene in mice defines its physiological role in the kidney. *Mol Cell Biol* **23**(9): 3247-3252.

Sabharanjak S and Mayor S (2004) Folate receptor endocytosis and trafficking. *Adv Drug Deliv Rev* **56**(8): 1099-1109.

Sadasivan E and Rothenberg SP (1989) The complete amino acid sequence of a human folate binding protein from KB cells determined from the cDNA. *J Biol Chem* **264**(10): 5806-5811.

Salazar MD and Ratnam M (2007) The folate receptor: what does it promise in tissue-targeted therapeutics? *Cancer Metastasis Rev* **26**(1): 141-152.

Scarpulla RC (2002) Transcriptional activators and coactivators in the nuclear control of mitochondrial function in mammalian cells. *Gene* **286**(1): 81-89.

Scarpulla RC (2006) Nuclear control of respiratory gene expression in mammalian cells. *Journal of cellular biochemistry* **97**(4): 673-683.

Scarpulla RC (2008) Transcriptional paradigms in mammalian mitochondrial biogenesis and function. *Physiological reviews* **88**(2): 611-638.

Scarpulla RC (2011) Nucleus-encoded regulators of mitochondrial function: Integration of respiratory chain expression, nutrient sensing and metabolic stress. *Biochim Biophys Acta*.

Schirch L (1978) Formyl-methenyl-methylenetetrahydrofolate synthetase from rabbit liver (combined). Evidence for a single site in the conversion of 5,10-methylenetetrahydrofolate to 10-formyltetrahydrofolate. *Arch Biochem Biophys* **189**(2): 283-290.

Schmid FA, Sirotnak FM, Otter GM and DeGraw JI (1985) New folate analogs of the 10-deaza-aminopterin series: markedly increased antitumor activity of the 10-ethyl analog compared to the parent compound and methotrexate against some human tumor xenografts in nude mice. *Cancer treatment reports* **69**(5): 551-553.

Schmid M, Malicki D, Nobori T, Rosenbach MD, Campbell K, Carson DA and Carrera CJ (1998) Homozygous deletions of methylthioadenosine phosphorylase (MTAP) are more frequent than p16INK4A (CDKN2) homozygous deletions in primary non-small cell lung cancers (NSCLC). *Oncogene* **17**(20): 2669-2675.

Segal MB (2000) The choroid plexuses and the barriers between the blood and the cerebrospinal fluid. *Cellular and molecular neurobiology* **20**(2): 183-196.

Seither RL, Trent DF, Mikulecky DC, Rape TJ and Goldman ID (1989) Folate-pool interconversions and inhibition of biosynthetic processes after exposure of L1210 leukemia cells to antifolates. Experimental and network thermodynamic analyses of the role of dihydrofolate polyglutamylates in antifolate action in cells. *J Biol Chem* **264**(29): 17016-17023.

Sennoune SR, Bakunts K, Martinez GM, Chua-Tuan JL, Kebir Y, Attaya MN and Martinez-Zaguilan R (2004) Vacuolar H+-ATPase in human breast cancer cells with distinct metastatic potential: distribution and functional activity. *Am J Physiol Cell Physiol* **286**(6): C1443-1452.

Shane B (1989) Folylpolyglutamate synthesis and role in the regulation of one-carbon metabolism. *Vitam Horm* **45**: 263-335.

Shayeghi M, Latunde-Dada GO, Oakhill JS, Laftah AH, Takeuchi K, Halliday N, Khan Y, Warley A, McCann FE, Hider RC, Frazer DM, Anderson GJ, Vulpe CD, Simpson RJ and McKie AT (2005) Identification of an intestinal heme transporter. *Cell* **122**(5): 789-801.

Shen F, Ross JF, Wang X and Ratnam M (1994) Identification of a novel folate receptor, a truncated receptor, and receptor type beta in hematopoietic cells: cDNA cloning, expression, immunoreactivity, and tissue specificity. *Biochemistry* **33**(5): 1209-1215.

Shen F, Wang H, Zheng X and Ratnam M (1997) Expression levels of functional folate receptors alpha and beta are related to the number of N-glycosylated sites. *Biochem J* **327 (Pt 3)**: 759-764.

Shen F, Wu M, Ross JF, Miller D and Ratnam M (1995) Folate receptor type gamma is primarily a secretory protein due to lack of an efficient signal for glycosylphosphatidylinositol modification: protein characterization and cell type specificity. *Biochemistry* **34**(16): 5660-5665.

Shih C, Barnett, C. J., Grindey, G. B., Pearce, H. L., Engelhardt, J. A., Todd, G. C., Rinzel, S. M., Worzalla, J. F., Gossett, L. S., Everson, T. P., Wilson, T. M., Kobierski, M. E., Winter, M. A., Moran, R. G., Kuhnt, D., Taylor, E. C. (1993) Structural Features That Determine the Biological Activity of Pyrrolo[2,3-d]pyrimidine Based Antifolates, in *The 10th International Symposium, Chemistry and Biology of Pteridines and Folates*, Orange Beach, AL.

Shih C, Chen VJ, Gossett LS, Gates SB, MacKellar WC, Habeck LL, Shackelford KA, Mendelsohn LG, Soose DJ, Patel VF, Andis SL, Bewley JR, Rayl EA, Moroson BA, Beardsley GP, Kohler W, Ratnam M and Schultz RM (1997) LY231514, a pyrrolo[2,3-d]pyrimidine-based antifolate that inhibits multiple folate-requiring enzymes. *Cancer Res* **57**(6): 1116-1123.

Shih C and Thornton DE (1999) Preclinical Pharmacology Studies and the Clinical Development of a Novel Multitargeted Antifolate, MTA (LY231514), in *Anticancer Drug Development Guide: Antifolate Drugs in Cancer Therapy* (Jackman AL ed) pp 183-201, Humana Press, Inc., Totowa, NJ.

Shin DS, Mahadeo K, Min SH, Diop-Bove N, Clayton P, Zhao R and Goldman ID (2011) Identification of novel mutations in the proton-coupled folate transporter (PCFT-SLC46A1) associated with hereditary folate malabsorption. *Mol Genet Metab* **103**(1): 33-37.

Shin DS, Min SH, Russell L, Zhao R, Fiser A and Goldman ID (2010) Functional roles of aspartate residues of the proton-coupled folate transporter (PCFT-SLC46A1); a D156Y mutation causing hereditary folate malabsorption. *Blood* **116**(24): 5162-5169.

Shin DS, Zhao R, Yap EH, Fiser A and Goldman ID (2012) A P425R mutation of the proton-coupled folate transporter causing hereditary folate malabsorption produces a highly selective alteration in folate binding. *Am J Physiol Cell Physiol*.

Shum KY, Kris MG, Gralla RJ, Burke MT, Marks LD and Heelan RT (1988) Phase II study of 10-ethyl-10-deaza-aminopterin in patients with stage III and IV non-small-cell lung cancer. *Journal of clinical oncology : official journal of the American Society of Clinical Oncology* **6**(3): 446-450.

Sigmond J, Backus HH, Wouters D, Temmink OH, Jansen G and Peters GJ (2003) Induction of resistance to the multitargeted antifolate Pemetrexed (ALIMTA) in WiDr human colon cancer cells is associated with thymidylate synthase overexpression. *Biochem Pharmacol* **66**(3): 431-438.

Simon GR, Verschraegen CF, Janne PA, Langer CJ, Dowlati A, Gadgeel SM, Kelly K, Kalemkerian GP, Traynor AM, Peng G, Gill J, Obasaju CK and Kindler HL (2008) Pemetrexed plus gemcitabine as first-line chemotherapy for patients with peritoneal mesothelioma: final report of a phase II trial. *Journal of clinical oncology : official journal of the American Society of Clinical Oncology* **26**(21): 3567-3572.

Sirotnak FM, DeGraw JI, Colwell WT and Piper JR (1998) A new analogue of 10-deazaaminopterin with markedly enhanced curative effects against human tumor xenografts in mice. *Cancer Chemother Pharmacol* **42**(4): 313-318.

Sirotnak FM, DeGraw JI, Schmid FA, Goutas LJ and Moccio DM (1984) New folate analogs of the 10-deaza-aminopterin series. Further evidence for markedly increased antitumor efficacy compared with methotrexate in ascitic and solid murine tumor models. *Cancer Chemother Pharmacol* **12**(1): 26-30.

Sirotnak FM, Kurita S and Hutchison DJ (1968) On the nature of a transport alteration determining resistance to amethopterin in the L1210 leukemia. *Cancer Res* **28**(1): 75-80.

Sirotnak FM, Moccio DM, Kelleher LE and Goutas LJ (1981) Relative frequency and kinetic properties of transport-defective phenotypes among methotrexate-resistant L1210 clonal cell lines derived in vivo. *Cancer Res* **41**(11 Pt 1): 4447-4452.

Sirotnak FM, Otter GM and Schmid FA (1993) Markedly improved efficacy of edatrexate compared to methotrexate in a high-dose regimen with leucovorin rescue against metastatic murine solid tumors. *Cancer Res* **53**(3): 587-591.

Sirotnak FM and Tolner B (1999) Carrier-mediated membrane transport of folates in mammalian cells. *Annu Rev Nutr* **19**: 91-122.

Smith-Jones PM, Pandit-Taskar N, Cao W, O'Donoghue J, Philips MD, Carrasquillo J, Konner JA, Old LJ and Larson SM (2008) Preclinical radioimmunotargeting of folate receptor alpha using the monoclonal antibody conjugate DOTA-MORAb-003. *Nuclear medicine and biology* **35**(3): 343-351.

Smith A, Hum M, Winick NJ and Kamen BA (1996) A case for the use of aminopterin in treatment of patients with leukemia based on metabolic studies of blasts in vitro. *Clin Cancer Res* **2**(1): 69-73.

Smith GK, Mueller WT, Benkovic PA and Benkovic SJ (1981) On the cofactor specificity of glycinamide ribonucleotide and 5-aminoimidazole-4-carboxamide ribonucleotide transformylase from chicken liver. *Biochemistry* **20**(5): 1241-1245.

Smith GK, Mueller WT, Wasserman GF, Taylor WD and Benkovic SJ (1980) Characterization of the enzyme complex involving the folate-requiring enzymes of de novo purine biosynthesis. *Biochemistry* **19**(18): 4313-4321.

Smith SG, Lehman NL and Moran RG (1993) Cytotoxicity of antifolate inhibitors of thymidylate and purine synthesis to WiDr colonic carcinoma cells. *Cancer Res* **53**(23): 5697-5706.

Spannuth WA, Sood AK and Coleman RL (2010) Farletuzumab in epithelial ovarian carcinoma. *Expert opinion on biological therapy* **10**(3): 431-437.

Srimatkandada S, Schweitzer BI, Moroson BA, Dube S and Bertino JR (1989) Amplification of a polymorphic dihydrofolate reductase gene expressing an enzyme with decreased binding to methotrexate in a human colon carcinoma cell line, HCT-8R4, resistant to this drug. *J Biol Chem* **264**(6): 3524-3528.

Stark M, Gonen N and Assaraf YG (2009) Functional elements in the minimal promoter of the human proton-coupled folate transporter. *Biochem Biophys Res Commun* **388**(1): 79-85.

Steinfeld R, Grapp M, Kraetzner R, Dreha-Kulaczewski S, Helms G, Dechent P, Wevers R, Grosso S and Gartner J (2009) Folate receptor alpha defect causes cerebral folate transport deficiency: a treatable neurodegenerative disorder associated with disturbed myelin metabolism. *American journal of human genetics* **85**(3): 354-363.

Stokstad ELR (1990) Historical perspective on key advances in biochemistry and physiology of folates, in *Folic Acid Metabolism in Health and Disease* (E.L.R. PMFS ed) pp 1-21, Wiley-Liss.

Stuwe L, Muller M, Fabian A, Waning J, Mally S, Noel J, Schwab A and Stock C (2007) pH dependence of melanoma cell migration: protons extruded by NHE1 dominate protons of the bulk solution. *The Journal of physiology* **585**(Pt 2): 351-360.

Subramanian VS, Marchant JS and Said HM (2008) Apical membrane targeting and trafficking of the human proton-coupled transporter in polarized epithelia. *Am J Physiol Cell Physiol* **294**(1): C233-240.

Sun Y, Sun J, Shi S, Jing Y, Yin S, Chen Y, Li G, Xu Y and He Z (2009) Synthesis, transport and pharmacokinetics of 5'-amino acid ester prodrugs of 1-beta-D-arabinofuranosylcytosine. *Molecular pharmaceutics* **6**(1): 315-325.

Swietach P, Patiar S, Supuran CT, Harris AL and Vaughan-Jones RD (2009) The role of carbonic anhydrase 9 in regulating extracellular and intracellular ph in three-dimensional tumor cell growths. *J Biol Chem* **284**(30): 20299-20310.

Taber LD, O'Brien P, Bowsher RR and Sportsman JR (1991) Competitive particle concentration fluorescence immunoassay for measuring 5,10-dideaza-5,6,7,8-tetrahydrofolic acid (lometrexol) in serum. *Clinical chemistry* **37**(2): 254-260.

Taylor AM, Zhu Q and Casey JR (2001) Cysteine-directed cross-linking localizes regions of the human erythrocyte anion-exchange protein (AE1) relative to the dimeric interface. *Biochem J* **359**(Pt 3): 661-668.

Taylor EC (1993) Design and synthesis of inhibitors of folate-dependent enzymes as antitumor agents. *Advances in experimental medicine and biology* **338**: 387-408.

Taylor EC, Harrington PJ, Fletcher SR, Beardsley GP and Moran RG (1985) Synthesis of the antileukemic agents 5,10-dideazaaminopterin and 5,10-dideaza-5,6,7,8-tetrahydroaminopterin. *J Med Chem* **28**(7): 914-921.

Taylor EC, Kuhnt D, Shih C, Rinzel SM, Grindey GB, Barredo J, Jannatipour M and Moran RG (1992) A dideazatetrahydrofolate analogue lacking a chiral center at C-6, N-[4-[2-(2-amino-3,4-dihydro-4-oxo-7H-pyrrolo[2,3-d]pyrimidin-5- yl)ethyl]benzoyl]-L-glutamic acid, is an inhibitor of thymidylate synthase. *J Med Chem* **35**(23): 4450-4454.

Theti DS, Bavetsias V, Skelton LA, Titley J, Gibbs D, Jansen G and Jackman AL (2003) Selective delivery of CB300638, a cyclopenta[g]quinazoline-based thymidylate synthase inhibitor into human tumor cell lines overexpressing the alpha-isoform of the folate receptor. *Cancer Res* **63**(13): 3612-3618.

Thigpen AE, West MG and Appling DR (1990) Rat C1-tetrahydrofolate synthase. cDNA isolation, tissue-specific levels of the mRNA, and expression of the protein in yeast. *J Biol Chem* **265**(14): 7907-7913.

Thompson CA (2009) FDA approves pralatrexate for treatment of rare lymphoma. *American journal of health-system pharmacy : AJHP : official journal of the American Society of Health-System Pharmacists* **66**(21): 1890.

Tibbetts AS and Appling DR (2010) Compartmentalization of Mammalian folate-mediated one-carbon metabolism. *Annu Rev Nutr* **30**: 57-81.

Toffoli G, Cernigoi C, Russo A, Gallo A, Bagnoli M and Boiocchi M (1997) Overexpression of folate binding protein in ovarian cancers. *Int J Cancer* **74**(2): 193-198.

Toner LE, Vrhovac R, Smith EA, Gardner J, Heaney M, Gonen M, Teruya-Feldstein J, Sirotnak F and O'Connor OA (2006) The schedule-dependent effects of the novel antifolate

pralatrexate and gemcitabine are superior to methotrexate and cytarabine in models of human non-Hodgkin's lymphoma. *Clin Cancer Res* **12**(3 Pt 1): 924-932.

Tong Y, Liu-Chen X, Ercikan-Abali EA, Zhao SC, Banerjee D, Maley F and Bertino JR (1998) Probing the folate-binding site of human thymidylate synthase by site-directed mutagenesis. Generation of mutants that confer resistance to raltitrexed, Thymitaq, and BW1843U89. *J Biol Chem* **273**(47): 31209-31214.

Trent JM, Buick RN, Olson S, Horns RC, Jr. and Schimke RT (1984) Cytologic evidence for gene amplification in methotrexate-resistant cells obtained from a patient with ovarian adenocarcinoma. *Journal of clinical oncology : official journal of the American Society of Clinical Oncology* **2**(1): 8-15.

Tse A, Brigle K, Taylor SM and Moran RG (1998) Mutations in the reduced folate carrier gene which confer dominant resistance to 5,10-dideazatetrahydrofolate. *J Biol Chem* **273**(40): 25953-25960.

Tse A and Moran RG (1998) Cellular folates prevent polyglutamation of 5, 10-dideazatetrahydrofolate. A novel mechanism of resistance to folate antimetabolites. *J Biol Chem* **273**(40): 25944-25952.

Tsujimoto Y (1997) Apoptosis and necrosis: intracellular ATP level as a determinant for cell death modes. *Cell Death Differ* **4**(6): 429-434.

Umapathy NS, Gnana-Prakasam JP, Martin PM, Mysona B, Dun Y, Smith SB, Ganapathy V and Prasad PD (2007) Cloning and functional characterization of the proton-coupled electrogenic folate transporter and analysis of its expression in retinal cell types. *Invest Ophthalmol Vis Sci* **48**(11): 5299-5305.

Unal ES, Zhao R, Chang MH, Fiser A, Romero MF and Goldman ID (2009a) The functional roles of the His247 and His281 residues in folate and proton translocation mediated by the human proton-coupled folate transporter SLC46A1. *J Biol Chem* **284**(26): 17846-17857.

Unal ES, Zhao R and Goldman ID (2009b) Role of the glutamate 185 residue in proton translocation mediated by the proton-coupled folate transporter SLC46A1. *Am J Physiol Cell Physiol* **297**(1): C66-74.

Unal ES, Zhao R, Qiu A and Goldman ID (2008) N-linked glycosylation and its impact on the electrophoretic mobility and function of the human proton-coupled folate transporter (HsPCFT). *Biochim Biophys Acta* **1778**(6): 1407-1414.

Urquhart BL, Gregor JC, Chande N, Knauer MJ, Tirona RG and Kim RB (2010) The human proton-coupled folate transporter (hPCFT): modulation of intestinal expression and function by drugs. *Am J Physiol Gastrointest Liver Physiol* **298**(2): G248-254.

Vandenberg TA, Pritchard KI, Eisenhauer EA, Trudeau ME, Norris BD, Lopez P, Verma SS, Buckman RA and Muldal A (1993) Phase II study of weekly edatrexate as first-line chemotherapy for metastatic breast cancer: a National Cancer Institute of Canada Clinical Trials Group study. *Journal of clinical oncology : official journal of the American Society of Clinical Oncology* **11**(7): 1241-1244.

Varela-Moreiras G and Selhub J (1992) Long-term folate deficiency alters folate content and distribution differentially in rat tissues. *J Nutr* **122**(4): 986-991.

Vavere AL, Biddlecombe GB, Spees WM, Garbow JR, Wijesinghe D, Andreev OA, Engelman DM, Reshetnyak YK and Lewis JS (2009) A novel technology for the imaging of acidic prostate tumors by positron emission tomography. *Cancer Res* **69**(10): 4510-4516.

Veenhoff LM, Heuberger EH and Poolman B (2001) The lactose transport protein is a cooperative dimer with two sugar translocation pathways. *The EMBO journal* **20**(12): 3056-3062.

Veggian R, Fasolato S, Menard S, Minucci D, Pizzetti P, Regazzoni M, Tagliabue E and Colnaghi MI (1989) Immunohistochemical reactivity of a monoclonal antibody prepared against human ovarian carcinoma on normal and pathological female genital tissues. *Tumori* **75**(5): 510-513.

Visentin M, Chang MH, Romero MF, Zhao R and Goldman ID (2012) Substrate- and pH-Specific Antifolate Transport Mediated by Organic Anion-Transporting Polypeptide 2B1 (OATP2B1-SLCO2B1). *Mol Pharmacol* **81**(2): 134-142.

Wang L, Cherian C, Kugel Desmoulin S, Mitchell-Ryan S, Hou Z, Matherly LH and Gangjee A (2012) Synthesis and biological activity of 6-substituted pyrrolo[2,3-d]pyrimidine thienoyl regioisomers as inhibitors of de novo purine biosynthesis with selectivity for cellular uptake by high affinity folate receptors and the proton-coupled folate transporter over the reduced folate carrier. *J Med Chem*.

Wang L, Cherian C, Kugel Desmoulin S, Polin L, Deng Y, Wu J, Hou Z, White K, Kushner J, Matherly LH and Gangjee A (2010) Synthesis and antitumor activity of a novel series of 6-substituted pyrrolo[2,3-d]pyrimidine thienoyl antifolate inhibitors of purine biosynthesis with selectivity for high affinity folate receptors and the proton-coupled folate transporter over the reduced folate carrier for cellular entry. *J Med Chem* **53**(3): 1306-1318.

Wang L, Kugel Desmoulin S, Cherian C, Polin L, White K, Kushner J, Fulterer A, Chang MH, Mitchell-Ryan S, Stout M, Romero MF, Hou Z, Matherly LH and Gangjee A (2011)

Synthesis, biological, and antitumor activity of a highly potent 6-substituted pyrrolo[2,3-d]pyrimidine thienoyl antifolate inhibitor with proton-coupled folate transporter and folate receptor selectivity over the reduced folate carrier that inhibits beta-glycinamide ribonucleotide formyltransferase. *J Med Chem* **54**(20): 7150-7164.

Wang W, Marsh S, Cassidy J and McLeod HL (2001a) Pharmacogenomic dissection of resistance to thymidylate synthase inhibitors. *Cancer Res* **61**(14): 5505-5510.

Wang X, Shen F, Freisheim JH, Gentry LE and Ratnam M (1992) Differential stereospecificities and affinities of folate receptor isoforms for folate compounds and antifolates. *Biochem Pharmacol* **44**(9): 1898-1901.

Wang Y, Zhao R and Goldman ID (2004) Characterization of a folate transporter in HeLa cells with a low pH optimum and high affinity for pemetrexed distinct from the reduced folate carrier. *Clin Cancer Res* **10**(18 Pt 1): 6256-6264.

Wang Y, Zhao R, Russell RG and Goldman ID (2001b) Localization of the murine reduced folate carrier as assessed by immunohistochemical analysis. *Biochim Biophys Acta* **1513**(1): 49-54.

Wasson GR, McGlynn AP, McNulty H, O'Reilly SL, McKelvey-Martin VJ, McKerr G, Strain JJ, Scott J and Downes CS (2006) Global DNA and p53 region-specific hypomethylation in human colonic cells is induced by folate depletion and reversed by folate supplementation. *J Nutr* **136**(11): 2748-2753.

Webb BA, Chimenti M, Jacobson MP and Barber DL (2011) Dysregulated pH: a perfect storm for cancer progression. *Nature reviews Cancer* **11**(9): 671-677.

Weitman SD, Weinberg AG, Coney LR, Zurawski VR, Jennings DS and Kamen BA (1992) Cellular localization of the folate receptor: potential role in drug toxicity and folate homeostasis. *Cancer Res* **52**(23): 6708-6711.

Westerhof GR, Schornagel JH, Kathmann I, Jackman AL, Rosowsky A, Forsch RA, Hynes JB, Boyle FT, Peters GJ, Pinedo HM and et al. (1995) Carrier- and receptor-mediated transport of folate antagonists targeting folate-dependent enzymes: correlates of molecular-structure and biological activity. *Mol Pharmacol* **48**(3): 459-471.

Wettergren Y, Odin E, Nilsson S, Willen R, Carlsson G and Gustavsson B (2005) Low expression of reduced folate carrier-1 and folylpolyglutamate synthase correlates with lack of a deleted in colorectal carcinoma mRNA splice variant in normal-appearing mucosa of colorectal carcinoma patients. *Cancer detection and prevention* **29**(4): 348-355.

Whetstine JR, Flatley RM and Matherly LH (2002a) The human reduced folate carrier gene is ubiquitously and differentially expressed in normal human tissues: identification of seven non-coding exons and characterization of a novel promoter. *Biochem J* **367**(Pt 3): 629-640.

Whetstine JR, Witt TL and Matherly LH (2002b) The human reduced folate carrier gene is regulated by the AP2 and sp1 transcription factor families and a functional 61-base pair polymorphism. *J Biol Chem* **277**(46): 43873-43880.

White JC and Goldman ID (1981) Methotrexate resistance in al L1210 cell line resulting from increased dihydrofolate reductase, decreased thymidylate synthetase activity, and normal membrane transport. Computer simulations based on network thermodynamics. *J Biol Chem* **256**(11): 5722-5727.

Wong SC, McQuade R, Proefke SA, Bhushan A and Matherly LH (1997) Human K562 transfectants expressing high levels of reduced folate carrier but exhibiting low transport activity. *Biochem Pharmacol* **53**(2): 199-206.

Wong SC, Proefke SA, Bhushan A and Matherly LH (1995) Isolation of human cDNAs that restore methotrexate sensitivity and reduced folate carrier activity in methotrexate transport-defective Chinese hamster ovary cells. *J Biol Chem* **270**(29): 17468-17475.

Wong SC, Zhang L, Proefke SA, Hukku B and Matherly LH (1998) Gene amplification and increased expression of the reduced folate carrier in transport elevated K562 cells. *Biochem Pharmacol* **55**(7): 1135-1138.

Wong SC, Zhang L, Witt TL, Proefke SA, Bhushan A and Matherly LH (1999) Impaired membrane transport in methotrexate-resistant CCRF-CEM cells involves early translation termination and increased turnover of a mutant reduced folate carrier. *J Biol Chem* **274**(15): 10388-10394.

Worm J, Kirkin AF, Dzhandzhugazyan KN and Guldberg P (2001) Methylation-dependent silencing of the reduced folate carrier gene in inherently methotrexate-resistant human breast cancer cells. *J Biol Chem* **276**(43): 39990-40000.

Wu D, Li Y, Song G, Cheng C, Zhang R, Joachimiak A, Shaw N and Liu ZJ (2009) Structural basis for the inhibition of human 5,10-methenyltetrahydrofolate synthetase by N10-substituted folate analogues. *Cancer Res* **69**(18): 7294-7301.

Wu M, Gunning W and Ratnam M (1999) Expression of folate receptor type alpha in relation to cell type, malignancy, and differentiation in ovary, uterus, and cervix. *Cancer epidemiology, biomarkers & prevention : a publication of the American Association for*

Cancer Research, cosponsored by the American Society of Preventive Oncology **8**(9): 775-782.

Wykoff CC, Beasley NJ, Watson PH, Turner KJ, Pastorek J, Sibtain A, Wilson GD, Turley H, Talks KL, Maxwell PH, Pugh CW, Ratcliffe PJ and Harris AL (2000) Hypoxia-inducible expression of tumor-associated carbonic anhydrases. *Cancer Res* **60**(24): 7075-7083.

Yang R, Sowers R, Mazza B, Healey JH, Huvos A, Grier H, Bernstein M, Beardsley GP, Krailo MD, Devidas M, Bertino JR, Meyers PA and Gorlick R (2003) Sequence alterations in the reduced folate carrier are observed in osteosarcoma tumor samples. *Clin Cancer Res* **9**(2): 837-844.

Yin CC, Aldema-Ramos ML, Borges-Walmsley MI, Taylor RW, Walmsley AR, Levy SB and Bullough PA (2000) The quarternary molecular architecture of TetA, a secondary tetracycline transporter from Escherichia coli. *Molecular microbiology* **38**(3): 482-492.

Yin MB, Voigt W, Panadero A, Vanhoefer U, Frank C, Pajovic S, Azizkhan J and Rustum YM (1997) p53 and WAF1 are induced and Rb protein is hypophosphorylated during cell growth inhibition by the thymidylate synthase inhibitor ZD1694 (Tomudex). *Mol Pharmacol* **51**(4): 630-636.

Zain J and O'Connor O (2010a) Pralatrexate: basic understanding and clinical development. *Expert opinion on pharmacotherapy* **11**(10): 1705-1714.

Zain JM and O'Connor O (2010b) Targeted treatment and new agents in peripheral T-cell lymphoma. *International journal of hematology* **92**(1): 33-44.

Zhang CC, Boritzki TJ and Jackson RC (1998a) An inhibitor of glycinamide ribonucleotide formyltransferase is selectively cytotoxic to cells that lack a functional G1 checkpoint. *Cancer Chemother Pharmacol* **41**(3): 223-228.

Zhang L, Taub JW, Williamson M, Wong SC, Hukku B, Pullen J, Ravindranath Y and Matherly LH (1998b) Reduced folate carrier gene expression in childhood acute lymphoblastic leukemia: relationship to immunophenotype and ploidy. *Clin Cancer Res* **4**(9): 2169-2177.

Zhang S, Wu K and Sherry AD (1999) A Novel pH-Sensitive MRI Contrast Agent. *Angew Chem Int Ed Engl* **38**(21): 3192-3194.

Zhang X, Lin Y and Gillies RJ (2010) Tumor pH and its measurement. *Journal of nuclear medicine : official publication, Society of Nuclear Medicine* **51**(8): 1167-1170.

Zhang Y, Desharnais J, Greasley SE, Beardsley GP, Boger DL and Wilson IA (2002) Crystal structures of human GAR Tfase at low and high pH and with substrate beta-GAR. *Biochemistry* **41**(48): 14206-14215.

Zhao R, Assaraf YG and Goldman ID (1998) A Reduced Folate Carrier Mutation Produces Substrate-dependent Alterations in Carrier Mobility in Murine Leukemia Cells and Methotrexate Resistance with Conservation of Growth in 5-Formyltetrahydrofolate. *J Biol Chem* **273**(14): 7873-7879.

Zhao R, Babani S, Gao F, Liu L and Goldman ID (2000a) The mechanism of transport of the multitargeted antifolate (MTA) and its cross-resistance pattern in cells with markedly impaired transport of methotrexate. *Clin Cancer Res* **6**(9): 3687-3695.

Zhao R, Chattopadhyay S, Hanscom M and Goldman ID (2004a) Antifolate resistance in a HeLa cell line associated with impaired transport independent of the reduced folate carrier. *Clin Cancer Res* **10**(24): 8735-8742.

Zhao R, Diop-Bove N, Visentin M and Goldman ID (2011a) Mechanisms of membrane transport of folates into cells and across epithelia. *Annu Rev Nutr* **31**: 177-201.

Zhao R, Gao F, Babani S and Goldman ID (2000b) Sensitivity to 5,10-dideazatetrahydrofolate is fully conserved in a murine leukemia cell line highly resistant to methotrexate due to impaired transport mediated by the reduced folate carrier. *Clin Cancer Res* **6**(8): 3304-3311.

Zhao R, Gao F and Goldman ID (2001a) Marked suppression of the activity of some, but not all, antifolate compounds by augmentation of folate cofactor pools within tumor cells. *Biochem Pharmacol* **61**(7): 857-865.

Zhao R, Gao F, Hanscom M and Goldman ID (2004b) A prominent low-pH methotrexate transport activity in human solid tumors: contribution to the preservation of methotrexate pharmacologic activity in HeLa cells lacking the reduced folate carrier. *Clin Cancer Res* **10**(2): 718-727.

Zhao R, Gao F, Wang Y, Diaz GA, Gelb BD and Goldman ID (2001b) Impact of the reduced folate carrier on the accumulation of active thiamin metabolites in murine leukemia cells. *J Biol Chem* **276**(2): 1114-1118.

Zhao R and Goldman ID (2003) Resistance to antifolates. *Oncogene* **22**(47): 7431-7457.

Zhao R and Goldman ID (2007) The molecular identity and characterization of a Proton-coupled Folate Transporter--PCFT; biological ramifications and impact on the activity of pemetrexed. *Cancer Metastasis Rev* **26**(1): 129-139.

Zhao R, Hanscom M, Chattopadhyay S and Goldman ID (2004c) Selective preservation of pemetrexed pharmacological activity in HeLa cells lacking the reduced folate carrier: association with the presence of a secondary transport pathway. *Cancer Res* **64**(9): 3313-3319.

Zhao R, Matherly LH and Goldman ID (2009a) Membrane transporters and folate homeostasis: intestinal absorption and transport into systemic compartments and tissues. *Expert Rev Mol Med* **11**: e4.

Zhao R, Min SH, Qiu A, Sakaris A, Goldberg GL, Sandoval C, Malatack JJ, Rosenblatt DS and Goldman ID (2007) The spectrum of mutations in the PCFT gene, coding for an intestinal folate transporter, that are the basis for hereditary folate malabsorption. *Blood* **110**(4): 1147-1152.

Zhao R, Min SH, Wang Y, Campanella E, Low PS and Goldman ID (2009b) A role for the proton-coupled folate transporter (PCFT-SLC46A1) in folate receptor-mediated endocytosis. *J Biol Chem* **284**(7): 4267-4274.

Zhao R, Qiu A, Tsai E, Jansen M, Akabas MH and Goldman ID (2008) The proton-coupled folate transporter: impact on pemetrexed transport and on antifolates activities compared with the reduced folate carrier. *Mol Pharmacol* **74**(3): 854-862.

Zhao R, Sharina IG and Goldman ID (1999) Pattern of mutations that results in loss of reduced folate carrier function under antifolate selective pressure augmented by chemical mutagenesis. *Mol Pharmacol* **56**(1): 68-76.

Zhao R, Shin DS, Diop-Bove N, Ovits CG and Goldman ID (2011b) Random mutagenesis of the proton-coupled folate transporter (SLC46A1), clustering of mutations, and the bases for associated losses of function. *J Biol Chem* **286**(27): 24150-24158.

Zhao R, Titus S, Gao F, Moran RG and Goldman ID (2000c) Molecular analysis of murine leukemia cell lines resistant to 5, 10-dideazatetrahydrofolate identifies several amino acids critical to the function of folylpolyglutamate synthetase. *J Biol Chem* **275**(34): 26599-26606.

Zhao R, Unal ES, Shin DS and Goldman ID (2010) Membrane topological analysis of the proton-coupled folate transporter (PCFT-SLC46A1) by the substituted cysteine accessibility method. *Biochemistry* **49**(13): 2925-2931.

Zottola RJ, Cloherty EK, Coderre PE, Hansen A, Hebert DN and Carruthers A (1995) Glucose transporter function is controlled by transporter oligomeric structure. A single, intramolecular disulfide promotes GLUT1 tetramerization. *Biochemistry* **34**(30): 9734-9747.

Zvelebil MJ, Barton GJ, Taylor WR and Sternberg MJ (1987) Prediction of protein secondary structure and active sites using the alignment of homologous sequences. *J Mol Biol* **195**(4): 957-961.

ABSTRACT

THE PROTON-COUPLED FOLATE TRANSPORTER: BIOLOGY AND THERAPEUTIC APPLICATIONS TO CANCER

by

SITA KUGEL DESMOULIN

August 2012

Advisor: Larry H. Matherly, Ph.D.

Major: Cancer Biology (Pharmacology)

Degree: Doctor of Philosophy

Folates are essential cofactors of tumor cell proliferation and survival required for nucleotide biosynthesis and amino acid metabolism. In cancer therapy, inhibition of folate-dependent metabolic pathways has been achieved through the use of antifolates. Unfortunately, the efficacy of many clinically approved antifolates is limited by a lack of tumor selectivity. Facilitative transport of folates into mammalian cells is achieved by the reduced folate carrier (RFC) and proton-coupled folate transporter (PCFT). As PCFT is a folate-proton symporter with an acidic pH optimum, PCFT may provide a mechanism for targeting cytotoxic antifolates to tumors, based on their acidic microenvironments. To establish the feasibility of this approach, we systematically determined the expression profiles for PCFT and RFC. In various human malignant cell lines and tissues PCFT was highly expressed and functional, while its expression in normal tissue was more limited compared to RFC.

Screening and characterization of multiple series of novel antifolates led to the identification of 6-substituted pyrrolo[2,3-*d*]pyrimidine benzoyl and thienoyl antifolates, which were selective for PCFT-mediated uptake, but not RFC. Upon internalization, these novel

antifolates were extensively polyglutamylated, as detected by high performance liquid chromatography (HPLC). Growth inhibition assay paired with nucleoside protection identified glycinamide ribonucleotide (GAR) formyltransferase (GARFTase) in the *de novo* purine biosynthesis pathway as the principle drug target. This was confirmed by *in situ* measurement of [^{14}C]glycine incorporation into [^{14}C]formylGAR in treated cells. Furthermore, contraction of intracellular purine nucleotide triphosphate pools occurred in a dose- and time-dependent manner, as demonstrated by quantitative HPLC analysis. Further, drug treatment induced S-phase accumulation eventually leading to irreversible cell death. Drug treatment caused a significant delay in tumor growth in an *in vivo* efficacy trial of SCID mice implanted with subcutaneous human tumors where PCFT was the sole mechanism of drug uptake.

Although these compounds are not substrates for RFC, its expression does impact drug efficacy by influencing intracellular tetrahydrofolate (THF) cofactor pools. Loss of functional RFC leads to increased polyglutamylation of these analogs within the cell causing enhanced cytotoxicity. Similarly, these novel PCFT-selective antifolates displayed increased *in vivo* efficacy in subcutaneously implanted human tumors lacking RFC.

Our finding of widespread PCFT expression in human solid tumors paired with our discovery of novel antifolates internalized via PCFT offers exciting new therapeutic possibilities for selectively targeting tumors based on their acidic microenvironments. These compounds display immense therapeutic potential, especially in tumors with *de novo* or acquired resistance to classic antifolates caused by lack of RFC function.

AUTOBIOGRAPHICAL STATEMENT

EDUCATION

Wayne State University Detroit, MI 2007 – 2012
Doctor of Philosophy: Cancer Biology (Minor in Pharmacology)
Simon Fraser University Burnaby, British Columbia, CANADA 2001 – 2006
Bachelor of Science: Kinesiology (Minor in Anatomy and Physiology)

GRANTS

Pre-doctoral Training Grant - Canadian Institutes of Health Research (CIHR) 2009 – 2012

SELECTED PUBLICATIONS

Kugel Desmoulin, S. & Matherly, L.H. The Human Proton-coupled Folate Transporter: Biology and Therapeutic Applications to Cancer. *Cancer Biology & Therapy*. Invited Review. **2012**.

Wang, L., Cherian, C., **Kugel Desmoulin, S.**, Mitchell-Ryan, S., Hou, Z., Matherly, L.H. & Gangjee, A. Synthesis and biological activity of 6-substituted pyrrolo[2,3-d]pyrimidine thienoyl regioisomers as inhibitors of de novo purine biosynthesis with selectivity for cellular uptake by high affinity folate receptors and the proton-coupled folate transporter over the reduced folate carrier. *J Med Chem*. 55(4): 1758-70. **2012**.

Hou, Z., **Kugel Desmoulin, S.**, Etnyre, E., Olive, M., Hsiung, B., Cherian, C., Wloszczynski, P.A., Moin, K. & Matherly, L.H. Identification and functional impact of homo-oligomers of the human proton-coupled folate transporter. *J Biol Chem*. 287(7): 4982-95. **2012**.

Kugel Desmoulin, S., Wang, L., Polin, P., White, K., Kushner, J., Hales, E., Stout, M., Hou, Z., Cherian, C., Gangjee, A. & Matherly, L.H. Therapeutic targeting of a novel 6-substituted pyrrolo[2,3d]pyrimidine thienoyl antifolate to human solid tumors based on selective uptake by the proton-coupled folate transporter. *Mol Pharmacol*. 80(6): 1096-107. **2011**.

*****Wang , L., ***Kugel Desmoulin, S**., Cherian, C., Polin, L., White, K., Kushner, J., Fulterer, A., Chang, M.H., Mitchell-Ryan, S., Stout, M., Romero, M.F., Hou, Z., Matherly, L.H. & Gangjee A. Synthesis, biological, and antitumor activity of a highly potent 6-substituted pyrrolo[2,3-d]pyrimidine thienoyl antifolate inhibitor with proton-coupled folate transporter and folate receptor selectivity over the reduced folate carrier that inhibits β-glycinamide ribonucleotide formyltransferase. *J Med Chem*. 54(20): 7150-64. **2011**.
***** These authors contributed equally to this work

Kugel Desmoulin, S., Wang, Y., Wu, J., Stout, M., Hou, Z., Fulterer, A., Chang, M.H., Romero, M.F., Cherian, C., Gangjee, A. & Matherly, L.H. Targeting the proton-coupled folate transporter for selective delivery of 6-substituted pyrrolo[2,3-d]pyrimidine antifolate inhibitors of de novo purine biosynthesis in the chemotherapy of solid tumors. *Mol Pharmacol*. 78(4): 577-87. **2010**.

Wang, L., Cherian, C., **Kugel Desmoulin, S**., Polin, L., Deng, Y., Wu, J., Hou, Z., White, K., Kushner, J., Matherly, L.H. & Gangjee, A. Synthesis and biological activity of a novel series of 6-substituted pyrrolo[2,3-*d*]pyrimidine thienoyl antifolate inhibitors of purine biosynthesis with selectivity for high affinity folate receptors and the proton-coupled folate transporter over the reduced folate carrier for cellular entry. *J Med Chem*. 53(3): 1306-18. **2010**.

Deng, Y., Zhou, X., **Kugel Desmoulin, S**., Wu, J., Cherian, C., Hou, Z., Matherly, L.H. & Gangjee, A. Synthesis and biological activity of a novel series of 6-substituted thieno[2,3-*d*]pyrimidine antifolate inhibitors of purine biosynthesis with selectivity for high affinity folate receptors over the reduced folate carrier and proton-coupled folate transporter for cellular entry. *J. Med. Chem*. 52(9): 2940-2951. **2009**.